Università degli Studi di Ferrara

DOTTORATO DI RICERCA IN

SCIENZE CHIMICHE

CICLO XXVII

COORDINATORE Prof. Carlo Alberto Bignozzi

Studio, sintesi e caratterizzazione di nuovi materiali microporosi funzionalizzati per la realizzazione di processi reattivi e separativi in sistemi dinamici

Settore Scientifico Disciplinare CHIM/06

Dottorando
Dott. Greco Roberto

_____
(firma)

Tutore
Prof. Cavazzini Alberto

_____
(firma)

Anni 2012/2014

Alla mia famiglia e a mio nonno Gino

Sommario

Il progetto di questa tesi di dottorato ha riguardato lo studio, la preparazione e la caratterizzazione di nuovi materiali microporosi funzionalizzati per applicazioni innovative in sistemi dinamici in flusso di tipo cromatografico e simil-cromatografico, inclusa la possibilità di eseguire reazioni chimiche in continuo (flow-chemistry).

Le tematiche sviluppate nel lavoro di dottorato hanno natura multidisciplinare includendo competenze di chimica analitica, di chimica organica, di scienze dei materiali e delle superfici e di modellizzazione di processo.

Un primo utilizzo di materiali porosi è stato quello di impiegarli per la creazione di microreattori a letto impaccato per la realizzazione in flusso continuo di sofisticate trasformazioni chimiche (quali, ad esempio, reazioni stereoselettive per l'ottenimento di molecole enantiomericamente pure). La progettazione e la realizzazione dei microreattori ha richiesto diverse fasi che vanno dalla preparazione del materiale di riempimento dei microreattori attraverso l'immobilizzazione di opportuni catalizzatori su materiale inerte (supporto) di tipo siliceo o polistirenico fino all'ottimizzazione dell'impaccamento dei microreattori (necessario per la preparazione del letto fisso) e al loro interfacciamento con sistemi di pompaggio (ad alta pressione) necessari per far percolare la soluzione di reazione nel letto impaccato. Abbiamo studiato il comportamento di questi sistemi cercando di descrivere tutti i processi che avvengono prima (trasferimento dei reattivi al sito catalitico di reazione), durante (cinetica del processo) e dopo (separazione dei prodotti dai reagenti) la reazione chimica. Pertanto, i nuovi materiali sintetizzati sono stati caratterizzati in dettaglio in termini chimico-fisici, cinetici e geometrici. In particolare, si sono caratterizzazione studiati: (1) i processi di trasferimento di massa di un composto dalla "fase mobile" (la fase mobile in questo contesto può essere la miscela dei reagenti pompati dentro il microreattore) alla "fase stazionaria" (che, a sua volta, può essere la superficie del catalizzatore supportato o di una fase stazionaria cromatografica); (2) la termodinamica del processo di adsorbimento attraverso la determinazione delle isoterme di adsorbimento dei composti di interesse sulla superficie del solido; e (3) una serie di proprietà del solido poroso quali, ad esempio, l'area superficiale, la dimensione dei pori, il grado di funzionalizzazione, etc.

I microreattori e la possibilità di utilizzarli per trasformazioni continue in flusso hanno un valore aggiunto importante dal momento che, per una serie di caratteristiche, rispondono ai fondamentali requisiti della cosiddetta chimica verde (green chemistry), consentendo una produzione sostenibile per l'ambiente e, allo stesso tempo, economicamente vantaggiosa.

Un secondo obiettivo è stato quello di utilizzare questi materiali funzionalizzati come nuove fasi stazionarie per il riconoscimento selettivo di molecole. Nel caso di organocatalizzatori chirali immobilizzati su matrici inerti, l'idea è stata quella di verificare se gli stessi meccanismi di induzione chirale (che portano alla produzione dei prodotti nei sistemi reattivi in flusso) possano essere sfruttati anche per il processo di discriminazione chirale da parte dello stesso organocatalizzatore. Un simile approccio ha trovato un'applicazione, ad esempio, nell'utilizzo di un'innovativa fase stazionaria impiegata per la separazione di oligonucleotidi di sintesi (la matrice silicea funzionalizzata con selettori organici ha consentito la realizzazione di una colonna cromatografica operante sia a fase inversa sia come debole scambiatore anionico).

Il lavoro di tesi è culminato nella pubblicazione di sette lavori scientifici (su riviste internazionali peer-reviewed) consultabili in allegato alla fine di questo elaborato e di un ulteriore lavoro in fase di stesura.

Abstract

This PhD program has focused on the study, preparation and characterization of new functionalized microporous materials for applications in chromatographic and chromatographic-like flow systems, including the possibility of performing chemical transformations in flow-mode (flow chemistry).

The work has been multidisciplinary in nature, including elements of analytical and organic chemistry, material science and process modeling.

The materials prepared in this work have been used for different purposes. They have been employed, on the one hand, for the preparation of packed-bed microreactors to perform advanced stereoselective chemical transformations by means of organocatalysts anchored to solid supports (polystyrene and silica gel based) and, on the other, as new stationary phases for chromatographic separations. In the case of organocatalyst-functionalized silicon packed-bed microreactors, we followed the idea that mechanisms of chiral induction due to organocatalysts (asymmetric synthesis) might be exploited for chiral discrimination (chiral chromatography) with their immobilized counterparts.

The new materials have been thoroughly characterized in terms of chemico-physical, geometric and thermodynamic properties by investigating the mass transfer phenomena in packed beds, by measuring the adsorption isotherms of different substrates on different porous materials and by characterizing some of their fundamental properties such as porosity, superficial area, functionalization degree, etc.

In addition, their dynamic behavior in reactive systems has been studied and modeled to understand not only the thermodynamics but also the kinetics of the process and to optimize, based on this information, the experimental conditions as to maximize production yield.

Microreactors and the possibility of performing flow-chemistry through them satisfy the fundamental criteria of green chemistry, allowing for the realization of sustainable processes in terms of environmental impact and cost.

The activities of my work have produced seven papers on international peer-reviewed journals. These publications are included at the end of my dissertation. One additional paper is in preparation.

Sommario

1. Introduzione e obiettivi della tesi

Il progetto di ricerca sviluppato in questo lavoro di tesi è stato principalmente svolto presso il Dipartimento di Scienze Chimiche e Farmaceutiche (DSCF) dell'Università di Ferrara e ha avuto come obiettivo la preparazione e la caratterizzazione di nuovi materiali microporosi funzionalizzati per applicazioni innovative in sistemi dinamici in flusso di tipo cromatografico e simil-cromatografico, incluse reazione chimiche in continuo (flow-chemistry).[1]

Questi materiali sono stati pensati e progettati con lo scopo di realizzare due possibili obiettivi.
Il primo è stato quello di utilizzarli per la realizzazione in flusso di sofisticate trasformazioni chimiche (quali, ad esempio, trasformazioni di tipo stereoselettivo).[2] A questo scopo, attraverso l'ausilio di pompe da cromatografia, abbiamo fatto percolare la soluzione di reazione attraverso il materiale microporoso opportunamente funzionalizzato (nel caso di trasformazioni stereoselettive attraverso l'ancoraggio di organocatalizzatori chirali sulla superficie di silice o polistirene)[3] e abbiamo studiato il comportamento di questi sistemi cercando di descrivere tutti i processi che avvengono prima (trasferimento dei reattivi al sito catalitico di reazione), durante (cinetica del processo), e dopo (separazione dei prodotti dai reagenti) la reazione chimica.

Il secondo scopo è quello di utilizzare questi materiali come nuove fasi stazionarie per il riconoscimento selettivo di molecole. Nel caso di fasi funzionalizzate con organocatalizzatori chirali, ad esempio, l'idea che sta alla base di questo approccio è quella di studiare se i meccanismi di induzione chirale (da parte dell'organocatalizzatore) possano essere sfruttati anche nel processo di discriminazione chirale (ad esempio in applicazioni di cromatografia chirale) da parte dello stesso organocatalizzatore opportunamente ancorato ad un supporto inerte.[4]

Visto il carattere multidisciplinare dell'attività di ricerca, il lavoro è stato svolto in collaborazione con i gruppi di chimica analitica e di chimica organica del DSCF.
Competenze di chimica organica e tecniche avanzate di sintesi sono, infatti, indispensabili per l'individuazione del tipo di organocatalizzatore e del processo da sviluppare, da una parte, e per la progettazione e la preparazione dei nuovi materiali porosi, dall'altra. Questi

materiali sono stati ottenuti sostanzialmente attraverso due approcci diversi: (1) la funzionalizzazione di supporti inerti di tipo siliceo o polimerico (disponibili in commercio in formato di sferette di diverse dimensioni e caratteristiche) e (2) la preparazione di strutture monolitiche generate in situ all'interno di opportuni contenitori. In entrambi i casi, i materiali possono essere utilizzati sia come supporti fissi per promuovere reazioni catalizzate eterogenee in flusso (in quelli che sono definiti rispettivamente packed-bed o monolithic microreactors), sia come fasi stazionarie per colonne cromatografiche (di tipo impaccato o monolitico).[5]

Le competenze di chimica analitica sono, d'altra parte, fondamentali per la caratterizzazione di questi materiali da un punto di vista chimico-fisico, cinetico e geometrico.

Per caratterizzazione cinetica si intende lo studio di tutti i processi di trasferimento di massa (responsabili del non-equilibrio) di un composto da quella che, per usare la terminologia cromatografica, è definita "fase mobile" (nel nostro caso, la fase mobile può essere la miscela dei reagenti pompati dentro il microreattore) alla "fase stazionaria" (che, a sua volta, può essere la superficie del catalizzatore supportato o il solido adsorbente di una fase cromatografica). In mezzi porosi, questi fenomeni includono la diffusione in fase mobile, la cinetica del processo di adsorbimento/desadsorbimento,[6] la diffusione all'interno di mezzi porosi e sulla superficie del solido e le cosiddette inomogeneità del flusso dovute alla presenza di percorsi multipli all'interno di letti impaccati o di strutture monolitiche (con una terminologia derivata dell'ingegneria chimica si parla, per quest'ultimo fenomeno, di diffusione di tipo "eddy").

La caratterizzazione termodinamica di un materiale adsorbente, invece, costituisce lo studio della termodinamica del processo di adsorbimento/desadsorbimento, cioè la determinazione delle isoterme di adsorbimento dei composti di interesse sui solidi in studio. L'isoterma di adsorbimento è la relazione funzionale che lega, all'equilibrio, la concentrazione di un dato componente in fase mobile alla sua concentrazione in fase stazionaria.[7] Queste misure possono essere estese a sistemi competitivi, cioè quelli in cui più componenti possono competere per l'adsorbimento sul solido. I sistemi competitivi sono certamente i casi più significativi da un punto di vista pratico, in quanto tutti i sistemi di tipo liquido/solido (e specialmente quelli reattivi) sono per loro stessa natura dei sistemi competitivi. Dall'interpretazione dell'isoterma di adsorbimento si possono determinare alcune proprietà fondamentali dell'interazione molecola/superficie, come ad esempio il

modo in cui le molecole si adsorbono (adsorbimento monolayer o di tipo Langmuir o adsorbimento anti-langmuiriano multistrato), la costante di equilibrio del processo di adsorbimento/desadsorbimento o ancora la cosiddetta capacità di saturazione (che rappresenta la massima concentrazione di un analita che può essere adsorbita per grammo di solido a una data temperatura) e come queste proprietà vengano influenzate dalle variabili sperimentali (quali, concentrazione di altri analiti, temperatura, composizione della fase mobile, etc.).

La caratterizzazione geometrica, infine, comprende lo studio di una serie di proprietà del solido poroso quali, ad esempio, l'area superficiale, la dimensione dei pori, il grado di funzionalizzazione (numero di gruppi legati per grammo di supporto solido)[8] e ancora come i gruppi ancorati al supporto sono orientati nell'ambiente in cui si trovano (se, ad esempio, sono in forma "estesa" o "collassata" e/o quando una delle due forme prevale sull'altra in funzione del mezzo in cui si trova). Si tratta, come si può facilmente intuire, di uno studio indispensabile per comprendere alcune caratteristiche fondamentali (che tra l'altro ne determinano il potenziale) del materiale funzionalizzato quali, ad esempio, la sua bagnabilità (che dipende, sostanzialmente, dal numero di gruppi idrofobici che sono stati ancorati al supporto inerte e/o di quelli polari presenti sulla superficie del materiale adsorbente e dalla dimensione dei pori) o l'estensione dell'area superficiale. E' evidente, ad esempio, che un solido poroso non bagnabile nell'ambiente di reazione in cui si intende utilizzarlo è un materiale di scarso valore pratico, dal momento che in queste condizioni la superficie a disposizione per il processo di adsorbimento/reazione/desadsorbimento sarà molto limitata e la resa del processo molto bassa.

***

Le moderne tecniche strumentali di indagine superficiale oggi a disposizione (e in parte anche utilizzate per la caratterizzazione dei materiali funzionalizzati nel lavoro di tesi) includono, tra le altre, la risonanza magnetica nucleare allo stato solido (solid state NMR), la microscopia elettronica a scansione (SEM), la microanalisi elementare. Queste tecniche consentono la caratterizzazione fine della superficie del solido. Permettono di evidenziare il grado di eterogeneità della superficie, di mettere in evidenza la presenza di micropori,[9] di descrivere nel dettaglio la chimica delle fasi legate o di studiare la composizione dell'interfaccia liquido/solido[10] (cioè di quella regione complessa e dinamica che si forma ogniqualvolta un solido e un liquido vengono messi a contatto e che si estende per qualche

diametro molecolare a partire dalla superficie del solido) dalla quale, in ultima analisi, dipendono moltissime delle proprietà del sistema.

Queste informazioni aumentano molto la possibilità di capire e di interpretare la natura dei processi di riconoscimento molecolare o dei processi di reazione e di correlarli alla struttura della superficie e alla composizione dell'interfaccia. Ci consentono anche di pensare a nuovi materiali opportunamente preparati con lo scopo di creare, ad esempio, delle zone idrofiliche in prossimità di un centro di reazione (cosiddette tasche idrofiliche) per massimizzare la concentrazione di uno specifico reagente (idrofilico) in quella zona e favorire così uno specifico processo di trasformazione o per mimare il comportamento di sistemi biologici avanzati.

La scelta di considerare materiali polimerici o silicei microporosi come base di partenza per la preparazione di materiali funzionalizzati adottata in questo lavoro è dipesa essenzialmente dalle caratteristiche di versatilità ed economicità a loro associate e dalla possibilità di utilizzare una grande quantità di informazioni (sia dalla letteratura che dall'esperienza pregressa dei gruppi di ricerca con cui ho svolto il lavoro di dottorato) per ancorare sulla loro superficie molecole di diversa natura con tecniche in grado di preservarne le caratteristiche fondamentali. Questo aspetto rappresenta spesso un elemento di criticità e deve essere considerato con attenzione nella fase di progettazione di un materiale funzionalizzato. E' evidente, infatti, che l'ancoraggio va effettuato preservando il o i centri della molecola che sono riconosciuti responsabili dell'attività di riconoscimento molecolare o di catalisi. Se si tratta di ancorare biomolecole alla superficie, è necessario operare in condizioni di reazioni blande per preservare le proprietà biologiche delle molecole e quindi la loro attività. Da un punto di vista di applicazioni tecnico-scientifiche, materiali funzionali ottenuti a partire da supporti inerti silicei o polistirenici sono importanti per esempio nel campo dell'ottica, della medicina, dell'elettronica, delle tecnologie avanzate per l'ambiente, della catalisi, solo per citare alcune esempi.

***

La flow chemistry rappresenta un campo avanzato di ricerca in rapido e continuo sviluppo. Il concetto fondamentale è che molto spesso la trasformazione di processi in batch (discontinui) in processi continui in flusso è vantaggiosa in termini economici e pratici.

Un primo esempio è dato dalla facile scalabilità del processo. Si supponga, ad esempio, di avere preparato un microreattore per lo svolgimento di una specifica reazione (per inciso, nel linguaggio della chimica in flusso la definizione di "micro" non è univoca potendo essa riferirsi alle dimensioni vere e proprie del reattore usato per il processo, ad esempio un canale microfluidico stampato su wafer di silice, oppure alle dimensioni dei canali, ad esempio i pori di un materiale microporoso, in cui avviene la reazione). Lo scaling-up del processo può essere semplicemente ottenuto utilizzando in parallelo una serie di questi microreattori. Se si confronta questo modo di procedere con quanto avviene tipicamente in un processo industriale, in cui quasi sempre lo scaling up di una reazione comporta la messa a punto di un approccio sintetico completamente diverso da quello impiegato per la produzione su piccola scala della molecola di interesse, ci si rende conto come un approccio in flow consenta una riduzione nei costi di preparazione e produzione del prodotto.

La trasformazione in flusso ha poi altri vantaggi rispetto alla modalità discontinua, quali ad esempio quasi sempre un miglioramento nella miscelazione e nel trasferimento di massa e di calore con un impatto positivo in termini di produttività del processo.

Un altro concetto a volte sottovalutato ma che rappresenta un valore aggiunto per la scelta di un processo continuo rispetto a uno discontinuo è quello che il sistema dinamico consente di superare i limiti imposti dall'equilibrio (in base al principio di Le Chatelier), dal momento che grazie all'azione convettiva del flusso di eluente si verifica la rimozione in continuo dei reattivi prodotti "nell'ambiente di reazione" (che può anche essere inteso, considerando la geometria del microreattore, come una porzione longitudinale del letto impaccato o del monolita).

Infine, la trasformazione in flusso in microreattori (in particolare se si utilizzano organocatalizzatori) ha per sua stessa natura aspetti di sostenibilità economica ed ambientale (green chemistry concepts) che rendono il processo moderno e particolarmente attrattivo per la grande industria.
Il modello concettuale che abbiamo seguito nello sviluppo del lavoro di dottorato è basato sul parallelismo tra sistemi flow-mode di reazione per la preparazione di prodotti chimici in continuo, che stanno prendendo un grande sviluppo nella moderna chimica organica e

concetti di cromatografia di reazione liquida non-lineare (il cosiddetto reattore cromatografico), cioè sistemi cromatografici in cui oltre alla separazione dei componenti si ha anche la trasformazione di uno o più di loro sulla superficie adsorbente con formazione di prodotto (cromatografia di reazione). Non-lineare in questo contesto significa che le concentrazioni iniettate nel sistema separativo appartengono alla zona non-lineare dell'isoterma di adsorbimento.

La termodinamica del processo in queste condizioni ci dice che una semplice analisi basata sul concetto di fattore di ritenzione (condizioni lineari) non è sufficiente per descrivere la complessità del sistema, dal momento che a seguito della competizione delle molecole per l'adsorbimento su una fase di dimensioni comunque finite (competizione che aumenterà all'aumentare della concentrazione dei reattivi in fase mobile e che, quindi, "naturalmente" aumenta nel momento in cui si cerca di massimizzare la resa del processo attraverso l'incremento delle concentrazioni dei reattivi) il tempo di ritenzione non può essere considerato una parametro di riferimento univoco essendo funzione delle concentrazione iniettata. Se poi si immagina che durante il processo, a seguito della reazione sulla superficie, si produce un nuovo componente (il prodotto della reazione), che a sua volta può interagire con la fase stazionaria, ci si rende conto che la complessità del problema aumenta in modo considerevole.

Da un punto di vista della modellizzazione del processo, si ha quindi la necessità di utilizzare equazioni differenziali di bilancio di massa in cui siano presenti anche termini che descrivono la cinetica della reazione e, quindi, la scomparsa di reagenti a seguito di formazione di prodotti. Una volta che queste equazioni siano state risolte (generalmente per via numerica) e che si sia verificata la loro effettiva capacità di descrivere il sistema reale, abbiamo a disposizione uno strumento estremamente efficace, e molto più efficiente del tradizionale approccio "trial-and-error", per l'ottimizzazione di processi di reazione in flusso e/o la determinazione di parametri (ad esempio le costanti cinetiche del processo) non sempre facilmente determinabili.

***

Questa tesi ha rappresentato uno sforzo rilevante anche in termini di "comunicazione" tra due settori di ricerca, la chimica analitica e la chimica organica, apparentemente lontani.

Gran parte del problema, soprattutto all'inizio, è stato nel linguaggio da adottare per far comunicare questi due mondi.

La multidisciplinarietà del lavoro ha costituito però un valore aggiunto inestimabile e ha offerto la possibilità di interpretare uno stesso fenomeno da punti di partenza diversi consentendo di ottenere, alla fine, una descrizione dei fenomeni osservati più completa e integrata.

Il lavoro di tesi ha portato alla produzione di 7 lavori scientifici tutti pubblicati su riviste peer-to-peer appartenenti al primo quartile (Q1) dei settori scientifici di riferimento (allegati alla fine della tesi) e a un manoscritto in fase di stesura. Le attività del mio lavoro di tesi sono state presentate in congressi scientifici Nazionali ed Internazionali

2. Premessa

Il seguente capitolo ha lo scopo di illustrare i fondamenti logici ed applicativi di ciascuno dei lavori scientifici pubblicati durante il dottorato di ricerca.

Ogni paragrafo che seguirà vuole illustrare le premesse scientifiche e lo scenario di base che ha condotto a degli studi accurati i cui esiti possono essere approfonditi nelle pubblicazioni riportate in allegato al termine di questo elaborato.

2.1 Introduzione

Come già accennato nella prima parte di questa dissertazione, i materiali porosi stanno acquisendo una sempre maggiore rilevanza scientifica e tecnologica; particolare interesse è stato rivolto verso i materiali mesoporosi che presentano una disposizione ordinata dei pori (ordine su mesoscala), come ossidi di silicio, titanio o alluminio o gli organosilicati, che presentano peculiari caratteristiche quali porosità di dimensione controllabile, elevati valori di area superficiale e di volume libero e la possibilità di inserire gruppi funzionali di varia natura modificando le proprietà del materiale, rendendoli adatti a molteplici attività in svariati campi, come la produzione di sensori di gas, la formazione di film "low-k" per applicazioni nell'ambito della microelettronica, l'utilizzo nel contesto della catalisi e fotocatalisi o la fabbricazione di dispositivi ottici. Sulla base delle peculiari dimensioni molecolari, delle elevate aree superficiali e della porosità, i materiali funzionalizzati vengono studiati e sintetizzati per trovare applicazioni industriali, nell'adsorbimento e nella catalisi.[11]

Dopo aver quindi descritto le tecniche più comuni utilizzate per caratterizzare tali materiali, ci addentreremo in casi specifici di sintesi, caratterizzazione e applicazione di materiali funzionalizzati. Per fare ciò, si prenderà come riferimento la produzione scientifica che mi ha riguardato durante questi anni di dottorato al fine di presentarvi casi-studio interessanti al fine di comprendere i potenziali impieghi di nuovi materiali.

2.2 Flow-Chemistry: principi introduttivi

Le reazioni chimiche svolte in condizioni di flusso continuo rappresentano senza dubbio uno dei campi applicativi più importanti al quale ho dedicato gran tempo della mia ricerca scientifica. Infatti, il fine principale (ma come vedremo non unico) della sintesi e caratterizzazione di nuovi materiali funzionalizzati è stato usare essi stessi per impaccare microreattori attraverso i quali condurre e ottimizzare metodiche di sintesi di reazioni note, al fine di porre l'accento sui benefici di questo approccio metodologico.

Risulta fin da ora evidente la necessità di descrivere i principi base della flow-chemistry soffermandoci sugli aspetti più inerenti alla ricerca che ho condotto durante il mio dottorato.

L'impiego di microreattori a flusso continuo per scopi sintetici cominciò ad essere teorizzato già negli anni '60, ma questa tecnologia ha preso effettivamente piede negli anni 2000.[5]

In cosa consiste esattamente un microreattore a flusso continuo? Quali sono i vantaggi associati al suo impiego? Un reattore a flusso è un insieme di canali di diametro pari a 10-1000μm per un microreattore, 1-10mm per un mesoreattore, attraverso cui vengono fatte fluire le soluzioni contenenti i reattivi.[12] Utilizzare questa moderna metodologia ha dimostrato un'indubbia utilità alla comunità scientifica, fornendo una valida alternativa in ogni fase di esecuzione di un processo di sintesi, dall'ottimizzazione alla realizzazione (addizione dei reagenti, mixing, reazione chimica, work-up), comprese la separazione dei prodotti e la loro analisi. Esistono diversi materiali costituenti e diverse tipologie di reattori a flusso; seguirà una brevissima descrizione con un particolare focus per quel che riguarda i vantaggi da essi offerti al fine di introdurre e motivare lo studio applicativo che mi ha visto coinvolto. Diversi materiali sono utilizzabili per la costruzione dei reattori a seconda del tipo di reazione che deve essere eseguita: acciaio inossidabile, PDMS (polidimetilsilossano), vetro, quarzo, PTFE (teflon) sono solo alcuni esempi di materiali comunemente impiegati. I reattori a flusso possono anche essere abbinati a tecniche di monitoraggio in-line, quali spettroscopia UV/Vis o IR, NMR, spettrometria MS o LC/MS.

Esistono differenti tipologie di reattori. Oltre al riscaldamento o raffreddamento un reattore può essere sottoposto a interazioni fisiche quali sonicazione, radiazioni UV, micro-onde allo scopo di facilitare la reazione.

Reattori a bobina (coil reactors): Sono i più semplici reattori usati per chimica in flusso. Sono tubi o capillari in acciaio inossidabile o polimerici (PTFE, PEEK, etc.) il cui volume

interno può essere facilmente determinato come pure il tempo di residenza. Lunghezza e diametro interno sono infatti definiti, il materiale si sceglie in funzione dell'aggressività dei reattivi da usare, sono infine ideali per reazioni omogenee. Il loro vantaggio è la possibilità si sostituire i tubi con facilità, tali reattori sono flessibili e facilmente interconnettibili in caso di reazioni multi-steps.

Reattori Chip: Sono quelli utilizzati per reazioni altamente esotermiche al fine di operare in condizioni di sicurezza, ciò vale anche per quelle reazioni condotte a temperatura e/o pressione levatissime[13]. Vetro, quarzo, silicone sono sottoposti a tecniche di lavorazione per l'ottenimento dei reattori chip: litografia, sinterizzazione, stampa 3D. In tali sistemi il trasferimento di calore è elevatissimo, il volume interno ridotto consente di lavorare su piccola scala e per le stesse ragioni la fase di mixing è ottimale.

Reattori Packed-bed o Fixed-bed: Possiamo descrivere questi reattori semplicemente come tubi in acciaio inox o in vetro borosilicato riempiti con particelle solide di diversa forma e dimensione[14]. Le estremità sono delimitate da filtri che impediscono al materiale impaccato di fuoriuscire durante la reazione; in questo contesto si muove anche il fine di sintetizzare materiali funzionalizzati con molecole che conferiscono a essi attività catalitica al fine di modulare reazioni a flusso continuo. Oltre all'importanza nella scelta delle dimensioni del materiale impaccante, questi sistemi si caratterizzano per una bassa contropressione, un elevato loading di catalizzatore in proporzione al volume del reattore; un quasi-assente leaching del catalizzatore; un prolungato utilizzo nel tempo (recycling); un'elevata resa di reazione. Quel che solitamente si sfrutta di tali sistemi è la possibilità di condurre reazioni eterogenee in seguito all'immobilizzazione di reagenti o catalizzatori su di un supporto solido che è per l'appunto il materiale impaccante. Vedremo come questo passaggio risulti cruciale all'interno dei miei studi.

Il flusso dei fluidi all'interno di un microreattore può essere garantito in diversi modi, a seconda del materiale costituente il reattore e alle esigenze applicative.

Flusso capillare: sebbene consenta un preciso controllo della quantità di fluido attraverso il reattore[15], risulta poco diffuso a causa della ridotta portata di esercizio.

Flusso elettroosmotico (EOF): viene ottenuto applicando una differenza di potenziale alle estremità del reattore; se da una parte questo tipo di flusso ha il vantaggio di poter essere controllato con estrema precisione elettronicamente e di non utilizzare parti meccaniche in movimento, dall'altra richiede solventi polari, dipende dalla concentrazione del soluto e può generare reazioni elettrochimiche indesiderate.

Flusso idrodinamico: risulta il metodo può diffuso poiché facilmente effettuabile con semplici apparecchi come premi-siringa o pompe HPLC; garantisce un flusso principalmente di tipo laminare[16] in un ampio range di velocità, dai µl/min ai ml/min.

Di seguito saranno descritti brevemente i reali vantaggi che dovrebbero discriminare nella scelta tra batch e flow; essi sono derivanti principalmente dall'elevato rapporto superficie/volume e dalle piccole quantità di sostanze coinvolte in ogni momento della sintesi.

Mixing: Quando si eseguono reazioni in batch si ricorre ad agitazione meccanica per miscelare i reattivi con evidenti svantaggi dovuti al crearsi di moti convettivi turbolenti e caotici, che spesso decrescono rapidamente con l'allontanarsi dall'agitatore. In un microreattore il mixing è al quanto immediato (microsecondi) a causa delle ridotte dimensioni dei volumi interni e poiché il flusso laminare è predominante.[5]

Il trasferimento di Massa: Le piccole dimensioni facilitano anche il trasferimento di massa. Comparando un'estrazione liquido-liquido effettuata sia in batch che in flow si può vedere come il flusso laminare attraverso un'elevata superficie interfacciale consente tale beneficio.[17] Da queste premesse, risulterà un incremento della velocità di reazione e in taluni casi migliora anche la resa e la selettività.

Il controllo della temperatura: a determinare la variazione di temperatura in un reazione è cruciale l'area superficiale per unità di volume; i sistemi batch danno un ampio profilo di distribuzione di temperatura al loro interno,[18] facilitando la formazione di prodotti secondari indesiderati, mentre i microreattori consentono una rapida e precisa variazione di temperatura grazie all'elevato valore del rapporto superficie/volume e alle ridotte quantità di materia coinvolte.

Efficienza: Effettuare un processo in flow implica la possibilità di incrementare la quantità di prodotto ottenuto in un dato tempo, riducendo le quantità di sostanze di scarto; il miglioramento dei processi di trasferimento di massa e di calore, può consentire, infatti, di impiegare i reagenti in concentrazioni maggiori e di ridurre il quantitativo di catalizzatore: questo si traduce in una minor quantità di solvente e di scarti per unità di prodotto.

Solitamente, una delle problematiche che ricercatori e progettisti devono affrontare risiede nello scale-up del processo, ovvero nelle differenze che si riscontrano nel passaggio da una scala ridotta come quella di laboratorio ad una maggiore come quella di un impianto industriale: con l'impiego di sistemi di tipo microfluidico, le cui caratteristiche risiedono proprio nelle piccole dimensioni, questo passaggio viene evitato lasciando in funzione il

sistema per un tempo maggiore (*scale-on*) o facendo lavorare più unità in parallelo (*numbering-up*).[19]

2.3 Catalisi asimmetrica eterogenea e catalizzatori immobilizzati su matrice

La richiesta di molecole enantiomericamente pure da parte dell'industria farmaceutica ed agrochimica ha contribuito all' affermarsi della catalisi asimmetrica nelle ultime decadi.[20]
In tale ambito, considerando l'uso di catalizzatori che richiedono costi elevati e che devono essere successivamente smaltiti, è vantaggioso rivolgersi alla catalisi asimmetrica dal momento che i catalizzatori possono essere utilizzati in quantità minime rispetto ai reagenti. La potenza della catalisi asimmetrica consiste nel fatto che un catalizzatore garantisce cammini di reazione con un'energia di attivazione più bassa rispetto al processo non catalizzato.
Un catalizzatore chirale converte molecole achirali in composti enantiomericamente arricchiti o puri. Nel corso di ogni ciclo catalitico esso poi si rigenera rilasciando facilmente il prodotto (le sue interazioni con la molecola prodotta sono, infatti, di natura debole e quindi non covalente) e rientrando in circolo.
In particolare, la catalisi eterogenea si basa sull'immobilizzazione di efficaci leganti, di complessi metallo-legante, di organocatalizzatori o di enzimi su supporti solidi insolubili come materiali inorganici, polimeri organici, dendrimeri, membrane, ma anche liquidi ionici o altri sistemi bifasici.
Il catalizzatore in particolare può essere legato al supporto tramite uno spaziatore (spacer), oppure strettamente coordinato al supporto senza spaziatori, oppure infine inglobato direttamente nel polimero.[21]
L'ancoraggio di un catalizzatore ad una matrice inerte richiede la formazione di legami covalenti tra catalizzatore e supporto solido e può avvenire secondo diverse vie, tra cui spiccano:
a) L'introduzione di molecole di legante in maniera casuale lungo la catena polimerica, tramite modifica del polimero preformato;
b) L'incorporamento tramite co-polimerizzazione di molecole di legante all'interno della catena polimerica principale (approccio più comune a supporti di natura organica);[22]
c) L'ancoraggio del legante o del complesso di coordinazione tramite un linker o direttamente all'estremità di una molecola di polimero (supporto) (anche questo approccio è più comune a supporti di natura organica);
d) Una strategia di self-supporting in cui il polimero viene formato in situ mediante l'assemblamento di leganti (monomeri) e ioni metallici o organocatalizzatori e senza

bisogno di introdurre alcun supporto solido. In tale tipologia di sintesi il metallo assume, accanto alla classica funzione di centro catalitico della reazione, anche un ruolo strutturale in quanto elemento "connettore" delle unità monomeriche di legante.

Un'utile strategia per la funzionalizzazione di supporti è sicuramente quella fornita dalla ***"click chemistry"***[23]. Si tratta di un termine che è stato introdotto da K.B. Sharpless nel 2001 per descrivere le reazioni che sono ad alto rendimento, ampia portata, capaci di creare solo sottoprodotti che possono essere rimossi senza cromatografia, che sono stereospecifiche, semplici da eseguire e che possono avvenire in solventi facilmente rimovibili o solventi "green".

Diversi tipi di reazione sono stati identificati soddisfare tali criteri, reazioni termodinamicamente favorite che portano specificamente ad un prodotto, come la reazione di apertura nucleofila dell'anello di epossidi e aziridine, come la formazione di idrazoni ed eterocicli, reazioni di tipo carbonio-carbonio da legami multipli , come la formazione ossidativa di epossidi e le addizioni di Michael, e le reazioni di cicloaddizione azide-alchino.

Una ricca letteratura dimostra come si ricorra a queste strategie sintetiche per l'immobilizzazione di selettori e catalizzatori sulla superficie di supporti solidi[24].

A conferma di quel che abbiamo descritto fin ora, descriveremo un caso di sintesi e applicazione di nuovi materiali funzionalizzati, nell'ambito della chimica in flusso, al fine di dare una concreta visione dei potenziali utilizzi di tali substrati attivati.

La catalisi da prolina applicata alla reazione di condensazione aldolica: L'organocatalisi usa come catalizzatori piccole molecole organiche principalmente composte da carbonio, idrogeno e eteroatomi come ossigeno, azoto, zolfo e fosforo, in grado di aumentare la velocità ma anche la selettività delle reazioni.

Poiché la capacità catalitica deriva dalla struttura stessa della molecola, gli organocatalizzatori consentono di ottenere processi efficienti (sia per resa che stereoselettività) senza la presenza di ioni metallici: è quindi possibile evitare lunghi processi di purificazione e il costoso smaltimento dei loro residui, il che rende questo tipo di catalisi molto interessante anche dal punto di vista applicativo su scala industriale oltre che per la ricerca in laboratorio.

Generalmente, all'interno dell'organocatalisi, si distinguono dei sottogruppi, a seconda del modo di attivazione della specie catalitica (che si formi cioè un'iterazione covalente o non covalente catalizzatore-substrato) e della sua natura chimica (acido o base di Lewis o acido o base di Brønsted); nonostante questo, è importante porre l'accento come, e qui risiede un

ulteriore aspetto positivo degli organocatalizzatori, queste molecole agiscano spesso attraverso meccanismi sia di tipo covalente che non covalente, o che contengano al loro interno gruppi funzionali diversi (catalizzatori polifunzionali).

All'interno della catalisi asimmetrica ad opera di basi di Lewis, rientra l'amminocatalisi in cui ammine primarie e secondarie agiscono attraverso due possibili meccanismi: uno che sfrutta la formazione di uno ione **imminio** (specie più reattiva del corrispettivo carbonilico perché abbassa il livello energetico del LUMO del sistema) che facilita processi come le reazioni di cicloaddizione e di addizione nucleofilica, l'altro che prevede la formazione di un intermedio di tipo **enamminico** (formato per deprotonazione dello ione imminio, alza il livello energetico dell' HOMO), capace di reagire con vari elettrofili e di dare reazioni pericicliche. Questo tipo di reazioni ricalcano processi quali le aldolasi di tipo I (catalisi via enammina) e chetoacidi decarbossilasi (catalisi via ione imminio).

List, Lerner e Barbas[25] descrissero la semplicità d'uso di ammine secondarie chirali cicliche nel catalizzare efficacemente la reazione di funzionalizzazione di composti carbonilici. Essi riportarono che una quantità catalitica di L-prolina era in grado di promuovere la reazione aldolica diretta in maniera enantioselettiva tra un chetone, come ad esempio l'acetone, e una varietà di aldeidi.

Questo amminoacido quindi si può impiegare come efficiente organocatalizzatore per reazioni di sintesi asimmetrica. La prolina, inoltre, è una molecola chirale facilmente disponibile in entrambe le sue forme enantiomeriche e si presenta con una struttura bifunzionale, in cui il gruppo carbossilico e il gruppo amminico possono agire in maniera concertata. Inoltre la struttura ciclica dell'anello pirrolidinico e il gruppo amminico secondario (con una pKa maggiore rispetto agli altri amminoacidi) le conferiscono una particolare reattività, che le consente di poter formare una specie contenente uno ione imminio o un'enammina con composti carbonilici in maniera più efficiente di altri amminoacidi o di altre ammine cicliche come la piperidina[26]; anche il gruppo carbossilico partecipa attivamente al meccanismo di reazione, fungendo da co-catalizzatore come acido di Brønsted. Grazie a queste caratteristiche la prolina risulta capace di mimare le trasformazioni enzimatiche in modo efficiente ed altamente stereoselettivo.

Al fine di sfruttare le sue potenzialità catalitiche sono state sintetizzate molecole mimetiche della prolina che, pur mantenendo una struttura chimica di base simile, hanno dimostrato di migliorarne le prestazioni (di resa, regio- o stereoselettività) per una specifica reazione, o in particolari condizioni (come nel passaggio da solventi organici a solventi acquosi) o che sono risultate più stabili nel tempo; altri organocatalizzatori mimetici della prolina,

chimicamente progettati ad-hoc, sono stati utilizzati per funzionalizzare specifici supporti solidi, oppure hanno dimostrato di poter fornire una selettività (diastero- o enantioselettività) invertita rispetto ai precursori (attraverso l'aggiunta di gruppi ingombranti e/o l'inversione di un centro stereogenico), ampliando così il numero di prodotti di sintesi a disposizione dei chimici organici.

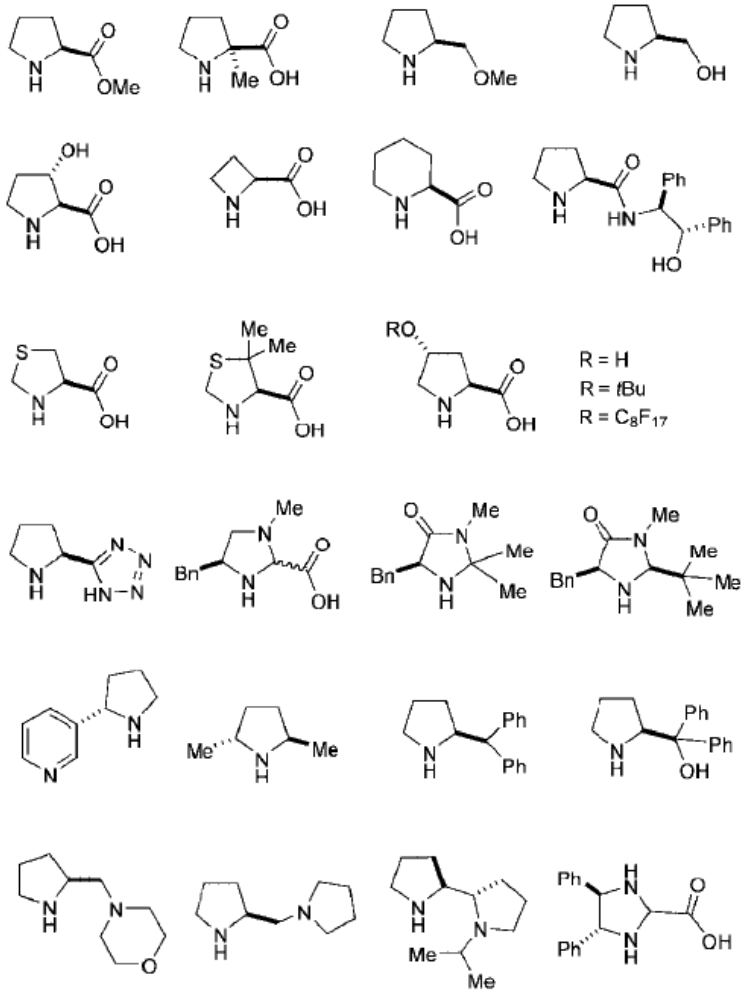

Figura 1 – Alcuni dei catalizzatori mimetici della prolina noti in letteratura

Nel vastissimo mondo dell'organocatalisi e nell'altrettanto vasto campo di applicabilità della stessa, ho concentrato i miei studi sulla prolina e su un mimetico della prolina per applicazioni in flusso continuo prendendo in esame in particolare la reazione di condensazione aldolica come caso applicativo.

La condensazione aldolica è una reazione in cui due molecole di un'aldeide o di un chetone, che abbiano almeno un atomo di idrogeno in posizione α al gruppo carbonilico (C=O), si combinano tra loro formando una β-idrossialdeide o un β-idrossichetone.

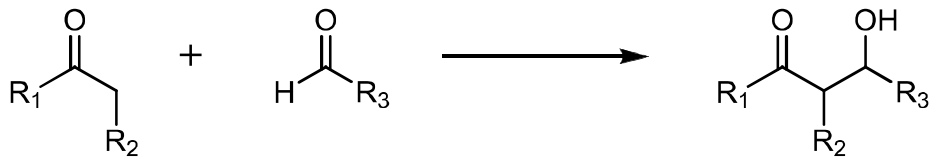

Figura 2 – Reazione di condensazione aldolica: schema generale

Il primo esempio di reazione di condensazione aldolica asimmetrica mediata da prolina fu condotto da Hajos–Parrish–Eder–Sauer–Wiechert nel 1971. Nonostante l'utilizzo di questa reazione nel corso dei decenni, il suo meccanismo è stato scarsamente investigato fino a poco tempo fa: molti meccanismi di reazione, compreso quello dei primi autori, sono stati proposti e successivamente esclusi[27] [28] [29], fino a giungere a quello suggerito da List, Lerner e Barbas (Figura 3), e successivamente confermato da Houk e collaboratori attraverso calcoli meccanicistici[30], che prevede la formazione di una specie enamminica in modo simile a quanto avviene con le aldolasi di tipo I.

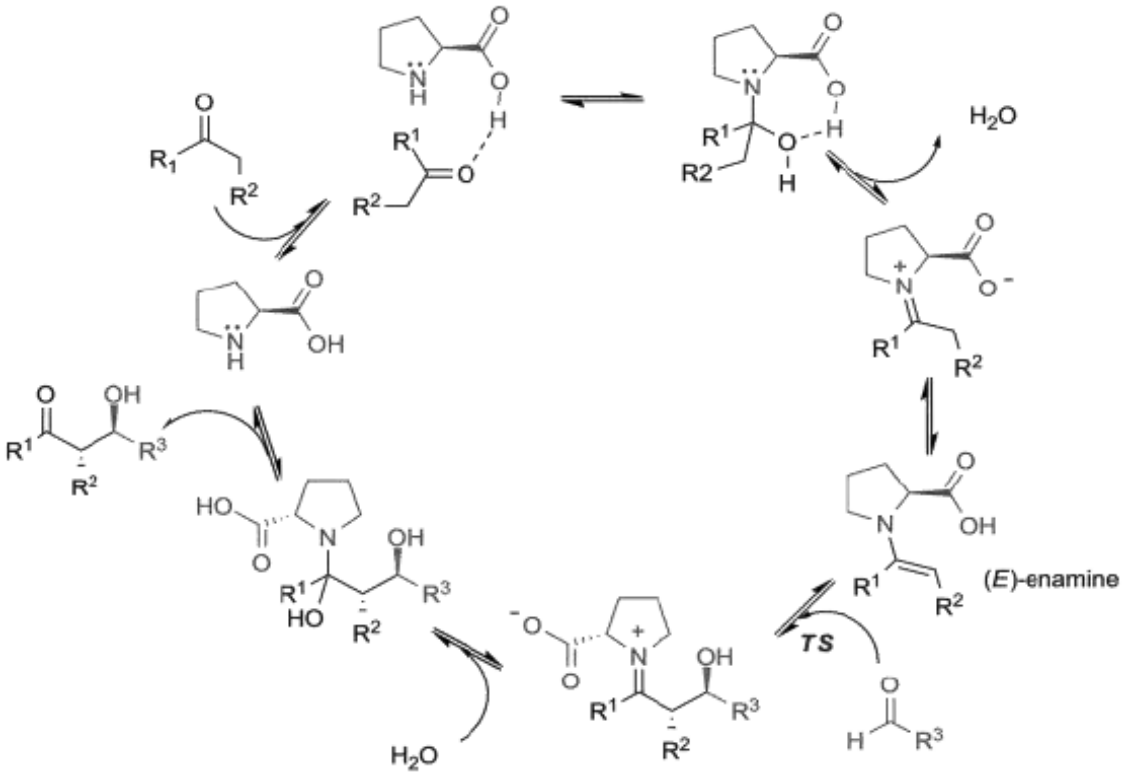

Figura 3 – Meccanismo catalitico mediato da L-Prolina per la reazione di condensazione aldolica fra un chetone e un'aldeide

Questo meccanismo prevede l'iniziale coordinazione, attraverso un legame ad idrogeno, di una molecola di chetone da parte del gruppo carbossilico della L-prolina e successivamente la formazione di un addotto prolina-chetone; attraverso l'eliminazione di una molecola di

acqua si ha poi la formazione di uno **ione imminio**, che risulta in equilibrio con la corrispettiva **enammina**. È proprio quest'ultima specie ad effettuare un attacco nucleofilo sull'aldeide (il cui processo di avvicinamento è coordinato dal legame ad idrogeno tra l'ossigeno del carbonile aldeidico e l'idrogeno del carbossile della prolina) e a generare lo stato di transizione nel quale si determina la stereoselettività della reazione. È opportuno evidenziare come diversi fattori contribuiscano all'elevata capacità stereoselettiva dell'organocatalizzatore in questo passaggio: nel passaggio da ione imminio ad enammina, l'(E)-enammina risulta favorita rispetto a quella a configurazione di tipo (Z) per ingombro sterico e, per lo stesso motivo, la conformazione **anti** risulta favorita rispetto a quella **syn** (Figura 4).

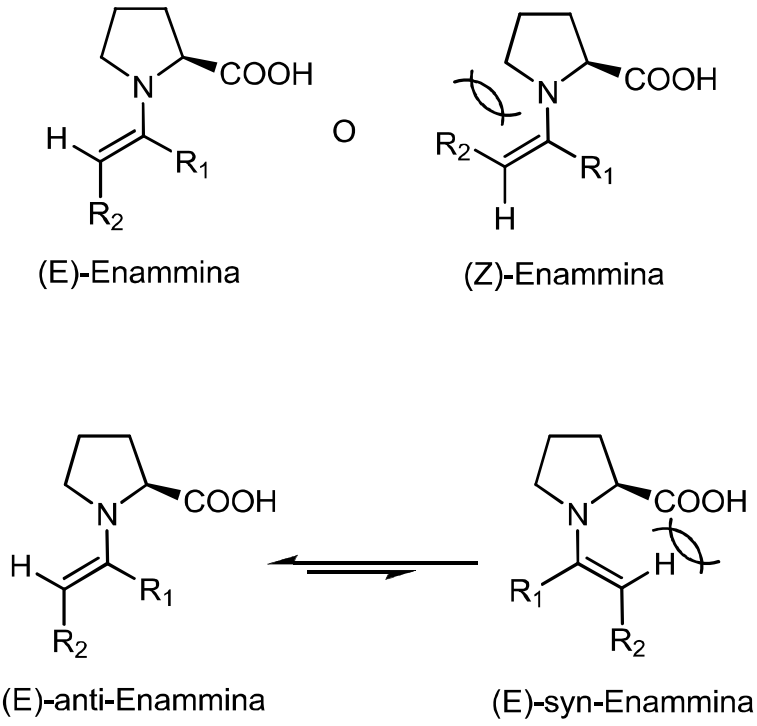

Figura 4 – Formazione dell'enammina in una specifica conformazione: (E)-anti-enammina

L'aldeide si avvicina quindi all'enammina per formare lo stato di transizione, coordinata dal gruppo carbossilico della L-prolina: essendo questo gruppo funzionale legato all'anello pirrolidinico su un carbonio asimmetrico, l'avvicinamento avverrà esclusivamente su una delle due facce dell'organocatalizzatore; anche per quanto riguarda l'aldeide entrante, l'attacco avverrà preferenzialmente su una delle due facce (quella *re*), così da disporre, nello stato di transizione, il suo sostituente in posizione equatoriale, minimizzando

l'interazione sterica (Figura 4). La geometria dello stato di transizione è il risultato di tutti questi fattori e porta quindi alla formazione preferenziale del diastereoisomero *anti* e ad un'elevata capacità di stereoinduzione da parte dell'organocatalizzatore.

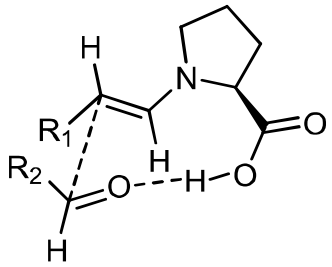

Figura 5 – Stato di transizione del processo catalitico

Il ciclo catalitico si chiude poi attraverso la reintroduzione di una molecola d'acqua, la successiva formazione del prodotto e il ripristino della molecola di L-prolina nel suo stato iniziale.

Un'alternativa a questo modello, proposta nel 2007 da Seebach,[31] prevede che il ruolo chiave nel meccanismo di reazione sia rivestito da una specie ossazolidinonica invece che dall'enammina (Figura 6).

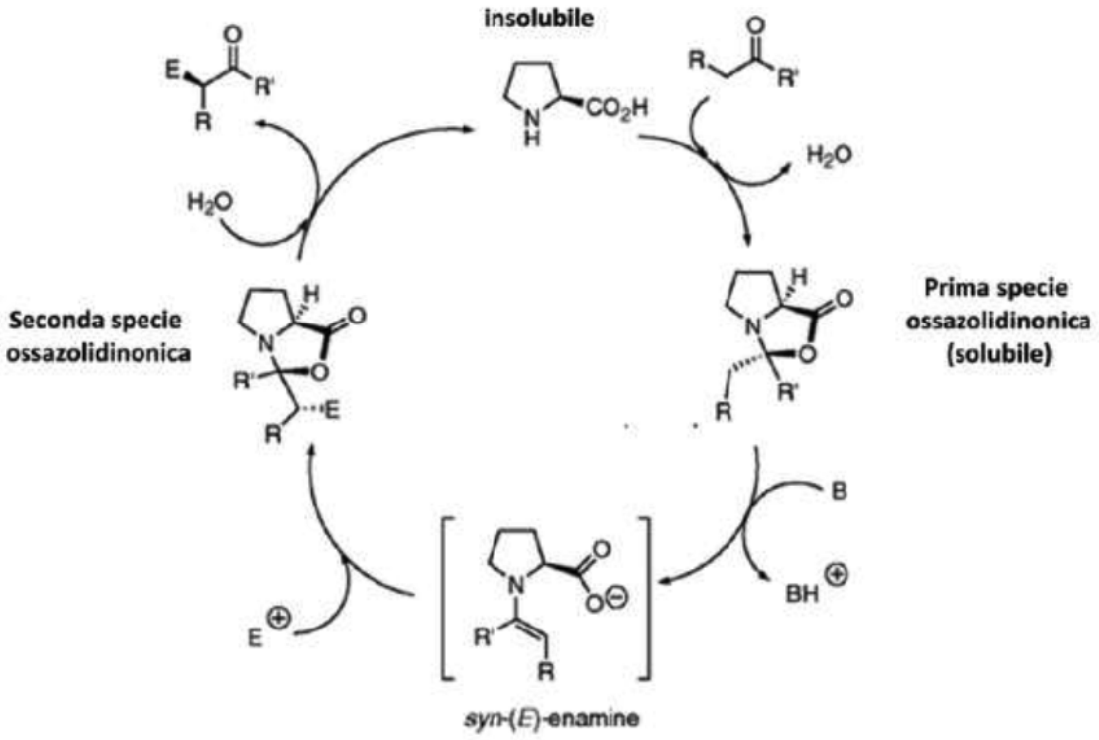

Figura 6 – Meccanismo di reazione proposto da Seebach nel 2007

Questo meccanismo di reazione, che si prevede avvenire in un solvente organico, ipotizza la formazione iniziale di un *ossazolidinone* tra la prolina e il composto carbonilico con l'eliminazione di una molecola d'acqua: questa nuova specie dovrebbe contribuire a portare la prolina (altrimenti scarsamente solubile) in soluzione. Questo passaggio è seguito dalla lenta trasformazione della specie ossazolidinonica in un intermedio *enammina carbossilato* attraverso un processo di β-eliminazione con una base esterna; successivamente è previsto che avvenga una trans-addizione al doppio legame dell'enammina indotta da un elettrofilo con la formazione di un *γ-lattone* (in questo passaggio si determina la stereoselettività della reazione).

Il ciclo catalitico si chiude quindi con il *cleavage* idrolitico dell'ossazolidinone (con la reintroduzione nel ciclo di una molecola d'acqua) che porta alla rigenerazione della molecola di prolina nel suo stato iniziale e alla formazione del prodotto. In questo modello l'attivazione intramolecolare dell'elettrofilo da parte dell'acido di Brønsted prevista nel modello di Houk-List, è rimpiazzata da un trasferimento protonico esterno da parte di un solvente protico o da parte della prolina; anche la base necessaria per la generazione dell'enammina carbossilato può essere di nuovo derivante o dal solvente o dalla prolina stessa. La formazione di una specie ossazolidinonica proposta da Seebach, era stata prevista anche da Houk e List, ma era stata indicata come una reazione parallela il cui prodotto era una specie indesiderata e soprattutto inattiva. L'esistenza della specie ossazolidinonica è stata ampiamente dimostrata da indagini spettroscopiche ma si dibatte sulla possibilità che questa sia l'intermedio chiave nel meccanismo di azione della prolina o se la catalisi proceda attraverso un meccanismo mediato da una specie enamminica.[32]

La reazione di condensazione aldolica può essere eseguita sia fra un chetone e un'aldeide (dove il chetone funge da donatore e l'aldeide da accettore), portando alla formazione di un β-idrossichetone, che fra due aldeidi (con la formazione di una β-idrossialdeide): in questo caso esistono esempi sia di reazioni *self-aldol* (dove si impiega la stessa aldeide sia come accettore che come donatore), sia di *cross-aldol* (fra aldeidi diverse).[33]

Infine, il principale processo secondario che può avvenire durante la reazione di condensazione aldolica, è la disidratazione del prodotto desiderato, con la formazione di un chetone (o un'aldeide) α,β-insaturo (Figura 7).

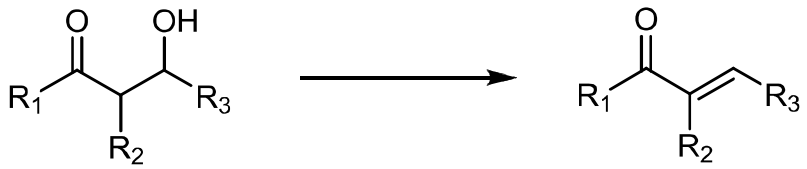

Figura 7 – Formazione del prodotto secondario di disidratazione

Un'altra problematica riguardante la reazione di condensazione aldolica è la disattivazione del catalizzatore attraverso la formazione irreversibile di una specie ossazolidinonica con aldeidi elettron-povere come la p-nitrobenzaldeide: la molecola di prolina può infatti formare una specie contenente uno ione imminio esattamente come fa nel corso del ciclo catalitico; in seguito ad una successiva reazione di decarbossilazione e ad un processo di cicloaddizione dipolare di un'ulteriore molecola di p-nitrobenzaldeide si può giungere alla disattivazione dell'organocatalizzatore (Figura 8). Si può ovviare a questo problema attraverso l'impiego di derivati della L-prolina incapaci di formare la specie ossazolidinonica con l'aldeide, come il derivato tetrazolico, che riesce a riprodurre gli ottimi valori di resa e stereoselettività del suo precursore risultando più stabile ed efficace nel tempo.[34]

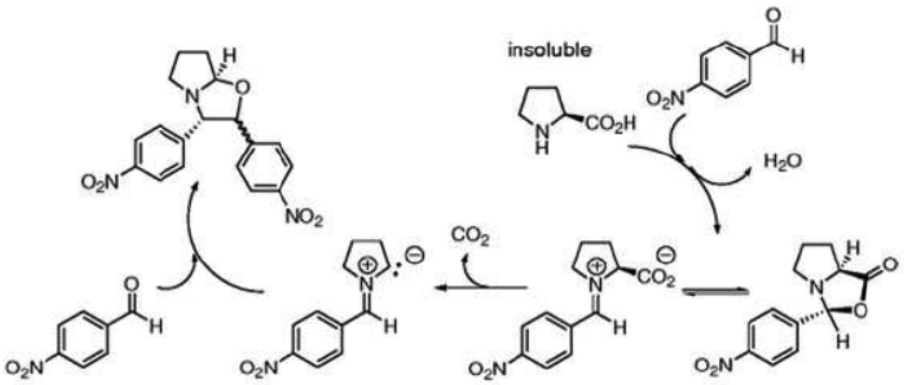

Figura 8 – Processo di disattivazione della L-Prolina con p-nitrobenzaldeide

Maggiori dettagli in merito all'utilizzo dell'organocatlizzatore prolina-like, il pirrolidiniltetrazolo immobilizzato su matrice silicea, sono stati discussi nell'articolo allegato dal titolo *"Silica-supported 5-(pyrrolidin-2-yl)tetrazole: development of organocatalytic processes from batch to continuous·flow conditions"*. Il supporto inerte selezionato, il gel di silice, è stato funzionalizzato con il 5-(pirrolidin-2-il)tetrazolo, il derivato tetrazolico della L-prolina, mediante reazione radicalica fra un alchene e un tiolo

(detta thiol-ene coupling, TEC), e successivamente usato per impaccare microreattori a colonna per esperimenti in flusso continuo condotti su reazioni di condensazione aldolica (e anche su reazioni di Mannich, di Michael, e di α-amminazione). L'utilizzo del supporto funzionalizzato rivolto a questa metodica di sintesi, si rivela ottimale confermando ottima stereoselezione, completa conversione, efficienza, e una stabilità nel tempo del materiale impaccato.

Thiol-ene coupling, TEC: il meccanismo prevede la formazione di un *sulfanil-radicale* mediante l'azione di un iniziatore, diverso a seconda che la reazione sia termica o fotoindotta. Si ha quindi il legame con la molecola di alchene secondo un andamento anti-Markovnikov con la conseguente formazione di una nuova specie radicalica al carbonio; avviene quindi uno step di propagazione in cui quest'ultima specie reagisce con un'ulteriore molecola di tiolo strappandole un radicale idrogeno: sia ha quindi la formazione del prodotto (un tio-etere) e la prosecuzione della reazione attraverso un nuovo ciclo radicalico (Figura 9).

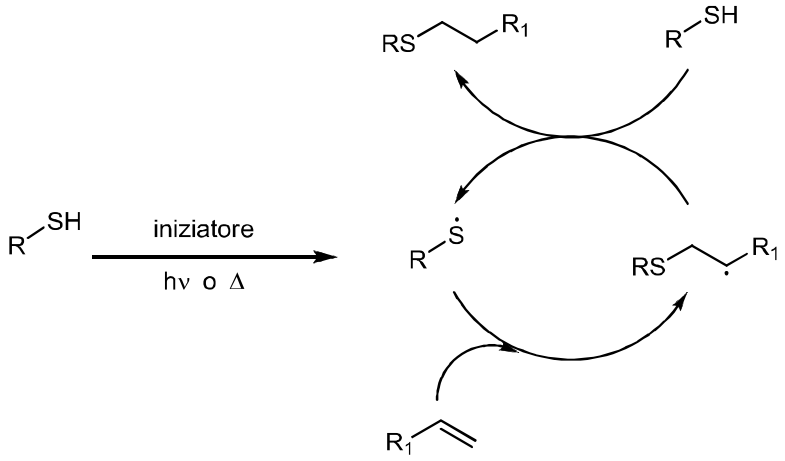

Figura 9 – Tiolene coupling: schema generale

É stata quindi progettata ed eseguita la sintesi del derivato della prolina funzionalizzato con un doppio legame e parallelamente è stata effettuata la reazione di derivatizzazione di particelle di silice con un gruppo tiolico, così da poter effettuare il *coupling*.

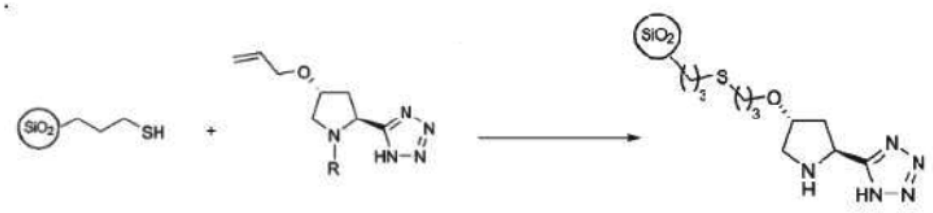

Figura 10 - Struttura del catalizzatore eterogeneo in seguito al coupling.

2.4 RPKA, un approccio cinetico e termodinatico per l'interpretazione di processi catalitici eterogenei in flusso continuo.

Un'applicazione basata sull'impiego di materiali funzionalizzati molto interessante è rappresentato da uno studio effettuato durante il mio dottorato e riguardante una matrice silicea funzionalizzata con organocatalizzatore ed impiegata per processi in flow. L'aspetto innovativo ed interessante è aver sfruttato questi microreattori a letto impaccato per studi di reaction-progress kinetic analysis, RPKA. Questa tecnica è stata combinata con metodi di cromatografia non lineare per interpretare in condizioni sinteticamente rilevanti, aspetti meccanicistici interessanti come la determinazione del rate-determining step di una reazione.[35]

Reaction-progress kinetic analysis, RPKA: Gli studi cinetici di una reazione organica sono da sempre un problema importante da risolvere; soprattutto in ambito farmaceutico è importantissimo conoscere l'ordine cinetico di una reazione in termini efficaci e non troppo complessi. In chimica , il reaction-progress kinetic analysis[36] appartiene un sottoinsieme di una vasta gamma di tecniche cinetiche utilizzate per determinare l'ordine di reazioni chimiche e per aiutare nella delucidazione dei meccanismi di reazione. Questa strategia è stata messa a punto dalla professoressa Donna Blackmond e da allora ha visto un uso sempre più diffuso. L'RPKA si basa sulla capacità di monitorare con precisione la conversione di reazione nel tempo *in situ*. Questo obiettivo può essere realizzato mediante una serie di tecniche, talune classificate come *differenziali* (controllo della velocità di reazione nel tempo), altre *integrali* (monitorano la quantità di substrato e/o prodotto nel tempo); una semplice manipolazione matematica (differenziazione o integrazione) permette l'interconversione dei dati ottenuti da uno delle due .

Solitamente le tecniche utilizzate sono spettroscopia NMR (una reazione avviene nel tubo e si può monitorare ad ogni istante); FT-IR *in situ* (per valutare la variazione di assorbanza tra reagenti e prodotti che si vengono a formare); UV-Vis *in situ*(misura la variazione di assorbanza nella regione del visibile); calorimetria (misura il cambiamento di entalpia durante la reazione).

Solitamente si fa uso di tue tecniche per monitorare lo sviluppo cinetico di una reazione al fine di validare l'andamento della frazione convertita nel tempo. Ad esempio, il monitoraggio FT-IR permette di plottare la concentrazione rispetto il tempo e la derivata fornisce la *velocità* di reazione. Parallelamente la calorimetria permette di plottare la velocità in funzione del tempo e l'integrale fornisce la *concentrazione del substrato*.

A questo punto questi dati possono essere convertiti in quel che si definisce *equazione grafica della velocità* e che plotta la velocità rispetto alla concentrazione. La concordanza tra due metodi di monitoraggio cinetico in situ, conferma la validità dell'equazione grafica della velocità, che correla la velocità alla concentrazione di reazione.
Solitamente si può descrivere la velocità di reazione in termini semplificati tramite forma *power law*[37] anche in casi in cui non ci siano sufficienti informazioni per correlare l'odine cinetico al meccanismo (nel caso di una reazione di condensazione aldolica tra acetone **1** e aldeide **2** per dare un aldolo **3** mediante catalisi da prolina **4**):

$$\text{rate} = k\,[\mathbf{1}]^x\,[\mathbf{2}]^y\,[\mathbf{4}]^z$$

L'obiettivo è trovare i valori di x, y e z; da notare che la concentrazione di **4** rimane invece costante durante il corso della reazione. La chiave dell'RPKA consiste nello sfruttare la stechiometria della reazione. Ad esempio, nel caso di una generica condensazione aldolica, per ciascuna molecola di chetone **1** consumata, una molecola di aldeide è anche consumata. Il parametro di interesse in questa analisi è la differenza tra le concentrazioni iniziali dei due substrati. Questo parametro è costante in ciascun esperimento che si effettua e prende il nome di eccesso, [*e*], che è misura della molarità; la quantità di [*e*] ci permette di correlare la concentrazione dei due ipotetici substrati dell'esempio precedente, ad ogni punto della reazione:

$$[e] = [\mathbf{1}]_0 - [\mathbf{2}]_0$$
$$[\mathbf{1}] = [e] + [\mathbf{2}]$$

[*e*][38] può essere grande, piccolo, positivo o negativo. Con una cinetica di pseudo-ordine-zero rispetto a **2,** [*e*] è >>[**1**]. Le migliori condizioni operative sono quando [*e*] è piccolo. Per sviluppare questi concetti tramite un'equazione grafica che sveli con semplicità la cinetica di reazione ci si avvale di due protocolli, gli esperimenti allo stesso eccesso e gli esperimenti ad eccesso differente.
Gli esperimenti eseguiti allo stesso eccesso rappresentano un protocollo semplice in cui si esegue per due volte una reazione in cui cambia la concentrazione iniziale dei due substrati ma tale che in entrambi i casi il valore di [*e*] sia identico. Solitamente le condizioni iniziali della reazione 2 sono identiche alle condizioni della reazione 1 quando la si considera al 50% della conversione. Operando questa scelta, le due reazioni mostrano da quel punto in

avanti la stessa [acetone] ad ogni [aldeide] durante il corso del loro avanzamento (teniamo come esempio sempre la reazione di condensazione aldolica).

Se i due esperimenti condotti allo stesso eccesso vengono plottati mettendo in grafico la velocità di reazione in funzione dell'[aldeide] verranno prodotte due curve per ciascuna reazione che andranno a sovrapporsi (overlay) nel range di [aldeide] comune indicando che la concentrazione di catalizzatore non varia nel corso della reazione: il che vuol dire che non siamo in situazioni di deattivazione o di product inhibition.

L'equazione della velocità scritta in forma power-low, può essere scritta normalizzando la velocità rispetto alla concentrazione di un substrato, ad esempio il substrato **2**:

$$normalized\ rate = rate\ /\ [\mathbf{1}]^x = k\,[\mathbf{2}]^y\,[\mathbf{4}]^z$$

In tal caso, eseguendo il protocollo degli esperimenti a differente eccesso, ne verrà che, in seguito a questa considerazione, i dati che andremo a mettere in grafico saranno caratterizzati da un' asse *y* del tipo *rate* / $[\mathbf{1}]^x$ e da un'asse *x* del tipo [**2**]. Considerando la definizione di eccesso, eseguendo due reazioni con differente valore di [*e*], vi sarà una diversa concentrazione di [**1**] per ogni concentrazione di [**2**].

Obiettivo di questo protocollo è quello di trovare un valore di *x* in seguito alle equazioni grafiche ottenute da i dati provenienti da esperimenti condotti a diversi eccesso:

asse *y*: $\frac{rate}{[\mathbf{1}]^x}$

asse *x*: [**2**]

Dai grafici derivanti da questi esperimenti possiamo stimare l'odine cinetico rispetto a ciascun substrato:

• Overlay (ipotizzando vi sia sovrapposizione tra le due curve) rivela che la reazione presenta una cinetico di primo ordine per il substrato normalizzato, $[\mathbf{1}]^x$ e x=1.

• La forma della curva rivela l' ordine di reazione del substrato plottato come variabile asse x; per esempio, quando le curve sovrapponendosi generano una linea retta, questo rivela che y = 1, il che significa che la reazione presenta una cinetica di primo ordine in [**2**].

La pendenza di questa retta è uguale a $k\cdot[\mathbf{4}]^z$. Ordini di reazione diversi possono essere valutati dalla forma della curva (concava per y < 1; convessa per y > 1).

Riassumendo, la tecnica RPKA, attraverso due esperimenti a differente eccesso ci fornisce l'ordine cinetico rispetto ai due substrati; attraverso due esperimenti con lo stesso eccesso ci informa sulla stabilità del catalizzatore durante la reazione.

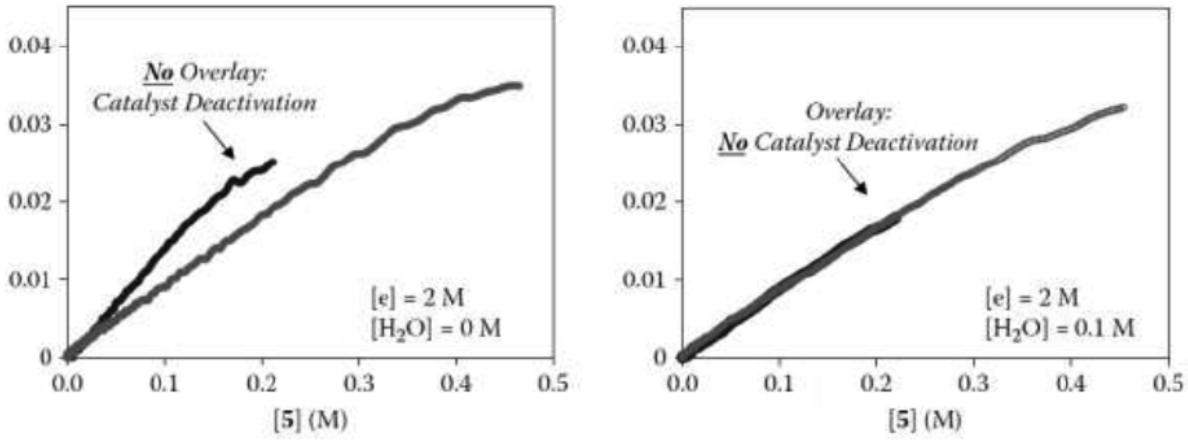

Questa tecnica semplice ed efficace è stata sfruttata e inserita all'interno di uno studio riguardante un'interessante indagine meccanicistica della reazione di condensazione aldolica eseguita in flusso continuo all'interno di microreattori a letto impaccato con silice funzionalizzata con catalizzatore prolina.

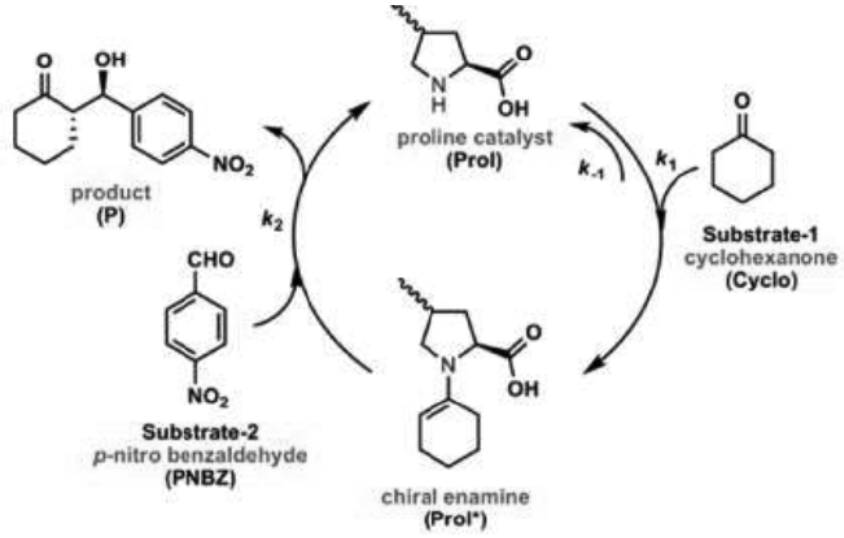

Per il meccanismo descritto per questa reazione possiamo scrivere, come già detto sopra, la più semplice equazione di velocità nella forma power-law:

$rate = k^*[\text{PNBZ}]^n\,[\text{Cyclo}]^m$

dove: $k^* = k\,[\text{Prol}]$

Nel nostro studio l'equazione cinetica può essere riscritta inglobando la concentrazione della prolina nella costante k^*.

Con i protocolli suggeriti dal metodo RPKA è stato individuato il valore di *m* ed *n* eseguendo degli esperimenti a flusso continuo piuttosto che in batch.

Per applicare il protocollo di esperimenti a differente eccesso, abbiamo considerato la velocità normalizzata rispetto alla concentrazione di cicloesanone.

normalized rate = *rate* / $[Cyclo]^m = k*[PNBZ]^n$

Si produce un grafico del profilo di reazione per ciascuno dei 3 esperimenti a differente eccesso (ne basterebbero 2) eseguiti in flusso continuo.

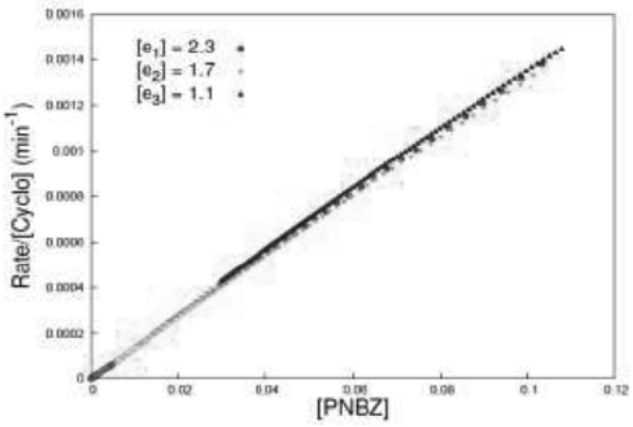

I profili di reazione ottenuti sono risultati essere tre rette sovrapponibili. Ciò impone dall'equazione matematica in alto, che l'ordine di reazione sia **1** rispetto all'aldeide; il fatto che si sovrappongano indica un ordine di reazione **1** anche per il cicloesanone, altrimenti avremmo avuto rette con pendenze differenti.

Gli esperimenti ad uguale eccesso hanno confermato la stabilità del catalizzatore nel corso della reazione condotta in flow. Due esperimenti con lo stesso valore di eccesso ma con diversi valori iniziali di concentrazione dei reattivi rappresentano la stessa reazione effettuata da due punti di partenza differenti. Riportando in grafico la velocità in funzione della concentrazione di aldeide per entrambi gli esperimenti, notiamo una sovrapposizione delle due rette che di ottengono per ciascuno di essi nel range di concentrazione di aldeide comune. Ciò vuol dire che la velocità non è significativamente influenzata dalle variazioni della concentrazione totale di catalizzatore all'interno del ciclo di reazione, cioè la concentrazione totale di catalizzatore è costante.

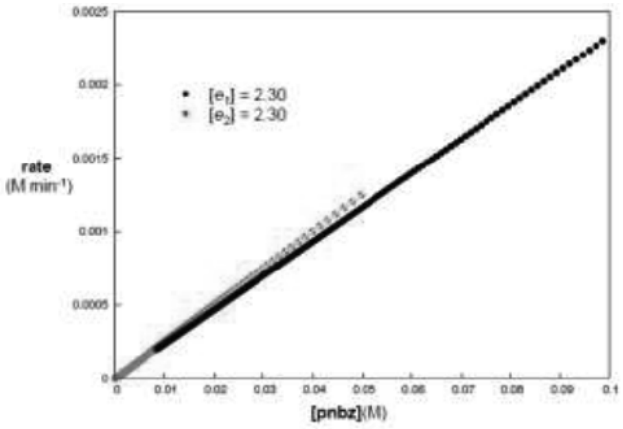

Individuato l'ordine cinetico mediante la tecnica RPKA, si dovrà confermare se l'ordine trovato è legato alle condizioni sperimentali adoperate e comprendere lo stadio lento della reazione di condensazione aldolica in condizioni di flusso continuo. Per far ciò dovremo prendere in considerazione l'equazione cinetica completa in stato stazionario che proviene dalla cinetica di Michaelis-Menten[39] che descrive l'andamento della velocità di una reazione catalizzata da enzimi, al variare della concentrazione del substrato e dell'enzima.

$$rate = \frac{k_1 k_2\,[\text{cycl}][\text{pnbz}][\text{prol}]_{tot}}{k_{-1} + k_1[\text{cycl}] + k_2[\text{pnbz}]}$$

La *prolina totale* tiene conto della concentrazione di enammina, cioè la specie attivata direttamente derivante dal catalizzatore, durante il ciclo catalitico.
Si valutano ora due possibili casi limite:

- se la formazione dell'enammina fosse lo stadio lento della reazione, la prolina totale sarebbe essenzialmente tutta in forma di prolina e con semplici elaborazioni matematiche si avrebbe:

  $$rate \propto k_1 k_2\,[\text{cycl}][\text{prol}]$$

  Ma questo si può escludere in quanto implicherebbe un ordine zero rispetto alla pnbz, e questo è in disaccordo con quello trovato sperimentalmente (RPKA).
- Nel caso in cui invece fosse l'addizione dell'aldeide ad essere lo stadio lento la prolina totale sarebbe essenzialmente tutta enammina e dopo semplici elaborazioni matematiche si avrebbe che la velocità risulta proporzionale a:

  $$rate \propto k_2\,[\text{pnbz}][\text{enam}] \propto k_2'[\text{pnbz}][\text{cycl}]$$

In base al meccanismo di reazione, la concentrazione di enammina, che non possiamo direttamente misurare, è proporzionale alla concentrazione del cicloesanone adsorbito sul letto catalitico e la concentrazione del cicloesanone assorbito è funzione della concentrazione di cicloesanone nella fase mobile. Queste informazioni potranno essere isolate mediante isoterma di adsorbimento per determinare la quantità di cicloesanone adsorbito sul letto catalitico in funzione del cicloesanone nella fase mobile. La correlazione trovata tra le due espressioni della velocità di reazione ci permette di dire che anche in fase eterogenea lo stadio lento della reazione è l'addizione dell'aldeide, confermando quanto trovato per questa reazione eseguita in condizioni classiche.

Per valutare l'andamento della quantità di cicloesanone adsorbito sul letto catalitico in funzione del cicloesanone nella fase mobile, si elabora l'isoterma di adsorbimento del cicloesanone sul letto catalitico a base di prolina attraverso diversi esperimenti a velocità di flusso costante mantenendo costante il rapporto tra le concentrazioni iniziali dei due substrati. All'aumentare della concentrazione iniziale di cicloesanone aumenta la concentrazione di cicloesanone adsorbito in maniera quasi lineare per un primo tratto per poi stabilizzarsi in un secondo tratto.

Quest'ultima situazione implica una saturazione cinetica per il cicloesanone, ovvero stiamo facendo entrare più cicloesanone di quanto il reattore lo riesca a trasformare, in un certo senso stiamo sprecando reattivo. Questo studio di interpretazione meccanicistica consente di ottimizzare il feed di reazione in condizioni di flusso continuo al fine di utilizzare la massima produttività del reattore.

Maggiori dettagli in merito a tale esempio di applicazione cinetico-termodinamica di materiale funzionalizzato nell'ambito della microreattoristica, sono stati discussi nell'articolo allegato dal titolo *"A Combined Kinetic and Thermodynamic Approach for the Interpretation of Continuous-Flow Heterogeneous Catalytic Processes"*.[35]

2.5 Analisi comparata di catalizzatori eterogenei al Palladio immobilizzati con ligandi fosfinici per reazioni di cross-coupling in flusso continuo: efficienza, durata, e studi di leaching.

Il palladio (Pd) è un raro e brillante metallo bianco-argenteo scoperto nel 1803; da allora, insieme al platino, rodio, rutenio e altri metalli viene sfruttato per le sue capacità catalitiche in chimica organica. Questi metalli di transizione catalizzano molte reazioni fondamentali quali cross-coupling, ossidazione e idrogenazione e quindi sono impegnati nella formazione di nuovi legami carbonio-carbonio e carbonio-eteroatomo e per tale motivo hanno avuto un impatto significativo sulla sintesi di prodotti farmaceutici e agrochimici.

Le reazioni di cross-coupling catalizzate dal palladio (Pd), sviluppate nel corso degli ultimi 30 anni, come Suzuky-Miyaura, Mizoroki, Heck, Negishi, Stille, Kumada e Sonogashira sono considerate tra le più potenti e versatili metodologie di sintesi largamente impiegate dall'industria per la formazione, in fase omogenea, di legami carbonio-carbonio (C-C).

Palladio su carbone (Pd/C) e palladio su allumina (Pd/Al_2O_3) sono stati i primi catalizzatori supportati a base di palladio disponibili in commercio e oggi sono frequentemente utilizzati sia nella ricerca che nell'industria della chimica fine. Un catalizzatore commerciale come il Pd/C ottimizzato per la reazione di Heck, di Suzuki-Miyaura e di Sonogashira può raggiungere valori elevati di **TON** (turnover number). Tuttavia il recupero del catalizzatore, specialmente nel casi di Pd/C risulta molto difficile.

Negli ultimi dieci anni, sono stati introdotti molti nuovi materiali catalitici a base di Pd ma la prima *review* completa sui catalizzatori solidi supportati al Pd per le reazioni di *cross-coupling*, apparve solo nel 2007,[40] seguita poi dalla presentazione dei risultati di Pd/C e palladio su silice (Pd/SiO_2).[41]

Purtroppo molti dei catalizzatori solidi sviluppati finora, sono in realtà omogenei, cioè si comportano come serbatoi, o "pre-catalizzatori"[42] delle specie catalitiche realmente attive in soluzione. Infatti, l'uso di "scavengers per Pd" sembra essere il metodo di scelta per risolvere il problema del leaching, cioè il distacco del Pd dal suo supporto.

La ricerca intensa nell'ottimizzazione della chimica del *cross-coupling* negli ultimi due decenni ha portato allo sviluppo di "condizioni di reazione *green*", nonché a numerosi sistemi di catalizzatori diversamente supportati al fine di poterli sfruttare per una catalisi eterogenea, più precisamente per reazioni in condizioni di flusso continuo, sulla premessa che il metallo attivo supportato sul solido può essere facilmente riutilizzato e il prodotto di reazione facilmente isolato dal catalizzatore che rimane intrappolato sul letto catalitico

piuttosto che inquinare la miscela di reazione. Tuttavia, nel caso del Palladio, è importante, come già accennato, il fenomeno del *leaching*.

Il problema del leaching e le reazioni di cross-coupling : numerosi catalizzatori al Pd immobilizzato sono stati impiegati sia in procedure batch che applicazioni in flusso continuo.[43] In un processo a flusso continuo il catalizzatore al Pd viene generalmente collocato in reattori a letto impaccato e la miscela di reazione viene condotta attraverso il reattore utilizzando un sistema di pompaggio adeguato.[44] Il materiale cataliticamente attivo rimane localizzato in una parte specifica del reattore durante il passaggio della miscela di reazione, e pertanto, la reazione e la separazione del catalizzatore dal feed di reazione (contenente il prodotto) si svolgono contemporaneamente. In questo modo, il riutilizzo del catalizzatore e il suo riciclaggio sono semplificati, infatti la fase di separazione/filtrazione del catalizzatore può essere evitata. Inoltre, piccole quantità della miscela di reazione sono in contatto simultaneamente con il letto catalitico che viene raggiunto dal feed di reazione, con conseguente aumento delle velocità di reazione e possibilità di avere alte conversioni estendendo i tempi di residenza.

Ma quando si esegue la chimica di *cross-coupling* in flusso continuo utilizzando microreattori a letto impaccato, accade che si riscontra una sostanziale quantità di palladio "dissolto" nella miscela in uscita dal reattore[45]. Il leaching del Pd non solo implica una disattivazione del letto catalitico ma anche un inquinamento del prodotto ottenuto. Tali reazioni possono dunque essere definite veramente eterogenee, o sono da considerarsi omogenee a causa del Pd passato in soluzione? Qual è la vera specie attiva responsabile della catalisi osservata?

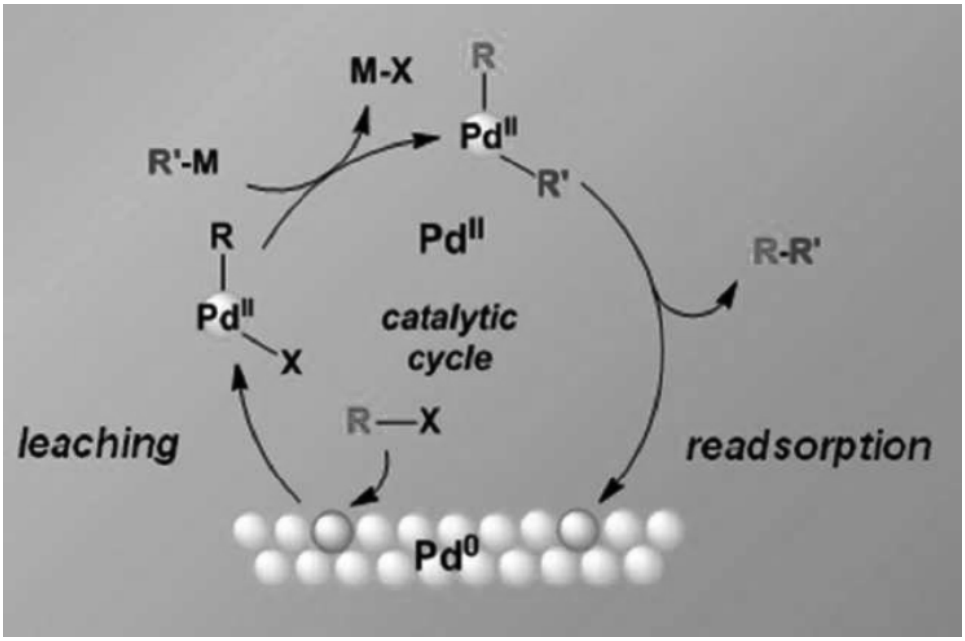

La reazione di Suzuki avviene tra un acido boronico e un alogenuro o triflato. Il meccanismo di reazione procede per **addizione ossidativa** di alogenuro vinilico o aromatica al Pd (0) che complessa e genera un intermedio Pd (II). Tale intermedio subisce una **transmetallazione** (così chiamata perché il nucleofilo R' viene trasferito dal metallo del reattivo organometallico al palladio e il controione [X = alogenuro o triflato] si muove nella direzione opposta) con l' alchenil boronato, da cui il prodotto viene espulso per **eliminazione riduttiva**, rigenerando il Pd (0).

La reazione di Heck avviene tra un arile o alogenuro di vinile (o triflato) e un alchene in presenza di Pd (0) per formare una nuovo alchene. Il meccanismo prevede l'**addizione ossidativa** dell' alogenuro, l' **inserimento** dell'olefina, e il rilascio del prodotto grazie a **β-eliminazione** di idruro. Una base quindi rigenera il Pd (0) via **eliminazione riduttiva** e chiude il ciclo catalitico.

In entrambi i casi di cross-coupling presi in esame, quando l'elettrofilo organico reagisce con il palladio per formare un complesso di Pd(II), la specie Pd(II) subisce un distacco dalla superficie del supporto solido e passa in soluzione durante il ciclo catalitico spiegando così il leaching, supportando l'idea che tale fenomeno avviene principalmente durante l'addizione ossidativa[46].

Al termine della reazione la concentrazione di Pd supportato può nuovamente aumentare a causa del ri-assorbimento (ri-precipitazione) del metallo sul supporto solido se si opera in batch.

Quando si sfrutta il flusso continuo la situazione può essere molto diversa poiché la dinamica del flusso impedisce la riprecipitazione del metallo, inoltre le specie solubilizzate di Pd(II) vengono coinvolte dal flusso laminare all'interno del reattore e perciò si verifica leaching.

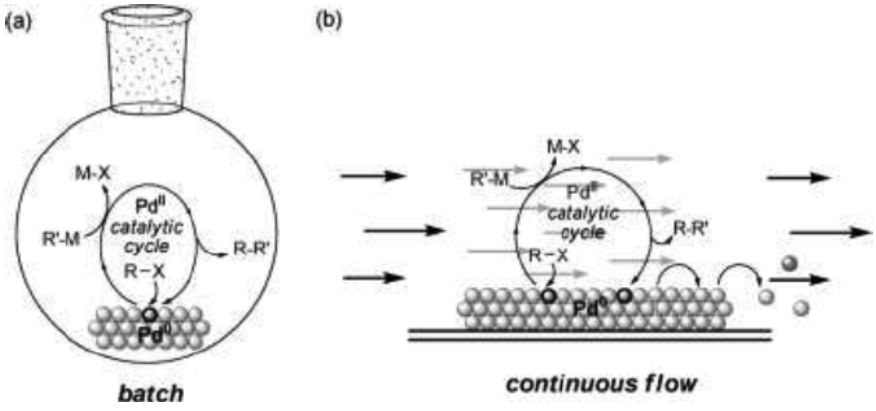

Figura 11 - leaching del Pd in condizioni batch(a) e flow (b)

Uno studio dettagliato relativamente al fenomeno del leaching di questo metallo nell'ambiente di reazione ha riguardato alcuni dei più comuni catalizzatori immobilizzati mediante ligandi arilfosfinici: Pd Tetrakis, FiberCat 1001, EnCat TPP30, e SiliaCat DPP - Pd. Questa indagine valuta efficienza, durata e leaching in condizioni di flusso continuo qualora sia considerato il Pd (diversamente) supportato per la catalisi di reazioni di Heck e Suzuki e può essere approfondito nell'articolo scientifico dal titolo: *"Benchmarking Immobilized Di- and Triarylphosphine Palladium Catalysts for Continuous-Flow Cross-Coupling Reactions: Efficiency, Durability, and Metal Leaching Studies"*[47].

2.6 Realizzazione di bioreattori a letto impaccato per lo studio di reazioni enzimatiche di formazione di legami C-C in flusso continuo: immobilizzazione di acetilacetoino sintasi

Anche nel caso di reazioni bio-catalizzate, che utilizzano enzimi, è possibile operare oltre che con un enzima libero (disperso nella miscela di reazione), con enzima immobilizzato su matrice.

In tal caso è possibile operare in flusso continuo, evitando di effettuare la rimozione degli enzimi dalla miscela di reazione.

Può essere conveniente procedere all'immobilizzazione degli enzimi perché:

1. Molti enzimi non sono sufficientemente stabili nelle condizioni operative e perdono la loro attività catalitica per ossidazione, denaturazione da parte del solvente o a causa di forze meccaniche.
2. Dal momento che gli enzimi sono molecole solubili in acqua, il loro uso ripetuto, che è necessario per l'economia del processo, è problematico a causa della difficoltà nel separarli da substrato e prodotto.
3. La produttività dei processi industriali è spesso bassa perché gli enzimi non tollerano alte concentrazioni di substrati (rapporto E:S troppo piccolo).

Le tecniche di immobilizzazione più diffuse possono essere raggruppate in quattro categorie

- adsorbimento, deposizione, formazione di legami ionici o comunque di legami non covalenti;
- legame covalente (particolarmente usato per enzimi isolati);
- intrappolamento in gel polimerici (particolarmente adatto per immobilizzare cellule intere), membrane o capsule;
- cross-linking di enzimi.

Più di recente, sono stati proposti materiali innovativi, quali silicati mesoporosi, idrogels, "polimeri intelligenti" (smart polymers), e metodi di intrappolamento non convenzionali, che, tuttavia, essendo ancora in via di sperimentazione, hanno avuto finora un'assai limitata applicabilità a livello industriale.

Un esempio di come l'efficiente immobilizzazione di enzimi abbia consentito l'applicazione di processi biocatalizzati in condizioni di flusso continuo è rappresentato dall'immobilizzazione di acetilacetoino sintasi (AAS) isolata da Bacillus licheniformis che è stato parzialmente purificato e immobilizzato su un supporto di silice. AAS è stato

impiegato nella sintesi enzimatica di una serie di α-idrossi-β-dichetoni ottenuti a partire da 1,2-dichetoni attraverso reazioni di homo- e cross-coupling. Ad eccezione di acetilacetoino, prodotto naturale di AAS, gli α-idrossi-β-dichetoni ottenuti sono tutti composti nuovi: si tratta di alcoli terziari, chirali e prochirali, che costituiscono degli interessanti building blocks per la sintesi asimmetrica.[48]

In natura, numerosi gruppi di reazioni biochimiche complesse sono catalizzate da enzimi; le acilazioni nucleofiliche sono catalizzate da enzimi transchetolasi in presenza del coenzima tiamina (**vitamina B1**):

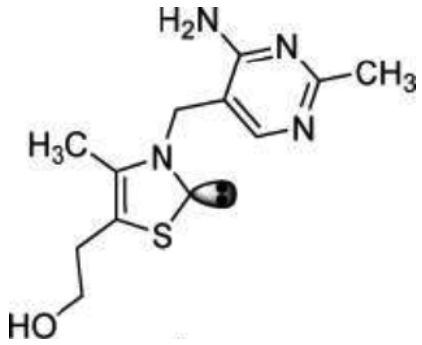

Questo coenzima, che si trova comunemente nel lievito di birra, catalizza reazioni chimiche, compiute in vivo, in maniera altamente selettiva.

Nel 1954, Mizuhara e il suo gruppo di ricerca scoprirono che la specie cataliticamente attiva del coenzima tiamina è un carbene nucleofilico.

Nel caso affrontato, l'acetilacetoino sintasi isolato da Bacillus licheniformis è un "nuovo" enzima tiamina-dipendente in grado di promuovere l'umpolung (inversione di polarità) di α-dichetoni con alta stereo-specificità. La tiamina è il cofattore che nella sua forma di ilide costituisce un carbene nucleofilo.

La catalisi enzimatica tiamina-dipendente è stata ripresa dall'organocatalisi per quella che è la chimica degli N-eterocicli carbeni (NHC). I carbeni che mimano il ruolo della tiamina sono per lo più il tiazolo e sali di triazolo.

Le caratterisciche degli NHC e quindi della tiamina, sono la neutralità e la presenza nella struttura di un atomo di carbonio bivalente con un sestetto elettronico[49].

Negli NHC, il doppietto di elettroni non condiviso degli eteroatomi (quale l'azoto) dona densità elettronica all'orbitale *p* vuoto del carbonio bivalente perpendicolare al piano dell'anello (stabilizzazione via π della reattività elettrofila del carbene):

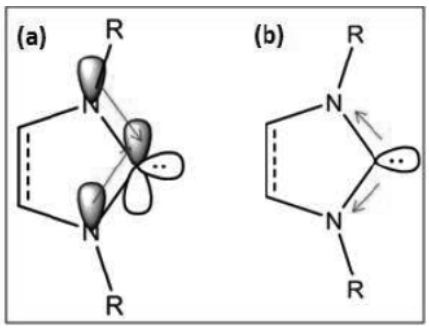

Figura 12 - Stabilizzazione degli N-eterocicli Carbeni per effetto push-pull degli eteroatomi.

L'elettronegatività degli eteroatomi adiacenti al carbonio C-2 ha un ruolo cruciale, portando una stabilità addizionale attraverso il legame σ che risulta in una reattività nucleofila più moderata[50].

Gli NHC si differenziano dalle classiche basi di Lewis perché mentre queste donano una coppia elettronica, gli NHC mostrano allo stesso tempo basicità σ e acidità π.[51], [52]

A monte di queste considerazioni si colloca questo lavoro che tratta α-dichetoni impiegati per la sintesi stereoselettiva e bio-catalizzata di α-idrossi-1,3-dichetoni usando l'enzima tiamina dipendente AAS:

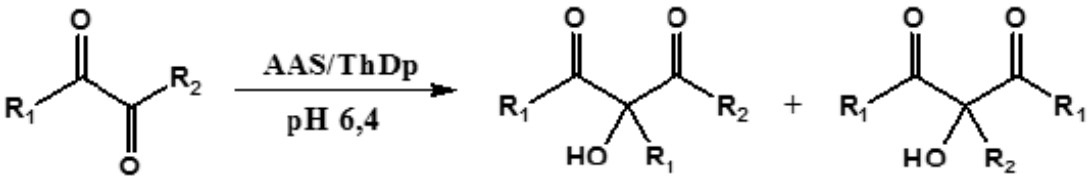

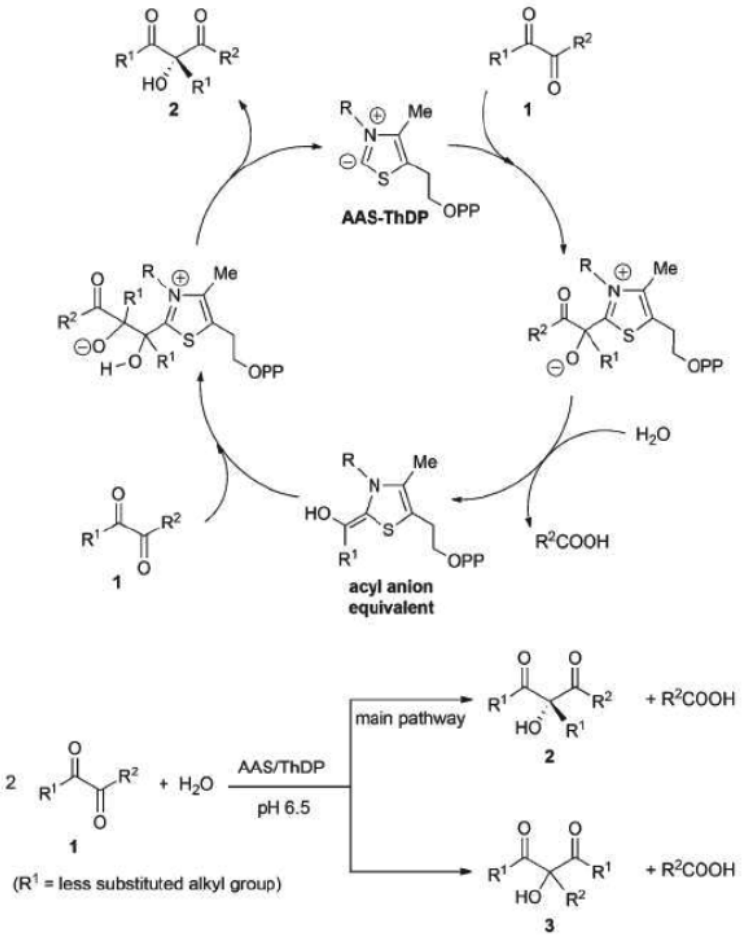

Figura 13 - Ciclo catalitico proposto per l'enzima tiamina dipendente

il carbene cataliticamente attivo procede con un meccanismo discusso da Breslow ad oggi ancora accettato.

Si presume che la molecola di sale di tiazolio sia deprotonata sulla sua posizione più acida, formando un tiazolin-2-ilidene; il successivo attacco nucleofilico sulla funzione carbonilica di un α-dichetone genera un addotto (vedi schema_). Un processo di eliminazione dell'acido carbossilico R^2COOH porta quindi alla formazione di una specie idrossienamminica (comunemente nota come intermedio di Breslow) in grado di agire chimicamente come un acil-anione.

È proprio quest'ultimo intermedio ad essere responsabile dell'attacco nucleofilo su un substrato elettrofilico come il gruppo carbonilico di una seconda molecola di α-dichetone: l'intermedio così ottenuto, attraverso un processo di riarrangiamento, elimina l'α-idrossi-chetone rigenerando contemporaneamente il catalizzatore nel suo stato iniziale. Come anticipato sopra, l'efficacia della catalisi eterogenea indotta da AAS è stata valutata sotto condizioni di flusso continuo in microreattori a letto impaccato.

È stato dimostrato che l'immobilizzazione covalente su silice porosa non solo garantisce resistenza meccanica al regime di flusso, ma contribuisce anche a conservare l'attività enzimatica nel tempo, permettendo il funzionamento a lungo termine (fino a 15 giorni) dei bioreattori preparati per impaccamento di tale materiale funzionalizzato. Maggiori dettagli sono stati discussi nella pubblicazione scientifica intitolata: "*Expanding the scope of enzymatic carboligation reactions in flow-mode: production of optically active tertiary alcohols with packed-bed micro-bioreactors"*

2.7 Separazione di oligonucleotidi di sintesi mediante tecnica cromatografica mixed-mode basata sull'utilizzo di una fase stazionaria innovativa a fase inversa e a scambio anionico debole.

Un utilizzo scientificamente rilevante di un materiale poroso funzionalizzato è l'impiego per realizzare fasi stazionarie per separazioni cromatografiche.

L'ottenimento di un particolare prodotto comporta molto spesso lo sviluppo di un metodo di purificazione che permetta di ottenere la molecola con parametri definiti e un profilo di purezza adeguato. Dietro la necessità di sviluppare e ottimizzare interi processi di purificazione, si giustifica l'impiego di metodiche di progettazione e sintesi di materiale funzionalizzato atto a costituire le fasi stazionarie più adatte a ogni specifica applicazione.

In particolare, prenderemo in esame la cromatografia liquida mixed-mode che è usata sempre di frequente per la purificazione di biomolecole, come peptidi e proteine. In molti casi infatti mostra migliori valori di selettività e di conseguenza migliora l'efficienza di purificazione in confronto con i metodi classici. Tali vantaggi sono essenzialmente merito di fasi stazionarie "multi-funzionali" che generano più di una forma d'interazione con gli analiti essendo progettate come fasi copolimeriche con meccanismo idrofobico e di scambio ionico che si combinano.

Nello studio che presentiamo, la fase stazionaria investigata, è frutto di una progettazione pregressa del gruppo di ricerca guidato dal Professor Michael Lämmerhofer.[53] Il carattere mixed-mode di tale fase stazionaria si basa su una fase inversa e su uno scambio anionico come modalità di interazione con l'analita. Come si può vedere in figura_, essa consiste in un selettore organico immobilizzato su gel di silice porosa (100 o 200 Å) a sua volta funzionalizzata con dei tioli. Il sito dove avviene lo scambio anionico debole si colloca nello strato più esterno della fase stazionaria idrofoba resa tale poichè la superficie idrofilica della silice è stata inizialmente rivestita con spacer apolari responsabili di una separazione a fase inversa.[54]

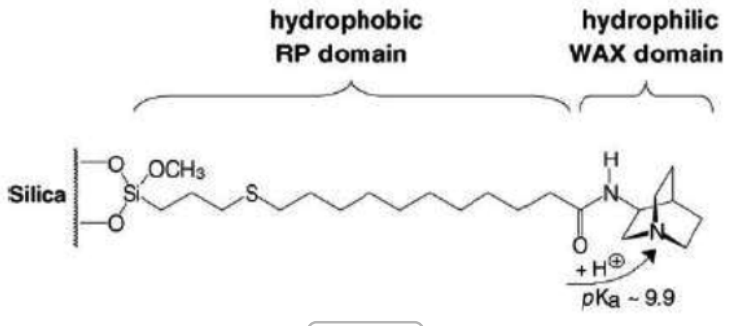

Nel presente studio, il comportamento cromatografico mixe-mode, fase inversa e debole scambio anionico (RP/WAX), è stato sfruttato per la separazione di oligonucleotidi di sintesi.

Da un punto di vista chimico un oligonucleotide è un oligomero di un acido nucleico (deossiribunucleico, DNA o ribonucleico, RNA). Esso consiste in una successione ordinata testa-coda di nucleotidi contentenenti un fosfato e un nucleside ossia uno zucchero e una base azotata.

La loro sintesi serve per un'infinità di scopi, dallo studio delle proprietà dei farmaci, all'analisi del genoma, alla realizzazione di strutture supramolecolari.[55]

Gli oligonucleotidi vengono sintetizzati usando un sintetizzatore di DNA programmabile, dove ciascun ciclo di reazione da come risultato l'aggiunta di una singola base di DNA. Una catena di basi di DNA può essere costruita grazie alla ripetizione di diversi cicli di sintesi fino ad ottenere la lunghezza desiderata. Sequenze fallimentari di oligonucleotidi o altre impurezze possono essere generate sia durante il processo di sintesi che durante il processo di post-sintesi. È raccomandabile che gli olignucleotidi siano purificati mediante cartucce a fase inversa, HPLC o PAGE al fine di avere un elevato grado di purezza per applicazioni biologiche e farmacologiche.[56]

La fase stazionaria mixed-mode mostra una grande flessibilità nello sviluppo di un metodo per separare/purificare oligonucleotidi. È stato messo a punto un metodo di eluizione in gradiente, esplorando parametri differenti quali il pH del tampone, la concentrazione di buffer, e il modificatore organico per trovare condizioni ottimali di eluizione. In comparazione con colonea a fase inversa e a scambio ionico, separazione e selettività risultano migliorate per una serie di oligonucleotidi lunghi 20-23 paia di basi. Gli oligonucleotidi scelti, posseggono alto grado di similitudine, con la stessa sequenza ma differenti per avere 1,2 o 3 unità di differenza, oppure con lo stesso numero di unità ma differenti per una singola base, SNP (single nucleotide polymorphisms). La risoluzione dipende dalla posizione del polimorfismo fra nucleotidi, con una diminuzione nell'ordine: SNP all'estremo 3' > SNP nel mezzo > SNP all'estremo 5'. Per quanto riguarda il tipo di basi che sono state scambiate, la selettività (e quindi la risoluzione) cala nell'ordine: C / G > A / G ~ G / T > A / C ~ C / T > A / T. Scegliendo una fase stazionaria con silice a porosità maggiore, da 100 a 200 Å, si riscontra un vantaggio dovuto all'aumento dell'area superficiale che permettono condizioni di eluizione più blande.

Maggiori dettagli in merito alle potenzialità di questa innovativa fase stazionaria applicata alla separazione di oligonucleotidi di sintesi si possono ritrovare nella pubblicazione dal titolo: *"Synthetic oligonucleotide separations by mixed-modereversed-phase/weak anion-exchange liquid chromatography"*.

2.8 Un nuovo metodo per investigare l'intrusione dell'acqua all'interno di strutture idrofobiche attraverso condizioni dinamiche

Dopo aver accennato all'importanza di valutare la bagnabilità di un solido, verrà illustrata in breve una procedura innovativa per stimare la bagnatura di un mezzo poroso funzionalizzato.

L'equazione fondamentale per valutare le caratteristiche di pori cilindrici[44] è l'equazione di Young-Laplace modificata opportunamente, denominata anche equazione di Washburn,[45] che stabilisce la relazione tra la pressione applicata *P* (pressione capillare di Laplace) e il d_p (diametro dei pori):

$$P = -4\gamma/d_p \cos\theta$$

dove γ è la tensione superficiale del liquido non-wetting e θ è l'angolo di contatto del sistema liquido - superficie - aria (per una situazione si non bagnabilità, $\theta > 90°$ e questo spiega il segno meno nell'equazione del Washburn). Per quanto riguarda l'angolo di contatto θ sono stati segnalati per l'acqua su superfici idrofobe valori come 93° (nel caso di gel di silice funzionalizzata), o 126° (per la silice commerciale idrofoba legata a catene C18). Questa variabilità induce ad osservare che, in particolare quando si considerano le superfici di supporti idrofilici, la porosimetria dell'acqua dovrebbe dare informazioni molto più dettagliate sulla struttura e le proprietà della superficie considerata.

In questo studio, si illustra attraverso un metodo *tracer-pulse*, una nuova tecnica per studiare l'intrusione di acqua in solidi porosi idrofobi in condizioni dinamiche. Come primo esempio di applicazioni, si è preso in esame alcuni tipi di silice porosa resa idrofoba in seguito a funzionalizzazione con gruppi alchilici e perfluoro-alchilici, che sono comunemente usati per realizzare fasi stazionarie nella cromatografia liquida: la silice porosa modificata chimicamente è un materiale particolarmente adatto per questo tipo di indagine.

Lo scopo di questo lavoro è, da un lato, mostrare che questo metodo promette di fornire informazioni sul comportamento dinamico d'acqua rispetto interfacce idrofobe e, dall'altro, contribuire alla ricerca del comportamento cromatografico di adsorbenti in fase inversa utilizzati con fasi acquose[46,47].

Quattro colonne cromatografiche sono state impiegate in questo studio: due colonne in fase inversa (C8 e C18 a base silicea); due colonne impaccate con perfluoroesiletilsilossano e

pentafluorofenilpropilsilossano legati su silice (rispettivamente abbreviate come PFH- e PFP-).
Secondo la tecnica tracer-pulse, quando la fase mobile è composta da un solo componente (diciamo A), si ha che il volume vuoto della colonna, V_0, è dato dal volume di ritenzione, V_A*, di un tracciante rilevabile di tale componente:

$$V_0 = V_A^*$$

Il volume di acqua contenuto in ciascuna colonna è funzione della pressione applicata e ci dice il grado di bagnabilità del solido in acqua. Tale volume è determinabile misurando tramite spettrometro di massa il tempo di ritenzione del D_2O iniettato. Implicitamente si presume che il liquido A bagna completamente il solido. Nel caso in cui questo non avviene, il "reale" volume del liquido nella colonna dovrebbe differire dal volume vuoto. In particolare, se il liquido non sarà in grado di penetrare nei pori del materiale adsorbente, il volume effettivo sarà corrisponde al volume interstiziale dei pori. Riscrivendo la precedente equazione nel caso sia l'acqua il liquido intercalante, si ha:

$$V_{H_2O} = V^*_{D_2O}$$

dove $V^*_{D_2O}$ è il volume di ritenzione dell'acqua deuterata e V_{H_2O} è il volume "reale" dell'acqua nella colonna. Per un materiale idrofobo, V_{H_2O} non necessariamente corrisponde a V_0.
Tuttavia, poiché la penetrazione nei pori di un liquido "non-wetting" può essere forzata dall'azione di una pressione esterna, la dipendenza del volume effettivo V_{H_2O}, quando viene applicata una pressione esterna, può essere intesa come la stima del grado di bagnabilità del materiale poroso da parte dell'acqua.
Il calo di pressione di un fluido che scorre attraverso il letto impaccato di una colonna cromatografica dipende in modo complesso da vari fattori, tra cui la portata, la viscosità della fase mobile, la lunghezza e il raggio della colonna, la porosità interstiziale (indicato anche come esterna o interparticellare), e le dimensioni delle particelle. Ipotizzando un impaccamento omogeneno della colonna, si può approssimare che la pressione diminuisce linearmente dall'ingresso e all'uscita della colonna stessa (poiché si risente della pressione atmosferica). L'acqua all'interno è sottoposta a diverse pressioni e può penetrare nei pori del solido a diversi livelli. Per minimizzare questo effetto, la velocità di flusso è stata

impostata a 20 µlmin^{-1} per rendere la contropressione proveniente dal flusso dell'acqua attraverso il letto impaccato trascurabile. La contropressione (costante) è stata invece generata utilizzando una serie di riduttori posti in coda alla colonna.

Come è stato detto, i limiti entro i quali il volume effettivo dovrebbe variare sono date dal volume interstiziale della colonna Ve, se l'acqua è totalmente escluso dai pori della fase solida, e V_0, se penetrazione dell'acqua nei pori è completa. Dal momento che è generalmente ritenuto che la picnometria fornisce la migliore stima migliore del volume occupato, questo valore è stato preso come V_0.

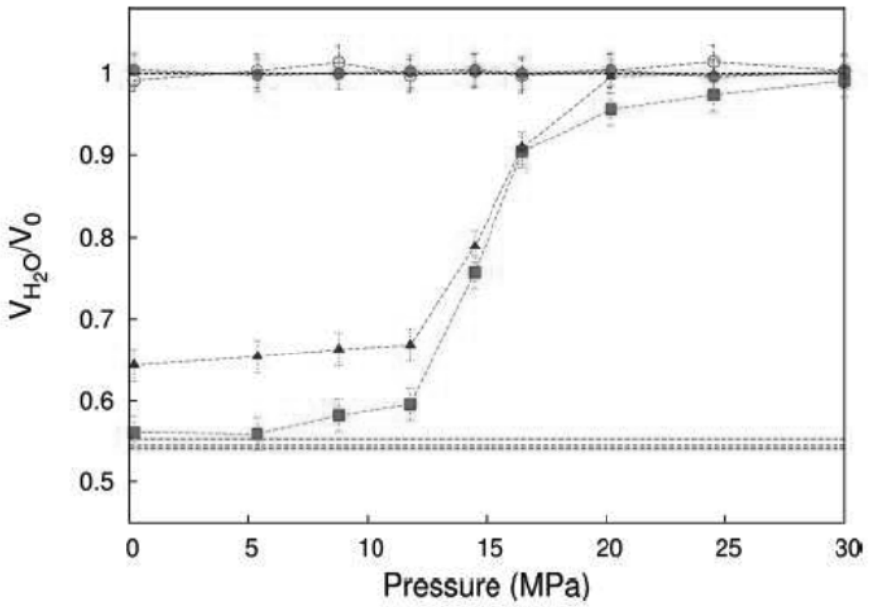

Figura 14 - Le curve rappresentano la dipendenza del volume normalizzato dell'acqua contenuta nella colonna rispetto la pressione applicata . La retta $VH_2O / V_0 = 1$ rappresenta la condizione di bagnatura totale. Le rette colorate tratteggiate nella parte inferiore della sono i volumi interstiziali normalizzati per le quattro colonne . La linea con i quadri rossi: C18 su silice; la linea con i triangoli verdi: PFH su silice ; la linea con i cerchi blu vuoti: C8 su silice ; la linea con cerchi fucsia: PFP su silice.

La figura 14 mostra la dipendenza del volume effettivo dalla pressione applicata. Prima di avviare la parte sperimentale, tutte le colonne sono state accuratamente condizionate con acqua.

La linea orizzontale nella parte superiore della figura rappresenta la condizione $V_{H_2O} = V_0$ (cioè, la situazione di bagnatura totale). Le linee nella parte inferiore del grafico

corrispondono invece ai volumi interstiziali normalizzati (cioè , la frazione di volume vuoto occupata dai pori interstiziali) delle quattro colonne. I volumi interstiziali sono stati determinatati grazie alla cromatografia di esclusione a fase inversa (ISEC= Tramite una serie di iniezioni di molecole a peso molecolare noto sono state effettuate delle misure per determinare la porosità delle colonne. Mettendo in grafico il volume di ritenzione delle molecole iniettate, contro il loro peso molecolare, si ottiene un grafico da cui è possibile estrapolare, considerando un PM pari a zero, il volume esterno (Ve) delle particelle porose. La porosità esterna della colonna (ε) è determinata dal rapporto tra Ve e $V_{colonna}$. Dalla differenza tra l'hold-up volume e il volume esterno si può determinare il volume interno (Vi). Da questo parametro è possibile poi calcolare il valore di porosità interna (ε_i)).

È importante osservare il diverso comportamento mostrato dall'acqua sulle quattro tipologie di materiale adsorbente. In particolare, due tendenze differenti possono essere riscontrate considerando le linee in Figura 14. La colonna C18- e quella PFH- (quadrati rossi e triangoli verde, rispettivamente) presentano un andamento analogo a forma di ***S***. I volumi effettivi misurati per gli altri due adsorbenti (C8- e PFP -, rispettivamente cerchi blu e cerchi fucsia vuoti) praticamente non dipendono dalla pressione applicata e, con una approssimazione accettabile, corrispondono all'hold-up volume. C18- e PFH- sono infatti materiali più idrofobici e la loro dimensione dei pori è comparabile. D'altra parte, la colonna di tipo C8-, che è meno idrofoba rispetto a quella C18- ma comunque altamente idrofobica, ha pori di 30 nm di diametro, cioè , circa tre volte più grandi di quelli di C18-; l'equazione per il calcolo della bagnabilità (vedi sopra) mostra che la bagnatura è fortemente influenzata dalla dimensione dei pori. In conclusione, il volume di acqua contenuto in ciascuna colonna, come risultato della pressione applicata, riflette il grado di bagnabilità del supporto solido ad opera dell'acqua. Tale volume è misurabile grazie ad uno spettrometro di massa in funzione del tempo di ritenzione del D_2O iniettato. Le informazioni ottenute spiegano il comportamento ritentivo di ciascun materiale rendendo il metodo proposto un promettente strumento per la caratterizzazione di materiali porosi in condizioni dinamiche.

2.9 Caratterizzazione geometrica di fasi stazionarie perflorurate impiegate in cromatografia liquida ad alta prestazione.

La modificazione chimica di un supporto poroso attraverso ligandi organici modifica la geometria del supporto stesso e influenza di un meccanismo di separazione nel caso questa fase solida sia impiegata per realizzare colonne cromatografiche. Dopo la derivatizzazione del supporto, i ligandi organici legati occupano certo volume all'interno dello spazio dei pori.

Nello studio presentato, sono stati considerati materiali a base di silice alchil-perfluorurata, impiegati come fasi stazionarie. In HPLC, tali materiali, hanno mostrato una specifica affinità verso composti contenenti fluoro (questa proprietà, denominata fluorophilicity o fluorous-affinity, nasce da forti interazioni non covalenti tra porzioni di ligandi altamente fluorurati) e una bassissima polarità.

Su questo tipo di fasi solide, i normali composti organici presentano una scarsa ritenzione mentre quelli fluorurati risultano più trattenuti, grazie alla contemporanea natura lipofobica e idrofobica delle catene fluorurate; inoltre, nel processo separativo, è proprio il numero di atomi di fluoro a fare da discriminante: miscele, anche complesse, di analiti chimicamente simili, ma a diverso contenuto di atomi di fluoro possono essere separati su colonne fluorurate. Inoltre questi materiali florurati risultano immiscibili anche con i più comuni solventi organici inrapporto alla loro bassissima polarità.

In questo lavoro, viene proposto uno studio volto a caratterizzare le caratteristiche geometriche di una fase stazionaria a base di gel di silice funzionalizzato con catene lineari perfluoroesilpropiliche, combinando le informazioni ottenute da analisi LTNA (low twmperature nitrogen adsorption) e analisi elementare con quelle provenienti da diversi tipi di misure cromatografiche, tra cui tracer-pulse (TP) e cromatografia inversa ad esclusione (ISEC). Queste informazioni possono aiutare la comprensione dei meccanismi di ritenzione su fasi stazionarie alchil-perfluorurate.

I parametri fondamentali di questi materiali florurati sono la superficie esposta e la dimensione media dei pori. In genere esse vengono dedotte attraverso la misura delle isoterme di adsorbimento. Queste curve rappresentano la massa di gas N_2 adsorbito sulla matrice porosa in funzione della pressione di equilibrio del vapore circostante (tipicamente il gas N_2 si trova alla temperatura dell'azoto liquido). L'iniezione in colonna di dosi successive di N_2 fino al raggiungimento della pressione di saturazione consente di determinare l'isoterma di adsorbimento, detta LTNA isotherm o BET plot che riporta la

quantità di gas adsorbito per unità di massa del solido adsorbente, la teoria BET ipotizza che le molecole adsorbite si trovano nello strato più alto sono in equilibrio dinamico con il vapore. Questo significa che dove la superficie è coperta con solo uno strato di adsorbato, questo sarà in equilibrio con il vapore; dove, invece, sono presenti più strati, solo lo strato esterno sarà in equilibrio. Dato che l'equilibrio è dinamico, la posizione dei siti superficiali coperti da uno o più strati può variare ma il numero di molecole in ogni strato rimarrà costante.

L'azoto totale (adsorbimento e desorbimento) misurato dall' isoterma per il gel di silice perfluorurato è rappresentato nella parte principale della figura seguente:.

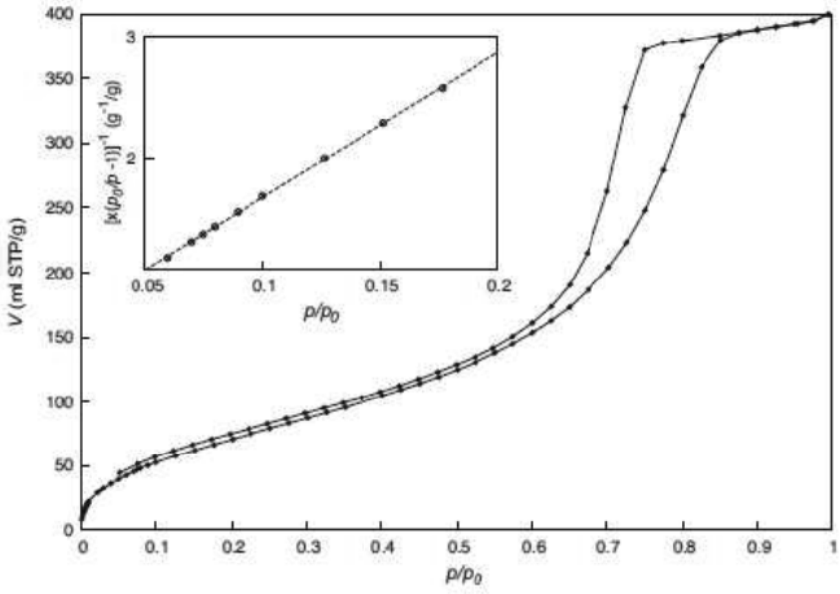

Secondo la classificazione IUPAC, l'isoterma appartiene al tipo IV. Il plateau della parte superiore corrispondente al riempimento completo dei pori.

Per stimare la densità di bonding si è ricorsi all'analisi elementare stimando il loading della porzione florurata rispetto alla silice bare. Il volume interstiziale dei pori è stato valutato mediante tecnica cromatografica ISEC iniettando il polistirene a massa molecolare nota. Il volume vuoto invece sì è determinato per picnometria.

Tali tecniche già sfruttate e descritte nel corso di studi precedenti, hanno evidenziato alcune importanti caratteristiche: in particolare, è stato dimostrato che, in condizioni cromatografiche le tipiche catene alchiliche perfluorurate assumono una disposizione compatta. L'altro aspetto importante è legato alla scarsa bagnabilità di questi mezzi ad opera dell'acqua. L'approccio proposto di studiare il comportamento di bagnatura di questa fase stazionaria in acqua, sulla base di tecniche cromatografiche tracer pulse (vedi paragrafo 2.7) sfruttando con acqua come fase mobile e ossido di deuterio come tracciante marcato, sembra essere molto promettente per indagare problemi di bagnabilità correlati

alla fase stazionaria: senza una contropressione di almeno 200 bar, il volume dei pori delle particelle impaccate non è completamente accessibile alle molecole di acqua. Pertanto, la superficie disponibile per l'adsorbimento in queste condizioni è significativamente inferiore al valore teorico, con ripercussioni importanti per l'efficienza cromatografica.

3 **Bibliografia**

[1] J. Y. Ying, C. P. Mehnert, M. S. Wong, *Angew. Chem. Int. Ed.* **1999**, *11*, 56–77.

[2] T. Carofiglio, M. Maggini, E. Menna, P. Salice, S. Silvestrini, **2012**, *30*, 37-39

[3] B. Lee, Y. Kim, H. Lee, Y. Jongheop, *Microporous Mesoporous Mater.* **2001**, *50*, 77–90.

[4] N. End, K. Schöning, *Top. Curr. Chem.* **2004**, *242*, 241–271.

[5] K. Jähnisch, V. Hessel, H. Löwe, M. Baerns, *Angew. Chemie Int. Ed. Ed.* **2004**, 406–446.

[6] F. Gritti, G. Guiochon, **2003**, *1010*, 153–176.

[7] A. J. GREGG, *J. Catal.* **1967**, *314*, 313–314.

[8] J. Sandoval, *J Chromatogr A.* **1999**, *13*, 375–381.

[9] K. S. W. Sing, **2004**, *241*, 3–7.

[10] E. Byström, *Porous Polymeric Materials for Chromatography Synthesis , Functionalization and Characterization,* KBC tryckeriet, Umeå University Umeå, Sweden, **2009**.

[11] L. C. Di Geoffrey A. Ozin, André C. Arsenault, *Nanochemistry: A Chemical Approach to Nanomaterials*, **2009**.

[12] A. Rencurosi, *Chim. Ind.* **2011**, 98–101.

[13] P. Watts, C. Wiles, *Chem. Commun* **2007**.

[14] W. Liu, *Chem. Eng. Sci.* **2007**, *62*, 3502–3512.

[15] N. Nikbin, P. Watts, *Org. Process Res. Dev.* **2004**, 2003–2005.

[16] C. R. N. J. Branebjerg, J. P. Krog, in *San Diego, USA, 1996*, **1996**, p. 441.

[17] K. Mawatari, Y. Kazoe, A. Aota, T. Tsukahara, K. Sato, T. Kitamori, *J. Flow Chem.* **2011**, 3–12.

[18] W. S. T. Schwalbe, V. Autze, M. Hohmann, *Org. Process Res. Dev.* **2004**, *8*, 440.

[19] T. Schwalbe, D. Kadzimirsz, G. Jas, *QSAR Comb. Sci.* **2005**, *24*, 758.

[20] E. E. N. Jacobsen, A. Pfaltz, H. Yamamoto, D. A. Evans, J. S. Johnson, **1999**.

[21] M. Leadbeater, Nicholas E.; Marco, *Chem. Rev.* **2002**, *102*, 0009–2665.

[22] L. Xing, J. H. Xie, Y. S. Chen, L. X. Wang, Q. L. Zhoua, *Adv. Synth. Catal.* **2008**, *350*, 1013–1016.

[23] H. C. Kolb, M. G. Finn, K. B. Sharpless, *Angew. Chem. Int. Ed.* **2001**, *40*, 2004-2021.

[24] W. H. Binder, R. Sachsenhofer, *Macromol. Rapid Commun.* **2007**, 15–54.

[25] B. List, R. A. Lerner, C. F. B. Iii, N. Torrey, P. Road, L. Jolla, R. V December, *J. Am. Chem. Soc.* **2000**, *122*, 2395–2396.

[26] P. W. Hickmott, *Tetrahedron* **1982**, *38*, 1975–2050.

[27] C. P. C Agami, F Meynier, C Puchot, J Guilhem, *Tetrahedron* **1984**.

[28] C Agami, *Bull. Soc. Chim. Fr.* **1987**, *3*, 499.

[29] D. Rajagopal, M. S. Moni, S. Subramanian, and S. Swaminathan, *Tetrahedron: Asymmetry* **1999**, *6*, 1997–2000.

[30] S. Bahmanyar, K. N. Houk, V. Uni, L. Angeles, R. V July, *J. Am. Chem. Soc.* **2001**, *17*, 12911–12912.

[31] D. Seebach, A. K. Beck, D. M. Badine, M. Limbach, A. Eschenmoser, A. M. Treasurywala, R. Hobi, *Helv. Chim. Acta* **2007**, *90*, 425–471.

[32] R. R. Torres, *Stereoselective Organocatalysis: Bond Formation Methodologies and Activation Modes*, **2013**.

[33] A. B. Northrup, I. K. Mangion, F. Hettche, D. W. C. Macmillan, *Angew.Chem.Int.Ed* **2004**, 2152–2154.

[34] S. V. L. A. J. A. Cobb, D. M. Shaw, D. A. Longbottom, J. B. Gold, *Org. Biomol. Chem.* **2005**, *3*, 84–96.

[35] O. Bortolini, A. Cavazzini, P. P. Giovannini, R. Greco, N. Marchetti, A. Massi, L. Pasti, *Chem. - A Eur. J.* **2013**, *19,* 7802-7808.

[36] N. Zotova, S. P. Mathew, H. Iwamura, D. G. Blackmond, in *Process Chem. Pharm. Ind. Vol. 2 Challenges an Ever Chang. Clim.*, **2008**, 455–464.

[37] J. S. Mathew, M. Klussmann, H. Iwamura, F. Valera, A. Futran, E. a C. Emanuelsson, D. G. Blackmond, *J. Org. Chem.* **2006**, *71*, 4711–4722.

[38] D. G. Blackmond, *Angew. Chemie - Int. Ed.* **2005**, *44*, 4302–4320.

[39] R. S. G. Kenneth A. Johnson, *Biochemistry* **2011**, *50*, 8264–8269.

[40] J. L. L. Yin, *Chem. Rev.* **2007**, *107*, 133–173.

[41] V. Polshettiwar, C. Len, A. Fihri, *Coord. Chem. Rev.* **2009**, *253*, 2599.

[42] M. B. A. Biffis, M. Zecca, *Eur. J. Inorg. Chem.* **2001**, 1131.

[43] S. L. B. T. Noël, *Chem. Soc. Rev.* **2011**, *40*.

[44] L. MUtton, C. G. Frost, *Green Chem.* **2010**, *12*, 1687–1703.

[45] D. Cantillo, C. O. Kappe, *ChemCatChem* **2014**, *6*, 3286–3305.

[46] M. Pagliaro, V. Pandarus, R. Ciriminna, F. Bland, P. Demma Car, *Chem- CatChem* **2012**, *4*, 432 –445.

[47] R. Greco, W. Goessler, D. Cantillo, C. O. Kappe, *ACS Catal.* **2015**, *5*, 1303–1312

[48] Y. Monguchi, T. Takahashi, Y. Iida, Y. Fujiwara, Y. Inagaki, T. Maegawa, H. Sajiki, *Synlett* **2008**, 2291–2294.

[49] D. Enders, O. Niemeier, A. Henseler, *Chem. Rev.* **2007**, *107*, 5606–5655.

[50] H. Y. S Saito, K Hatanaka, *Tetrahedron* **2001**, *57*, 875.

[51] E. . Philips, A. Chan, K. Scheidt, *Anal. Chim. Acta.* **2009**, *42*, 55–66.

[52] T. . Biju, N. . Kuhul, F. Glorious, *Acc. Chem. Res.* **2011**, *44*, 1182–1195.

[53] M. Lämmerhofer, M. Richter, J. Wu, R. Nogueira, W. Bicker, W. Lindner, *J Sep Sci.* **2008**, *31*, 2572–2588.

[54] R. Nogueira, M. Lämmerhofer, W. Lindner, *J. Chromatogr. A* **2005**, *1089*, 158–169.

[55] F. Rigo, Y. Hua, A. R. Krainer, C. F. Bennett, *J. Cell Biol.* **2012**, *199*, 21–5.

[56] R. R. Deshmukh, T. N. Warner, F. Hutchison, M. Murphy, W. E. Leitch, P. De Leon, G. S. Srivatsa, D. L. Cole, Y. S. Sanghvi, *J. Chromatogr. A* **2000**, *890*, 179–192.

Green Chemistry

Dynamic Article Links

Cite this: *Green Chem.*, 2012, **14**, 992

www.rsc.org/greenchem

PAPER

Silica-supported 5-(pyrrolidin-2-yl)tetrazole: development of organocatalytic processes from batch to continuous-flow conditions†

Olga Bortolini,[a] Lorenzo Caciolli,[a] Alberto Cavazzini,*[b] Valentina Costa,[b] Roberto Greco,[b] Alessandro Massi*[a] and Luisa Pasti[b]

Received 27th December 2011, Accepted 19th January 2012
DOI: 10.1039/c2gc16673a

5-(Pyrrolidin-2-yl)tetrazole functionalized silica prepared by photoinduced thiol–ene coupling is packed into a short stainless steel column. The resulting packed-bed microreactor is conveniently heated to perform environmentally benign continuous-flow aldol reactions with good stereoselectivities, complete conversion efficiencies, and long term stability of the packing material.

Introduction

In the context of a growing competition in which time, cost, and sustainability issues of the synthesis play an increasingly important role even at a research stage, chemical efficiency has become one of the leading concepts for chemists working in both industry and academia. Key criteria include intrinsic (yield, (stereo)selectivity, atom economy) and extrinsic (time, waste, equipment, environment, safety) factors of the synthetic process.[1] Hence, the booming field of asymmetric organocatalysis is opening, on the one hand, new and unique opportunities towards efficient and highly stereoselective metal-free catalytic syntheses.[2] On the other hand, microreactor technology is offering safe, environmentally benign, and high-throughput processes typically intensified by a fast postreaction phase (workup and purification) and direct scalability.[3] Very recently, we have embarked on a research program aimed at preparing and testing organocatalytic packed-bed microreactors[4] to prove the potential benefits arising from the combination of the above synthetic methodology and production technology.[5] Currently, this program is being developed on the basis of the following general thread: (i) heterogenization of a successful asymmetric organocatalyst on silica and optimization of its performance (yield and stereoselectivity) under batch conditions; (ii) preparation of the corresponding packed-bed microreactor and preliminary testing in continuous-flow regime; (iii) development of a suitable in-line analysis method and final optimization of the continuous-flow process based on kinetic and thermodynamic characterization thereof. It is worth noting that while a (limited) number of notable examples of asymmetric syntheses in continuous-flow have been reported,[6] only a few studies have dealt with the use of immobilized organocatalysts.[7] Indeed, peculiar benefits of heterogeneous organocatalysis in conjunction with microreactor technology are the absence of metal leaching (a problematic issue especially in pharmaceutical applications), the enhanced resistance of supports to mechanical degradation, and the potential long-term usage of (micro)reactors that is highly desirable for complex and costly immobilized catalysts. As a matter of fact, the main limitation encountered in our first investigation[4] on the proline-catalyzed continuous-flow aldol reaction of cyclohexanone with *p*-nitro benzaldehyde was the progressive loss of catalytic activity of the packing material **1** (Fig. 1). Deactivation of immobilized proline **1** occurred through irreversible decarboxylation[8] after 24 h on stream at room temperature and was greatly accelerated by increasing the process temperature. Herein, we report on the synthesis and catalytic activity under batch conditions of immobilized proline mimetics, namely heterogeneous prolyl amide **2**,[9] sulfonamide **3**,[10] and pyrrolidinyl tetrazole **4**,[11] which are not prone to the above deactivation pathway and thus are expected to provide organocatalytic packed-bed

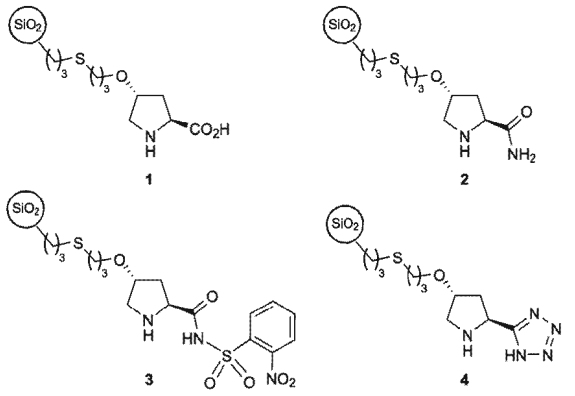

Fig. 1 Silica-immobilized proline and proline-like organocatalysts **1**–**4**.

[a]*Dipartimento di Chimica, Laboratorio di Chimica Organica, Università di Ferrara, Via L. Borsari 46, I-44121 Ferrara, Italy. E-mail: alessandro.massi@unife.it; Fax: +39 0532 455183; Tel: +39 0532 455183*
[b]*Dipartimento di Chimica, Laboratorio di Chimica Analitica, Università di Ferrara, Italy. E-mail: alberto.cavazzini@unife.it; Fax: +39 0532 455133; Tel: +39 0532 455133*

†Electronic supplementary information (ESI) available: Copies of ^{1}H and ^{13}C NMR spectra for new compounds, FT-IR spectra of silicas **2**–**4**, chiral HPLC chromatograms. See DOI: 10.1039/c2gc16673a

microreactors with improved stability and, eventually, better reaction profiles.[9–11] Preliminary results on the continuous-flow aldol reaction promoted by the best performing silica-supported 5-(pyrrolidin-2-yl)tetrazole catalyst **4** are finally presented.

Results and discussion

The thermal/photoinduced thiol–ene coupling (TEC)[12] was chosen as the covalent immobilization strategy for the preparation of heterogeneous proline-like organocatalysts **2–4** in analogy with the synthesis of the previously reported immobilized proline **1**. Accordingly, the novel *N*-Boc pyrrolidine 2-carboxyamide **7** and sulfonamide **8** equipped with the ene functionality (4-allyloxy group) were readily prepared in a single step from (2*S*,4*R*)-*N*-Boc-4-*O*-allyl-hydroxyproline **5**[4] by standard chemistry (Scheme 1). The tetrazolyl alkene **13** bearing a Cbz protecting group at the pyrrolidine nitrogen atom was next synthesized by adapting the procedures already optimized by Ley *et al.*,[11m] Hartikka and Arvidsson,[11i] and Saito, Yamamoto *et al.*[11j] for the synthesis of a *N*-Cbz protected pyrrolidinyl tetrazole analogue. Accordingly, (2*S*,4*R*)-*N*-Cbz-4-*O*-allyl-hydroxyproline **6**[13] was almost quantitatively converted to the corresponding amide **9** by *in situ* activation of the carboxylic acid. Subsequent dehydration promoted by cyanuric chloride gave the nitrile **11** in high yield (82%), which in turn was transformed into the corresponding tetrazole **13** (85%) by cycloaddition with sodium azide.

The thermally (toluene, 90 °C) and photochemically (MeOH, room temperature, λ_{max} 365 nm) induced TECs of thiol–silica **14**[14] with alkenes **7** or **8** (3 equiv.) were next carried out under the previously optimized conditions[4] by using 2,2′-azobis(2-methylpropionitrile) (AIBN) and 2,2-dimethoxy-2-phenyl-acetophenone (DMAP) as the radical initiators, respectively. Both immobilization strategies resulted equally effective producing, after TFA-promoted Boc deprotection, the target prolyl amide and sulfonamide functionalized silicas **2** and **3**, respectively, with a comparable degree of functionalization (0.75–0.70 mmol g^{-1}), as determined by elemental analysis (Scheme 2). A lower loading (0.15 mmol g^{-1}) was instead achieved for the tetrazole functionalized silica **4** prepared by TEC (thermal or photoinduced) of **14** with *N*-Cbz pyrrolidinyl tetrazole **13**. This unsatisfactory result was determined by the harsh acidic conditions required for Cbz group removal (6N HCl, 80 °C). Nevertheless, while milder Cbz deprotection procedures proved to be unsuccessful on silica support, the synthetic sequence optimized for the preparation of *N*-Cbz pyrrolidinyl tetrazole **13** was practicable and effective for the synthesis of the *N*-Boc analogue **12** as well (Scheme 1). Gratifyingly, TEC of **14** with **12** followed by Boc deprotection afforded the tetrazole functionalized silica **4** with a suitable loading (0.76 mmol g^{-1}; Scheme 2).

Next, on the basis of our previous experience with proline catalyst **1**, the activity of the newly prepared heterogeneous proline mimetics **2–4** was evaluated in selected solvents (acetonitrile, toluene, DMSO, and dichloromethane) by using the aldol condensation of cyclohexanone **15** with *p*-nitro benzaldehyde **16a** as the benchmark (Table 1). Proline amide **2** was the less active catalyst in terms of both chemical yield and stereoselectivity (entries 1–4). As already observed for immobilized proline **1**,[4] the use of the low-polarity toluene produced the best results for the sulfonamide **3** and tetrazole **4** as well, the latter being much more active than the former (entries 6 and 10). Different solvents were then screened to further improve catalyst **4** profile (entries 13–15). Pleasingly, the utilization at room temperature of diisopropyl ether allowed isolation of the mixture of *anti–syn* adducts (d.r. = 2 : 1) in quantitative yield and high enantioselectivity (95% ee_{anti}) after 12 h reaction time (entry 15). It is important to note that tetrazole catalyst **4** outperforms the supported proline **1**, which promoted the formation of **17a** (d.r. = 4 : 1) in lower yield (67%) and enantioselectivity (78% ee_{anti}; entry 16).[4] Finally,

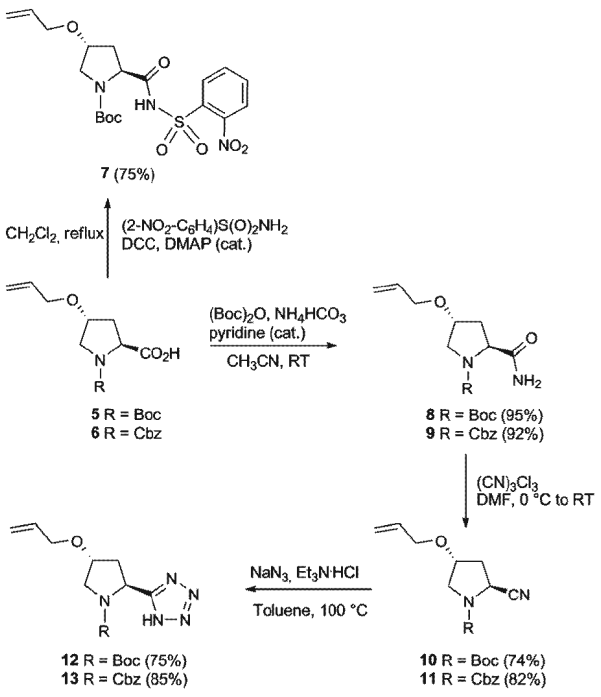

Scheme 1 Synthesis of the ene-functionalized proline mimetics **7**, **8**, **12**, and **13**.

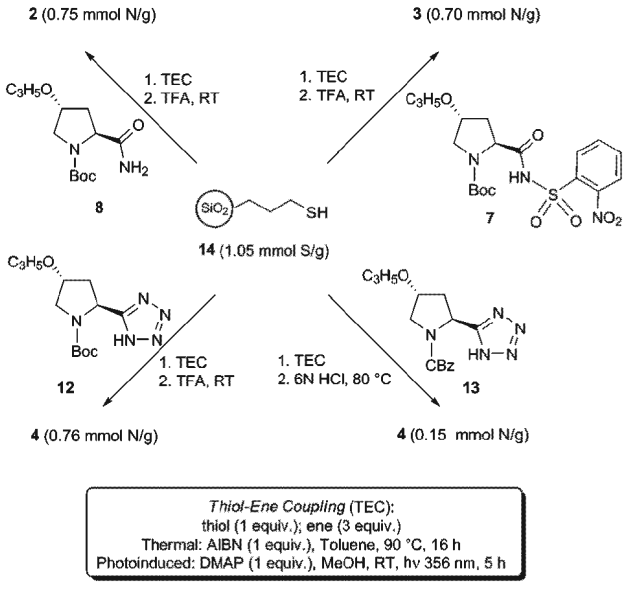

Scheme 2 Thermally and photochemically induced TEC of thiol silica **14** with 4-*O*-allyl-hydroxyroline derivatives **7**, **8**, **12**, and **13**.

Table 1 Evaluation of catalysts **2–4** performance under batch conditions[a]

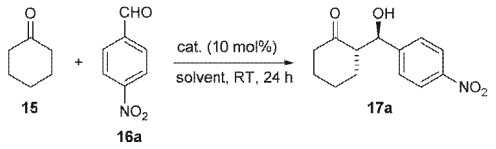

Entry	Cat.	Solvent	Yield[b] [%]	d.r. *anti–syn*[c]	ee$_{anti}$[d] [%]
1	**2**	CH_3CN	24	2 : 1	26
2	**2**	Toluene	45	4 : 1	23
3	**2**	DMSO	12	3 : 1	23
4	**2**	CH_2Cl_2	18	4 : 1	8
5	**3**	CH_3CN	21	4 : 1	9
6	**3**	Toluene	58	3 : 1	30
7	**3**	DMSO	25	2 : 1	9
8	**3**	CH_2Cl_2	15	4 : 1	15
9	**4**	CH_3CN	75	4 : 1	74
10	**4**	Toluene	>95	3 : 1	82
11	**4**	DMSO	>95	1 : 1	50
12	**4**	CH_2Cl_2	84	3 : 1	51
13	**4**	MeOH	45	3 : 1	32
14	**4**	Et_2O	>95	2 : 1	90
15	**4**	$(iPr)_2O$	>95[e]	2 : 1	95
16	**1**	Toluene	68	4 : 1	78
17	**4**	$(iPr)_2O$[f]	>95	2 : 1	92

[a] Reactions performed in the stated solvent with 0.25 mmol of aldehyde (0.15 M) and 0.75 mmol of ketone. [b] Isolated yield of the *anti–syn* diastereomeric mixture. [c] Estimated by ^{1}H NMR analysis of crude reaction mixtures. [d] Determined by chiral HPLC analysis. [e] Reaction time: 12 h. [f] Reactions performed with recycled catalyst.

Table 2 Short study on the catalytic activity of **4** in model organocatalytic reactions[a]

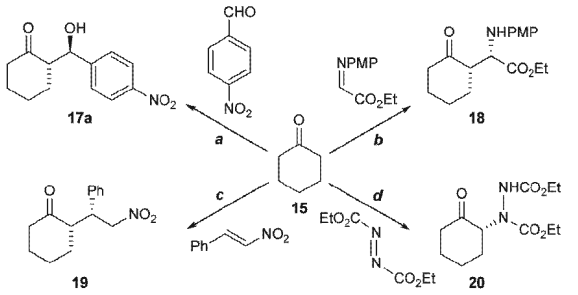

Entry	React.	Solvent	Yield[b] [%]	d.r. *anti–syn*[c]	ee[d] [%]
1	*a*	$(iPr)_2O$	90 (**17a**)	2 : 1	95$_{anti}$
2	*a*	DMSO	92 (**17a**)	1 : 1	50$_{anti}$
3[e]	*b*	$(iPr)_2O$	82[f] (**18**)	1 : >19	90$_{syn}$
4[e]	*b*	Toluene	>95[f] (**18**)	1 : >19	95$_{syn}$
6	*c*	$(iPr)_2O$	80 (**19**)	1 : 15	55$_{syn}$
5	*c*	DMSO	92 (**19**)	1 : 9	45$_{syn}$
7[e]	*d*	CH_3CN	95[f] (**20**)	—	42
8[e]	*d*	Toluene	72[f] (**20**)	—	71
9[g]	*a*	DMSO	92 (**17a**)	1 : 1	95$_{anti}$

[a] Reactions performed at room temperature for 24 h in the stated solvent with 0.25 mmol of acceptor (0.1 M), 0.75 mmol of cyclohexanone, and 0.075 mmol of **4**. [b] Isolated yield of the stereomeric mixture of adducts. [c] Estimated by ^{1}H NMR analysis of crude reaction mixtures. [d] Determined by chiral HPLC analysis. [e] Reaction performed with 20 vol % of **15**. Reaction time: 2 h. [f] Yield determined by ^{1}H NMR analysis. [g] Reaction performed under homogeneous conditions with (*S*)-5-(pyrrolidin-2-yl)-1*H*-tetrazole catalyst (10 mol%).

a substantial maintenance of catalyst efficiency was detected in diisopropyl ether for recycled **4** (entry 17). Indeed, the evaluation of catalyst stability (recyclability) was a crucial experiment to envisage the potential application of **4** in continuous-flow processes.

Since its discovery,[11g,h,j] the unsupported (*S*)-5-(pyrrolidin-2-yl)-1*H*-tetrazole has proven to be a successful catalyst due to its efficacy in a wide range of organocatalytic reactions.[11a] Therefore, with the aim to gain more information about the potential applications of the supported analogue **4** in continuous-flow heterogeneous catalysis, the activity of **4** was tested in model Mannich (eq. *b*, Table 2), Michael (eq. *c*), and α-amination (eq. *d*) reactions. Table 2 summarizes the results of this short study reporting for each transformation the best reaction profiles based on product yield and/or stereoselectivity.[15] Selected outcomes of the model aldol reaction are also included in Table 2 (eq. *a*). It appears from these preliminary results that heterogeneous catalyst **4** behaves in a comparable manner to the unsupported counterpart in terms of yield[16] and diastereo- and enantioselectivity. A direct comparison with literature data was, in fact, possible for the Mannich,[11c] Michael,[11c,16] and α-amination reactions.[11b] As far as the aldol reaction is concerned (entries 1–2), the observed poor diastereoselectivity was demonstrated to be an intrinsic feature of tetrazole catalysis. Indeed, an experiment (entry 9) performed in DMSO (room temperature, 24 h) with the unsupported (*S*)-5-(pyrrolidin-2-yl)-1*H*-tetrazole catalyst (10 mol%) gave the mixture of aldol products in identical quantitative yield and 1 : 1 diastereomeric ratio (entries 9 and 2).

Mechanistically, though the general mode of pyrrolidinyl tetrazole catalysis is still the subject of debate and discussion,[11a] it can be speculated that the suitable choice of low-polarity solvents such as diisopropyl ether and toluene prevents the free hydroxyls on the silica support of **4** from perturbing the hydrogen-bonding network responsible for the high selectivities detected in homogeneous catalysis.[17]

As anticipated, the tetrazole catalyst **4** was finally tested in the continuous-flow aldol reaction of cyclohexanone with *p*-nitro benzaldehyde with the hope of setting up an effective process with potential long term stability.[18] Thus, a micro-HPLC was suitably adapted for this study with minimized extra-columns volumes. The packed-bed microreactor **R4** (Table 3) was then prepared by filling (packing by gravity) a stainless steel column (50 mm length, 2.1 mm diameter) with tetrazole-functionalized silica **4** (pore size 60 Å, particle size ~50 μm, superficial area 500 m^2 g^{-1}, loading 0.76 mmol g^{-1}). Main features of **R4** were determined by pycnometry and included the hold-up (dead) volume (V_0 = 125 μL), and the total porosity (0.72). The packing amount of silica (154 mg) was calculated by weighing the column before and after filling. In addition, chromatographic retention factors k' of cyclohexanone and *p*-nitro benzaldehyde were measured under linear conditions in diisopropyl ether (DIP) and toluene.[19] These solvents, in fact, were selected as the optimal reaction media for the subsequent continuous-flow experiments (Table 3). Importantly, the determination of k' values was crucial for roughly calculating the retention times (t_r) of the above reactants at different flow rates,[19] and thus for

Table 3 Optimization of continuous-flow aldol reaction in packed-bed microreactors **R4** and short substrate scope study[a]

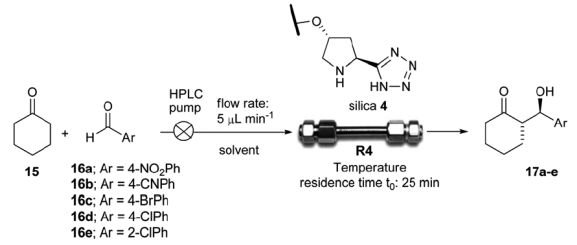

Entry	Solvent	**16** (*c* [M])	$k'_{\mathbf{16}}$[b]	$t_{r(\mathbf{16})}$[b] (min)	Temp.[c] [°C]	Conv.[d] [%]	Productivity[e]/10^3 [mmolh^{-1} mmol$_{cat}^{-1}$]	d.r. *anti–syn*[f]	ee$_{anti}$[g] [%]
1	$(iPr)_2O$	**16a** (0.03)	8.56	239	25	65	50	2 : 1	95
2	Toluene	**16a** (0.10)	0.91	48	25	62	159	3 : 1	82
3	$(iPr)_2O$[h]	**16a** (0.10)	—	—	25	58	149	2 : 1	85
4	$(iPr)_2O$[i]	**16a** (0.03)	8.56	239	50	>95	77	1 : 1	92
5	Toluene	**16a** (0.10)	0.91	48	50	95	256	2 : 1	80
6	Toluene	**16b** (0.10)	0.60	45	50	>95	256	3 : 1	75
7	Toluene	**16c** (0.10)	0.26	31	50	95	256	3 : 1	78
8	Toluene	**16d** (0.10)	0.27	32	50	>95	256	3 : 1	82
9	Toluene	**16e** (0.10)	0.28	32	50	>95	236	2 : 1	68

[a] See the Experimental section for a description of the experimental setup. All reactions were performed with a three-fold excess of cyclohexanone. [b] Chromatographic retention factors k' and retention times t_r have been estimated at RT in the reaction solvent as described in ref. 19. $k'_{\mathbf{15}}$(DIP) = 0.84 (t_r = 46 min); $k'_{\mathbf{15}}$(Tol) = 0.30 (t_r = 33 min)). [c] All temperatures were measured by a thermometer placed inside the thermostatted unit containing the microreactor. [d] Instant conversion in steady-state regime as established by ^{1}H NMR analysis. [e] Productivities are measured in mmol(product) h^{-1} mmol(catalyst)$^{-1}$ × 10^3. [f] Estimated by ^{1}H NMR analysis of crude reaction mixtures. [g] Determined by chiral HPLC analysis. [h] Reaction performed with 10 vol% of DMF. [i] The same reaction outcome was observed in a control experiment performed at the end of the substrate scope study.

estimating the duration of the process.[20] An initial continuous-flow experiment was performed in DIP by using a three-fold excess of cyclohexanone in analogy to the batch study. The optimal compromise between aldehyde solubility, conversion efficiency, and productivity was obtained by pumping a 0.03 M solution of aldehyde at 5 μL min^{-1} (residence time t_0 = 25 min; $t_{r(\mathbf{16a})}$: 239 min). As previously observed with proline catalyst **1**,[4] the stereoselectivity of the batch experiment with **4** (Table 1, entry 15) was replicated (d.r. 2 : 1; 95 ee$_{anti}$, Table 3, entry 1) and maintained constant during the continuous process in steady-state regime.[20] The use of toluene or a 9 : 1 DIP–DMF mixture as the solvent improved the process productivity because of the higher concentration of reactants but, at the same time, slightly lowered the reaction conversion and the level of enantioselectivity (entries 2–3). Therefore, having in mind that reaction completion is a fundamental goal in continuous process optimization for easier product purification, the effect of temperature on conversion efficiency was finally examined.[21] To our delight, we found that warming the microreactor **R4** in the HPLC oven set a 50 °C resulted in complete conversion and selectivity (no formation of dehydration by-product was detected) both in DIP and toluene, thus allowing the isolation of the aldol product **17a** by simple evaporation of the solvent and excess cyclohexanone (entries 4 and 5). Notably, the increase of the process temperature did not compromise the enantioselectivity of the process, which proceeded with higher productivity (*ca.* 8 mg h^{-1}) in toluene (entry 5).

The scope and the applicability of the method were shortly investigated by reacting cyclohexanone with various aromatic aldehydes having electron-withdrawing substituents (entries 6–9). Gratifyingly, the corresponding mixtures of aldol adducts **17b–e** were produced in toluene at 50 °C with high conversion efficiency (≥95%) and a satisfactory level of enantioselectivity (68–82 ee$_{anti}$). We would like to emphasize that the whole optimization and substrate scope study was carried out with the same packed-bed microreactor **R4**, which functioned at 50 °C for an overall time of 80 hours. Remarkably, the packing silica **4** did not show any evidence of deactivation during that period, as demonstrated by a final control experiment that reproduced the optimal **15**/**16a** coupling outcome (entry 4). A progressive loss of catalytic activity was observed, however, after 120 hours at 50 °C, with catalyst **4** fully deactivated after *ca.* 7 days on stream.

Conclusions

In summary, we have synthesized a heterogeneous version of the valuable Ley–Arvidsson–Yamamoto (*S*)-5-(pyrrolidin-2-yl)-1*H*-tetrazole organocatalyst and ascertained that the utilization of silica as the support and thiol–ene coupling (TEC) as the immobilization strategy enables tetrazole organocatalyst **4** to maintain the level of stereoselectivity of its homogeneous counterpart in model batch transformations. Crucial for successful experiments with supported tetrazole **4** was the selection of low-polarity reaction solvents. In addition, we have provided a further example of the effective combination of heterogeneous asymmetric organocatalysis and microreactor technology by preparing a packed-bed microreactor filled with silica **4** and demonstrating its efficacy in the continuous production of optically active aldol products. Further improvements, in particular pertaining to process productivity, are in progress through chemical optimization of the

described catalytic system and by taking advantage of a deeper understanding of the kinetics and thermodynamics of the continuous-flow-process. Nevertheless, we believe this work may represent a useful contribution to the current search for more efficient, economic, and environmentally benign production strategies of valuable chiral targets.

Experimental section

All moisture-sensitive reactions were performed under a nitrogen atmosphere using oven-dried glassware. Solvents were dried over standard drying agent and freshly distilled prior to use. Flash column chromatograph was performed on silica gel 60 (230–400 mesh). Reactions were monitored by TLC on silica gel 60 F_{254} with detection by charring with sulfuric acid and/or ninhydrin. Flash column chromatography was performed on silica gel 60 (230–400 mesh). Optical rotations were measured at 20 ± 2 °C in the stated solvent; $[\alpha]_D$ values are given in 10^{-1} deg cm^2 g^{-1}. ^1H (300 MHz) and ^{13}C (75 MHz) NMR spectra were recorded for $CDCl_3$ solutions at room temperature unless otherwise specified. Peak assignments were aided by ^1H–^1H COSY and gradient-HMQC experiments. Enantiomeric excess (ee) values were determined by HPLC. A two-pump high pressure micro system (Agilent 1100 micro series) equipped with a DAD detector was employed. The column was 150 × 2 mm Lux-1 Cellulose (from Phenomenex), 3 μm particle diameter. The mobile phase was a binary mixture hexanes–i-PrOH 90 : 10 (v/v). ESI MS (LTQ-XL Linear Trap from Thermo Scientific) analyses were performed in positive ion mode with samples dissolved in 10 mM solution of HCO_2NH_4 in 1 : 1 MeCN–H_2O. FT-IR analyses were performed with the Bruker Instrument Vertex 70. Elemental analyses were performed with FLASH 2000 Series CHNS/O analyzer (ThermoFisher Scientific). Vertical agitation was performed with the FirstMate™ synthesizer, Argonaut Technology. The household UVA lamp apparatus was equipped with four 15 W tubes (1.5 × 27 cm each). Photoinduced reactions were carried out in a glass vial (diameter: 1 cm; wall thickness: 0.65 mm), sealed with a natural rubber septum, located 2.5 cm away from the UVA lamp (irradiation on sample: 365 nm, 1.04 W m^{-2}). The system used for continuous-flow reactions was composed of an HPLC pump (Agilent 1100 micro series), an in-line pressure transducer, a thermostated microreactor holder (Peltier unit), a system to collect fractions and a data acquisition system (Agilent ChemStation). The units were connected by peek tubing (internal diameter 0.01 inch from Upchurch Scientific). The system hold-up volume was smaller than 80 μL. The temperature was controlled by inserting a thermometer inside the Peltier unit (temperature measurement error: ±0.5 °C). Silica gel (grade 9385, pore size 60 Å, particle size ~50 μm, superficial area 500 m^2 g^{-1}) was purchased from Sigma-Aldrich. (2*S*,4*R*)-*N*-Boc-4-(allyloxy)proline **5**[4] and (2*S*,4*R*)-*N*-Cbz-4-(allyloxy)proline **6**[13] were synthesized as described. Thiol–silica **14**[22] was prepared according to reported procedures with minor modifications. For microreactor **R4** preparation and characterization see the ESI.† Adducts **17a–e**, **18**, **19**, and **20** are known compounds. The self-disproportionation of enantiomers (SDE) test for achiral chromatography[23] has been carried out for derivatives **17a–e**, **19**, and **20** without noting any significant magnitude of SDE.

(2*S*,4*R*)-*tert*-Butyl 4-(allyloxy)-2-(2-nitrophenylsulfonylcarbamoyl)pyrrolidine-1-carboxylate (7)

To a stirred solution of (2*S*,4*R*)-*N*-Boc-4-(allyloxy)proline **5**[4] (500 mg, 1.85 mmol) in CH_2Cl_2 (8 mL) were added 2-nitrobenzenesulfonamide (337 mg, 1.67 mmol), 4-(dimethylamino)pyridine (DMAP, 61 mg, 0.50 mmol), and *N*,*N*′-dicyclohexylcarbodiimide (DCC, 419 mg, 2.03 mmol). The resulting mixture was refluxed for 72 h, then cooled to room temperature, filtered, and washed with fresh portions of CH_2Cl_2 (4 × 5 mL). The combined filtrates were washed with cold 1 M HCl (5 mL) and brine (5 mL) Then, the organic phase was dried (Na_2SO_4), concentrated, and eluted from a column of silica gel with 2.5 : 1 cyclohexane–AcOEt to give the sulfonamide **7** (631 mg, 75%) as a white amorphous solid. $[\alpha]_D = -51.2$ (*c* 1.6, $CHCl_3$). ^1H NMR: δ = 8.50–8.38 (bm, 2 H, Ar), 7.85–7.62 (bm, 3 H, Ar), 5.90–5.78 (m, 1 H, CH_2═C*H*), 5.28–5.15 (m, 2 H, CH_2═CH), 4.50–4.29 (bm, 1 H, H-2), 4.08–3.74 (bm, 3 H, OCH_2, H-4), 3.52 (bdd, 1 H, $J_{4,5a}$ = 2.0 Hz, $J_{5a,5b}$ = 8.5 Hz, H-5a), 3.40 (bdd, 1 H, $J_{4,5b}$ = 5.0 Hz, $J_{5a,5b}$ = 10.5 Hz, H-5b), 2.50–2.00 (bm, 2 H, 2 H-3), 1.42 and 1.38 (2 s, 9 H, C(CH_3)$_3$). ^{13}C NMR (major conformer): δ = 171.1, 157.0, 154.2, 148.1, 134.2, 133.3, 132.3, 124.7, 117.2, 82.3, 76.0, 70.1, 59.5, 51.9, 32.6, 28.2. ESI MS (455.1): 473.4 (M + NH_4^+). Found: C, 50.02; H, 5.78; N, 9.51; S 7.22. $C_{19}H_{25}N_3O_8S$ requires C, 50.10; H, 5.53; N, 9.23; 7.04%.

(2*S*,4*R*)-*tert*-Butyl 4-(allyloxy)-2-carbamoylpyrrolidine-1-carboxylate (8)

To a stirred mixture of (2*S*,4*R*)-*N*-Boc-4-(allyloxy)proline **5**[4] (1.28 g, 4.72 mmol), di-*tert*-butyl dicarbonate (1.54 g, 7.08 mmol,), NH_4HCO_3 (559 mg, 7.08 mmol), and anhydrous CH_3CN (20 mL) anhydrous pyridine (286 μL, 3.54 mmol) was added in one portion. The mixture was stirred at room temperature until TLC analysis revealed the disappearance of the starting acid (*ca.* 5 h), then the volume was reduced under vacuum to approximately 5 mL. Subsequently, AcOEt (20 mL) and H_2O (20 mL) were added and the organic phase separated. The aqueous phase was extracted further with AcOEt (2 × 20 mL) and the combined organic phases washed with brine (10 mL), dried (Na_2SO_4), and concentrated to give the amide **8** (1.21 g, 95%) at least 90% pure as judged by ^1H NMR analysis. An analytical sample of **8** was obtained by column chromatography with 1 : 9 cyclohexane–AcOEt. $[\alpha]_D = -58.8$ (*c* 0.6, $CHCl_3$). ^1H NMR: δ = 6.80 and 5.90 (2 bs, 1 H, NH), 6.00–5.80 (m, 1 H, CH_2═C*H*), 5.60–5.45 (bm, 1 H, NH), 5.35–5.15 (m, 2 H, CH_2═CH), 4.45–4.15 (bm, 2 H, H-2, H-4), 4.05–3.90 (bm, 2 H, OCH_2), 3.80–3.40 (m, 2 H, 2 H-5), 2.55–2.00 (bm, 2 H, 2 H-3), 1.42 (s, 9 H, C(CH_3)$_3$). ^{13}C NMR (major conformer): δ = 173.9, 154.0, 134.3, 117.2, 80.8, 75.9, 70.2, 58.2, 51.8, 33.7, 28.3. ESI MS (270.2): 309.8 (M + K^+). Found: C, 57.48; H, 8.41; N, 10.09. $C_{13}H_{22}N_2O_4$ requires C, 57.76; H, 8.20; N, 10.36%.

(2*S*,4*R*)-Benzyl 4-(allyloxy)-2-carbamoylpyrrolidine-1-carboxylate (9)

To a stirred mixture of (2*S*,4*R*)-*N*-Cbz-4-(allyloxy)proline **6**[13] (1.00 g, 3.28 mmol), di-*tert*-butyl dicarbonate (1.07 g,

4.92 mmol), NH_4HCO_3 (389 mg, 4.92 mmol), and anhydrous CH_3CN (15 mL) anhydrous pyridine (199 μL, 2.46 mmol) was added in one portion. The mixture was stirred at room temperature until TLC analysis revealed the disappearance of the starting acid (*ca.* 5 h), then the volume was reduced under vacuum to approximately 5 mL. Subsequently, AcOEt (20 mL) and H_2O (20 mL) were added and the organic phase separated. The aqueous phase was extracted further with AcOEt (2 × 20 mL) and the combined organic phases washed with brine (10 mL), dried (Na_2SO_4), and concentrated to give the amide **9** (917 mg, 92%) at least 90% pure as judged by ^{1}H NMR analysis. An analytical sample of **9** was obtained by column chromatography with pure AcOEt. $[\alpha]_D = -49.9$ (*c* 1.4, $CHCl_3$). ^{1}H NMR: δ = 7.40–7.20 (m, 5 H, Ar), 6.65 and 5.82 (2 bs, 1 H, NH), 5.92–5.78 (m, 1 H, CH_2═C*H*), 5.45–5.30 (bm, 1 H, NH), 5.28–5.10 (m, 2 H, CH_2═CH), 4.50–4.35 (m, 1 H, H-2), 4.26–4.10 (m, 1 H, H-4), 4.00–3.90 (m, 2 H, OCH_2), 3.86–3.50 (m, 2 H, 2 H-5), 2.60–2.40 and 2.30.2.00 (2 bm, 2 H, 2 H-3). ^{13}C NMR (major conformer): δ = 173.4, 156.2, 136.1, 134.2, 128.5, 128.2, 127.8, 117.3, 76.1, 70.2, 67.5, 58.7, 51.7, 33.9. ESI MS (344.1): 343.9 (M + K^+). Found: C, 63.38; H, 6.51; N, 9.01. $C_{16}H_{20}N_2O_4$ requires C, 63.14; H, 6.62; N, 9.20%.

(2S,4*R*)-*tert*-Butyl 4-(allyloxy)-2-cyanopyrrolidine-1-carboxylate (10)

To a cooled (0 °C), stirred solution of crude amide **8** (1.21 g, 4.48 mmol) in anhydrous DMF (20 mL) cyanuric chloride (537 mg, 2.91 mmol) was added in one portion. The mixture was stirred at 0 °C for 1 h, then warmed to room temperature, and stirred at that temperature for additional 24 h. The mixture was then cooled to 0 °C, diluted with H_2O (15 mL), and extracted with AcOEt (3 × 50 mL). The combined organic phases were washed with brine (10 mL), dried (Na_2SO_4), concentrated, and eluted from a column of silica gel with 4 : 1 cyclohexane–AcOEt to give **11** (835 mg, 74%) as a pale yellow oil. $[\alpha]_D = -65.4$ (*c* 1.1, $CHCl_3$). ^{1}H NMR: δ = 5.98–5.82 (m, 1 H, CH_2═C*H*), 5.34–5.20 (m, 2 H, CH_2═CH), 4.64–4.50 (m, 1 H, H-2), 4.30–4.10 (m, 1 H, H-4), 4.08–3.90 (m, 2 H, OCH_2), 3.70–3.60 and 3.58–3.48 (2 bm, 2 H, 2 H-5), 2.60–2.30 (bm, 2 H, 2 H-3), 1.48 and 1.4 (2 s, 9 H, C(CH_3)$_3$). ^{13}C NMR (major conformer): δ = 152.8, 133.7, 118.7, 117.2, 81.3, 74.9, 69.9, 50.5, 45.4, 37.0, 27.9. ESI MS (252.1): 275.7 (M + Na^+). Found: C, 61.67; H, 7.81; N, 11.28. $C_{13}H_{20}N_2O_3$ requires C, 61.88; H, 7.99; N, 11.10%.

(2S,4*R*)-Benzyl 4-(allyloxy)-2-cyanopyrrolidine-1-carboxylate (11)

To a cooled (0 °C), stirred solution of crude amide **9** (1.60 g, 5.26 mmol) in anhydrous DMF (18 mL) cyanuric chloride (630 mg, 3.41 mmol) was added in one portion. The mixture was stirred at 0 °C for 1 h, then warmed to room temperature, and stirred at that temperature for additional 12 h. The mixture was then cooled to 0 °C, diluted with H_2O (10 mL), and extracted with AcOEt (3 × 40 mL). The combined organic phases were washed with brine (10 mL), dried (Na_2SO_4), concentrated, and eluted from a column of silica gel with 2 : 1 cyclohexane–AcOEt to give **11** (1.23 g, 82%) as a white foam. $[\alpha]_D = -61.5$ (*c* 0.7, $CHCl_3$). ^{1}H NMR: δ = 7.45–7.25 (m, 5 H, Ar), 6.00–5.78 (m, 1 H, CH_2═C*H*), 5.40–5.25 (m, 2 H, CH_2═CH), 4.80–4.58 (m, 1 H, H-2), 4.30–4.12 (m, 1 H, H-4), 4.10–3.80 (m, 2 H, OCH_2), 3.80–3.72 and 3.64–3.50 (2 m, 2 H, 2 H-5), 2.60–2.20 (m, 2 H, 2 H-3). ^{13}C NMR (major conformer): δ = 162.0, 135.7, 133.8, 128.6, 128.3, 128.2, 128.1, 128.0, 118.7, 117.8, 75.9, 70.3, 68.1, 51.3, 45.5, 37.6. ESI MS (286.1): 309.5 (M + Na^+). Found: C, 67.42; H, 6.60; N, 9.98. $C_{16}H_{18}N_2O_3$ requires C, 67.12; H, 6.34; N, 9.78%.

(2S,4*R*)-*tert*-Butyl 4-(allyloxy)-2-(1*H*-tetrazol-5-yl)pyrrolidine-1-carboxylate (12)

A mixture of nitrile **10** (800 mg, 3.17 mmol), NaN_3 (268 mg, 4.12 mmol), Et_3N·HCl (567 mg, 4.12 mmol), and toluene (5 mL) was stirred at 95 °C under an atmosphere of argon for 24 h. The mixture was then cooled to room temperature and extracted with AcOEt (3 × 40 mL). The combined organic phases were washed with brine (10 mL), dried (Na_2SO_4), concentrated, and eluted from a column of silica gel with 6 : 4 : 1 cyclohexane–AcOEt–AcOH to give **12** (701 mg, 75%) as a white amorphous solid. $[\alpha]_D = -92.0$ (*c* 0.6, $CHCl_3$). ^{1}H NMR: δ = 6.02–5.88 (m, 1 H, CH_2═C*H*), 5.37–5.22 (m, 2 H, CH_2═CH), 5.17 (dd, 1 H, $J_{2,3a}$ = 7.0 Hz, $J_{2,3b}$ = 7.5 Hz, H-2), 4.35–4.25 (m, 1 H, H-4), 4.15–4.00 (m, 2 H, OCH_2), 3.64 (dd, 1 H, $J_{4,5a}$ = 3.0 Hz, $J_{5a,5b}$ = 11.5 Hz, H-5a), 3.48 (dd, 1 H, $J_{4,5b}$ = 5.0 Hz, $J_{5a,5b}$ = 11.5 Hz, H-5b), 3.10–3.00 (m, 1 H, H-3a), 2.63–2.51 (m, 1 H H-3b), 1.42 (s, 9 H, C(CH_3)$_3$). ^{13}C NMR (major conformer): δ = 157.0, 155.9, 134.1, 117.3, 81.6, 76.0, 70.1, 52.0, 49.7, 35.5, 28.2. ESI MS (295.2): 296.6 (M + H^+). Found: C, 52.55; H, 7.41; N, 23.46. $C_{13}H_{21}N_5O_3$ requires C, 52.87; H, 7.17; N, 23.71%.

(2S,4*R*)-Benzyl 4-(allyloxy)-2-(1*H*-tetrazol-5-yl)pyrrolidine-1-carboxylate (13)

A mixture of nitrile **11** (800 mg, 2.80 mmol), NaN_3 (237 mg, 3.64 mmol), Et_3N·HCl (501 mg, 3.64 mmol), and toluene (5 mL) was stirred at 95 °C under an atmosphere of argon for 24 h. The mixture was then cooled to room temperature, diluted with cold 1 M HCl until pH = 3, and extracted with CH_2Cl_2 (3 × 40 mL). The combined organic phases were washed with brine (10 mL), dried (Na_2SO_4), concentrated, and eluted from a column of silica gel with 6 : 4 :1 cyclohexane–AcOEt–AcOH to give **13** (783 mg, 85%) as a white amorphous solid. $[\alpha]_D = -42.2$ (*c* 0.9, $CHCl_3$). ^{1}H NMR (DMSO-d_6 + D_2O, 120 °C): δ = 7.45–7.15 (m, 5 H, Ar), 6.00–5.84 (m, 1 H, CH_2═C*H*), 5.32–5.05 (m, 2 H, CH_2═CH), 5.29 (dd, 1 H, $J_{2,3a}$ = 5.0 Hz, $J_{2,3b}$ = 5.5 Hz, H-2), 4.36–4.28 (m, 1 H, H-4), 4.04–3.98 (m, 2 H, OCH_2), 3.72 (dd, 1 H, $J_{4,5a}$ = 5.0 Hz, $J_{5a,5b}$ = 11.5 Hz, H-5a), 3.64 (dd, 1 H, $J_{4,5b}$ = 1.5 Hz, $J_{5a,5b}$ = 11.5 Hz, H-5b), 2.42 (ddd, 1 H, $J_{2,3a}$ = 5.0 Hz, $J_{3a,4}$ = 7.5 Hz, $J_{3a,3b}$ = 12.5 Hz, H-3a), 2.21 (ddd, 1 H, $J_{2,3a}$ = 5.5 Hz, $J_{3a,4}$ = 6.0 Hz, $J_{3a,3b}$ = 12.5 Hz, H-3b). ^{13}C NMR (major conformer): δ = 156.7, 156.3, 135.8, 134.1, 128.5, 128.2, 128.0, 127.8, 117.4, 75.7, 70.2, 67.7, 51.9, 50.3, 35.5. ESI MS (329.1): 330.5 (M + H^+). Found: C, 58.62; H,

5.99; N, 21.58. $C_{16}H_{19}N_5O_3$ requires C, 58.35; H, 5.81; N, 21.26%.

Preparation of 3-mercaptopropyl silica gel 14

To preserve silica particles from mechanical degradation, this derivatization step was carried out in a standard rotary evaporator in which a two-necked flask was fitted with solvent condenser, solvent collector, and nitrogen inlet for syringe addition of reactant solutions under an inert atmosphere. Mixing was obtained by spinning the flask around its axis and warming by means of a standard oil-bath. Silica gel (grade 9385, pore size 60 Å, particle size ~50 μm, superficial area 500 m^2 g^{-1}) was dried before its use (0.1 mbar, T = 110 °C, 2 h).

To a stirred slurry of silica gel (5.00 g), anhydrous toluene (60 mL), and freshly distilled triethylamine (0.25 mL) was slowly added a solution of (3-mercaptopropyl)-trimethoxysilane (2.5 mL) in anhydrous toluene (10 mL). The resulting mixture was then warmed to 60 °C and stirred for 20 h. Subsequently, the mixture was refluxed until *ca.* 15 mL of solvent were collected (eventually by the aid of a nitrogen stream). The mixture was then refluxed for an additional 1 h, cooled to room temperature, and centrifuged with 20 mL portions of toluene, MeOH, EtOH, and cyclohexane. The resulting thiol-functionalized silica gel **14** was finally dried at reduced pressure (0.1 mbar, 60 °C, 6 h). FT-IR (KBr): ν 2577(SH) cm^{-1}. Elemental analysis (%) found: S 3.36 (estimated loading f = 1.05 mmol g^{-1}).

General procedure for the synthesis of silica-supported proline mimetics 2–4 *via* thermally induced TEC

To preserve silica particles from mechanical degradation, this derivatization step was carried out with the FirstMate™ synthesizer.

A vertically-stirred mixture of thiol–silica **14** (1.00 g, 1.05 mmol; f = 1.05 mmol S g^{-1}), (4-allyloxy)pyrrolidine derivative **7**, **8** or **12** (3.15 mmol), 2,2′-azobis(2-methylpropionitrile) (AIBN, 172 mg, 1.05 mmol), and anhydrous toluene (8 mL) was degassed under vacuum, and saturated with argon (by an Ar-filled balloon) three times. The mixture was then warmed to 90 °C, stirred for 16 h, cooled to room temperature, diluted with AcOEt (8 mL), and centrifuged with 5 mL portions AcOEt (4×). The resulting *N*-Boc protected silica-supported proline mimetic ***N*-Boc 2**, ***N*-Boc 3** or ***N*-Boc 4** was finally dried at reduced pressure (0.1 mbar, 40 °C, 6 h). Excess pyrrolidine derivative **7**, **8** or **12** can be easily recycled by column chromatography of the centrifugate.

Silica *N*-Boc 2. Elemental analysis (%) found: N 2.15 (estimated loading f = 0.77 mmol g^{-1}). FT-IR (KBr): ν 1745 (CO), 1690 (CO), 1455 (*t*-Bu), 1370 (*t*-Bu) cm^{-1}.

Silica *N*-Boc 3. Elemental analysis (%) found: N 3.18 (estimated loading f = 0.76 mmol g^{-1}). FT-IR (KBr): ν 1740 (CO), 1610 (CO), 1545 (SO_2N), 1450 (*t*-Bu), 1370 (*t*-Bu) cm^{-1}.

Silica *N*-Boc 4. Elemental analysis (%) found: N 5.45 (estimated loading f = 0.78 mmol g^{-1}). FT-IR (KBr): ν 1699 (CO), 1650 (CO), 1457 (*t*-Bu), 1396 (*t*-Bu) cm^{-1}.

To a cooled (0 °C), vertically-stirred mixture of silica-supported proline mimetic ***N*-Boc 2**, ***N*-Boc 3** or ***N*-Boc 4** (~1.00 g) and anhydrous CH_2Cl_2 (4 mL) was slowly added a solution of TFA (4 mL) in anhydrous CH_2Cl_2 (4 mL). The mixture was then warmed to room temperature, stirred for 12 h, and centrifuged with 5 mL portions of CH_2Cl_2 (2×), 1 : 2/Et_3N–CH_2Cl_2 (2×; addition at 0 °C), CH_2Cl_2 (2×), MeOH (2×), CH_2Cl_2 (2×). The resulting silica-supported proline mimetics **2**, **3** or **4** was finally dried at reduced pressure (0.1 mbar, 40 °C, 6 h).

Silica 2. Elemental analysis (%) found: N 2.10 (estimated loading f = 0.75 mmol g^{-1}). FT-IR (KBr): ν 2938 (CH), 1681 (CO) cm^{-1}.

Silica 3. Elemental analysis (%) found: N 2.94 (estimated loading f = 0.70 mmol g^{-1}). FT-IR (KBr): ν 2930 (CH), 1613 (CO), 1546 (SO_2N), 1130 (SO_2N) cm^{-1}.

Silica 4. Elemental analysis (%) found: N 5.32 (estimated loading f = 0.76 mmol g^{-1}). FT-IR (KBr): ν 2938 (CH), 1674 (CO), 1445 (CN) cm^{-1}.

General procedure for the synthesis of silica-supported proline mimetics 2–4 *via* photoinduced TEC

To preserve silica particles from mechanical degradation, this derivatization step was carried out with the FirstMate™ synthesizer.

A vertically-agitated mixture of thiol–silica **14** (1.00 g, 1.05 mmol; f = 1.05 mmol S g^{-1}), (4-allyloxy)pyrrolidine derivative **7**, **8** or **12** (3.15 mmol), 2,2-dimethoxy-2-phenyl-acetophenone (DMAP, 269 mg, 1.05 mmol), and MeOH (6 mL) was irradiated at room temperature for 5 h, and then centrifuged with 5 mL portions of MeOH (4×). The resulting *N*-Boc protected silica-supported proline mimetic ***N*-Boc 2**, ***N*-Boc 3** or ***N*-Boc 4** was finally dried at reduced pressure (0.1 mbar, 40 °C, 6 h). Excess pyrrolidine derivative **7**, **8** or **12** can be easily recycled by column chromatography of the centrifugate. Silicas ***N*-Boc 2**, ***N*-Boc 3**, and ***N*-Boc 4** were obtained with levels of functionalization which were comparable to those detected in the corresponding thermally induced TECs.

To a cooled (0 °C), vertically-agitated mixture of silica-supported proline mimetic ***N*-Boc 2**, ***N*-Boc 3** or ***N*-Boc 4** (~1.00 g) and anhydrous CH_2Cl_2 (4 mL) was slowly added a solution of TFA (4 mL) in anhydrous CH_2Cl_2 (4 mL). The mixture was then warmed to room temperature, stirred for 12 h, and centrifuged with 5 mL portions of CH_2Cl_2 (2×), 1 : 2/Et_3N–CH_2Cl_2 (2×; addition at 0 °C), CH_2Cl_2 (2×), MeOH (2×), CH_2Cl_2 (2×). The resulting silica-supported proline mimetics **2**, **3** or **4** was finally dried at reduced pressure (0.1 mbar, 40 °C, 6 h). Silicas **2**, **3**, and **4** were obtained with levels of functionalization which were comparable to those detected in the corresponding thermally induced TECs.

Procedure for the model aldol reaction under batch conditions (Table 1)

A mixture of *p*-nitro benzaldehyde (38 mg, 0.25 mmol), cyclohexanone (78 μL, 0.75 mmol), the stated catalyst (0.075 mmol), and the stated solvent (1.7 mL) was vertically-stirred at room temperature for 24 h, and then centrifuged with 2.5 mL-portions of CH_2Cl_2 (2×). The combined centrifugates were concentrated and the resulting residue analyzed by ^1H NMR to determine the

diastereomeric ratio and conversion. Subsequently, the residue was eluted from a column of silica gel with 5 : 1 toluene–AcOEt to determine the yield of the *anti–syn* diastereomeric mixture and obtain the pure *anti*-adduct **17a** whose enantiomeric excess value[23] was determined by chiral HPLC analysis: Lux-1 cellulose (hexanes–i-PrOH 98 : 2 v/v, 400 μL min^{-1}; λ_{max} = 258 nm); t_R (major) = 18.5 min; t_R (minor) = 25.4).

Procedure for the model Mannich reaction under batch conditions (Table 2)

A mixture of *N-p*-methoxybenzyl-α-iminoglyoxalate (52 mg, 0.25 mmol), cyclohexanone (340 μL, 20 vol%), catalyst **4** (99 mg, 0.075 mmol), and the stated solvent (1.7 mL) was vertically-stirred at room temperature for 2 h, and then centrifuged with 2.5 mL-portions of CH_2Cl_2 (2×). The combined centrifugates were concentrated and the resulting residue analyzed by ^1H NMR to determine the diastereomeric ratio and estimate the yield of the *syn–anti* diastereomeric mixture. The enantiomeric excess of the *syn*-adduct **18** was determined by chiral HPLC analysis: Lux-1 Cellulose (hexanes–i-PrOH 99 : 1 v/v, 300 μL min^{-1}; λ_{max} = 246 nm); t_R (minor) = 16.5 min; t_R (major) = 17.7).

Procedure for the model Michael reaction under batch conditions (Table 2)

A mixture of *trans*-β-nitrostyrene (37 mg, 0.25 mmol), cyclohexanone (78 μL, 0.75 mmol), the stated catalyst (99 mg, 0.075 mmol), and the stated solvent (1.7 mL) was vertically-stirred at room temperature for 24 h, and then centrifuged with 2.5 mL-portions of CH_2Cl_2 (2×). The combined centrifugates were concentrated and the resulting residue analyzed by ^1H NMR to determine the diastereomeric ratio and conversion. Subsequently, the residue was eluted from a column of silica gel with 2 : 1 cyclohexane–AcOEt to determine the yield of the *anti–syn* diastereomeric mixture and obtain the pure *syn*-adduct **19** whose enantiomeric excess value[23] was determined by chiral HPLC analysis: Lux-1 Cellulose (hexanes–i-PrOH 92 : 8 v/v, 50 μL min^{-1}; λ_{max} = 220 nm); t_R (minor) = 34.8 min; t_R (major) = 36.3).

Procedure for the model α-amination reaction under batch conditions (Table 2)

A mixture of diethyl azodicarboxylate (97% purity, 41 μL, 45 mg, 0.25 mmol), cyclohexanone (340 μL, 20 vol%), catalyst **4** (99 mg, 0.075 mmol), and the stated solvent (1.7 mL) was vertically-stirred at room temperature for 2 h, and then centrifuged with 2.5 mL portions of CH_2Cl_2 (2×). The combined centrifugates were concentrated and the resulting residue analyzed by ^1H NMR to estimate the yield of **20**. The enantiomeric excess of **20** was determined by chiral HPLC analysis: Lux-1 cellulose (hexanes–i-PrOH 95 : 5 v/v, 200 μL min^{-1}; λ_{max} = 220 nm); t_R (minor) = 7.7 min; t_R (major) = 10.4).

Continuous-flow aldol reactions (Table 3)

Microreactor **R4** was fed with a solution in the stated solvent of cyclohexanone and the aromatic aldehyde **16a–e**, and operated at the stated temperature for 4 h (under steady-state conditions) at 5 μL min^{-1} (see Table 3 for molarity concentrations). Instant conversion was determined (^1H NMR analysis) every 30 minutes by taking a sample of the eluate. The collected solution was finally concentrated and eluted from a column of silica gel with the suitable elution system to give the corresponding mixture of *anti–syn* adducts whose diastereomeric ratio was determined by ^1H NMR analysis. The enantiomeric excess[23] of the *anti*-adducts **17a–e** was evaluated by chiral HPLC analysis.

17b. Lux-1 cellulose (hexanes–i-PrOH 99 : 1 v/v, 500 μL min^{-1}; λ_{max} = 220 nm); t_R (major) = 30.5; t_R (minor) = 46.2 min.

17c. Lux-1 cellulose (hexanes–i-PrOH 99 : 1 v/v, 100 μL min^{-1}; λ_{max} = 220 nm); t_R (major) = 57.8; t_R (minor) = 77.9 min.

17d. Lux-1 cellulose (hexanes–i-PrOH 98 : 2 v/v, 500 μL min^{-1}; λ_{max} = 220 nm); t_R (major) = 5.3; t_R (minor) = 7.3 min.

17e. Lux-1 cellulose (hexanes–i-PrOH 99 : 1 v/v, 500 μL min^{-1}; λ_{max} = 220 nm); t_R (major) = 5.4; t_R (minor) = 6.8 min.

Acknowledgements

We gratefully acknowledge the University of Ferrara (Progetto FAR 2010) and the Italian Ministry of University and Scientific Research (Progetto FIRB Chem-Profarma-Net Grant RBPR05NWWC 008, Progetto PRIN Grants 2009ZSC5K2 004 and 20098SJX4F 004) for financial supports. Thanks are also given to Mr Paolo Formaglio for NMR experiments and to Mrs Ercolina Bianchini for elemental analyses.

Notes and references

1 (*a*) A. J. von Wangelin, H. Neumann, D. Gördes, S. Klaus, D. Strübing and M. Beller, *Chem.–Eur. J.*, 2003, **9**, 4286–4294; (*b*) J. Andraos, *Org. Process Res. Dev.*, 2005, **9**, 149–163.

2 (*a*) *Enantioselective Organocatalysis*, ed. P. I. Dalko, Wiley-VCH, Weinheim, 2007; (*b*) *Chem Rev.*, guest ed. B. List, 2007, **107**, 5413–5883 (*c*) A. Dondoni and A. Massi, *Angew. Chem., Int. Ed.*, 2008, **47**, 4638–4660; (*d*) E. N. Jacobsen and D. W. C. MacMillan, *Proc. Natl. Acad. Sci. U. S. A.*, 2010, **107**, 20618–20619.

3 (*a*) K. Geyer, T. Gustafsson and P. H. Seeberger, *Synlett*, 2009, **15**, 2382–2391; (*b*) B. P. Mason, K. E. Price, J. L. Steinbacher, A. R. Bogdan and D. T. McQuade, *Chem. Rev.*, 2007, **107**, 2300–2318; (*c*) I. R. Baxendale, S. V. Ley, A. C. Mansfield and C. D. Smith, *Angew. Chem., Int. Ed.*, 2009, **48**, 4017–4021; (*d*) I. R. Baxendale, J. J. Hayward, S. Lanners, S. V. Ley and C. D. Smith, in *Microreactors in Organic Synthesis and Catalysis*, ed. T. Wirth, Wiley-VCH, Weinheim, 2008, ch. 4.2, pp. 84–122; (*e*) I. R. Baxendale, J. J. Hayward and S. V. Ley, *Comb. Chem. High Throughput Screening*, 2007, **10**, 802–836; (*f*) A. R. Bogdan, S. L. Poe, D. C. Kubis, S. J. Broadwater and D. T. McQuade, *Angew. Chem., Int. Ed.*, 2009, **48**, 8547–8550. For a recent review, see: (*g*) C. Wiles and P. Watts, *Green Chem.*, 2012, **14**, 38.

4 A. Massi, A. Cavazzini, L. Del Zoppo, O. Pandoli, V. Costa, L. Pasti and P. P. Giovannini, *Tetrahedron Lett.*, 2011, **52**, 619–622.

5 In light of this new paradigm, Odera and Seeberger reported the first homogeneous organocatalytic aldol and Mannich reactions in microfluidic devices: (*a*) A. Odedra and P. H. Seeberger, *Angew. Chem., Int. Ed.*, 2009, **48**, 2699–2702. For a general discussion on the potential of this approach in the field of fine chemicals and pharmaceuticals production, see: (*b*) A. Kirschning, W. Solodenko and K. Mennecke, *Chem.–Eur. J.*, 2006, **12**, 5972–5990; (*c*) A. El Kadib, R. Chimenton, A. Sachse,

F. Fajula, A. Galarneau and B. Coq, *Angew. Chem., Int. Ed.*, 2009, **48**, 4969–4972; (*d*) F. E. Valera, M. Quaranta, A. Moran, J. Blacker, A. Armstrong, J. T. Cabral and D. G. Blackmond, *Angew. Chem., Int. Ed.*, 2010, **49**, 2478–2485. For a recent review on the combination of heterogeneous catalysis with microreactor technology, see: (*e*) C. G. Frost and L. Mutton, *Green Chem.*, 2010, **12**, 1687–1703.

6 For a review on continuous-flow asymmetric reactions, see: X. Y. Mak, P. Laurino and P. H. Seeberger, *Beilstein J. Org. Chem.*, 2009, **5**, DOI: 10.3762/bjoc.5.19.

7 (*a*) C. Ayats, A. H. Henseler and M. A. Pericàs, *ChemSusChem*, 2012, DOI: 10.1002/cssc.201100570; (*b*) X. C. Cambeiro, R. Martín-Rapún, P. O. Miranda, S. Sayalero, E. Alza, P. Llanes and M. A. Pericàs, *Beilstein J. Org. Chem.*, 2011, **7**, 1486–1493; (*c*) A. L. W. Demuynck, L. Peng, F. de Clippel and J. Vanderleyden, *Adv. Synth. Catal.*, 2011, **353**, 725–732; (*d*) E. Alza, S. Sayalero, X. C. Cambeiro, R. Martín-Rapún, P. O. Miranda and M. A. Pericàs, *Synlett*, 2011, 464–468; (*e*) E. Alza, C. Rodríguez-Escrich, S. Sayalero, A. Bastero and M. A. Pericàs, *Chem.–Eur. J.*, 2009, **15**, 10167–10172; (*f*) F. Bonfils, I. Cazaux, P. Hodge and C. Caze, *Org. Biomol. Chem.*, 2006, **4**, 493–497; (*g*) D. Bernstein, S. France, J. Wolfer and T. Lectka, *Tetrahedron: Asymmetry*, 2005, **16**, 3481–3483; (*h*) S. France, D. Bernstein, A. Weatherwax and T. Lectka, *Org. Lett.*, 2005, **7**, 3009–3012; (*i*) A. M. Hafez, A. E. Taggi, T. Dudding and T. Lectka, *J. Am. Chem. Soc.*, 2001, **123**, 10853–10859.

8 For a rationalization of the solvent/additive effect in the irreversible deactivation *via* decarboxylation of proline in the presence of electron-deficient aromatic aldehydes, see: N. Zotova, A. Franzke, A. Armstrong and D. G. Blackmond, *J. Am. Chem. Soc.*, 2007, **129**, 15100–15101.

9 For the utilization of homogeneous prolinamide organocatalysts, see: (*a*) W. Notz, F. Tanaka and C. F. Barbas III, *Acc. Chem. Res.*, 2004, **37**, 580–591; (*b*) J. Xu, X. Fu, C. Wu and X. Hu, *Tetrahedron: Asymmetry*, 2011, **22**, 840–850, and references therein.

10 For a recent review on proline sulfonamide based organocatalysts, see: H. Yang and R. G. Carter, *Synlett*, 2010, 2837–2828.

11 For the use of homogeneous 11(*S*)-5-(pyrrolidin-2-yl)-1*H*-tetrazole in organocatalytic strategies, see: (*a*) D. A. Longbottom, V. Franckevičius, S. Kumarn, A. J. Oelke, V. Wascholowski and S. V. Ley, *Aldrichim. Acta*, 2008, **41**, 3–11; (*b*) S. Kumarn, A. J. Oelke, D. M. Shaw, D. A. Longbottom and S. V. Ley, *Org. Biomol. Chem.*, 2007, **5**, 2678–2689; (*c*) A. J. A. Cobb, D. M. Shaw, D. A. Longbottom, J. B. Gold and S. V. Ley, *Org. Biomol. Chem.*, 2005, **3**, 84–96; (*d*) V. Franckevičius, K. R. Knudsen, M. Ladlow, D. A. Longbottom and S. V. Ley, *Synlett*, 2006, 889–892; (*e*) A. J. Oelke, S. Kumarn, D. A. Longbottom and S. V. Ley, *Synlett*, 2006, 2548–2552; (*f*) C. E. T. Mitchell, A. J. A. Cobb and S. V. Ley, *Synlett*, 2005, 611–614; (*g*) A. J. A. Cobb, D. M. Shaw and S. V. Ley, *Synlett*, 2004, 558–560; (*h*) A. Hartikka and P. I. Arvidsson, *Tetrahedron: Asymmetry*, 2004, **15**, 1831–1834; (*i*) A. Hartikka and P. I. Arvidsson, *Eur. J. Org. Chem.*, 2005, 4287–4295; (*j*) H. Torii, M. Nakadai, K. Ishihara, S. Saito and H. Yamamoto, *Angew. Chem., Int. Ed.*, 2004, **43**, 1983–1986; (*k*) N. Momiyama, H. Torii, S. Saito and H. Yamamoto, *Proc. Natl. Acad. Sci. U. S. A.*, 2004, **101**, 5374–5378; (*l*) N. S. Chowdari, M. Ahmad, K. Albertshofer, F. Tanaka and C. F. Barbas III, *Org. Lett.*, 2006, **8**, 2839–2842. For the optimized synthesis of 11(*S*)-5-(pyrrolidin-2-yl)-1*H*-tetrazole and previous reports on this matter, see: (*m*) V. Aureggi, V. Franckevičius, M. O. Kitching, S. V. Ley, D. A. Longbottom, A. J. Oelke and G. Sedelmeier, *Org. Synth.*, 2008, **85**, 72–87; (*n*) J. M. McManus and R. M. Herbst, *J. Org. Chem.*, 1959, **24**, 1643–1649; (*o*) R. G. Almquist, W.-R. Chao and C. Jennings-White, *J. Med. Chem.*, 1985, **28**, 1067–1071. For an application to natural product synthesis, see: (*p*) D. E. Ward, V. Jheengut and G. E. Beye, *J. Org. Chem.*, 2006, **71**, 8989–8992.

12 (*a*) A. B. Lowe, *Polym. Chem.*, 2010, **1**, 17–36; (*b*) P. Jonkheijm, D. Weinrich, M. Köhn, H. Engelkamp, P. C. M. Christianen, J. Kuhlmann, J. C. Maan, D. Nüsse, H. Schroeder, R. Wacker, R. Breinbauer, C. M. Niemeyer and H. Waldmann, *Angew. Chem., Int. Ed.*, 2008, **47**, 4421–4424.

13 F. Fache and O. Piva, *Tetrahedron: Asymmetry*, 2003, **14**, 139–143.

14 Thiol–silica **14** is commercially available from Sigma-Aldrich. Nevertheless, better results in continuous-flow experiments were detected by using immobilized proline mimetics **2–4** obtained from freshly prepared **14** (see Experimental section for details).

15 Screened solvents were toluene, acetonitrile, dichloromethane, DMSO, and diisopropyl ether. The effect of temperature and variation of reagent molar ratios were not considered at this stage of the study.

16 It has to be pointed out that reactions considered in this comparison have been optimized with a lower loading of homogeneous catalyst (typically, 5–15 mol% of unsupported tetrazole *vs.* 30 mol% of **4**). Moreover, modest enantioselectivities were also detected in Michael and α-amination reactions under homogeneous tetrazole catalysis. Higher enantioselectivities were achieved by Ley and co-workers in Michael additions to nitro-olefins by using a homo-proline tetrazole catalyst (ref. 11*f*).

17 The effect on catalyst **4** activity of free hydroxyls capping with hydrophilic and hydrophobic moieties is currently under investigation in our laboratories.

18 A detailed study on the kinetics and thermodynamics of the continuous-flow model aldol reaction promoted by either catalyst **1** or **4** will be reported in due course along with a suitable in-line analysis method.

19 The equation for the experimental determination of the retention factor k' is: $k' = (t_r - t_0)/t_0$, where t_r is the retention time of the species under evaluation and t_0 is the hold-up time of the column. The hold-up time t_0 can be easily calculated by dividing the hold-up volume V_0 by the flow rate. In microreactor technology literature, this is the so called residence time.

20 Typically, the steady-state regime is reached *ca.* 30 minutes after the first elution of the more retained aldehyde.

21 For a discussion on the beneficial effect of temperature on the catalytic activity of unsupported (*S*)-5-(pyrrolidin-2-yl)-1*H*-tetrazole, see ref. 5*d*.

22 (*a*) F. Gasparrini, D. Misiti and C. Villani, *J. Org. Chem.*, 1995, **60**, 4314–4315; (*b*) F. Gasparrini, G. Cancelliere, A. Ciogli, I. D'Acquarica, D. Misiti and C. Villani, *J. Chromatogr., A*, 2008, **1191**, 205–213.

23 V. A. Soloshonok, *Angew. Chem., Int. Ed.*, 2006, **45**, 766–769.

CHEMISTRY
A EUROPEAN JOURNAL

ChemPubSoc
Europe

DOI: 10.1002/chem.201300181

A Combined Kinetic and Thermodynamic Approach for the Interpretation of Continuous-Flow Heterogeneous Catalytic Processes

Olga Bortolini,[a] Alberto Cavazzini,*[b] Pier Paolo Giovannini,[a] Roberto Greco,[b] Nicola Marchetti,[b] Alessandro Massi,*[a] and Luisa Pasti[b]

Dedicated to Professor Alessandro Dondoni on the occasion of his retirement

Abstract: The heterogeneous proline-catalyzed aldol reaction was investigated under continuous-flow conditions by means of a packed-bed microreactor. Reaction-progress kinetic analysis (RPKA) was used in combination with nonlinear chromatography for the interpretation, under synthetically relevant conditions, of important mechanistic aspects of the heterogeneous catalytic process at a molecular level. The information gathered by RPKA and nonlinear chromatography proved to be highly complementary and allowed for the assessment of optimal operating variables. In particular, the determination of the rate-determining step was pivotal for optimizing the feed composition. On the other hand, the competitive product inhibition was responsible for the unexpected decrease in the reaction yield following an apparently obvious variation in the feed composition. The study was facilitated by a suitable 2D instrumental arrangement for simultaneous flow reaction and online flow-injection analysis.

Keywords: aldol reaction · flow chemistry · heterogeneous catalysis · nonlinear chromatography · organocatalysis

Introduction

Currently, continuous-flow microreactors are emerging as new synthetic platforms for the sustainable, safe, and intensified production of fine chemicals and pharmaceuticals.[1] In particular, heterogeneous catalysis under a flow regime provides a useful addition to microreactor technology and allows for simple product/catalyst separation, high resistance of supports to mechanical degradation, and long-term usage of (often costly) catalytic packing materials.[2] Very recently, organocatalytic packed-bed microreactors[3] have been demonstrated to show additional and unusual benefits, such as the absence of metal leaching and high levels of stereoselectivity in continuous-flow syntheses of valuable chiral molecules.[4] In those studies,[3,4] operative flow conditions (feed composition and temperature) typically result from the direct translation of batch-mode conditions with only minor empirical adjustments. Furthermore, shorter (minutes versus hours) residence/reaction times are normally detected in the flow regime to reach the same level of batch conversion. A rationalization for these observations, however, is generally not supported by a true understanding of the heterogeneous catalytic process. Indeed, although the microreactor inlet and outlet can be transparently examined during the course of the reaction, the catalytic bed is an opaque medium, which severely complicates the interpretation of the heterogeneous process. Therefore, despite some spectroscopic methods having been developed for in situ analysis of the active catalysts,[5] noninvasive and cost-effective measurements for investigating mechanism, kinetics, and thermodynamics of the process under the real working conditions are still a challenge. Herein, we propose a practical method to approach the above issues. This relies on the combination of reaction progress kinetic analysis (RPKA), a powerful methodology developed by Blackmond for the study of kinetic and mechanistic properties under synthetically relevant conditions,[6] and nonlinear chromatography tools (principally, frontal analysis measurements[7]) for the thermodynamic interpretation of the catalytic process in the flow regime. The data described herein finally show that merging kinetic and thermodynamic information with a deep understanding of mechanistic constraints might result in the effective design of productivity-enhancing improvements.

[a] O. Bortolini, P. P. Giovannini, Dr. A. Massi
Dipartimento di Scienze Chimiche e Farmaceutiche
Laboratorio di Chimica Organica
Università di Ferrara, Via L. Borsari 46
44121 Ferrara (Italy)
Fax: (+39) 0532-455183
E-mail: alessandro.massi@unife.it

[b] Dr. A. Cavazzini, R. Greco, N. Marchetti, L. Pasti
Dipartimento di Scienze Chimiche e Farmaceutiche
Laboratorio di Chimica Analitica
Università di Ferrara
44100 Ferrara (Italy)
E-mail: alberto.cavazzini@unife.it

Supporting information for this article is available on the WWW under http://dx.doi.org/10.1002/chem.201300181.

Results and Discussion

The previously investigated[4a,d] heterogeneous proline-catalyzed continuous-flow aldol reaction of cyclohexanone (**1**)

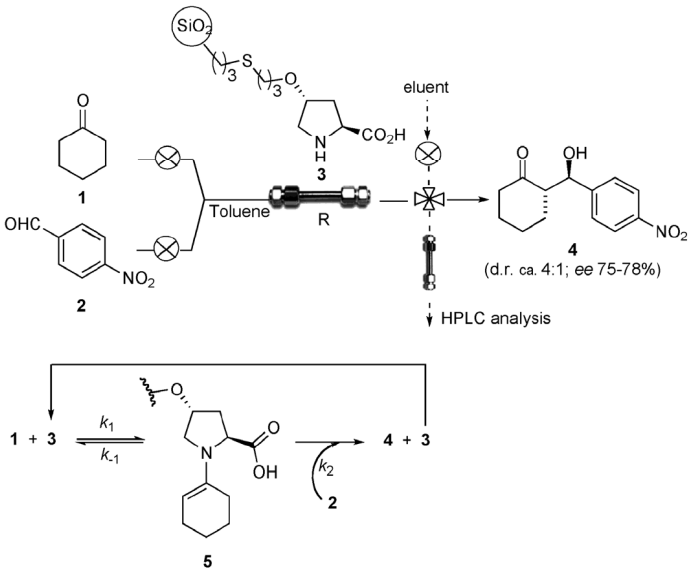

Scheme 1. Continuous-flow model aldol reaction.

with *p*-nitrobenzaldehyde (**2**) was considered as the benchmark for this proof-of-concept study. The generally accepted mechanism for the reaction in Scheme 1 involves the nucleophilic attack of silica-supported proline (**3**) on carbonyl compound **1** to form enamine **5**, followed by its attack on electrophile **2** to yield product **4** with release of catalyst **3**. The proposal of Scheme 1 simplifies the whole mechanistic picture as it omits the intrinsic effect of water within the catalytic cycle.[8] Accordingly, the possible kinetic role of added water, for which a negative order dependence was ascertained by Blackmond and coworkers in a similar process under homogeneous catalysis,[9] is not considered in the present study.

Hence, the overall sequence of Scheme 1 appears reminiscent of the Michaelis–Menten enzymatic reaction for which the applicable rate expression might be written in power-law form as in Equation (1), in which the constant proline **3** concentration (i.e., the loaded amount of catalyst) has been grouped into the constant k^*.

$$\text{Rate} = k[\mathbf{1}]^x[\mathbf{2}]^y[\mathbf{3}] = k^*[\mathbf{1}]^x[\mathbf{2}]^y \quad (1)$$

The determination of the reaction order and interpretation of the reaction mechanism by RPKA are, however, complicated by the heterogeneous nature of the process and its long timescale. A suitable instrumental setup facilitated the experimental work because it allowed online monitoring by HPLC analysis with a high density of data collection. For the sake of validation, correlation between the measured reactant/product concentrations and reaction progress was also confirmed by discontinuous sampling and NMR spectroscopic analysis of the eluate. Figure 1 describes the whole 2D equipment for simultaneous flow-reaction and flow-injection analysis. Concisely (for a more detailed description, see the Supporting Information), in direction-1, the microreactor R (stainless-steel packed column, 100×2.1 mm) is connected to pump-1 through a mixer chamber. Channels A and B are used to deliver the solutions of **1** and **2** in toluene, respectively. The effluent from the microreactor is redirected to a 6-port 2-position switching valve. In direction-2, the binary pump-2 delivers a hexane/*i*PrOH solution into a hydrophilic interaction liquid chromatography (HILIC) column by passing through the switching valve. This is controlled by software and allows for the switching from the "load" position (Figure 1, lower left), in which the sampling loop (2–5) is filled with the effluent from the microreactor, to the "inject" position (Figure 1, lower right), for flushing the content of the loop into the HILIC column for fraction conversion determination.

The main features of the packed-bed microreactor R (hold-up volume V_0, total porosity, and loading of silica **3**) were determined by pycnometry and elemental analysis (see the Supporting Information). They are summarized in Table 1.

According to RPKA, the concentration dependencies and the stability of the catalytic system can be probed using the

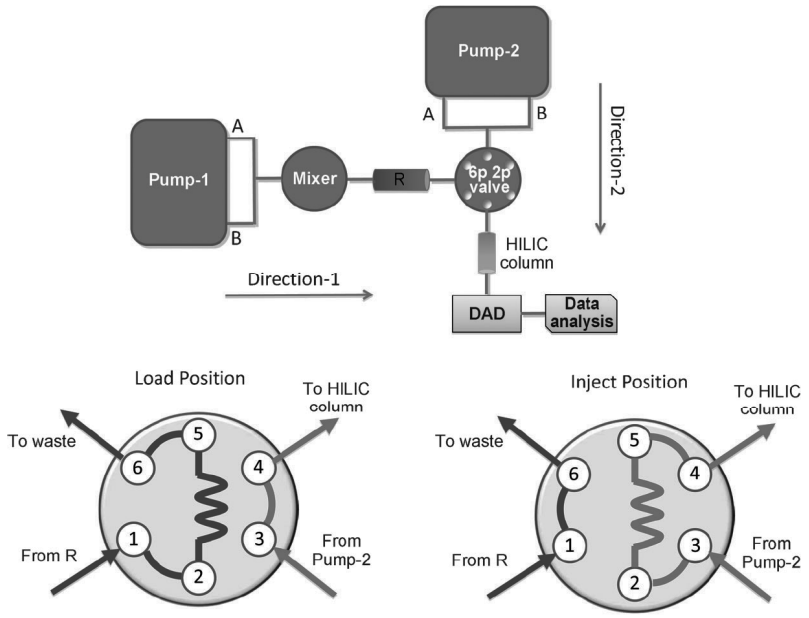

Figure 1. Scheme of the 2D instrumental setup for flow-reaction and flow-injection analysis. Top: Block diagram (R: microreactor; 6p2p valve: 6-port, 2-position switching valve). Bottom: Magnification on the 6-port 2-position valve to show the "load" (left) and the "inject" (right) position.

Table 1. Main features of microreactor R.

Loading of **3** [mmol g^{-1}][a]	Amount of **3** [mg][b]	V_0 [μL][b]	V_G [μL][b,c]	V_{bed} [μL][b,d]	t [min][e]	Total porosity[f]
0.81	190	230	346	110	46	0.67

[a] Determined by elemental analysis. [b] See the Supporting Information. [c] Geometric volume. [d] $V_{bed}=V_G-V_0$. [e] Residence time calculated at 5 μL min^{-1}. [f] Total porosity $\varepsilon_{tot}=V_0/V_G$.

"different excess" and "same excess" protocols, respectively.[6] In the context of RPKA, the term "excess" [*e*] defines the difference in initial concentrations of two reactants (i.e., $[e]=[\mathbf{1}]_0-[\mathbf{2}]_0$).[6] In the case of heterogeneous reactions, the excess must refer to the system taken as a whole.[10] However, as long as mass transfer and adsorption–desorption processes are so rapid that a constant equilibrium state can be assumed between the bulk and the solid phase,[11] RPKA can be properly employed.[10] Table 2 reports the initial concentrations of substrates **1** and **2** and the excess value for each of the four kinetic runs in this study.

Table 2. Experimental conditions for reaction-progress kinetic analysis of continuous-flow proline **3**-catalyzed aldol reaction of cyclohexanone **1** with aldehyde **2** at 25 °C in toluene.[a]

Entry	$[\mathbf{1}]_0$ [M]	$[\mathbf{2}]_0$ [M]	Excess [M]
1	2.40	0.10	2.30
2	2.35	0.05	2.30
3	1.80	0.10	1.70
4	1.20	0.10	1.10

[a] See the Supporting Information for experimental procedures.

Reaction results for the illustrative first experiment are plotted in Figure 2 as conversion of **2** relative to residence time. Indeed, to the best of our knowledge, this study represents the first example of application of RPKA under heterogeneous flow conditions.[12] Thus, the curve of Figure 2 was obtained by measuring the steady-state conversion of different experiments performed with the same reactor and feed composition but at different flow rates.[13]

The more informative rate versus [**2**] plot (Figure 3) was then generated by differentiation of the concentration profile of Figure 2; the same plot was also produced for run 2, which was performed at the half-life of run 1. The overlay in Figure 3 of these "same excess" experiments confirmed that the total concentration of active catalyst **3** remained constant during the continuous-flow process, and that the rate is not significantly influenced by product inhibition (at least under conditions of runs 1 and 2).[14]

Reaction orders of reactants **1** and **2** were next determined by the "different excess" protocol. Accordingly, kinetic profiles were obtained for runs 3 and 4 and plotted as in Figure 4 ("normalized" rate versus concentration). While the overlay between the two curves showed first-order kinetics in the "normalized" substrate [**1**] ($x=1$), the found

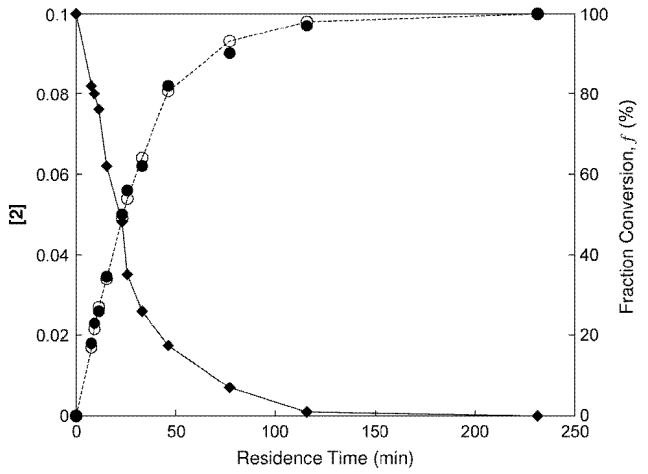

Figure 2. Kinetic profile for the model aldol reaction carried out under conditions shown in Table 2 (entry 1). Diamonds: **2** (left *y* axis); circles: percentage fraction conversion (right *y* axis) estimated by HPLC (○) and NMR spectroscopy (●).

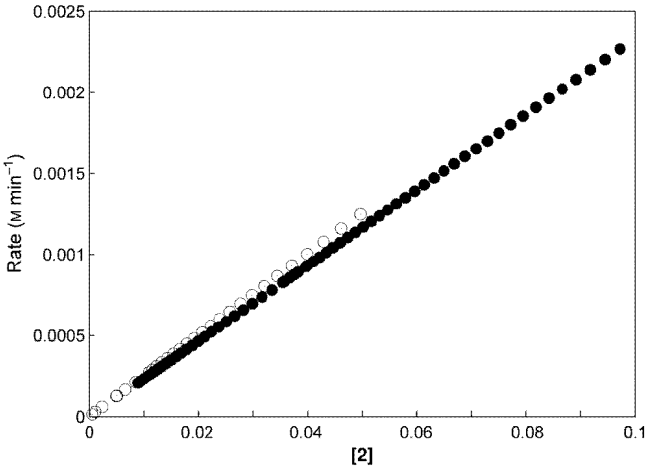

Figure 3. Rate versus [**2**] for "same excess" experiments as given in Table 1 (●: entry 1; ○: entry 2).

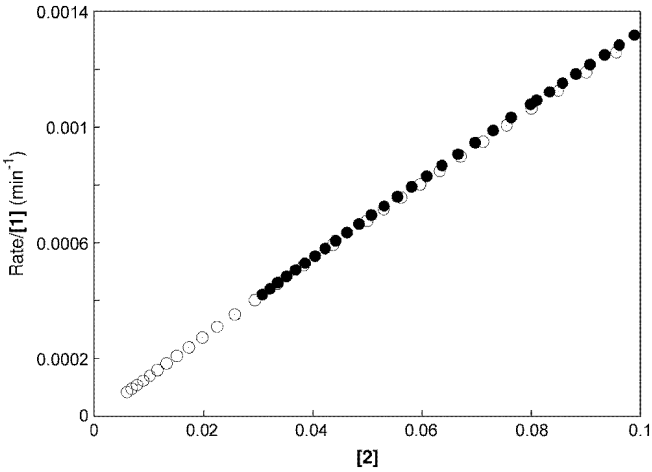

Figure 4. Rate/[**1**] versus **2** for "different excess" experiments as given in Table 2 (○: entry 3; ●: entry 4).

linear correlation reflected first-order kinetics in [**2**] ($y=1$).[6]

The catalytic network of Scheme 1 is suitably described by the full steady-state rate Equation (2), which is written in terms of the elementary-step rate constants.

$$\text{Rate} = k_1 k_2[\mathbf{1}][\mathbf{2}][\mathbf{3}_{tot}]/(k_{-1} + k_1[\mathbf{1}] + k_2[\mathbf{2}]) \quad [\mathbf{3}_{tot}] = [\mathbf{3}] + [\mathbf{5}] \tag{2}$$

It becomes evident from the presence of the denominator term in Equation (2) that simple first-order dependence in the concentration of reactants cannot be assumed as a general result, and that the intrinsic kinetic role of both substrates can be quite complicated. Hence, following the approach described by Blackmond and co-workers in their batch study on a homogeneous proline-catalyzed aldol reaction,[9] a possible correlation between the theoretical steady-state and experimentally found power-law rate equations was considered in the two limiting cases in which: 1) the reaction that consumes enamine **5** is the slow step [in this case, Eq. (2) is reduced to Eq. (3)]; 2) the rate-determining step is the formation of enamine **5**, and the unactivated catalyst **3** represents the "resting state" of the catalyst [Eq. (4)].

$$\text{Rate} = k_2[\mathbf{5}][\mathbf{2}] \tag{3}$$

$$\text{Rate} = k_1[\mathbf{1}][\mathbf{3}] \tag{4}$$

We shall see that the observed first-order dependence of rate on [**1**] and [**2**] is consistent only with Equation (3). Indeed, since for each molecule of cyclohexanone adsorbed on the immobilized proline ($\mathbf{1}_{ads}$), one molecule of enamine **5** is formed, Equation (3) can be recast in the form of Equation (5), provided that mass-transfer effects are negligible.[11]

$$\text{Rate} = k_2[\mathbf{1}_{ads}][\mathbf{2}] \tag{5}$$

The importance of this formulation is that it establishes a connection between the measurable quantity [$\mathbf{1}_{ads}$] and the reaction rate. In fact, [$\mathbf{1}_{ads}$] can be measured through the (competitive) adsorption isotherm, which relates the adsorbed amount to the bulk fluid phase concentrations of substrates **1**, **2**, and even product **4**, which is produced in the microreactor during the process.[7] Equation (5) thus gives an appropriate mathematical form to use in testing a proposed reaction rate expression. The basis for most analyses of this type is the Langmuir competitive isotherm [Eq. (6), in which q_s = monolayer saturation capacity [M], a, b, c = adsorption equilibrium constants[15] for substrates **1**, **2**, and **4**, respectively [M^{-1}]]. This model assumes that both **2** and product **4** might compete with **1** for the adsorption on the (homogeneous) silica surface.[16] The product terms, b[**2**] and c[**4**], quantify the competitive adsorption by **2** and **4**.[17]

$$[\mathbf{1}_{ads}] = q_s a[\mathbf{1}]/(1 + a[\mathbf{1}] + b[\mathbf{2}] + c[\mathbf{4}]) \tag{6}$$

If one assumes that, in the denominator of Equation (6), a[**1**] outweighs the other two product terms (which means the absence of competitive adsorption) and, simultaneously, that $a[\mathbf{1}] \ll 1$ (that is, [**1**] belongs to the linear range of the adsorption isotherm), [$\mathbf{1}_{ads}$] would be linearly proportional to the bulk concentration of cyclohexanone **1** ([$\mathbf{1}_{ads}$] = $q_s a$[**1**]), and the rate Equation (5) would reduce to Equation (7) [$k'_2 = k_2 q_s a$], which is consistent with our experimental finding (first-order dependence in either reactants).

$$\text{Rate} = k'_2[\mathbf{1}][\mathbf{2}] \tag{7}$$

Thus, the validity of the assumptions that lead to simplified rate Equation (7) has been examined for the experimental conditions of Table 2 by a chromatographic study. Essentially, our scope is to test that competitive adsorption can be neglected and that the isotherm is linear. To this end, both linear measurements (namely, the retention factors of **1**, **2**, and **4** on the silica-supported proline **3** using toluene as eluent) and nonlinear measurements (i.e., the adsorption isotherm of cyclohexanone **1** from toluene on silica-supported proline **3**)[18] were performed (details in the Supporting Information). Since, under the assumption of the same saturation factor, the ratio of the retention factors of two substrates corresponds to the ratio of their adsorption equilibrium constants,[19] the chromatographic study allows us to establish that the adsorption constant of **2** [b in Eq. (6)] is roughly twice that of **1** [a in Eq. (6)], and that c (the adsorption constant of product **4**) is about four times larger than a. Accordingly, the denominator of Equation (6) can be rewritten as Equation (8), which has the advantage of permitting an easier comparison of the relative magnitude of the terms in brackets.

$$1 + a([\mathbf{1}] + 2[\mathbf{2}] + 4[\mathbf{4}]) \tag{8}$$

Since the concentration ratio of feed components $[\mathbf{1}]_0/[\mathbf{2}]_0$ was 18:1 and 12:1, respectively, for entries 3 and 4 of Table 2, the assumption that *p*-nitrobenzaldehyde **2** does not compete for the adsorption with cyclohexanone **1** (i.e., $2[\mathbf{2}] \ll [\mathbf{1}]$) appears to be entirely reasonable. As for the competitive adsorption by product **4**, the situation is complicated by the fact that **4** is generated inside the reactor. RPKA, however, comes to our aid, as the "same excess" experiments excluded product inhibition (Figure 3). Inasmuch as the competitive adsorption by the product would reasonably be a source of catalyst deactivation, the conclusion that product **4** does not compete for the adsorption under the conditions of Table 2 would seem to be sound. Translated into a mathematical form, this means $4[\mathbf{4}] \ll [\mathbf{1}]$. A deeper examination of this last inequality is central to our subsequent rationalization, and it requires knowledge of fraction conversions. Under the conditions of Table 2, entry 3, a 52% conversion is achieved with a residence time of 45 min.[20] Accordingly, [**4**] at the microreactor outlet is about 0.05 M, and the term 4[**4**], which we might refer to as the competition factor of product **4**, results in roughly 10%

Table 3. Relationship between concentration of cyclohexanone **1** in the feed ($[\mathbf{1}]_0$) and amount of adsorbed cyclohexanone ($\mathbf{1}_{ads}$), relative surface coverage (θ), and percentage fraction conversion (f). Process conditions: residence time, 45 min; constant ratio of feed concentrations, $[\mathbf{1}]_0/[\mathbf{2}]_0 = 24{:}1$.

Entry	$[\mathbf{1}]_0$ [M]	$\mathbf{1}_{ads}$ [μmol][a]	θ[b]	f [%]
1	0.2	12	0.08	8
2	0.6	40	0.26	20
3	1.2	77	0.50	40
4	1.8	106	0.68	56
5	2.4	119	0.77	64
6	3.6	142	0.92	85
7	4.0	143	0.93	83
8	4.4	144	0.94	84
9	5.0	146	0.95	82

[a] Per reactor. Calculated by frontal analysis. [b] Calculated as the ratio between $\mathbf{1}_{ads}$ and the total amount of silica-supported proline **3** in the reactor (154 μmol). See the Supporting Information for details.

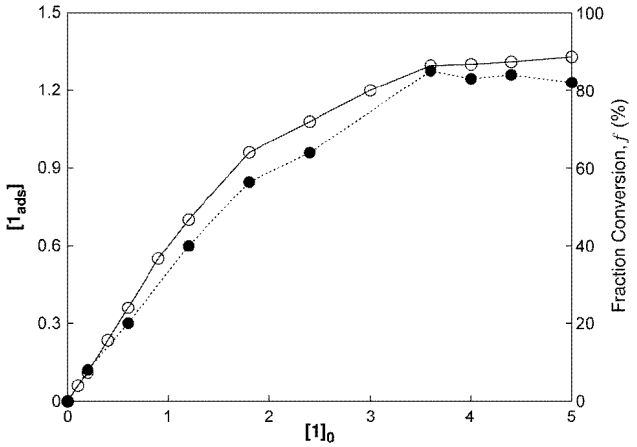

Figure 5. Adsorption isotherm of cyclohexanone from toluene on silica-supported proline **3** (○, left y axis) and percentage fraction conversion (●, right y axis) versus cyclohexanone concentration $[\mathbf{1}]_0$. Adsorbed concentration of cyclohexanone **1** ($[\mathbf{1}_{ads}]$) in micromole per microliter of packing (V_{bed}). Process conditions as in Table 3.

of the cyclohexanone concentration in the feed ($[\mathbf{4}]/[\mathbf{1}]_0 = 0.2{:}1.8$). Thus, this simple reasoning will be employed as an indication for estimating the presence of competitive adsorption by the product (see below).

The adsorption isotherm of cyclohexanone **1** (columns 2 and 3 in Table 3 and Figure 5) allowed us to evaluate the meaning of the last approximation introduced to obtain Equation (7) with regard to the linearity of the adsorption isotherm (or, $a[\mathbf{1}] \ll 1$). As the isotherm exhibits a substantially linear behavior until $[\mathbf{1}]_0 = 1.8$ M, the condition holds in the concentration ranges of entries 3 and 4 of Table 2. Hence, it is possible to conclude that under these conditions, the full steady-state rate Equation (2) simplifies to Equation (7), and that enamine addition to aldehyde is the rate-determining step, which is in agreement with the homogeneous case.[9]

By increasing the concentration of **1** in the feed above 1.8 M, however, the adsorption isotherm exhibits at first a curvature (for $1.8 < [\mathbf{1}]_0 < 3.6$), and then it flattens out ($[\mathbf{1}]_0 > 3.6$), which indicates that saturation capacity has been reached (fractional surface coverage is given in column 4 of Table 3). Thus for $[\mathbf{1}]_0 > 1.8$, the simple kinetic model given by Equation (7) is not expected to hold any longer. Consequently, a series of ad hoc experiments were conducted to investigate the process outcome under these regimes (entries 5–9 in Table 3) and eventually find a correlation between the estimated surface coverage (Table 3, column 4) and fraction conversion (Table 3, column 5).

In the concentration interval $1.8 < [\mathbf{1}]_0 < 3.6$, the steady-state rate Equation (2) assumes the form given by Equation (9), since the competitive adsorption by both *p*-nitrobenzaldehyde **2** and product **4** can be neglected under the conditions of runs 4 and 5 of Table 3. The statement on [**2**] is justified by the strongly unfavorable 24:1 feed ratio $[\mathbf{1}]_0/[\mathbf{2}]_0$, whereas that on [**4**] comes from the consideration that the product term $4[\mathbf{4}]$ is smaller than 10% of $[\mathbf{1}]_0$, as it was in the case in which RPKA excluded product inhibition.

$$\text{Rate} = k'_2[\mathbf{1}][\mathbf{2}]/(1 + a[\mathbf{1}]) \quad (9)$$

Since the first-order dependence of [**1**] in the numerator is tempered by the concentration term in the denominator, the fraction conversion is expected to increase more slowly as $[\mathbf{1}]_0$ increases than in the linear range of the isotherm. This is demonstrated by the change in the slope of the plot of fraction conversion relative to $[\mathbf{1}]_0$ (dotted line in Figure 5), which drops from about 30 when $[\mathbf{1}]_0 < 1.8$ (Table 3, entries 1–4) to less than 15 if $1.8 < [\mathbf{1}]_0 < 3.6$ (Table 3, entries 4–6). Finally, at the isotherm plateau (i.e., for $[\mathbf{1}]_0 > 3.6$), the fraction conversion is found to be practically constant (Table 3, entries 7–9).

Under these conditions, all the available silica-supported proline **3** is transformed to enamine **5** (Table 3, column 4), and any further increase in concentration (keeping the ratio $[\mathbf{1}]_0/[\mathbf{2}]_0$ and residence time constant) does not affect the conversion efficiency (Table 3, column 5). These considerations show that 3.6 M is the optimal cyclohexanone feed concentration for the reactor R employed in this work. The study was concluded with the evaluation of the optimal concentration of aldehyde **2** in the feed by performing different experiments in which $[\mathbf{1}]_0$ was kept constant at the 3.6 M value. After some experimentation, it turned out that $[\mathbf{2}]_0 = 0.1$ M furnished an almost quantitative conversion ($f = 98\%$). A full explanation of this result is not a trivial task, as it requires the modeling of the spatial and temporal distribution of the concentration profiles of all compounds (**1**, **2**, and **4**) between the bulk and the adsorbed phase inside the microreactor. This study is currently underway in our laboratories and will be the subject of a forthcoming publication.

Conclusion

In this proof-of-concept study, we have proposed an innovative approach for the characterization of heterogeneous catalytic reactions in flow mode. In particular, we have focused

on the proline-catalyzed aldol reaction, which has been extensively investigated under homogeneous batch conditions. Essentially, we have coupled the kinetic information that comes from the application of reaction-progress kinetic analysis (RPKA) with the thermodynamic information that results from nonlinear chromatographic measurements. Significantly, the two methodologies turned out to be strongly complementary and allowed for a clear understanding of important features of the heterogeneous continuous-flow process, such as the dependence of the reaction order on feed composition and saturation capacity of the catalytic bed.

Experimental Section

Microreactor packing: Microreactor R was fabricated by using a 100× 2.1 mm stainless-steel column, which was filled with silica **3** by slurry-packing. Slurry-packing was performed under constant pressure (300 bar, 30 min, toluene as solvent) by using an air-driven liquid pump. The slurry was prepared by suspending an excess in weight of functionalized silica in toluene.

Kinetic analysis: For the determination of reaction profiles at constant flow rate (reaction isotherm curve; Figure S2 in the Supporting Information), microreactor R was fed with a solution of **1** (2.40 M) and **2** (0.10 M) in toluene and operated at 25 °C for about 4 h at 2 μL min^{-1}. Fraction conversion was determined by online HPLC analysis (see Figure 1) and by ^{1}H NMR spectroscopic analysis (a sample of the eluate was taken every 40 min). The collected solution at the steady-state regime was finally concentrated and eluted from a column of silica gel with 5:1 toluene/AcOEt to give the corresponding mixture of *anti*/*syn* adducts **4**. This kinetic study was repeated with the same feed composition but at different flow rates to determine the kinetic profile depicted in Figure 2. To complete the RPKA of the model reaction, the above approach was then applied to all the experiments of Table 2.

Chromatographic measurements: The binary pump-2 delivered a hexanes/*i*PrOH 99.7:0.3 (v/v) solution into a 150×4.6 mm 5 μm-particle-diameter HILIC column by passing through the switching valve (see Figure 1). The flow rate along direction-2 was 1 mL min^{-1}. Under these conditions, the retention times of **2**, *syn*-, and *anti*-aldol product were 2.3, 6.4, and 11.2 min, respectively. The detector was calibrated at 290 nm for both **2** and **4** (different calibration curves were employed depending on the concentration of cyclohexanone **1** in the feed).

In separate experiments, microreactor R was used as a chromatographic column for determining the retention factors of **1**, **2**, and **4**. The mobile phase was pure toluene. The adsorption isotherm of **1** on silica **3** was measured from toluene by frontal analysis (see the Supporting Information for details).

Acknowledgements

We gratefully acknowledge the Italian Ministry of University and Scientific Research (Progetto PRIN grant nos. 2009ZSC5K2 004 and 20098SJX4F 004) for financial support. Thanks are also given to Mr. Paolo Formaglio for NMR spectroscopic experiments and to Mrs. Ercolina Bianchini for elemental analyses.

[1] a) J. Wegner, S. Ceylan, A. Kirschning, *Adv. Synth. Catal.* **2012**, *354*, 17–57; b) I. R. Baxendale, J. J. Hayward, S. Lanners, S. V. Ley, C. D. Smith, *Microreactors in Organic Synthesis and Catalysis* (Ed.: T. Wirth), Wiley, New York, **2008**; c) F. E. Valera, M. Quaranta, A. Moran, J. Blacker, A. Armstrong, J. T. Cabral, D. G. Blackmond, *Angew. Chem.* **2010**, *122*, 2530–2537; *Angew. Chem. Int. Ed.* **2010**, *49*, 2478–2485.

[2] C. G. Frost, L. Mutton, *Green Chem.* **2010**, *12*, 1687–1703.

[3] For a review of continuous-flow asymmetric reactions, see: a) X. Y. Mak, P. Laurino, P. H. Seeberger, *Beilstein J. Org. Chem.* **2009**, *5*, doi: 10.3762/bjoc.5.19; for the first homogeneous organocatalytic processes in microfluidic devices, see: b) A. Odedra, P. H. Seeberger, *Angew. Chem.* **2009**, *121*, 2737–2740; *Angew. Chem. Int. Ed.* **2009**, *48*, 2699–2702.

[4] a) O. Bortolini, L. Caciolli, A. Cavazzini, V. Costa, R. Greco, A. Massi, L. Pasti, *Green Chem.* **2012**, *14*, 992–1000; b) L. Osorio-Planes, C. Rodríguez-Escrich, M. A. Pericàs, *Org. Lett.* **2012**, *14*, 1816–1819; c) C. Ayats, A. H. Henseler, M. A. Pericàs, *ChemSusChem* **2012**, *5*, 320–325; d) A. Massi, A. Cavazzini, L. Del Zoppo, O. Pandoli, V. Costa, L. Pasti, P. P. Giovannini, *Tetrahedron Lett.* **2011**, *52*, 619–622; e) X. C. Cambeiro, R. Martín-Rapún, P. O. Miranda, S. Sayalero, E. Alza, P. Llanes, M. A. Pericàs, *Beilstein J. Org. Chem.* **2011**, *7*, 1486–1493; f) A. L. W. Demuynck, L. Peng, F. de Clippel, J. Vanderleyden, *Adv. Synth. Catal.* **2011**, *353*, 725–732; g) E. Alza, S. Sayalero, X. C. Cambeiro, R. Martín-Rapún, P. O. Miranda, M. A. Pericàs, *Synlett* **2011**, 464–468; h) E. Alza, C. Rodríguez-Escrich, S. Sayalero, A. Bastero, M. A. Pericàs, *Chem. Eur. J.* **2009**, *15*, 10167–10172; i) F. Bonfils, I. Cazaux, P. Hodge, C. Caze, *Org. Biomol. Chem.* **2006**, *4*, 493–497; j) D. Bernstein, S. France, J. Wolfer, T. Lectka, *Tetrahedron: Asymmetry* **2005**, *16*, 3481–3483; k) S. France, D. Bernstein, A. Weatherwax, T. Lectka, *Org. Lett.* **2005**, *7*, 3009–3012; l) A. M. Hafez, A. E. Taggi, T. Dudding, T. Lectka, *J. Am. Chem. Soc.* **2001**, *123*, 10853–10859; m) S. B. Ötvös, I. M. Mandity, F. Fulop, *ChemSusChem* **2012**, *5*, 266–269; n) Y. Arakawa, H. Wennemers, *ChemSusChem* **2013**, *6*, 242–245.

[5] For a recent review, see: W. Zhang, S. Xu, X. Han, X. Bao, *Chem. Soc. Rev.* **2012**, *41*, 192–210.

[6] a) D. G. Blackmond, *Angew. Chem.* **2005**, *117*, 4374–4393; *Angew. Chem. Int. Ed.* **2005**, *44*, 4302–4320; b) J. S. Mathew, M. Klussmann, H. Iwamura, F. Valera, A. Futran, E. A. C. Emanuelsson, D. G. Blackmond, *J. Org. Chem.* **2006**, *71*, 4711–4722.

[7] a) G. Guiochon, A. Felinger, D. G. Shirazi, A. M. Katti, *Fundamentals of Preparative and Nonlinear Chromatography*, 2nd ed., Academic Press, Amsterdam, **2006**; b) A. Cavazzini, L. Pasti, F. Dondi, M. Finessi, V. Costa, F. Gasparrini, A. Ciogli, F. Bedani, *Anal. Chem.* **2009**, *81*, 6735–6743; c) A. Cavazzini, F. Dondi, S. Marmai, E. Minghini, A. Massi, C. Villani, R. Rompietti, F. Gasparrini, *Anal. Chem.* **2005**, *77*, 3113–3122.

[8] The occurrence of the postulated oxazolidinone–enamine conversion process has not been considered in this study: a) M. B. Schmid, K. Zeitler, R. M. Gschwind, *Angew. Chem.* **2010**, *122*, 5117–5123; *Angew. Chem. Int. Ed.* **2010**, *49*, 4997–5003; b) A. K. Sharma, R. B. Sunoj, *Angew. Chem.* **2010**, *122*, 6517–6521; *Angew. Chem. Int. Ed.* **2010**, *49*, 6373–6377.

[9] N. Zotova, L. J. Broadbelt, A. Armstrong, D. G. Blackmond, *Bioorg. Med. Chem. Lett.* **2009**, *19*, 3934–3937.

[10] For application of RPKA to liquid–liquid biphasic media, see: a) M. Colladon, A. Scarso, P. Sgarbossa, R. A. Michelin, G. Strukul, *J. Am. Chem. Soc.* **2007**, *129*, 7680–7689; b) S. Xu, Z. Wang, Y. Li, X. Zhang, H. Wang, K. Ding, *Chem. Eur. J.* **2010**, *16*, 3021–3035.

[11] A criterion of whether a molecule, after being displaced a certain distance d_p (d_p: diameter of a packing particle), was moved primarily by diffusion or by flow is given by the dimensionless quantity Peclet number (in chromatography more often referred to as reduced velocity), $d_p v/D_m$, in which v and D_m are the linear velocity of flow and the diffusion coefficient, respectively. When this quantity is less than one, the diffusion time is less than the flow time, which indicates that the displacement by diffusion is the more rapid of the two. The opposite conclusion is reached for a ratio greater than one. See, for example: J. C. Giddings, *Dynamics of Chromatography, Part I*, Marcel Dekker, New York, **1965**. By considering the geometrical characteristics of microreactor R (10 cm length by 0.21 cm inner diameter) and those of the packing (d_p – 5 μm), in the range of employed flow rates (1–30 μL min^{-1}) reduced velocities smaller

than one were obtained in confirmation that mass-transfer effects can be neglected.
[12] For reaction-progress kinetic analysis of the continuous-flow aldol reaction in a liquid–liquid microfluidic device, see reference [1c].
[13] Achievement of the steady-state regime was assumed when constant reactants/product outlet concentrations accompanied by complete inlet mass recovery in the eluate were detected (see the reaction isotherm curve in the Supporting Information).
[14] Progressive loss of catalytic activity of the packing material **3** was observed at 25 °C after approximately 24 h on stream. For the utilization of the more stable 5-pyrrolidin-2-yl)tetrazole-functionalized silica in the same aldol process, see reference [4a].
[15] Adsorption constants can be determined by chromatographic experiments. The chromatographic retention factor, k_{chrom}, traditionally defined as the ratio between the correct retention time and the hold-up time, in fact, also corresponds to the product between the so-called Henry constant of adsorption (H) and the phase ratio, F (i.e., the ratio between the stationary and the mobile phase): $k_{chrom} = HF$. In turn, H is the product between the saturation constant (achievable by the adsorption isotherm) and the equilibrium adsorption constant a (i.e., $H = q_s a$).
[16] The assumption that only one type of adsorption site (namely, the catalytic sites) is present on the surface was verified by considering the retention behavior of cyclohexanone **1** on an alkylated silica gel (by TEC of mercaptopropyl thiol silica and 1-heptene) through a series of dedicated HPLC experiments using toluene as the eluent. See the Supporting Information for details.
[17] Incidentally, we want to remark here that, also in steady-state conditions, [**1**] and [**2**] in Equation (6) do not correspond to the feed concentrations $[\mathbf{1}]_0$ and $[\mathbf{2}]_0$ since the system is reactive.
[18] This is a necessary simplification. Equation (6) is in fact a competitive adsorption isotherm. Accordingly, the amount of adsorbed cyclohexanone should not be a function of only its bulk concentration (as we are assuming here) but also of the concentration of **2** and **4**. Nevertheless, as the system is reactive, the competitive isotherm of **1** cannot be experimentally measured. In light of the excess amount of **1** with respect to **2** and **4**, however, this appears a physically sound approximation at this stage of the study.
[19] By assuming the same saturation capacity for **1**, **2**, and **4** (which is reasonable in light of their similar molecular dimensions), the ratio of retention factors correspond to the ratio of the adsorption equilibrium constants, the phase ratio F being the same in all the cases (see also ref. [15]). The retention factors for **1**, **2**, and **4**, using toluene as eluent, were 0.52, 1.10, and 2.10, respectively (see the Supporting Information).
[20] Since the reaction studied in this work is quite slow, a residence time of 45 min was taken for these experiments as a reasonable compromise between fraction conversion and analysis time.

Received: January 17, 2013
Published online: April 15, 2013

ACS Catalysis

Research Article

pubs.acs.org/acscatalysis

Benchmarking Immobilized Di- and Triarylphosphine Palladium Catalysts for Continuous-Flow Cross-Coupling Reactions: Efficiency, Durability, and Metal Leaching Studies

Roberto Greco, Walter Goessler, David Cantillo,* and C. Oliver Kappe*

Institute of Chemistry, University of Graz, NAWI Graz, Heinrichstrasse 28, A-8010 Graz, Austria

Supporting Information

ABSTRACT: Leaching resistance and recyclability, in addition to efficiency, are key parameters which constrain the choice of a catalyst for performing metal-catalyzed cross-coupling reactions in continuous-flow mode. Comparison of commercially available immobilized catalysts is often difficult because literature data are typically obtained under a wide range of reaction conditions. Here we present a comparative investigation on some of the most common immobilized phosphine-based Pd catalysts, namely Pd Tetrakis (polymer bound), FiberCat 1001, EnCat TPP30, and SiliaCat DPP-Pd. The efficiency, recyclability, and leaching resistance of each of the catalysts has been carefully investigated under a standard set of conditions as well as a selection of literature-based protocols. The data presented herein enable a direct comparison of these catalysts and provide further insights into the leaching phenomena of these types of ligand-based palladium catalysts.

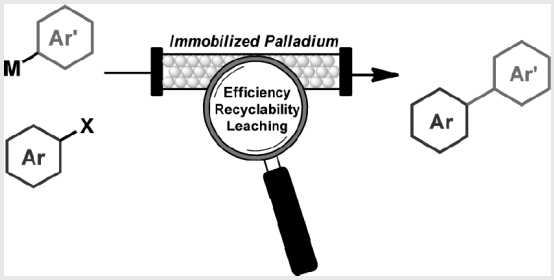

KEYWORDS: *continuous flow, cross-coupling, palladium, immobilized catalysts, leaching*

INTRODUCTION

There is little doubt that the development of cross-coupling chemistry over the past decades has revolutionized modern synthetic organic chemistry.[1] These transition-metal-catalyzed carbon−carbon and carbon−heteroatom bond forming reactions have had a significant impact on the synthesis of pharmaceuticals, agrochemicals, and natural products.[1,2] As a recognition of their seminal work, Richard Heck, Ei-ichi Negishi, and Akira Suzuki were awarded with the Nobel Prize in Chemistry in 2010.[3] The discoveries by these authors of Pd-catalyzed C−C bond formations changed how many organic syntheses are conceived and later on inspired other chemists to develop a wide range of additional cross-coupling reactions, including carbon−heteroatom coupling.[1,2,4] In the case of carbon−carbon bond forming reactions palladium is the most commonly used transition-metal catalyst. In a few cases metals other than palladium are used to perform these cross-couplings (typically copper or nickel), although the catalytic activity of these metals is generally significantly lower in comparison to that of palladium.[5]

The intense research in the field of cross-coupling chemistry during the past two decades has led to the development of "greener" reaction conditions as well as a large number of highly efficient catalyst/ligand combinations.[1−5] Apart from a plethora of homogeneous catalytic systems, several immobilized palladium catalysts have also been developed[6] and have been extensively utilized as heterogeneous catalysts, on the premise that the the solid-supported active metal could be easily removed from the reaction mixture and reutilized. In this context, several immobilized catalysts have been employed both in batch procedures and in continuous-flow applications.[7] In a continuous-flow process the catalyst is typically placed in a packed-bed reactor and the reaction mixture is flown through the reactor using an appropriate pumping system.[8] The catalytically active material remains located in a specific part of the reactor during processing of the reaction mixture, and therefore, the reaction and separation of the catalyst from the solution (including the product) take place simultaneously. In this way, catalyst reuse and recycling is simplified, as a catalyst separation/filtration step can be avoided. Furthermore, as small amounts of the reaction mixture are in contact simultaneously with the packed-bed reactor, high local concentrations of catalyst are achieved, resulting in increased reaction rates in comparison to that of a batch reaction.[8] Thus, high conversions can be obtained within residence times of a few seconds or minutes, although on the other hand the same local concentration effect can also sometimes lead to lower selectivities.

When cross-coupling chemistry and continuous flow using a packed-bed heterogeneous catalyst are combined, substantial amounts of "dissolved" palladium are typically observed in the reaction mixture collected from the reactor output.[9] Ultimately, deactivation of the catalyst bed and reduced product formation are inevitable. The leaching phenomenon in cross-coupling

Received: December 14, 2014
Revised: January 13, 2015
Published: January 15, 2015

DOI: 10.1021/cs5020089
ACS Catal. 2015, 5, 1303−1312

reactions is ascribed to the fact that the reaction mechanism for these kinds of transformations is (quasi)homogeneous and involves the transformation of Pd^0 species into soluble Pd^{II} during the oxidative addition step.[10] When an immobilized catalyst is used in a batch cross-coupling reaction, the leaching of palladium is not obvious because upon completion the metal readsorbs onto the solid support (thus acting as a "reservoir" of soluble, active Pd species). When continuous flow is used, the situation is different: in continuous-flow mode, the palladium metal will progressively be "chromatographed" through the packed-bed catalyst until eventually all Pd will be removed from the support owing to continuous metal leaching/readsorption.[9] This effect, which becomes especially relevant when long-run experiments are performed, leads to significant amounts of transition metal being leached out of the reactor, contaminating the product.

In 2009 our group carried out a detailed investigation on the mechanism and leaching phenomena for the Pd/C-catalyzed Mizoroki–Heck reaction of 4-iodobenzonitrile with butyl acrylate in microwave batch and continuous flow.[11] Although Pd/C is one of the most widely used catalysts for (batch) cross-coupling chemistry,[12] under the applied continuous-flow conditions a rapid metal leaching and catalyst deactivation was observed. Notably, novel and more sophisticated supported Pd catalysts for cross-coupling chemistry are being continuously reported in the literature.[1−5] In particular, incorporation of ligands to the immobilized catalyst often results in improved stability and leaching resistance of the solid material.[2] In some instances, continuous-flow applications have been also performed to test the leaching resistance and hence the recyclability and durability of the catalysts. However, the flow experiments have often been performed under very specific conditions (solvent, temperature) and at very low substrate concentrations. Low substrate concentrations obviously result in low amounts of metal being leached from the packed-bed reactor but compromise the practical use of a procedure that has no possibility of being scalable. A comparison of the performance of the different commercially available catalysts is therefore difficult, as the existing literature data have been obtained under a wide range of reaction conditions. Herein we present a benchmarking study of some of the most common immobilized diarylphosphine- and triarylphosphine-based palladium catalysts: namely, Pd Tetrakis (polymer-bound), FiberCat 1001, EnCat TPP30, and SiliaCat DPP-Pd. The efficiency, durability, and leaching resistance of these supported catalysts have been studied for continuous-flow Mizoroki–Heck and Suzuki–Miyaura reactions under analogous as well as selected literature conditions. The data presented herein enable a direct comparison of these catalysts and will help to understand the leaching phenomena of these types of ligand-based supported Pd catalysts.

RESULTS AND DISCUSSION

Initial Considerations. Four popular Pd-supported catalysts have been considered in our comparative study (Figure 1). Polymer-bound Pd Tetrakis, FiberCat 1001, EnCat TPP30, and SiliaCat DPP-Pd differ in the solid matrix hosting the active metal catalyst and the way in which the ligand is attached to the support (covalent bonding, encapsulation) (Figure 1). All of the catalysts evaluated herein have in common the presence of a substituted diphenylphosphine (DPP) or triphenylphosphine (TPP) as ligand. It has been shown that the presence of a ligand has beneficial effects in terms of catalyst stability and

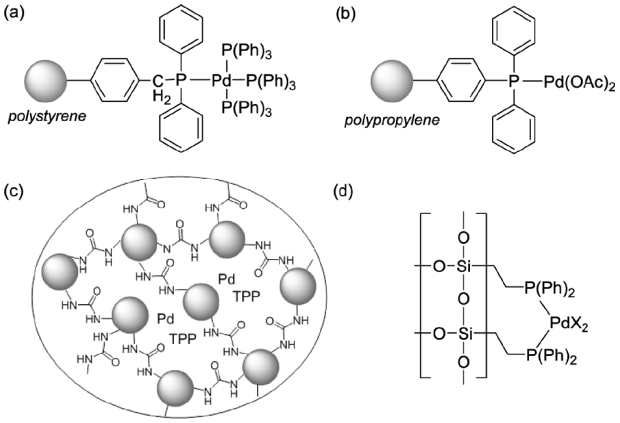

Figure 1. Structures of the (a) polymer-bound Pd Tetrakis, (b) FiberCat 1001, (c) EnCat TPP30, and (d) SiliaCat catalysts used in this work.

durability, as well as reaction selectivity and efficiency in some cases.[2] Two cross-coupling reactions have been selected as models for our continuous-flow experiments: the Mizoroki–Heck reaction of 4-iodobenzonitrile (**IBN**) with *n*-butyl acrylate (**BA**) (in analogy to our previous study on the Pd/C catalyst[11]) and the Suzuki–Miyaura reaction of **IBN** with phenylboronic acid (**PBA**) (Scheme 1). The use of aryl bromides in these

Scheme 1. Cross-Coupling Reactions Selected as Models in the Present Study[a]

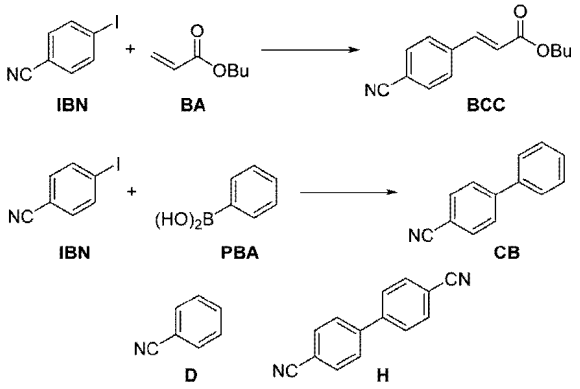

[a]Dehalogenation (**D**) and homocoupling (**H**) side products typically observed in these reactions are also shown.

transformations was troublesome, since their lower reactivity resulted in only moderate conversions in flow after a single pass through the packed-bed reactor.[11]

In all cases the temperature has been kept below 120 °C, even when low conversions were observed. It has been shown that at temperatures above 120 °C Pd catalysts are prone to form Pd black nanoparticles[13] which could provoke a faster deactivation and leaching of the active metal species. Selected literature-based reaction conditions (temperature, concentration, base, solvent) have been applied for each of the immobilized catalysts to independently assess their efficiency and stability. Furthermore, a set of reaction conditions which utilizes acetonitrile as solvent and triethylamine (TEA) or diisopropylethylamine (DIPEA) as base has been concurrently utilized in all cases. Acetonitrile is a relatively inert, weakly

DOI: 10.1021/cs5020089
ACS Catal. 2015, 5, 1303−1312

complexing solvent compatible with all solid-supported catalysts considered in this study.

Each of the immobilized catalysts has been tested for both the model Mizoroki–Heck and Suzuki–Miyaura reactions. In all cases a set of preliminary microwave (MW) batch experiments was performed to estimate an appropriate range of temperatures for the flow experiments.[14] Fresh catalyst cartridges were used for all flow runs, and typically 20 mL of the reaction mixture or 10 mmol of substrate was processed. For this purpose a commercial flow instrument (X-Cube, ThalesNano) was utilized (Figure 2).[15] Conversion profiles

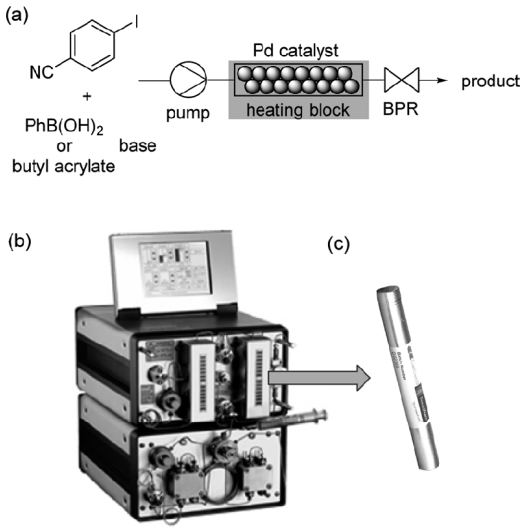

Figure 2. Schematic representation of the flow setup (a), performed in a X-Cube reactor from ThalesNano (b). The immobilized catalysts were loaded in a CatCart stainless steel column reactor (c).

were obtained by GC-FID monitoring of samples collected from the reactor output. To assess the amount of metal leaching produced during the flow processing, the Pd content of the crude reaction mixtures was determined by ICPMS analysis (see the Experimental Section for details).

Polymer-Bound Pd Tetrakis. This supported catalyst, developed by Fenger and Le Drian in 1998, consists of a diphenylphosphinated divinylbenzene (DVB) cross-linked polystyrene matrix treated with a solution of $Pd(PPh_3)_4$ in benzene.[16] In their original work the catalyst was tested for the batch Suzuki–Miyaura reaction of 4-bromopyridine with phenylboronic acid. Excellent yields analogous to those obtained when $Pd(PPh_3)_4$ was used as homogeneous catalyst were obtained, with the advantage that the heterogeneous catalyst could be easily separated from the reaction mixture and reused more than five times without any activity decrease. Recently, it has been shown by Gordon and co-workers that this catalyst can be applied for continuous-flow Suzuki–Miyaura reactions involving furylboronic acids,[17] although a detailed investigation on the stability of this particular catalyst was not carried out.

Our study started with a series of preliminary microwave batch experiments to evaluate the most appropriate reaction conditions. As an established literature protocol for cross-coupling reactions in flow using this catalytic system was not available, we decided to carry out all our experiments using acetonitrile as solvent and TEA or DIPEA as base. Thus, ~0.5 M solutions of the substrate in MeCN were treated with 1.5 equiv of the coupling partner (phenylboronic acid or *n*-butyl acrylate) and 1.5 equiv of base and mixed with 0.5 mol % of the supported catalyst. The mixture was heated in a single-mode microwave reactor for 15 min at temperatures ranging from 70 to 100 °C and the crude product analyzed by GC-FID (see Table S1 in the Supporting Information). A temperature of 100 °C was not exceeded, as this is the maximum working temperature recommended by the catalyst vendor. As expected, the best conversions were obtained at this temperature (56–57% and 36–40% for the Suzuki and Heck reactions, respectively) and a relatively good selectivity (90%) was observed for both transformations. The base employed did not affect the reaction outcome, and DIPEA and TEA gave analogous results.

We thus decided to move forward and utilize these conditions (100 °C, TEA or DIPEA as base in MeCN) in continuous-flow mode (see the Experimental Section for details). A volume of 20 mL of a 0.5 M reaction mixture was prepared for both cross-coupling reactions and pumped through the reactor utilizing fresh catalyst cartridges preheated at 100 °C. The reactor pump was set to a flow rate of 0.2 mL min^{-1}, which results in a residence time within the packed-bed reactor of approximately 2–3 min. Samples were collected from the reactor output and analyzed by GC-FID to monitor the reaction conversion and selectivity over time (Figure 3). In the case of the Heck reaction (Figure 3a) an essentially constant reaction profile was obtained under steady-state conditions. Full conversion was obtained within the relatively short contact time of the reaction mixture with the catalyst bed, although with a significantly lower selectivity with respect to batch processing (with formation of ~25% dehalogenation product and ~15% homocoupling). Both effects are typically ascribed to the high local concentrations of catalyst achieved using a packed-bed reactor.[11] Importantly, after 180 min working time and 10 mmol of starting material processed no drop in the conversion was noticeable.

For the Suzuki reaction the picture looked completely different (Figure 3b). In this case the substrate was fully consumed during the first 40 min of processing (after an initial period of stabilization) but then dropped dramatically to a conversion of <10%. Obviously the catalyst was rapidly degraded during this reaction, and significant amounts of metal were most likely leached from the support, contaminating the product.

The irregular contour of the conversion profiles during the first minutes of the continuous-flow processing is worth noting. Seemingly, only the desired cross-coupling is initially observed, followed by a drop in the selectivity until the system stabilizes. This effect, particularly pronounced for the Suzuki–Miyaura reaction, is due to the different affinities of each of the reaction components to the solid phase of the packed-bed reactor. Thus, the reactants as well as the formed products are "chromatographed" through the catalyst column, causing an initial incorrect reaction stoichiometry until steady-state conditions are reached. As could be observed in Figure 4, the cross-coupling product is eluted through the packed bed faster than other reaction products and therefore is the first species observed in the conversion profile. Butyl acrylate is also separated and eluted more rapidly than other reagents. This "chromatographic effect" results in an apparent poor selectivity at the initial stage of processing, with a greater amount of homocoupling product being obtained, due to the lower

DOI: 10.1021/cs5020089
ACS Catal. 2015, 5, 1303–1312

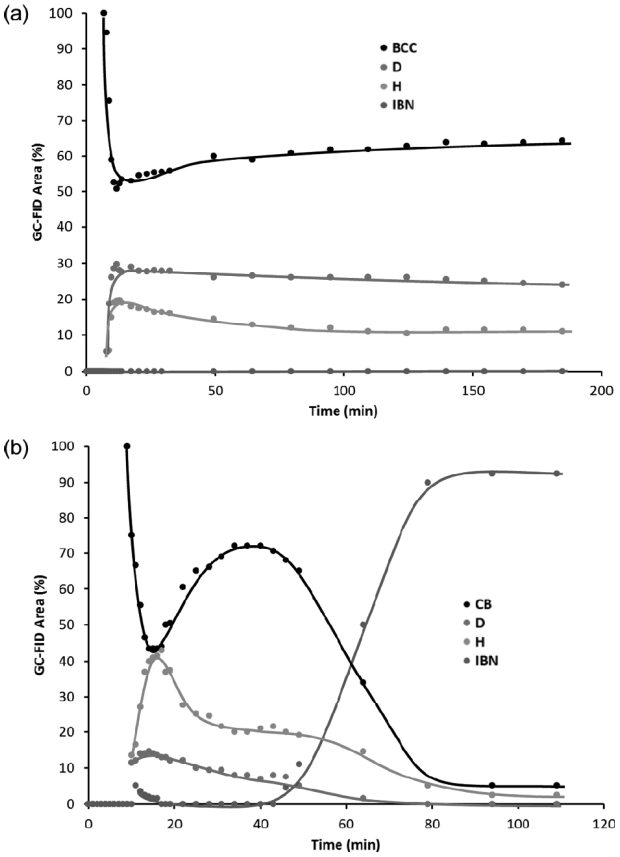

Figure 3. Conversion profiles obtained for the continuous-flow Mizoroki–Heck (a) and Suzuki–Miyaura (b) reactions catalyzed by polymer-bound Pd Tetrakis. The first ~10 min, in which no compound is observed in the GC-FID, corresponds to the dead volume of the reactor. Conditions: 0.5 M substrate in MeCN, 1.5 equiv of TEA, 1.5 equiv of $PhB(OH)_2$ or *n*-butyl acrylate, 100 °C, 0.2 mL min^{-1}.

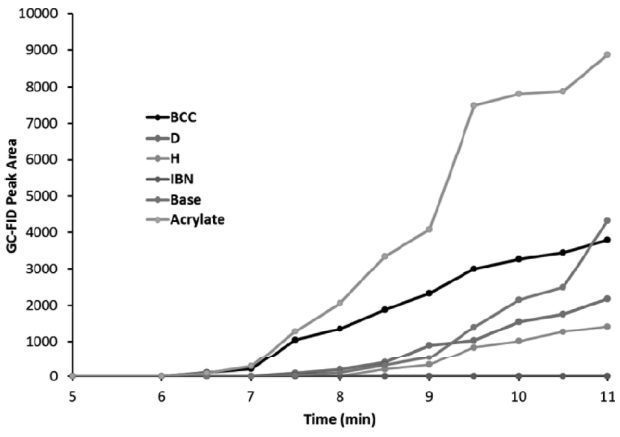

Figure 4. Differences in the retention of the components of the Mizoroki–Heck reaction within the polymer-bound Pd Tetrakis catalyst cartridge. Base: TEA.

effective amount of coupling partner until steady-state concentrations are reached. The effect is even more pronounced for the Suzuki–Miyaura reaction (for an analysis of the corresponding chromatographic effect, see Figure S9 in the Supporting Information).

ICPMS analyses revealed that significant amounts of Pd had leached from the packed-bed reactors for both cross-coupling reactions. Not surprisingly, a higher amount was determined for the Suzuki–Miyaura (4.61 mg) in comparison to that for the Mizoroki–Heck crude reaction mixture (2.25 mg) (the amount of palladium refers to that amount contained in the total crude reaction mixture), as in the former case the reaction conversion dramatically dropped after 40 min of processing. However, the amount of metal measured was small in comparison to the total amount of palladium contained in each catalyst cartridge. A close inspection of the packed-bed reactor denoted a substantial degradation of the material, with copious amounts of Pd black particles found in the reactor tubing and connections.

FibreCat 1001. A matrix of triphenylphosphine-functionalized polypropylene fibers serves as support for this palladium acetate based catalyst (Figure 1b).[18] Apart from a number of batch mode applications,[19] this immobilized catalyst has been utilized in continuous-flow mode for Sonogashira[20] and Suzuki–Miyaura[17,21] cross-coupling reactions. In this context, a catalyst reusability study was carried out by Dormán and coworkers for continuous-flow Sonogashira reactions.[20] The results revealed important substrate-dependent reductions in conversion after reusing the packed-bed reactors more than five times.

Our own initial microwave batch experiments showed excellent conversion (95%) and selectivity (>99%) for the Mizoroki–Heck reaction on heating to 120 °C for 15 min using DIPEA as base (see Table S2 in the Supporting Information). The Suzuki–Miyaura coupling was less efficient with this catalyst, and at the same temperature only 60% conversion was achieved. This temperature was thus selected for the long-run continuous-flow experiments. In this case DIPEA performed slightly better than TEA as the base for the reaction.

The conversion profiles resulting from the continuous-flow experiments were somewhat similar to those obtained with the polystyrene Pd Tetrakis immobilized catalyst (Figure 5). In the case of the Heck reaction, after an initial period of erratic selectivity due to the chromatographic effect, a more or less constant profile with full conversion and ca. 60% selectivity was achieved (Figure 5a). Evaluation of the retention of the reaction components in the FiberCat support was analogous to that for the polystyrene matrix, and similar chromatography curves were observed (see Figures S10 and S11 in the Supporting Information). Notably, after 80 min of processing the conversion started to drop slowly. Similar to the case for polymer-bound Pd Tetrakis, the Suzuki–Miyaura reaction provoked a very rapid degradation and deactivation of the supported catalyst, starting after approximately 20 min of flow processing (Figure 5b).

ICPMS analyses of the crude reaction mixtures again revealed significant amounts of Pd leached from the packed-bed reactors after processing 20 mL of the reaction mixture (2.58 and 2.43 mg of Pd for the Mizoroki–Heck and Suzuki–Miyaura reactions, respectively). However, the quantity of leached palladium was again relatively moderate in comparison with the total amount contained in the catalyst cartridge (ca. 15 mg), despite the rapid drop of conversion observed for the Suzuki–Miyaura reaction. In this particular case the content of the solid material inside the used catalyst cartridge was also examined (Figure 6). Apparently, the reaction provoked the formation of Pd black particles, which gradually moved through

DOI: 10.1021/cs5020089
ACS Catal. 2015, 5, 1303–1312

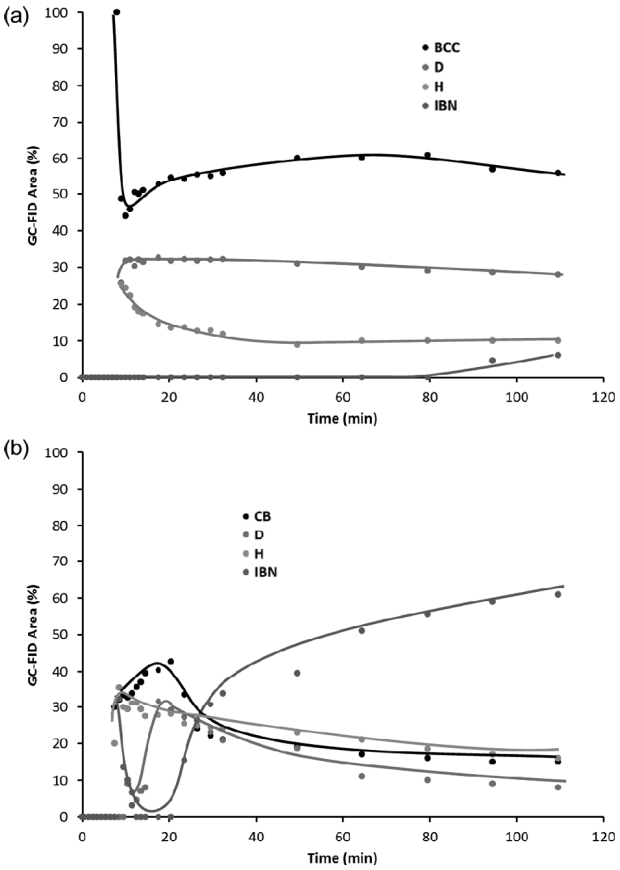

Figure 5. Conversion profiles obtained for the continuous flow Mizoroki–Heck (a) and Suzuki–Miyaura (b) reactions catalyzed by Fibercat 1001. The first ~10 min, in which no compound is observed in the GC-FID, corresponds to the dead volume of the reactor. Conditions: 0.5 M substrate in MeCN, 1.5 equiv of DIPEA, 1.5 equiv of $PhB(OH)_2$ or *n*-butyl acrylate, 120 °C, 0.2 mL min^{-1}.

the column with the flow of the reaction mixture. Thus, at the end of the flow run most of the metal was deposited in the final part of the packed-bed reactor. ICPMS analyses of the different portions of the solid material confirmed higher amounts of Pd in the final part of the packed-bed reactor after the Suzuki–Miyaura reaction (Figure 6). This catalyst degradation with migration of Pd through the supported catalyst would indeed result in a much shorter contact time of Pd-containing material with the reaction mixture. This effect, together with the metal leaching, can explain the significant reduction in conversion observed.

PdEncat TPP30. Polyurea encapsulated Pd is a popular, commercially available class of heterogeneous catalysts introduced by the Ley group in 2002.[22] The polyurea matrix provides the material with a good ability to ligate metal species and has been used in a wide range of applications, including cross-coupling reactions.[23] Although considered a hetereogeneous catalyst, it was shown by Broadwater and McQuade[24] that most likely soluble, catalytically active Pd species leached from the support are responsible for catalysis in cross-coupling reactions, with the encapsulated palladium species serving as a reservoir for soluble palladium. Suzuki–Miyaura cross-coupling reactions using PdEncat in a packed-bed reactor in continuous-flow mode have also been described.[25] Importantly, metal contamination in the products was observed in some cases and

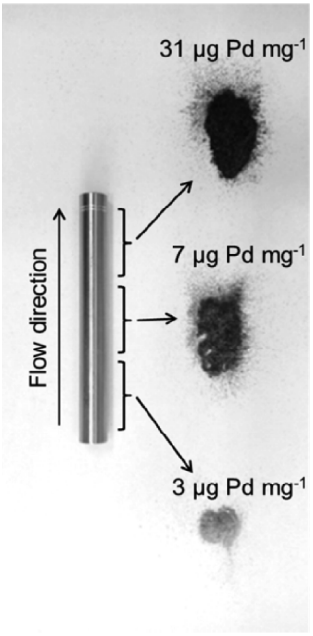

Figure 6. Visual representation of the contents of a used Fibrecat 1001 catalyst cartridge after a continuous-flow Suzuki–Miyaura reaction. The Pd black particles are clearly concentrated in the final part of the packed-bed reactor after the flow run.

a metal scavenging resin had to be installed into the flow setup. Attempts to process large-scale reaction mixtures failed, and the conversions dropped dramatically after a few hours of processing.[25c]

Our study again started with a series of preliminary microwave batch experiments to establish adequate reaction conditions for this catalyst (see Table S3 in the Supporting Information). Apart from an evaluation of the general acetonitrile/DIPEA conditions, other base and solvent systems utilized in the literature[25] were tested. In MeCN and DIPEA or TEA as base, low conversions (<25%) were observed in all cases after 15 min at 120 °C, in contrast to the high conversions achieved with Pd Tetrakis and FibreCat 1001 under analogous conditions. When EtOH was used as solvent instead and tetrabutylammonium acetate (TBAOAc) was used as base, higher conversions (60% and 75% for Suzuki–Miyaura and Mizoroki–Heck reactions, respectively) and excellent selectivities were achieved (Table S3, entries 4 and 13). Ultimately both solvent/base systems were translated into flow for comparative purposes.

The flow experiments carried out using the two systems and the Pd Encat catalyst highlight the importance of the solvent/base choice on the stability of the packed-bed reactor. When the Mizoroki–Heck coupling was performed in acetonitrile with TEA as base, a constant amount of product was observed (after the initial irregular selectivity due to the chromatographic effect) on processing 20 mL of the reaction mixture (10 mmol) (Figure 7a). Even when the amount of reaction mixture was doubled (40 mL), no drop in conversion could be seen (see Figure S1 in the Supporting Information). In stark contrast, when EtOH was used as the solvent in combination with TBAOAc as base (conditions based on the work of the Ley group[25]) a constant decrease in the product formation was observed during flow processing (Figure 7b). Again, Suzuki–Miyaura reactions resulted in much faster degradation of the

DOI: 10.1021/cs5020089
ACS Catal. 2015, 5, 1303–1312

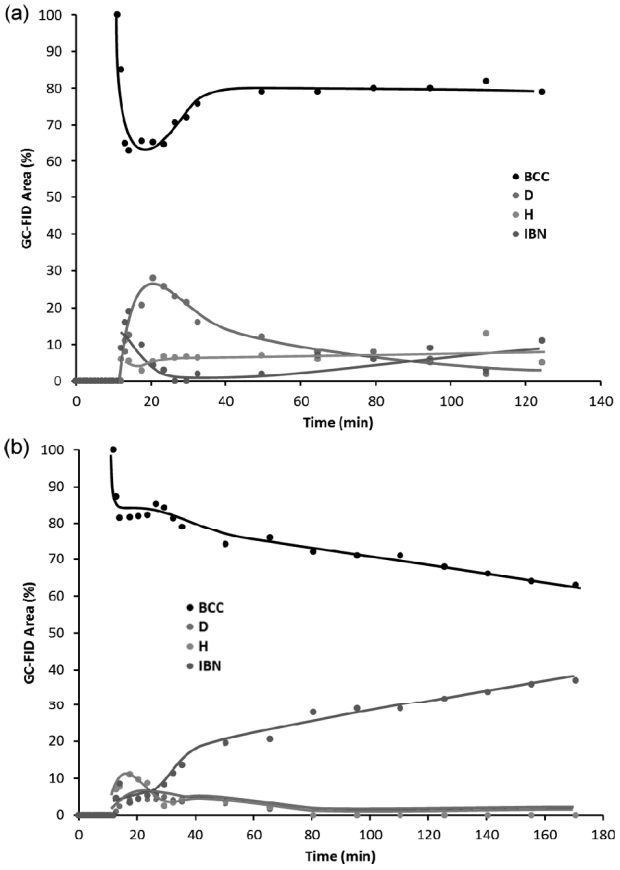

Figure 7. Conversion profiles obtained for the continuous-flow Mizoroki–Heck reactions catalyzed by Pd Encat TPP30 using the (a) acetonitrile/TEA and (b) ethanol/TBAOAc solvent/base systems. The first ~10 min, in which no compound is observed in the GC-FID, corresponds to the dead volume of the reactor. Conditions: (a) 0.5 M or (b) 0.25 M substrate, 1.5 equiv of base, 1.5 equiv of *n*-butyl acrylate, 120 °C, 0.2 mL min^{-1}.

immobilized catalyst (Figures S2 and S3 in the Supporting Information).

Despite the constant production of the desired Mizoroki–Heck cross-coupling product using acetonitrile as solvent, significant amounts of Pd (6.25 mg) were detected in the crude reaction mixture by ICPMS after processing 20 mmol of the substrate. Interestingly, lower amounts of Pd were found in the ethanolic crude mixture (1.03 mg), probably reflecting the fact that the catalyst is degraded or poisoned but that the Pd does not pass the packed-bed reactor filter. As for the previous catalyst studies, higher amounts of Pd were found in the Suzuki–Miyaura reaction mixtures (detailed information on the ICPMS Pd determination for all reactions is collected in Table S5 in the Supporting Information).

SiliaCat DPP-Pd. SiliaCat DPP-Pd is a commercially available sol–gel entrapped catalyst made out of an amorphous organosilica matrix functionalized with a diphenylphosphine ligand bound to Pd(II).[26] This immobilized catalyst has previously been evaluated for continuous-flow applications by the groups of Alcázar[27] and Pagliaro.[28,29] Notably, Alcázar and co-workers were able to perform a continuous Suzuki–Miyaura reaction in H_2O/THF for more than 8 h (0.125 M, 0.2 mL min^{-1}) without observing a decrease in the catalytic activity.[27a] In contrast, in the work by Pagliaro and co-workers a long-run experiment (also 8 h) utilizing this catalyst for a continuous-flow Suzuki–Miyaura reaction in THF/H_2O/EtOH as solvent clearly exhibited a significant decrease in conversion.[28a]

A wide range of reaction conditions and solvent/base combinations were evaluated for the SiliaCat DPP-Pd catalyst in our preliminary batch experiments. These incorporated THF/H_2O and THF/H_2O/EtOH mixtures as solvents as well as K_2CO_3, KOH, and KOAc as bases, in addition to our standard MeCN/DIPEA (or TEA) conditions concurrently used for all catalysts (see Table S4 in the Supporting Information). Remarkably, this catalyst had a relatively low performance in acetonitrile in batch processing, for both the Suzuki–Miyaura and Mizoroki–Heck reactions. Conversions considerably increased when mixtures including protic solvents and inorganic bases were employed. Thus, full conversion and complete selectivity were observed in H_2O/THF and H_2O/THF/EtOH mixtures and K_2CO_3 and KOH as bases, even at temperatures as low as 60–70 °C (see entries 5 and 6 in Table S4).

Given the good results obtained for a variety of solvent/base combinations, a large number of flow experiments were carried out using the SiliaCat catalyst. Although the conversion for the Mizoroki–Heck reaction in acetonitrile was not very high (Figure 8a), excellent selectivity was achieved. Interestingly, the

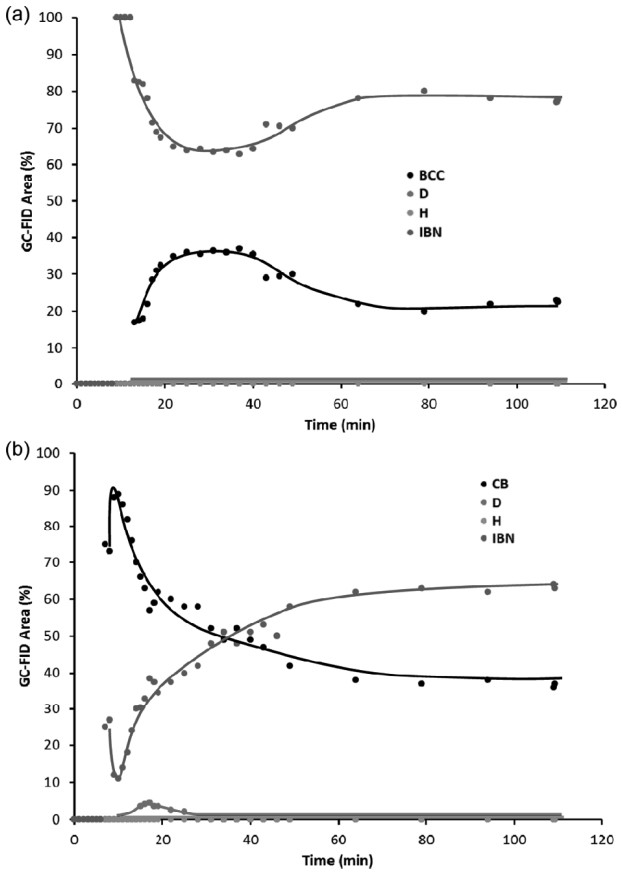

Figure 8. Conversion profiles obtained for the continuous-flow Mizoroki–Heck (a) and Suzuki–Miyaura (b) reactions catalyzed by SiliaCat DPP-Pd. The first ~10 min, in which no compound is observed in the GC-FID, corresponds to the dead volume of the reactor. Conditions: 0.5 M substrate in MeCN, 1.5 equiv of TEA, 1.5 equiv of $PhB(OH)_2$ or *n*-butyl acrylate, 120 °C, 0.2 mL min^{-1}.

DOI: 10.1021/cs5020089
ACS Catal. 2015, 5, 1303–1312

conversion profile was not stable until ca. 40 min of processing time. During the first stage of the processing a higher conversion (~35%) was obtained, which then dropped and stabilized at ca. 20% after 40 min. This behavior is possibly due to a modification of the metal species upon contact with the reaction mixture that partially decreases its initial activity. A similar pattern was observed for the Suzuki–Miyaura reaction (Figure 8b), with higher initial conversion rates which slowly stabilized during flow processing.

We decided to increase the residence time for the Mizoroki–Heck reaction by using a larger packed-bed reactor containing 2 g of supported catalyst. Under these conditions full conversion was obtained during the complete processing time but with decreased selectivity (~80%) (see Figure S4 in the Supporting Information). An Ommifit column reactor was utilized for this experiment. In contrast to the stainless steel CatCart catalyst cartridges, the Omnifit columns are made out of transparent borosilicate glass and we therefore could observe in situ changes in the appearance of the solid material during the processing (Figure 9). The SiliaCat DPP-Pd catalyst has an intense orange color which is maintained in contact with acetonitrile even when the temperature is increased (Figure 9a). However, as soon as the reaction mixture was introduced in the packed-bed reactor (Figure 9b) the catalyst material gradually turned black, indicating the formation of Pd(0) in the supported catalyst. Ultimately all of the supported catalyst acquired a black coloration (Figure 9c,d). This catalyst modification during the reaction is most probably responsible for the decrease of catalytic activity observed for the smaller scale experiment (Figure 8a).

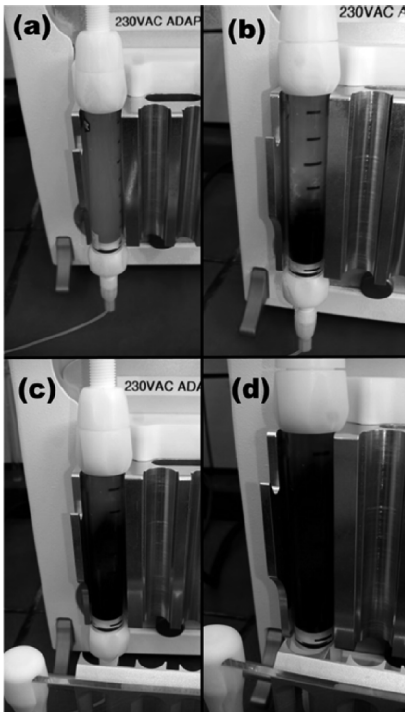

Figure 9. Visual appearance of SiliaCat DPP-Pd packed in a column reactor during the processing of a Mizoroki–Heck reaction using acetonitrile as solvent and TEA as base (a) in contact with hot solvent, (b) after 30 min, (c) after 60 min, and (d) after 120 min. The reaction stream flows from the bottom to the top of the packed-bed reactor.

As was experienced in batch processing, combinations with a protic solvent and an inorganic base resulted in very good conversions and selectivities in continuous flow. The conversion profiles depicted in Figure 10 were obtained using the THF/EtOH/H_2O and K_2CO_3 system described by Pagliaro and co-workers.[28] The reaction outcome rapidly stabilized, and a constant profile was achieved. It is possible that in this case the Pd catalyst is "preactivated" in contact with the hot protic solvent, with can be easily oxidized by Pd(II) to form Pd(0),[30] thus avoiding the initial stabilization time necessary when MeCN was used as solvent. Interestingly, under these conditions SiliaCat DPP-Pd performed much better for the Suzuki–Miyaura reaction (Figure 10b) than for the Mizoroki–Heck reaction (Figure 10a). Almost full conversion and excellent selectivity was obtained during all of the processing for the coupling with $PhB(OH)_2$. For the Mizoroki–Heck reaction a constant 65% conversion was obtained. This solvent/base system gave the best results in terms of conversion and catalyst stability. Several other solvent/base systems were tested, including THF/H_2O/KOH, THF/H_2O/K_2CO_3, and MeOH/H_2O/K_2CO_3 (the corresponding conversion profiles are collected in the Supporting Information).

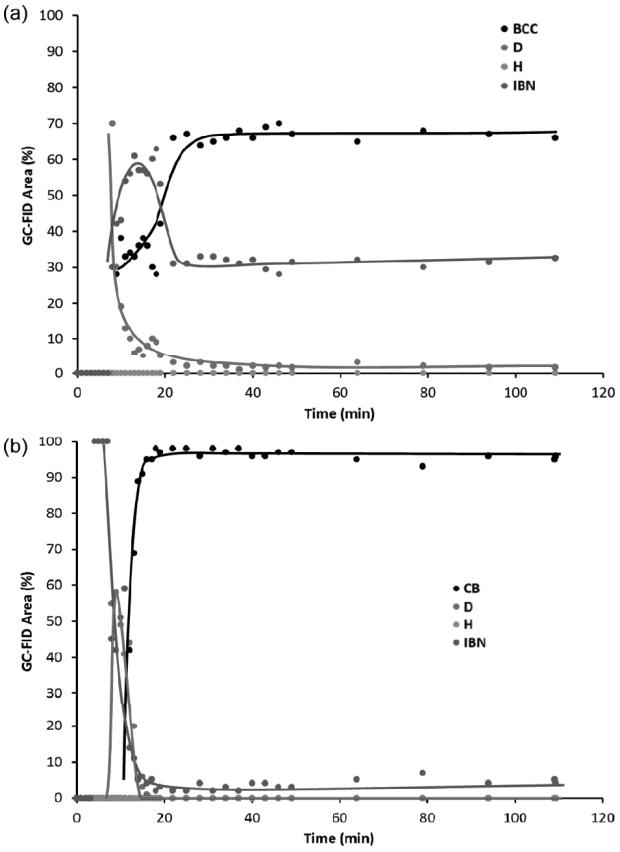

Figure 10. Conversion profiles obtained for the continuous-flow Mizoroki–Heck (a) and Suzuki–Miyaura (b) reactions catalyzed by SiliaCat DPP-Pd. The first ~10 min, in which no compound is observed in the GC-FID, corresponds to the dead volume of the reactor. Conditions: 0.25 M substrate in THF/EtOH/H_2O, 1.5 equiv of K_2CO_3, 1.25 equiv of $PhB(OH)_2$ or *n*-butyl acrylate, 80 °C, 0.2 mL min^{-1}.

DOI: 10.1021/cs5020089
ACS Catal. 2015, 5, 1303–1312

ICPMS analyses of all crude reaction mixtures obtained from the reactor output indicated a significantly lower amount of Pd being leached from the solid support with respect to that for the three previously studied supported catalysts. The amounts of metal encountered in the mixtures obtained with the MeCN/TEA system (Figure 8) were 0.81 and 1.25 mg for the Mizoroki–Heck and Suzuki–Miyaura reactions, respectively. For the THF/EtOH/H_2O/K_2CO_3 system the amount was even lower (332 and 39 μg for the Mizoroki–Heck and Suzuki–Miyaura reactions). The solid material from the catalyst cartridge utilized for this Suzuki–Miyaura reaction (Figure 10b) was placed out of the steel cylinder for a closer inspection. Similar to the reaction carried out in acetonitrile, the catalyst had acquired a black color as a result of the formation of Pd(0) black. More importantly, clear catalyst degradation could be visually observed at the first part of the material (Figure 11). Apparently, the Pd had been gradually

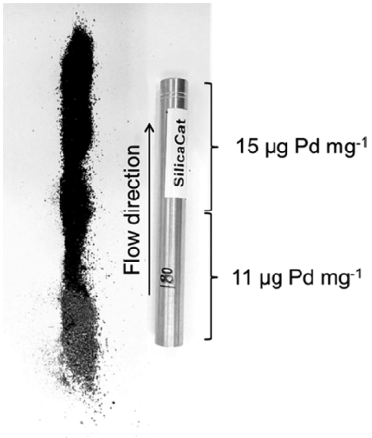

Figure 11. Visual appearance of the content of a used SiliaCat DPP-Pd catalyst cartridge after a continuous-flow Suzuki–Miyaura reaction with the THF/EtOH/H_2O/K_2CO_3 system. The Pd content of different fragments of the solid material, as determined by ICPMS analyses, is also incorporated. Degradation of the solid material at the beginning of the reactor is visually observable (gray coloration).

moved through the packed-bed reactor during the reaction processing, becoming a gray material. This hypothesis was confirmed by ICPMS analyses of the used solid material (Figure 11), which detected a higher concentration of Pd in the final part of the catalyst cartridge. Although no drop of conversion was observed during our flow experiment and the amount of metal contaminating the reaction mixture was not very high, this analysis revealed that most likely when larger reaction mixtures are processed all of the catalyst material will be degraded, ultimately losing its activity. A negligible amount of Pd leaching could only be obtained when very dilute reaction mixtures were processed. Thus, following a procedure described by the group of Pagliaro,[29] solutions for the Mizoroki–Heck and Suzuki–Miyaura reactions containing 0.05 M substrate concentration were processed using fresh catalyst cartridges. Although, as expected, the metal leached from the reactor was very low (15 μg and 5 μg of Pd), such dilute conditions arguably are not very useful for practical preparative purposes.

The results described above show SiliaCat DPP-Pd to be a superior catalyst with respect to those in the other case studies, especially in terms of stability and durability, even though metal leaching and catalyst degradation were still observable. An obvious question arises from the possibility that the silica matrix itself can retain Pd species by a simple physical affinity with the polar media and whether the presence of the phosphine ligand covalently bound to the support is essential for the low leaching. In order to address this question, a simple packed-bed reactor was built in a column containing unmodified silica gel. Then, a solution of $Pd(PhPh_3)_4$ in acetonitrile was pumped through the column reactor at room temperature. The solid material rapidly acquired a dark coloration while, after a second pass of the Pd solution, the solvent became completely colorless. The column was then utilized for a Suzuki–Miyaura reaction using the MeCN/TEA system. Notably, when only solvent was passed through the reactor, no leaching was appreciable even on heating to 120 °C. However, as soon as the reaction mixture was introduced, a rapid leaching was observed. The conversion rapidly dropped, and it could be clearly observed how the Pd Tetrakis was "washed out" from the silica (for a detailed description, see Figures S12 and S13 in the Supporting Information). This simple experiment demonstrated that the polarity of the silica matrix itself has no crucial effect on the recyclability of the SiliaCat DPP-Pd and the immobilized ligand plays an essential role in the Pd retention. This effect is in agreement with previous observations which indicated that the addition of external ligands often induces leaching of the metals.[31]

■ CONCLUSION

A comparative study of the efficiency, durability, and metal leaching resistance of some of the most common immobilized diarylphosphine- and triarylphosphine-based palladium catalysts toward continuous flow cross-coupling reactions has been performed. Pd Tetrakis (polymer-bound), FiberCat 1001, EnCat TPP30, and SiliaCat DPP-Pd have been independently evaluated using two model reactions: the Mizoroki–Heck reaction of 4-iodobenzonitrile with butyl acrylate and the Suzuki–Miyaura reaction of the same halide with phenylboronic acid. A set of reaction conditions combining acetonitrile as solvent and triethylamine or diisopropylethylamine as base has been concurrently used in all cases to directly compare the performance of the immobilized catalyst. Furthermore, selected literature protocols have been also reevaluated in terms of catalyst efficiency and durability.

Except for SiliaCat DPP-Pd, the Suzuki–Miyaura cross-coupling produced a much higher amount of metal leaching and catalyst degradation than the Mizoroki–Heck reaction. The choice of an appropriate solvent/base system is crucial for the durability of the supported catalyst. Thus, in the case of Pd EnCat TPP30 a constant drop in conversion was observed when EtOH as solvent and TBAOAc as base were utilized for the Mizoroki–Heck reaction, while in MeCN a much more constant conversion profile was achieved.

Variable amounts of Pd leached from the packed-bed reactors were always present in the crude reaction mixtures collected from the reactor output (for a comparison of Pd leaching data for all experiments performed, see Table S5 in the Supporting Information). In this context, SiliaCat DPP-Pd combined with THF/EtOH/H_2O as solvent and K_2CO_3 as base gave the best results regarding catalyst efficiency and leaching resistance. However, significant degradation of the immobilized catalyst was also observable in these cases. Negligible amounts of metal leaching are only achieved when

DOI: 10.1021/cs5020089
ACS Catal. 2015, 5, 1303–1312

rather diluted reaction mixtures (e.g., 0.05 M) are processed; this is not practical for preparative purposes.

The role of the covalent bonding of the ligand with the silica matrix for the stability of the SilicaCat DPP-Pd catalyst could be assessed by using a packed-bed reactor of unmodified silica loaded with $Pd(PPh_3)_4$. In this case, a rapid metal leaching and drop of conversion was observed during a continuous Suzuki–Miyaura reaction.

Given the problem of metal leaching and catalyst stability observed in most continuous-flow metal-catalyzed cross-coupling reactions,[7,9] it appears that in many cases it would be more appropriate to use a suitable homogeneous metal catalyst/ligand system. This would lead to more predictable and reproducible transformations, as the catalyst loading could be accurately adjusted. If necessary, recycling of the homogeneous metal catalyst could also be implemented and likely future research in this area will become increasingly important.[32] Notably, the SiliaCat DPP-Pd catalyst system described herein has shown superior leaching resistance and stability with respect to the other three case studies. Further development of this or other silica-based immobilized catalysts might lead to more leaching-resistant supports in the future, at least on a laboratory scale. Other strategies to circumvent the problem of metal leaching in continuous-flow cross-couplings using immobilized catalysts, such as "capture and release" systems[33] and recirculating reactors,[34] can also be useful on a small scale when telescoped reactions are not required.

EXPERIMENTAL SECTION

General Considerations. GC-FID analysis was performed on a standard GC instrument with a flame ionization detector, using an HP5 column (30 m, 0.250 mm, 0.025 mm). After 1 min at 50 °C the temperature was increased in 25 °C min^{-1} steps up to 300 °C and kept at 300 °C for 4 min. The detector gas for the flame ionization was H_2 and compressed air (5.0 quality). Curves drawn in the conversion profiles correspond to average plots of the experimental data. Solvents and chemicals were obtained from standard commercial vendors and were used without any further purification. The following catalyst cartridges were obtained from ThalesNano: Pd Tetrakis, polymer bound (0.5 mmol of Pd/g, THS X1178, ca. 565 mg of catalyst/cartridge); Pd Fibrecat 1001 (0.5 mmol of Pd/g, THS X1187, ca. 300 mg of catalyst/cartridge); Pd EnCat TPP30 (0.4 mmol of Pd/g, THS X1125, ca. 530 mg of catalyst/cartridge); SiliaCat DPP-Pd (0.2 mmol of Pd/g, ca. 220 mg of catalyst/cartridge). A fresh cartridge was used for every continuous-flow experiment described herein.

Leaching Studies. The amount of Pd leached from the immobilized catalyst for each of the flow runs was determined by ICPMS analysis of the crude reaction mixture. Thus, the solution collected from the reactor was evaporated under reduced pressure to remove all volatile compounds. The resulting residue was dissolved in acetonitrile/concentrated nitric acid to give a homogeneous solution, and the solution was diluted with nitric acid to 40 mL and placed in a vial for microwave digestion. Microwave-assisted acid digestion was carried out in an MLS UltraClave IV instrument. The temperature was ramped up in 30 min to 250 °C and kept at this temperature for a further 30 min. After appropriate dilution Pd was quantitatively determined at m/z 105 with an Agilent 7500ce inductively coupled plasma mass spectrometer. A calibration was performed with an external calibration curve established from 1.000 g of Pd/L standard (CPI International). Indium served as the internal standard.

General Procedure for Microwave Batch Experiments. In a 2 mL Pyrex vial were placed the Pd catalyst (0.5 mol %), 4-iodobenzonitrile (0.5 mmol), phenylboronic acid (Suzuki–Miyaura) (1.5 equiv) or *n*-butyl acrylate (Mizoroki–Heck) (1.5 equiv), the corresponding base (see Tables S1–S4 in the Supporting Information), and 1 mL of solvent. The vial was capped and heated in a single-mode microwave reactor (Biotage Initiator) for 15 min at the desired temperature. The reaction mixture was subsequently cooled to room temperature with compressed air, filtered, and analyzed by GC FID.

Continuous-Flow Procedures. *Procedure 1: Flow Reactions in MeCN as Solvent and TEA or DIPEA as Base (Figures 3, 5, 7, and 8).* A stock solution containing 4-iodobenzonitrile (0.5 M), phenylboronic acid (Suzuki–Miyaura) or *n*-butyl acrylate (Mizoroki–Heck) (1.5 equiv), and the corresponding base (1.5 equiv) in MeCN was prepared. A fresh catalyst cartridge was placed in the X-Cube flow reactor, and the system was set at the desired temperature and 20 bar of back pressure while pure acetonitrile was pumped at a rate of 0.2 mL min^{-1}. When the temperature and pressure were stable, the reactor inlet was switched to the reaction mixture, and 20 mL of the stock solution was pumped through the reactor before switching the inlet back to solvent. The crude reaction mixture was collected from the output, and the conversion was monitored by GC-FID.

Procedure 2: Flow Reactions in THF/EtOH/H_2O and K_2CO_3 as Base (Figure 10). Two separate stock solutions (A and B) were prepared. Solution A contained 4-iodobenzonitrile (0.83 M) in THF. Solution B contained phenylboronic acid (Suzuki–Miyaura) or *n*-butyl acrylate (Mizoroki–Heck) (0.45 M) and K_2CO_3 (0.55 M) in 1/1 EtOH/H_2O. A modified flow setup incorporating two feeds was employed. Feed A was set to 0.055 mL min^{-1} using THF as solvent. Feed B containing 1/1 EtOH/H_2O was set to 0.155 mL min^{-1}. At these flow rates the substrate/coupling partner proportion is 1/1.25 and the substrate/ base proportion is 1/1.5. A fresh catalyst cartridge was placed in the X-Cube flow reactor, and the system was set at the desired temperature and 20 bar of back pressure while pure THF and EtOH/H_2O were pumped through the system. When the temperature and pressure were stable, the reactor inlets were switched to the corresponding stock solutions A and B. The two reaction streams were mixed immediately before the heated column reactor in a T-mixer. The system was run until 10 mmol of the substrate had been processed (8.3 mL of solution A) before switching the inlets back to solvent. The crude reaction mixture was collected from the output, and the conversion was monitored by GC-FID.

ASSOCIATED CONTENT

Supporting Information

Supplementary Tables and Figures. This material is available free of charge via the Internet at http://pubs.acs.org.The following file is available free of charge on the ACS Publications website at DOI: 10.1021/cs5020089.

Preliminary MW-batch experiments, ICPMS data, continuous-flow conversion profiles, separation of the reaction components within the catalysts, and continuous-flow experiment with packed unmodified silica (PDF)

DOI: 10.1021/cs5020089
ACS Catal. 2015, 5, 1303–1312

AUTHOR INFORMATION

Corresponding Authors

*E-mail for D.C.: david.cantillo@uni-graz.at, .
*E-mail for C.O.K.: oliver.kappe@uni-graz.at.

Notes

The authors declare no competing financial interest.

ACKNOWLEDGMENTS

R.G. gratefully acknowledges the University of Ferrara (grant: Fondo Giovani-2012) for a fellowship. We thank ThalesNano for providing the catalyst cartridges and technical support.

REFERENCES

(1) Johansson Seechurn, C. C. C.; Kitching, M. O.; Colacot, T. J.; Snieckus, V. *Angew. Chem., Int. Ed.* **2012**, *51*, 5062−5085.

(2) (a) *Science of Synthesis: Cross Coupling and Heck Type Reactions*; Molander, G. A., Wolf, J. P., Larhed, M., Eds.; Georg Thieme Verlag: Stuttgart, Germany, 2013; Vols. *1*−*3*. (b) *Metal Catalyzed Cross-Coupling Reactions and More*; de Meijere, A., Bräse, S., Oestreich, M., Eds.; Wiley-VCH: Weinheim, Germany, 2014.

(3) (a) Negishi, E.-i. *Angew. Chem., Int. Ed.* **2011**, *50*, 6738−6764. (b) Suzuki, A. *Angew. Chem., Int. Ed.* **2011**, *50*, 6722−6737.

(4) (a) Bariwal, J.; van der Eycken, E. *Chem. Soc. Rev.* **2013**, *42*, 9283−9303. (b) Monnier, F.; Taillefer, M. *Angew. Chem., Int. Ed.* **2009**, *48*, 6954−6971. (c) Ley, S. V.; Thomas, A. W. *Angew. Chem., Int. Ed.* **2003**, *42*, 5400−5449.

(5) (a) Takahashi, T.; Kanno, K.-i. In *Modern Organonickel Chemistry*; Tamaru, Y., Ed.; Wiley-VCH: Weinheim, Germany, 2005; pp 41−53. (b) *Copper-Mediated Cross-Coupling Reactions*; Evano, G., Blanchard, N., Eds.; Wiley: Hoboken, NJ, 2014.

(6) (a) Molnár, A. *Chem. Rev.* **2011**, *111*, 2251−2320. (b) Anderson, E. B.; Buchmeiser, M. R. *ChemCatChem* **2012**, *4*, 30−33.

(7) Noël, T.; Buchwald, S. L. *Chem. Soc. Rev.* **2011**, *40*, 5010−5029.

(8) Frost, C. G.; Mutton, L. *Green Chem.* **2010**, *12*, 1687−1703.

(9) Cantillo, D.; Kappe, C. O. *ChemCatChem* **2014**, *6*, 3286−3305.

(10) (a) Pagliaro, M.; Pandarus, V.; Ciriminna, R.; Bland, F.; Demma Carà, P. *ChemCatChem* **2012**, *4*, 432−445. (b) Ananikov, V. P.; Beletskaya, I. P. *Organometallics* **2012**, *31*, 1595−1604. (b) Kashin, A. S.; Ananikov, V. P. *J. Org. Chem.* **2013**, *78*, 11117−11125.

(11) Glasnov, T. N.; Findenig, S.; Kappe, C. O. *Chem. Eur. J.* **2009**, *15*, 1001−1010.

(12) Yin, L.; Liebscher, J. *Chem. Rev.* **2007**, *107*, 133−173.

(13) de Vries, J. G. *Dalton Trans.* **2006**, 421−429.

(14) Glasnov, T. N.; Kappe, C. O. *Chem. Eur. J.* **2011**, *17*, 11956−11968.

(15) The ThalesNano X-Cube system is no longer commercially available and has been replaced by the H-Cube Pro, which enables working with identical cartridges, but under slightly decreased maximum conditions (150 °C, 100 bar) in "no hydrogen" mode.

(16) Fenger, I.; Le Drian, C. *Tetrahedron Lett.* **1998**, *39*, 4287−4290.

(17) Trinh, T. N.; Hizartidis, L.; Lin, A. J. A.; Harman, D. G.; McCluskey, A.; Gordon, C. P. *Org. Biomol. Chem.* **2014**, *12*, 9562−9571.

(18) Carole, W.; Colacot, T. J. *Chim. Oggi* **2010**, *28*, XXIII−XXV.

(19) (a) Colacot, T. J.; Carole, W. A.; Neide, B. A.; Harad, A. *Organometallics* **2008**, *27*, 5605−5611. (b) Colacot, T. J. *Top. Catal.* **2008**, *48*, 91−98.

(20) Borcsek, B.; Bene, G.; Szirbik, G.; Dormán, G.; Jones, R.; Ürge, L.; Darvas, F. *ARKIVOC* **2012**, *5*, 186−195.

(21) Estrada, G. O. D.; Flores, M. C.; Silva, J. F. M.; de Souza, R. O. M. A.; e Miranda, L. S. M. *Tetrahedron Lett.* **2012**, *53*, 4166−4168.

(22) Ramarao, C.; Ley, S. V.; Smith, S. C.; Shirley, I. M.; DeAlmeida, N. *Chem. Commun.* **2002**, *10*, 1132−1133.

(23) (a) Kuang, Y. Y.; Chen, F. R. *Helv. Chim. Acta* **2009**, *92*, 897−903. (b) Carpita, A.; Ribecai, A. *Tetrahedron Lett.* **2009**, *50*, 204−207.

(24) Broadwater, S. J.; McQuade, D. T. *J. Org. Chem.* **2006**, *71*, 2131−2134.

(25) (a) Lee, C. K. Y.; Holmes, A. B.; Ley, S. V.; McConvey, I. F.; Al-Duri, B.; Leecke, C. A.; Santos, R. C. D.; Seville, J. P. K. *Chem. Commun.* **2005**, 2175−2177. (b) Leeke, G. A.; Santos, R. C. D.; Al-Duri, B.; Seville, J. P. K.; Smith, C. J.; Lee, C. K. Y.; Holmes, A. B.; McConvey, I. F. *Org. Process Res. Dev.* **2007**, *11*, 144−148. (c) Baxendale, I. R.; Griffiths-Jones, C. M.; Ley, S. V.; Tranmer, C. K. *Chem. Eur. J.* **2006**, *12*, 4407−4416.

(26) (a) Pandarus, V.; Gingras, G.; Béland, F.; Ciriminna, R.; Pagliaro, M. *Org. Process Res. Dev.* **2012**, *16*, 117−122. (b) Lemay, M.; Pandarus, V.; Simard, M.; Marion, O.; Tremblay, L.; Béland, F. *Top. Catal.* **2010**, *53*, 1059−1062.

(27) (a) Muñoz, J. M.; Alcázar, J.; de la Hoz, A.; Díaz-Ortiz, A. *Adv. Synth. Catal.* **2012**, *354*, 3456−3460. (b) Egle, B.; Muñoz, J. M.; Alonso, N.; De Borggraeve, W. M.; de la Hoz, A.; Díaz-Ortiz, A.; Alcázar, J. *J. Flow. Chem.* **2014**, *4*, 22−25.

(28) (a) Pandarus, V.; Gingras, G.; Béland, F.; Ciriminna, R.; Pagliaro, M. *Org. Process Res. Dev.* **2014**, *18*, 1550−1555. (b) Pandarus, V.; Gingras, G.; Béland, F.; Ciriminna, R.; Pagliaro, M. *Org. Process Res. Dev.* **2014**, *18*, 1556−1559.

(29) Pandarus, V.; Ciriminna, R.; Gingras, G.; Béland, F.; Drobod, M.; Jina, O.; Pagliaro, M. *Tetrahedron Lett.* **2013**, *54*, 1129−1132.

(30) Brazier, J. B.; Nguyen, B. N.; Adrio, L. A.; Barreiro, E. M.; Leong, W. P.; Newton, M. A.; Figueroa, S. J. A.; Hellgardt, K.; Hii, K. K. M. *Catal. Today* **2014**, *229*, 95−103.

(31) Kobayashi, S.; Miyamura, H. *Aldrichim. Acta* **2013**, *46*, 3−19.

(32) (a) Li, P.; Moore, J. S.; Jensen, K. F. *ChemCatChem* **2013**, *5*, 1729−1733. (b) Ormerod, D.; Bongers, B.; Porto-Carrero, W.; Ciegas, S.; Vijt, G.; Lefevre, N.; Lauwers, D.; Brusten, W.; Buekenhoudt, A. *RSC Adv.* **2013**, *3*, 21501−21510. (c) Peeva, L.; Arbour, J.; Livingston, A. *Org. Process Res. Dev.* **2013**, *17*, 967−975. (c) Peeva, L.; da Silva Burgal, J.; Vartak, S.; Livingston, A. G. *J. Catal.* **2013**, *306*, 190−201.

(33) Suzuki, Y.; Laurino, P.; McQuade, D. T.; Seeberger, P. H. *Helv. Chim. Acta* **2012**, *95*, 2578−2588.

(34) (a) Pavia, C.; Ballerini, E.; Bivona, L. A.; Giacalone, F.; Aprile, C.; Vaccaro, L.; Gruttadauria, M. *Adv. Synth. Catal.* **2013**, *355*, 2007−2018. (b) Petrucci, C.; Strappaveccia, G.; Giacalone, F.; Gruttadauria, M.; Pizzo, F.; Vaccaro, L. *ACS Sustainable Chem. Eng.* **2014**, *2*, 2813−2819.

DOI: 10.1021/cs5020089
ACS Catal. 2015, 5, 1303−1312

Green Chemistry

PAPER

View Article Online
View Journal

Cite this: DOI: 10.1039/c4gc00838c

Expanding the scope of enzymatic carboligation reactions in flow-mode: production of optically active tertiary alcohols with packed-bed micro-bioreactors

P. P. Giovannini,* O. Bortolini, A. Cavazzini, R. Greco, G. Fantin and A. Massi*

Received 7th May 2014,
Accepted 6th June 2014

DOI: 10.1039/c4gc00838c

www.rsc.org/greenchem

Acetylacetoin synthase (AAS) from *Bacillus licheniformis* has been partially purified and immobilized on a silica support and its activity was tested under batch conditions in the homo-coupling of a set of α-diketones leading to valuable α-hydroxy ketone derivatives displaying a chiral tertiary alcohol functionality at the α-position. Next, the effectiveness of AAS heterogeneous catalysis has been evaluated under continuous-flow conditions by fabricating the corresponding packed-bed microreactors (pressure-resistant stainless-steel columns). It has been demonstrated that the covalent immobilization on a silica support and the flow regime synergistically contribute to preserve the enzyme activity over time, thus permitting the long-term operation (up to 15 days) of the prepared bioreactors for the production of the chiral targets *via* the umpolung strategy.

Introduction

In recent years continuous-flow asymmetric catalysis has been emerging as an attractive field of research in academic and industrial laboratories.[1] Following a critical and comprehensive cost analysis, the production of chiral organic synthons and fine chemicals by operation of meso- and micro-flow devices may offer several advantages over conventional batch reactors, including the safety and sustainability of the processes, the direct scalability, and the ease of automation and integration with in-line analysis methods.[2] Heterogenization of homogeneous chiral catalysts represents an effective strategy towards process implementation because of simple product/catalyst separation and catalyst recycling opportunities.[1a,c,3] Recently, our[4] and other groups[5] have demonstrated that heterogeneous organocatalysis in combination with flow technologies constitutes an efficient synthetic platform for the production of chiral target molecules, the absence of metal contamination being an additional and peculiar benefit of the synthetic strategy.

The design of asymmetric organocatalytic processes is often inspired by the mechanisms of enzyme catalysis with the aim to reproduce nature achievements in terms of chemo- and stereo-selectivity of the investigated synthesis.[6] Outstanding results in this direction have been obtained even under flow conditions;[1] nevertheless, it is a matter of fact that, to date, biocatalytic approaches still remain the preferred choice of chemical and pharma industries for the continuous-flow production of chiral molecules.[7] Biocatalytic processes, in fact, are unique in several ways: they occur under very mild conditions (pH and temperature), with high atom and stereochemical efficiency, and with diminished environmental concerns.[8] Immobilization of biocatalysts (enzymes and whole cells) together with their use in the flow-regime is frequently the key for success of industrial and lab-scale syntheses.[9] Typical advantages of this approach are improved biocatalyst stability and increased activity for those enzymes subjected to product inhibition thanks to the continuous elution of reaction mixtures. Immobilization strategies comprise covalent bonding to organic or inorganic solid supports, encapsulation, entrapment, and adsorption (specific and non-specific) methods.[10] In most cases, the fixed-bed configuration, in the form of either packed or monolithic columns, is the optimal choice for biocatalytic flow processes, overcoming the continuous stirred reactor set-up in terms of volumetric productivities.[7b,11] Therefore, microstructured fixed-bed bioreactors can be envisaged as useful scale-down systems for the fast screening of realistic flow process conditions.

Dominant in the field of (micro)flow biocatalysis is the utilization of hydrolases and oxidoreductases in single- and multiple-reactor processes,[1a,d,e,12,13] while more limited is the number of strategies involving the challenging asymmetric formation of carbon–carbon bonds (Fig. 1).[14–16] Optically active

Dipartimento di Scienze Chimiche e Farmaceutiche, Università di Ferrara, Via Fossato di Mortara 17, I-44121 Ferrara, Italy.
E-mail: pierpaolo.giovannini@unife.it, alessandro.massi@unife.it

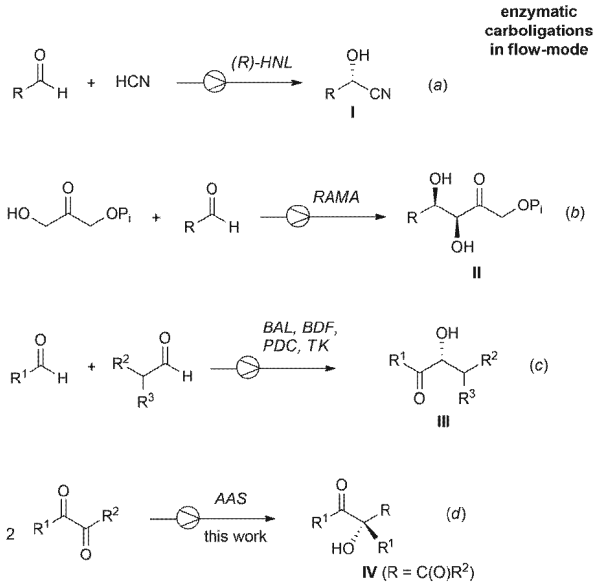

Fig. 1 Enzyme tool box for continuous-flow biocatalytic carboligation reactions.

cyanohydrins (Fig. 1, **I**) have been prepared from aldehydes using hydroxynitrile lyases (HNL) in both chip and column reactors (eqn (a)).[14] Recently, immobilized aldolases (*e.g.* fructose-1,6-diphosphate aldolase, RAMA) have been reported to promote the addition of dihydroxyacetone phosphate to aldehydes yielding phosphorylated α,β-dihydroxy ketones (Fig. 1, **II**) as intermediates of the flow synthesis of complex chiral carbohydrates (eqn (b)).[15] Also, several thiamine diphosphate (ThDP)-dependent enzymes such as benzaldehyde lyase (BAL), benzoylformate decarboxylase (BFD), pyruvate decarboxylase (PDC), and transketolase (TK) have been successfully utilized in different flow chemistry programs for the production of target molecules incorporating the chiral α-hydroxy ketone functionality (Fig. 1, **III**) as a common structural motif (eqn (c)).[16] It appears evident from the above survey that expanding the enzyme toolbox to access valuable chiral frameworks by biocatalytic continuous-flow carboligations is of timely significance. In this article we report on the flow synthesis of chiral tertiary α-hydroxy ketones (Fig. 1, **IV**) from α-diketones by operating fixed-bed microreactors fabricated with acetylacetoin synthase (AAS)-functionalized packing material (eqn (d)). The α-hydroxy ketone group **IV** displaying a chiral tertiary alcohol functionality at the α-position is not only the key feature of a range of natural products and antibiotics,[17] but also a densely functionalized building block for the asymmetric synthesis of important organic molecules such as diols, amino alcohols, and so forth.[18] Despite its synthetic utility and significance, the chiral quaternary structure **IV** is hardly accessible through direct, purely chemical approaches;[19] instead, straightforward routes to derivatives of type **IV** are realized with the ThDP-dependent enzymes AAS[20] and YerE,[21] which efficiently catalyze the formal carboligation of an aldehyde with a ketone through diketone–diketone and pyruvate–ketone couplings, respectively.

In a recent study we have described the continuous-flow, biomimetic synthesis of tertiary alcohols **IV** in racemic form using thiazolium-functionalized polystyrene monolithic microreactors.[4a] Herein, we demonstrate that the same derivatives **IV** can be produced with high enantioselectivities (up to 91% ee) and a comparable level of productivity with AAS covalently bound to mesoporous silica as the catalytic material of fixed-bed microreactors. Significantly, an elevated operational stability was observed for these bioreactors, which were continuously operated for more than 15 days without any significant decrease of enzyme activity.

Results and discussion

Acetylacetoin synthase (AAS) from *Bacillus licheniformis* is a 'new'[21b] ThDP-dependent enzyme capable to promote the umpolung (polarity reversal) of α-diketones **1** with high substrate specificity. Distinctive of AAS catalysis is the release of a carboxylic acid molecule in the key hydrolytic step leading to the reactive acyl anion equivalent, whose attack on a second molecule of α-diketone **1** yields the chiral α-hydroxy-β-diketone **2** together with minor amounts of the regioisomeric prochiral derivative **3** (Scheme 1).[20a]

AAS-catalyzed homo- and cross-coupling reactions of α-diketones **1** have been previously investigated by our group under conventional batch conditions using *Bacillus licheniformis* crude cell extracts.[20] Although this procedure was quite

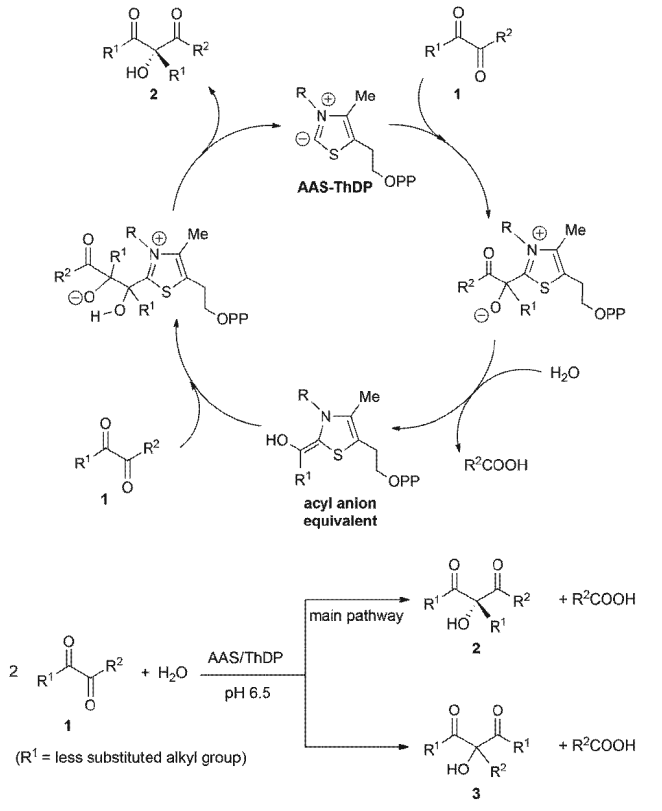

Scheme 1 AAS-catalyzed formation of chiral tertiary alcohols.

Table 1 Purification of acetylacetoin synthase (AAS) from *B. licheniformis* DSM13

Step	Volume (mL)	Total protein[a] (mg)	Total activity[b] (U)	Specific activity (U mg^{-1})	Purification (-fold)[c]	Recovery[d] (%)
Crude extract	26	314	1.8	5.7×10^{-3}	—	100
Ammonium sulfate precipitation	6	75	1.8	2.4×10^{-2}	4.2	100
DEAE chromatography	10	12	1.2	0.10	17.5	67

[a] The protein amount was determined by spectrophotometric UV measurements at 215 and 280 nm (see the Experimental section and ref. 30). [b] One unit (U) is defined as the enzyme amount catalyzing the formation of 1 μmol of products **2a** + **3a** in one minute from 2,3-pentanedione **1a**. [c] The ratio between the specific activity of the partially purified enzyme and the crude extract. [d] Referred to as the total activity recovery.

efficient for the preparation of tertiary alcohols **2** (yields: 30–68%; enantioselectivities: 44–91%), the purification of AAS was first addressed in this study with the hope to achieve a high volumetric activity (U g^{-1}) for the heterogenized enzyme and improved stereoselectivities. Thus, AAS from acetoin-grown cells was partially purified 17-fold by a two-step procedure with 67% recovery of enzyme activity as determined using the homo-coupling of 2,3-pentanedione **1a** as the activity test (Tables 1 and 3). Initially, proteins precipitated between 40 and 60% ammonium sulfate saturation were tested showing a 4.2-fold enzyme enrichment and total activity recovery. Next, the precipitated proteins were dissolved in phosphate buffer (50 mM, pH 7.0) and chromatographed on a DEAE-Sepharose column with a step gradient of NaCl.

The active fractions were collected and treated with ammonium sulfate (80% saturation); native polyacrylamide gel electrophoresis indicated AAS as the main component of the precipitated fraction (Fig. 2), whose specific activity (0.1 unit per mg) remained unchanged for at least one month under storage at 4 °C.

Having in mind the utilization of heterogeneous AAS under flow conditions as the ultimate goal of this study, an enzyme covalent immobilization method was next investigated. Indeed, out of different approaches, the covalent attachment of an enzyme to a functionalized solid support is undoubtedly one of the most efficient strategies to enhance protein stability and prevent protein leaching during elution;[10,22] on the other hand, these are critical issues that must be carefully considered to ensure flow bioreactors with long operational stability. Hence, mesoporous silica was chosen as the support and the classical glutaraldehyde method as the immobilization technique.[23] This involved three sequential steps: amino-silanization of silica, derivatization of surface amino groups with glutaraldehyde, and immobilization of partially purified AAS *via* the free aldehyde groups. Accordingly, 3-aminopropyl-silica was freshly prepared with a satisfactory loading (0.32 mmol g^{-1}) by treatment of mesoporous silica (particle size: 5 μm; pore size 30 nm) with 3-aminopropyl triethoxysilane in refluxing toluene (Scheme 2). Screening of optimal pH conditions for the coupling steps was carried out with reaction buffers in the pH range 5.0 to 8.0. Thus, aminopropyl-silica was suspended in phosphate buffer (pH 7.0), treated with excess glutaraldehyde for 2 h at 30 °C, and then washed. To the activated carrier was then added a solution of AAS in the appropriate buffer (enzyme/carrier ratio (w/w) = 0.12 : 1) and the coupling was continued for additional 2 h at 30 °C. Protein mass balance was determined by evaluating the protein concentration left in the solution after the anchoring step. As shown in Fig. 3, while an increase of pH corresponded to a decrease of immobilized AAS, the highest volumetric activity (2.9 U g^{-1}

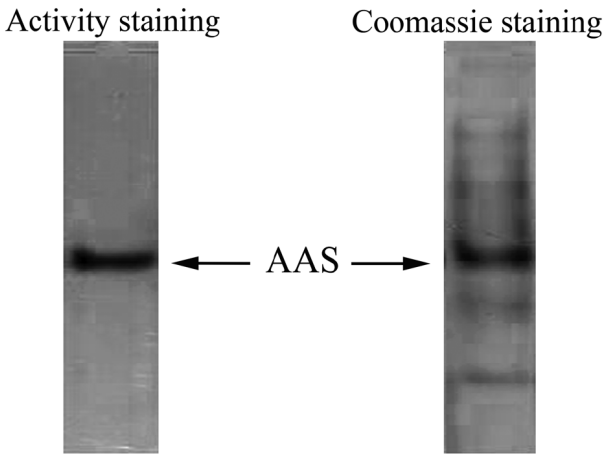

Fig. 2 Native gel electrophoresis of partially purified acetylacetoin synthase. Samples were applied to 4% (w/v) polyacrylamide gel and stained with the diacetyl–DCPIP–thiazolyl blue mixture (activity staining) and with Coomassie brilliant blue (Coomassie staining).

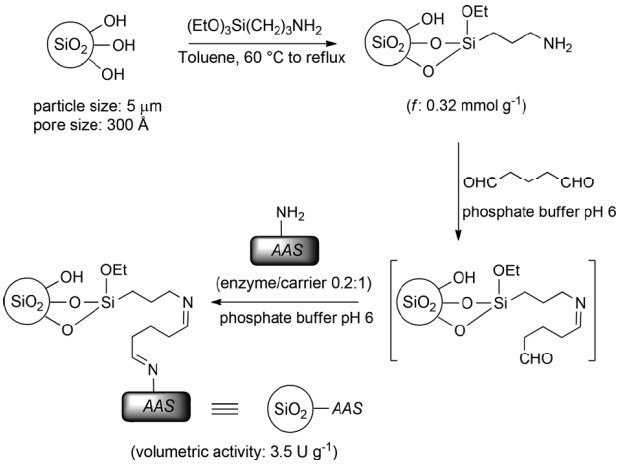

Scheme 2 Optimized procedure for the immobilization of AAS on the silica support.

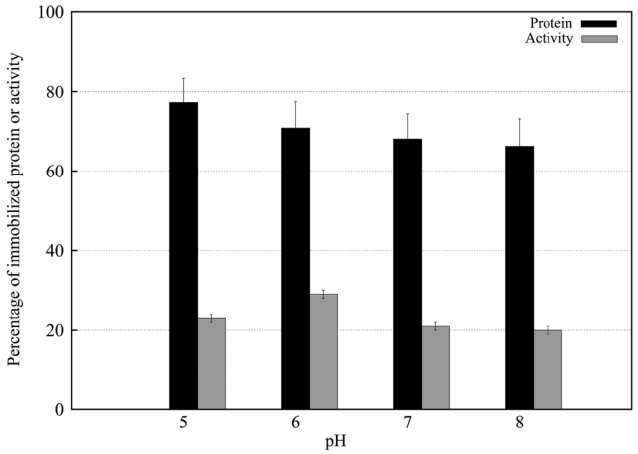

Fig. 3 Effect of the immobilization pH on the percentage amount (black histogram) and percentage activity (grey histogram) of the immobilized AAS relative to the starting carrier-free enzyme.

carrier) was detected at pH 6; under these conditions 78 mg of AAS were bound to one gram of the silica support.

Selection of the suitable enzyme/carrier (E/C) ratio (w/w) was next performed by dedicated coupling experiments performed as described before at the optimal pH 6 (Table 2).

Treatment of activated aminopropyl-silica with increasing amounts of AAS resulted in catalytic materials with progressively higher volumetric activities (up to 3.5 U g^{-1}, entries 1–4). This trend, however, reversed with enzyme/carrier ratios exceeding the critical 0.2 value (entry 4). According to similar immobilization studies,[24] this loss of efficiency may be attributed to the increase of steric hindrance on the support preventing the access of the substrate to the immobilized enzyme.[25] Alternatively, high protein concentrations might be responsible for the formation of multi-covalent linkages between the enzyme and the carrier, thus affecting the structure and activity of the native enzyme.[26]

Table 2 Effect of the enzyme/carrier ratio (E/C) on the activity of the immobilized AAS

Entry	Initial activity[a] (U)	Initial protein[b] (mg)	E/C ratio[c] (mg g $^{-1}$)	Volume activity[a,d] (U g $^{-1}$)	Imm. protein[e] (mg g $^{-1}$)
1	2.5	25	0.025	1.0	25
2	5	50	0.05	1.5	50
3	10	100	0.1	1.9	91
4	20	200	0.2	3.5	160
5	40	400	0.4	2.3	221

[a] The activity (U) of the free enzyme in the starting solution before immobilization. One unit (U) is defined as the enzyme amount catalyzing the formation of 1 μmol of products **2a** + **3a** in one minute from 2,3-pentanedione **1a**. [b] The protein amount in the starting solution as determined by spectrophotometric UV measurements at 215 and 280 nm (see the Experimental section and ref. 30). [c] Values normalized to 1 g of aminopropyl-silica. [d] Volumetric activity. [e] Immobilized protein. The protein mass balance was determined by evaluating the protein concentration left in the solution after the anchoring step.

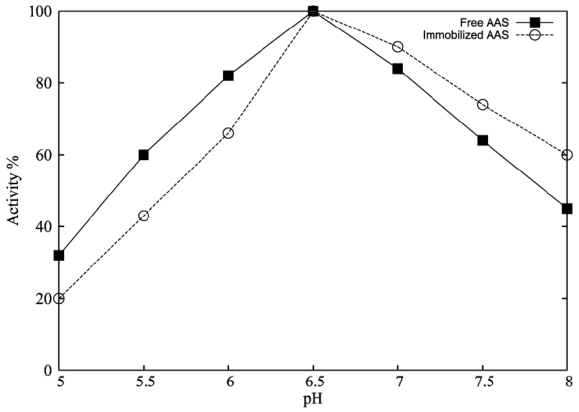

Fig. 4 Effect of pH on the activity of the free (black line) and immobilized AAS (grey line).

Quite surprisingly, sodium cyanoborohydride reducing treatment of immobilized AAS produced a marked decrease in volumetric activity (*ca.* 80%), which was not compensated for by an increase of enzyme stability (see the Experimental section). Finally, the effect of pH on the activity of free and immobilized AAS was determined in the pH range 5.0–8.0, and the results are shown in Fig. 4. The maximum value of relative activity was observed at pH 6.5 for the free and immobilized enzyme; overall, the absence of a significant pH shift in the two curves seems to be in accordance with no interaction between AAS and the silica support.[27]

The synthetic value of AAS heterogeneous catalysis was first evaluated in standard batch reactors (Table 3). Accordingly, different portions of AAS-functionalized silica (250 mg) were obtained with the optimal volumetric activity (3.5 U g^{-1}) and utilized in the homo-coupling (1 mmol scale) of unsymmetrically substituted diketones **1a–e** (entries 1–5) and symmetric diketones **1f,g** (entries 6 and 7). In all the investigated cases, the immobilized AAS showed the same level of activity of the free enzyme affording the target tertiary alcohols **2a–e** with comparable conversion efficiencies (35–58%, 16 h reaction time) and enantioselectivities (55–91% ee, *R*).[20a] Appreciably, the enantiomeric purity of **2a–e** was, on average, significantly higher (*ca.* 15%) than that detected with the not purified free enzyme.[20]

It is also important to point out that while the AAS-promoted coupling of diketones **1f,g** affords symmetrically substituted tertiary alcohols **3f,g**, these prochiral derivatives can be efficiently elaborated into valuable chiral molecules such as α-alkyl-α,β-dihydroxy ketones with high levels of stereocontrol.[18]

A final and crucial result of this batch investigation was that heterogeneous AAS could be re-used after reactivation with ThDP ten times for repeat or different couplings without any loss of activity.

The success in the above recycle experiment paved the way to the use of ASS-functionalized silica as the packing material of fixed-bed bioreactors with potential long-term stability. Enzyme immobilization was performed under flow conditions ('*in situ*' immobilization technique) with the fully assembled

Table 3 AAS heterogeneous catalysis under batch conditions[a]

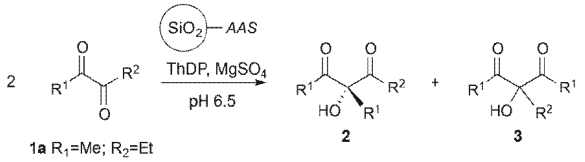

1a R_1=Me; R_2=Et
1b R_1=Me; R_2=*n*-Pr
1c R_1=Me; R_2=*n*-Bu
1d R_1=Me; R_2=*n*-Pent
1e R_1=Me; R_2=Ph
1f R_1=R_2=Me
1g R_1=R_2=Et

Entry	Diketone **1**	Chiral alcohol **2**[b] (ee [%])	Alcohol **3**	**2** + **3**[c] (Yield [%])
1	**1a**	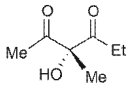 **2a** (85)	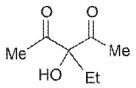 **3a**	46 + 35
2	**1b**	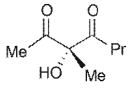 **2b** (91)	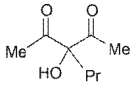 **3b**	48 + 22
3	**1c**	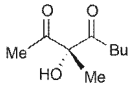 **2c** (72)	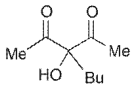 **3c**	45 + 19
4	**1d**	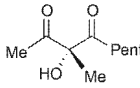 **2d** (55)	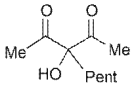 **3d**	58 + 13
5	**1e**	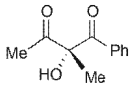 **2e** (80)	—	35 + 0
6	**1f**	—	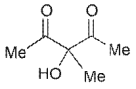 **3f**	0 + 85
7	**1g**	—	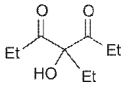 **3g**	0 + 78

[a] See the Experimental section. [b] Determined by chiral GC analysis. [c] Isolated yield.

microreactor.[28] This consisted of a stainless steel column (100 mm length, 2.1 mm internal diameter) slurry packed (toluene) with the previously prepared 3-aminopropyl silica.

The main features of the column were determined by pycnometry and included the hold-up (dead) volume (V_0 = 250 μL), and the total porosity (0.72). The packing amount of spherical silica (240 mg) was calculated by weighing the column before and after filling. After characterization, the column was conditioned with phosphate buffer (pH 7.0), flushed with glutaraldehyde solution, equilibrated to pH 6.0, and finally eluted with AAS solution to obtain the AAS-functionalized catalytic bed (see the Experimental section). Continuous-flow experiments were performed by first considering the homo-coupling of 2,3-pentanedione **1a** (Table 4, entries 1–4). It turned out from preliminary tests that the preparation of a fully homogeneous 10 mM solution of **1a** containing 0.04 mol % of ThDP and $MgSO_4$ (0.08 mol%) required the addition of DMSO (1% w/v), and that utilization of triethanolamine buffer (pH 6.5) gave feed solutions of **1a** with longer stability (25 °C, air) compared to the corresponding solutions prepared in phosphate buffer.[29] The optimal reaction mixture was then pumped at different flow rates through the bioreactor to evaluate the influence of the residence time on the conversion efficiency (%) and productivity (mmol d^{-1}). Therefore, portions of the outlet stream were analyzed (GC) at regular intervals (60 min) to determine the product distribution. While good levels of conversions (>50%) were detected at 30 °C with flow rates up to 30 μL min^{-1} (entries 1–4), full consumption of diketone **1a** was achieved with a flow rate of 5 μL min^{-1} (residence time: 56 min). Actually, driving the reaction to completion is an important goal in continuous process optimization for easier product purification; nevertheless, operation at the flow rate of 10 μL min^{-1} (residence time: 28 min) was considered the best compromise to provide a suitable balance between the productivity (0.11 mmol d^{-1}) and the conversion efficiency (78%, entry 2, Table 4). Therefore, the long-term stability of the AAS-functionalized catalytic bed was next examined with 10 mM **1a** under the above continuous-flow conditions. As evidenced in Fig. 5, the steady state-conversion was reached after *ca.* 1 h and maintained stable for 15 days on stream; significantly, 30 day operation determined a loss of only half the initial productivity.

The scope and the applicability of the disclosed flow procedure were investigated by considering the homo-couplings of diketones **1b–g**. Gratifyingly, satisfactory conversion efficiencies (>50%) could be obtained by suitably adjusting the flow rate of the optimized feed solutions (entries 5–10). As previously observed for the tertiary alcohol **2a** (Table 4, entry 1), enantioselectivities of alcohols **2b–e** detected in batch experiments (Table 3) were replicated under flow conditions and maintained constant during the process in the steady-state regime. Notably, the high selectivity of the flow procedure was confirmed by the unique formation of the target products **2** and **3** that are easily separable by chromatography and, in the case of incomplete conversions, by the recovery of the unmodified starting diketone **1**. This result indicated that the acetyl anion ($MeCO^-$) transfer was predominant over migration of its higher carbanion counterparts under heterogeneous continuous-flow conditions as well. Moreover, in full agreement with AAS reactivity,[20a] the selectivity towards the formation of chiral alcohols **2** improved with the increase of steric hindrance of the R^2 group, thus confirming the preferential attack of the acetyl anion on the less bulky carbonyl carbon of the starting diketone **1** (Scheme 1).

Table 4 AAS heterogeneous catalysis under flow conditions[a]

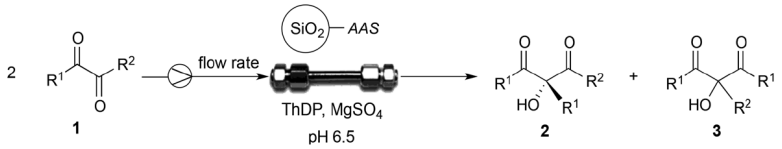

Entry	**1** (*c* [mM])	Flow rate [μL min^{-1}]	Residence time[b] [min]	Temperature [°C]	**2** + **3**[c] (Conv. [%])	**2**[d] (ee [%])	Productivity[e] [mmol d^{-1}]
1	**1a** (10)	5	56	30	56 + 43	85	0.07
2	**1a** (10)	10	28	30	44 + 34	85	0.11
3	**1a** (10)	15	19	30	33 + 25	85	0.13
4	**1a** (10)	30	9	30	28 + 21	85	0.21
5	**1b** (10)	10	28	30	47 + 23	91	0.10
6	**1c** (10)	10	28	30	46 + 20	74	0.10
7	**1d** (10)	10	28	30	48 + 15	55	0.09
8	**1e** (5)	10	56	30	51 + 0	81	0.02
9	**1f** (10)	10	28	30	0 + 88	—	0.13
10	**1g** (10)	10	28	30	0 + 81	—	0.12

[a] See the Experimental section for a description of the experimental setup. [b] Calculated residence time. [c] Instant conversions in the steady-state regime as established by GC analysis. [d] Determined by chiral GC analysis. [e] Productivities are measured in mmol (**2** + **3**) d^{-1}.

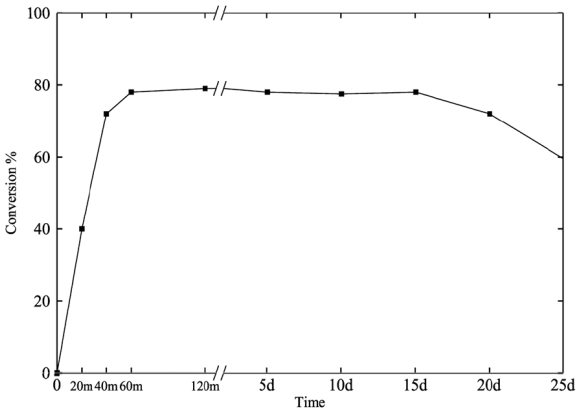

Fig. 5 Conversion of continuous-flow **1a** homo-coupling as a function of time.

Conclusions

In summary, we have initially described a method for the purification and immobilization on a silica support of acetylacetoin synthase (AAS). Interest towards this non-classical ThDP-dependent enzyme arises from its unique capability to furnish through the polarity reversal of α-diketone chiral tertiary alpha-hydroxyketones. These are densely functionalized derivatives containing a quaternary stereocenter of high synthetic utility and biological relevance. In preliminary batch experiments we have found that the immobilized AAS displayed a significantly enhanced stability compared to the free enzyme leading to high recyclability without the loss of catalytic activity. Subsequently, the synthetic potential of AAS catalysis has been evaluated under flow conditions using fixed-bed microreactors fabricated with the silica-supported AAS as the packing material. Results from the continuous-flow set-up were fully consistent with those obtained from the batch process in terms of both the conversion efficiency and stereoselectivity. Together with the ease of product/catalyst separation, a peculiar benefit of the flow-regime has been the remarkable long-term stability of the catalytic bed (more than 15 days on stream). While small-scale bioreactors have been presented in this study, an easy scale-up strategy may be envisaged through the use of multiple columns or the design of reactors with larger diameters. Therefore, we believe this work may represent a useful contribution to the current search for more efficient, economic, and environmentally benign production strategies of valuable chiral targets.

Experimental section

All moisture-sensitive reactions were performed under a nitrogen atmosphere using oven-dried glassware. Solvents were dried over a standard drying agent and freshly distilled prior to use. Reactions were monitored by TLC on silica gel 60 F_{254} with detection by charring with sulfuric acid and/or ninhydrin. Flash column chromatography was performed on silica gel 60 (230–400 mesh). Optical rotations were measured at 20 ± 2 °C in the stated solvent; $[\alpha]_D$ values are given in 10^{-1} deg cm^2 g^{-1}. ^{1}H (300 MHz) and ^{13}C (75 MHz) NMR spectra were recorded in $CDCl_3$ solutions at room temperature unless otherwise specified. Peak assignments were aided by ^{1}H–^{1}H COSY and gradient-HMQC experiments. Elemental analyses were performed with a FLASH 2000 Series CHNS/O analyzer (ThermoFisher Scientific). Gas chromatographic analyses were performed on a Carlo Erba 6000, equipped with a FID detector and a fused capillary column Megadex 5 (25 m × 0.25 mm) containing dimethyl-*n*-pentyl-β-cyclodextrin on OV 1701 from Mega snc (temperature program from 80 to 200 °C with a gradient of 1.5 °C min^{-1} unless otherwise specified); helium was used as

carrier gas (80 kPa). The mass spectra were obtained using a Varian 4000 GC/MS/MS equipped with a chiral column Megadex 5, using the same conditions described for GC analyses. UV spectroscopic measurements were performed on a Shimadzu UV-1601 UV-visible spectrophotometer. ESI MS (LTQ-XL Linear Trap from Thermo Scientific) analyses were performed in positive ion mode with samples dissolved in a 10 mM solution of HCO_2NH_4 in 1 : 1 MeCN–H_2O. For accurate mass measurements, the compounds were analyzed in positive ion mode on an Agilent 6520 HPLC-Chip Q/TOF-MS (nanospray) using a quadrupole, a hexapole, and a time-of-flight unit to produce spectra. The capillary source voltage was set at 1700 V; the gas temperature and drying gas were kept at 350 °C and 5 L min^{-1}, respectively. The MS analyzer was externally calibrated with an ESI-L low concentration tuning mix from *m*/*z* 118 to 2700 to yield accuracy below 5 ppm. Accurate mass data were collected by directly infusing samples in 40/60 H_2O–ACN 0.1% TFA into the system at a flow rate of 0.4 μL min^{-1}. Crude AAS was obtained from commercially available (DSMZ) *B. licheniformis* DSM13 as described.[18] Spherical silica gel (Microsorb 300-5 Si, particle size 5 μm, pore size 300 Å) was purchased from Varian. Diketones **1a**, **1b**, **1c**, **1e**, **1f**, and **1g** are commercially available from Sigma-Aldrich. The diketone **1d** was synthesized as described.[20b]

Preparation of 3-aminopropyl silica gel

To preserve the spherical shape of silica particles, this derivatization step was carried out in a standard rotary evaporator in which a two-necked flask was fitted with a solvent condenser, solvent collector, and nitrogen inlet for syringe addition of reactant solutions under an inert atmosphere. Mixing was performed by spinning the flask around its axis and warming by means of a standard oil-bath. Microsorb 300-5 Si silica gel was dried before its use (0.1 mbar, T = 110 °C, 2 h).

To a stirred slurry of Microsorb 300-5 Si (5.00 g), anhydrous toluene (60 mL), and freshly distilled triethylamine (0.25 mL) was slowly added a solution of (3-aminopropyl)-trimethoxysilane (4 mL) in anhydrous toluene (10 mL). The resulting mixture was then warmed to 60 °C and stirred for 20 h. Subsequently, the mixture was refluxed until *ca.* 15 mL of solvent were collected (eventually with the aid of a nitrogen stream). The mixture was then refluxed for an additional hour, cooled to room temperature, and centrifuged with 20 mL portions of toluene, MeOH, EtOH, and cyclohexane. The resulting 3-aminopropyl silica gel was finally dried at reduced pressure (0.1 mbar, 60 °C, 6 h). Elemental analysis (%) found: N 0.45 (estimated loading f = 0.32 mmol g^{-1}).

Acetylacetoin synthase (AAS) production and purification

The cells of *B. licheniformis* DSM13 were cultured and treated as described[18] in order to obtain the cell free extract that represents the starting material of the following purification procedure. The purification of the enzyme was checked by measuring the activity as reported below and determining the protein concentration through spectrophotometric measurements at 215 and 280 nm.[30] The extract (26 mL) was fractionated with ammonium sulfate and the proteins precipitated between 40 and 60% saturation were collected by centrifugation (6000 rpm, 15 min, r.t.). The pellet was dissolved in phosphate buffer 50 mM, pH 7 (5 mL) and desalted by repeated ultrafiltration (Amicon Ultra-4 membrane). The desalted protein solution (6 mL, 1.8 U) was loaded on a DEAE-Sepharose column (length 3.0 cm, diameter 1.5 cm), equilibrated with phosphate buffer 50 mM (pH 7), and eluted with a step-gradient of NaCl in the equilibration buffer (0.2, 0.4 and 0.6 M). The fractions were assayed for determining the enzyme activity and protein concentration; the active fractions eluted with 0.4 M NaCl were pooled (10 mL, 1.2 U). This enzyme solution was treated with ammonium sulfate (80% of the saturating concentration) in order to precipitate the partially purified AAS that, in this form, can be stored at 4 °C for at least two months without a significant loss of activity.

Enzyme assay

The enzyme solution (50–100 μL) was added to a reaction mixture (1 mL) containing 2,3-pentanedione **1a** (10 mM), ThDP (0.4 mM), and $MgSO_4$ (0.8 mM) dissolved in phosphate buffer 50 mM (pH 6.5). The reaction mixture was gently shaken at 30 °C and samples (0.15 mL) were withdrawn after 30, 60 and 120 min. The samples were extracted with AcOEt (0.2 mL) containing diethyl carbonate (0.05%) as the internal standard and the organic extracts were subjected to chiral GC analysis.[20a] One unit (U) of AAS was defined as the amount catalyzing the formation of 1 μmol of the mixture of products **2a** and **3a** (for the ratio see Table 3) in one minute.

AAS immobilization: optimization of pH

3-Aminopropyl silica gel (30 mg) was suspended in 50 mM phosphate buffer (pH 7, 1 mL), and then a 25% aqueous solution of glutaraldehyde (0.1 mL) was added in one portion. After shaking for 2 h at 30 °C silica was filtered and washed with water. The carrier was suspended in water (1 mL) and the resulting suspension was divided into four equivalent portions. After centrifugation (3000 rpm, 3 min) the supernatant was discharged and to each pellet a solution of the partially purified AAS (0.8 mg, 0.08 U) in different buffers (1 mL) was added. For pH 5, 50 mM acetate was used as the buffering agent while for pH 6, 7 and 8, 50 mM phosphate was employed. The suspensions were shaken at 25 °C for 2 h and then centrifuged and each pellet was washed with 50 mM phosphate at pH 7 (3 × 1 mL). The amount of immobilized proteins (see Fig. 3) was determined from the difference between the protein concentration of the supernatant before and after the immobilization, whereas the enzymatic activity of the solutions and pellets was determined as described before.

AAS immobilization: optimization of the enzyme/carrier ratio (w/w)

3-Aminopropyl silica gel (25 mg) was suspended in phosphate buffer (pH 7, 1 mL) and treated with the glutaraldehyde solution as described in the previous paragraph. Five equivalent portions of the resulting silica (5 mg) were suspended in

50 mM phosphate buffer at pH 6 (1 mL) containing different amounts of partially purified AAS (0.125, 0.25, 0.5, 1, and 2 mg). The suspensions were shaken at 25 °C for 2.5 h and then centrifuged. The amount of immobilized proteins and the activity of the carrier bound enzyme (Table 2) were determined as described before.

AAS immobilization: the effect of the Schiff's base double bond reduction

The immobilized AAS (20 mg) prepared as described in the previous paragraph (enzyme/carrier ratio 0.2 : 1) was suspended in 50 mM phosphate buffer at pH 6.5 (4 mL). The suspension was divided into two equivalent portions; the first one was used for the control experiment. To the second one sodium cyanoborohydride (13 mg, 0.20 mmol) was added in small portions. The two samples were shaken at 25 °C for 1.5 hours and then washed with the above buffer. The activity of the two heterogeneous catalysts was assayed by GC-analysis showing a volumetric activity of 3.5 and 0.8 U g^{-1} for the reference and the reduced catalyst, respectively. The assays were daily repeated for one month: the final volumetric activities are 2.8 and 0.6 U g^{-1}.

Effect of pH on the activity of free and immobilized AAS

The free and the immobilized AAS enzyme (*ca.* 0.01 U) were added to a reaction mixture (1 mL) containing 2,3-pentanedione **1a** (10 mM), ThDP (0.4 mM) and $MgSO_4$ (0.8 mM) dissolved in the appropriate buffer. The used buffers were 50 mM acetate for pH 5 and 50 mM phosphate for pH 6–8. After 2 h the reactions were treated and analyzed as described before. The results are summarized in Fig. 4.

Homo-coupling of α-diketones 1a–g with the immobilized AAS under batch conditions

The heterogeneous enzyme prepared under the above optimized immobilization conditions (pH 6.0, enzyme/carrier ratio = 0.2 : 1, no imine bond reduction) was used in this study. The silica supported AAS (250 mg, *ca.* 0.9 U) was added to a solution of ThDP (18 mg, 0.04 mmol) and $MgSO_4$ (10 mg, 0.08 mmol) in 50 mM phosphate buffer at pH 6.5 (100 mL). The α-diketone **1** (1 mmol) dissolved in DMSO (1 mL) was then added to the above suspension; the reaction was performed in a reciprocal shaker (100 rpm) at 30 °C for 10 h. After removing the catalyst by filtration, the aqueous mixture was extracted with Et_2O (3 × 20 mL) and the combined organic layers were washed with a saturated NaH_2CO_3 solution (5 mL). The ethereal solvent was then removed under a nitrogen stream and the residue containing the target α-hydroxyketones **2** and **3** was purified by either bulb-to-bulb distillation (compounds **3f** and **3g**) or flash chromatography (compounds **2a–d** and **3a–d**).

(*R*)-3-Hydroxy-3-methylhexane-2,4-dione (2a). Column chromatography with 12 : 1 cyclohexane–AcOEt afforded **2a**[20a] (66 mg, 46%) as a colorless oil; $[\alpha]_D$ = 18.2 (*c* 0.5, $CHCl_3$). ^{1}H NMR: δ = 1.05 (t, 3H, *J* = 7.5 Hz, CH_3), 1.55 (s, 3H, CH_3), 2.27 (s, 3H, CH_3CO), 2.51 (dq, 1H, *J* = 21 Hz, *J* = 7.5 Hz, CH_{2a}), 2.73 (dq, 1H, *J* = 21 Hz, *J* = 7.5 Hz, CH_{2b}), 4.65 (br s, 1H, OH); ^{13}C NMR: δ = 7.5, 22.8, 24.5, 87.4, 207.4, 210.2; GC–MS: retention time: 15.4 (*S*)-enantiomer and 15.9 (*R*)-enantiomer, ee 85%; MS (70 eV, EI); *m*/*z* (%) 145 (≤1), 102 (27), 88 (100), 57 (25), 43 (30). ESI MS (144.1): 145.1 (M + H^+). HRMS (ESI) *m*/*z* calcd for $C_7H_{13}O_3$ [M + H]$^+$ 145.0845, found 145.0892. Found: C, 58.55; H, 8.21. $C_7H_{12}O_3$ requires C, 58.32; H, 8.39%.

A chromatographic fraction containing 3-ethyl-3-hydroxy-2,4-pentanedione **3a** was collected for **3a**[20a] identification. Compound **3a** partially decomposes on silica gel. ^{1}H NMR: δ = 1.85 (t, 3H, *J* = 7.5 Hz, CH_3), 2.05 (q, 2H, *J* = 7.5 Hz, CH_2), 2.27 (s, 6H, $2CH_3CO$); 4.7 (br s, 1H, OH).

(*R*)-3-Hydroxy-3-methyl-2,4-heptanedione (2b). Column chromatography with 12 : 1 cyclohexane–AcOEt afforded **2b**[20a] (76 mg, 48%) as a colorless oil; $[\alpha]_D$ = 4.1 (*c* 0.5, $CHCl_3$). ^{1}H NMR: δ = 0.91 (t, 3H, *J* = 7.5 Hz, CH_3), 1.56 (s, 3H, CH_3), 1.58–1.65 (m, 2H, CH_2), 2.25 (s, 3H, CH_3CO), 2.49 (dt, 1H, *J* = 17.5 Hz, *J* = 7.5 Hz, CH_{2a}), 2.68 (dt, 1H, *J* = 17.5 Hz, *J* = 7.5 Hz CH_{2b}), 4.75 (br s, 1H, OH); ^{13}C NMR: δ = 13.5, 16.8, 22.6, 24.6, 38.6, 87.6, 207.4, 209.5; GC–MS: retention time (min) 20.8 (*S*)-enantiomer and 20.9 (*R*)-enantiomer, ee 91%; MS (70 eV, EI): *m*/*z* (%) 159 (≤1), 116 (21), 88 (100), 71 (37), 43 (46). ESI MS (158.2): 181.4 (M + Na^+). HRMS (ESI) *m*/*z* calcd for $C_8H_{14}O_3$ [M]$^+$ 158.0943, found 158.0912. Found: C, 60.98; H, 8.70. $C_8H_{14}O_3$ requires C, 60.74; H, 8.92%.

A chromatographic fraction containing 3-hydroxy-3-propylpentane-2,4-dione **3b** was collected for **3b**[20a] identification. Compound **3b** partially decomposes on silica gel. ^{1}H NMR: δ = 0.95 (t, 3H, *J* = 7.5 Hz, CH_3); 1.22 (m, 2H, CH_2); 1.93 (m, 2H, CH_2), 2.24 (s, 6H, 2 CH_3CO), 4.65 (br s, 1H, OH).

(*R*)-3-Hydroxy-3-methyl-2,4-octanedione (2c). Column chromatography with 12 : 1 cyclohexane–AcOEt afforded **2c**[18] (77 mg, 45%) as a colorless oil; $[\alpha]_D$ = 7.3 (*c* 0.2, $CHCl_3$). ^{1}H NMR: δ = 0.93 (t, 3H, *J* = 7.5 Hz, CH_3), 1.22–1.36 (m, 2H, CH_2), 1.48–1.62 (m, 2H, CH_2), 1.56 (s, 3H, CH_3), 2.25 (s, 3H, CH_3CO), 2.51 (dt, 1H, *J* = 17.5 Hz, *J* = 7.5 Hz, CH_2CO), 2.70 (dt, 1H, *J* = 17.5, *J* = 7.5 Hz, CH_2CO), 4.75 (br s, 1H, OH). ^{13}C NMR: δ = 13.8, 22.5, 22.7, 24.6, 25.5, 36.5, 87.6, 207.4, 209.6; GC–MS: retention time (min) 23.7 (*S*)-enantiomer and 23.8 (*R*)-enantiomer, ee 72%; MS (70 eV, EI): *m*/*z* (%) 172 (<1), 130 (20), 88 (100), 43 (45). ESI MS (172.2): 173.8 (M + H^+). HRMS (ESI) *m*/*z* calcd for $C_9H_{17}O_3$ [M + H]$^+$ 173.1178, found 173.1112. Found: C, 62.88; H, 9.12. $C_9H_{16}O_3$ requires C, 62.77; H, 9.36%.

A chromatographic fraction containing 3-butyl-3-hydroxypentane-2,4-dione **3c**[18] was collected for **3c** identification. Compound **3c** partially decomposes on silica gel. ^{1}H NMR: δ = 0.91 (t, 3H, *J* = 7.5 Hz, CH_3), 1.10–1.40 (m, 4H, $2CH_2$), 1.95–2.05 (m, 2H, CH_2), 2.25 (s, 6H, $2CH_3CO$), 4.65 (br s, 1H, OH).

(*R*)-3-Hydroxy-3-methylnonane-2,4-dione (2d). Column chromatography with 20 : 1 cyclohexane–AcOEt afforded **2d**[20b] (108 mg, 58%) as a colorless oil; $[\alpha]_D$ = 10.4 (*c* 0.2, $CHCl_3$). ^{1}H NMR: δ = 0.85 (t, *J* = 7.5 Hz, 3H, CH_3), 1.15–1.35 (m, 5H), 1.52 (s, 3H), 1.45–1.58 (m, 1H), 2.20 (s, 3H), 2.47 (dt, *J* = 7.0 Hz, *J* = 17.0 Hz, 1H), 2.65 (dt, *J* = 7.0 Hz, *J* = 17.0 Hz, 1H), 4.70 (s, 1H); ^{13}C NMR: δ = 13.8, 22.3, 22.6, 22.7, 23.0, 31.1, 36.7, 87.5, 207.4, 209.6; GC–MS: retention time (min) 22.7

(*S*)-enantiomer and 22.9 (*R*)-enantiomer, ee 55%; MS (70 eV, EI): *m*/*z* (%) 187 (3), 144 (20), 99 (55), 88 (100). ESI MS (186.2): 187.7 ($M + H^+$). HRMS (ESI) *m*/*z* calcd for $C_{10}H_{18}NaO_3$ $[M + Na]^+$ 209.1154, found 209.1180. Found: C, 64.88; H, 9.52. $C_{10}H_{18}O_3$ requires C, 64.49; H, 9.74%.

A chromatographic fraction containing 3-butyl-3-hydroxypentane-2,4-dione **3d**[20b] was collected for **3d** identification. ^{1}H NMR: δ = 0.92 (t, J = 7.0 Hz, 3H), 1.20 (m, 6H), 1.95–2.05 (m, 2H), 2.28 (s, 6H), 4.70 (s, 1H).

(*R*)-2-Hydroxy-2-methyl-1-phenyl-1,3-butanedione (2e). Column chromatography with 10 : 1 cyclohexane–AcOEt afforded **2e**[20a] (67 mg, 35%) as a colorless oil; $[\alpha]_D$ = 13.7 (*c* 0.5, $CHCl_3$). ^{1}H NMR: δ = 1.70 (s, 3H, CH_3), 2.24 (s, 3H, CH_3CO), 5.02 (br s, 1H, OH), 7.42–8.21 (m, 5H, Ph); ^{13}C NMR: δ = 23.4, 24.7, 85.8, 128.6, 129.8, 133.6, 133.9, 197.9, 206.5; GC–MS (temperature program from 100 to 200 °C with a gradient of 5 °C min^{-1}): retention time (min) 16.6 (*S*)-enantiomer and 16.7 (*S*)-enantiomer, ee 80%; MS (70 eV, EI): *m*/*z* (%) 193 (2), 150 (24), 105 (100), 77 (56). ESI MS (192.2): 215.8 ($M + Na^+$). HRMS (ESI) *m*/*z* calcd for $C_{11}H_{12}O_3$ $[M]^+$ 192.0786, found 192.0755. Found: C, 68.22; H, 6.45. $C_{11}H_{12}O_3$ requires C, 68.74; H, 6.29%.

3-Hydroxy-3-methylpentane-2,4-dione (3f). The crude reaction mixture was bulb-to-bulb distilled (50 °C, 5 mmHg) to give **3f**[20a,31] (111 mg, 85%) as a colorless liquid. Lit.:[31] bp 43–44 °C (4 mmHg). ^{1}H NMR: δ = 1.60 (s, 3H, CH_3), 2.30 (s, 6H, $2CH_3CO$), 4.70 (s, 1H, OH). ^{13}C NMR: δ = 22.6, 24.7, 87.6, 207.4; GC–MS (temperature program from 60 to 200 °C with a gradient of 2 °C min^{-1}): retention time (min) 15.1. ESI MS (130.1): 153.4 ($M + Na^+$). HRMS (ESI) *m*/*z* calcd for $C_6H_{10}NaO_3$ $[M + Na]^+$ 153.0528, found 153.0562. Found: C, 55.20; H, 7.88. $C_6H_{10}O_3$ requires C, 55.37; H, 7.74%. Compound **3f** partially decomposes on silica gel.

4-Ethyl-4-hydroxyheptane-3,5-dione (3g). The crude reaction mixture was bulb-to-bulb distilled (84 °C, 5 mmHg) to give **3g**[20a,32] (134 mg, 78%) as a colorless liquid. ^{1}H NMR: δ = 0.82 (t, 3H, J = 7.5 Hz, CH_3), 1.04 (t, 6H, J = 7.5 Hz, $2CH_3$), 2.04 (q, 2H, J = 7.5 Hz, CH_2), 2.51 (dq, 2H, J = 21.0 Hz, J = 7.5 Hz, CH_2), 2.73 (dq, 2H, J = 21.0 Hz, J = 7.5 Hz, CH_2), 4.65 (br s, 1H, OH); ^{13}C NMR: δ = 7.3, 7.4, 29.8, 30.6, 90.9, 210.2; GC–MS: retention time (min) 22.5. ESI MS (172.2): 173.5 ($M + H^+$). HRMS (ESI) *m*/*z* calcd for $C_9H_{16}O_3$ $[M]^+$ 172.1099, found 172.1028. Found: C, 55.20; H, 7.88. $C_9H_{16}O_3$ requires C, 62.77; H, 9.36%. Compound **3g** partially decomposes on silica gel.

Microreactor preparation/characterization and instrumental set-up

Microreactor packing. The microreactor was fabricated using a 100 × 2.1 mm stainless steel column, which was filled with 3-aminopropyl silica by slurry-packing. Slurry-packing was performed under constant pressure (300 bars, 30 min, toluene as the solvent) using an air driven liquid pump (by Haskel). Slurry was prepared by suspending excess in weight functionalized silica in toluene.

Determination of the microreactor void volume. The microreactor void volume (V_0) was determined by pycnometry.[33] This method consists of filling the microreactor successively with two distinct solvents (here noted as 1 and 2) and weighing the filled microreactors accurately. Simple math shows that[34]

$$V_0 = \frac{w_1 \quad w_2}{\delta_1 \quad \delta_2} \tag{1}$$

where w_1 and w_2 are the weights of the microreactor filled with solvents 1 and 2 and δ_1 and δ_2 are the densities of the solvents, respectively.

Determination of the packing amount inside the microreactor. The determination of the amount of material contained in the microreactor is based on the consideration that the microreactor weight, w_{tot}, can be expressed as:

$$w_{tot} = w_0 + w_{ads} + w_{hw} \tag{2}$$

where w_0 and w_{ads} are the weights of the liquid and the adsorbent inside the reactor (packing), respectively. w_{hw} is the weight of the stainless steel hardware (*i.e.* the weight of the empty microreactor). Eqn (2) can be rewritten as:

$$w_{tot} = V_0\delta_0 + w_{ads} + w_{hw} \tag{3}$$

where δ_0 is the density of the solvent with which the microreactor was filled. Since V_0 is known from eqn (1), w_{tot} is readily available and w_{hw} can be measured before packing, eqn (3) allows the estimation of w_{ads} for a slurry-packed microreactor without destroying the device.

Enzyme immobilization under flow conditions

The microreactor was provided with fittings, connected to an HPLC pump, and washed in sequence with isopropanol, water, and 50 mM phosphate buffer at pH 7. After that, a 2.5% glutaraldehyde solution in 50 mM phosphate buffer at pH 7 was flushed through the column (2 h; flow rate: 0.15 mL min^{-1}) and then washed with 50 mM phosphate buffer at pH 6 (2 h; flow rate: 0.15 mL min^{-1}). The aldehyde functionalized column was then fed (flow rate: 0.10 mL min^{-1}) with a 0.1% (w/v) solution of AAS in phosphate buffer pH 6 (20 mL) containing ThDP (0.4 mM) and $MgSO_4$ (0.8 mM). The resulting bioreactor was finally washed with the buffer until the eluate absorbance at 280 nm reached the background value.

Homo-coupling of α-diketones 1a–g under flow conditions

The microreactor was equilibrated with 50 mM triethanolamine at pH 6.5 and then fed with a solution of α-diketone **1** (10 mM; see Table 4 for different molarity concentrations), ThDP (0.04 mM) and $MgSO_4$ (0.08 mM) in the equilibration buffer containing DMSO (1% w/v). The microreactor was operated at 30 °C for 24 h (under steady-state conditions) at the stated flow rate. Instant conversion was determined (GC analysis) every 60 min by taking a sample of the eluate. The solution collected after 24 h was extracted with Et_2O (3 × 20 mL) and the combined organic layers were washed with a saturated NaH_2CO_3 solution (5 mL). The ethereal solvent was then removed under a nitrogen stream and the residue containing the target α-hydroxyketones **2** and **3** was purified by either bulb-to-bulb distillation (compounds **3f** and **3g**) or flash chromatography (compounds **2a–d** and **3a–d**).

The long-term stability experiment was performed using the α-diketone **1** (0.10 M) as the substrate; the microreactor was operated at 30 °C with a flow rate of 10 μL min^{-1} for 30 days. After the achievement of the steady-state regime (*ca*. 1 h), conversion of **1a** in the range 78–70% was maintained for 15 days, while a progressive loss of catalytic activity was observed after that time.

Acknowledgements

We gratefully acknowledge the University of Ferrara (fondi FAR) for financial support. Thanks are also given to Mr P. Formaglio for NMR spectroscopic experiments, to Mrs E. Bianchini for elemental analyses, to Dr T. Bernardi for high-resolution mass spectrometric experiments, and to Dr M. De Bastiani for electrophoretic analyses.

Notes and references

1 (*a*) T. Tsubogo, T. Ishiwata and S. Kobayashi, *Angew. Chem., Int. Ed.*, 2013, **52**, 6590; (*b*) A. Puglisi, M. Benaglia and V. Chiroli, *Green Chem.*, 2013, **15**, 1790; (*c*) T. Chinnusamy, S. Yudha, M. Hager, P. Kreitmeier and O. Reiser, *ChemSusChem*, 2012, **5**, 247; (*d*) D. Zhao and K. Ding, *ACS Catal.*, 2013, **3**, 928; (*e*) X. Y. Mak, P. Laurino and P. H. Seeberger, *Beilstein J. Org. Chem.*, 2009, **5**, DOI: 10.3762/bjoc.5.19.

2 (*a*) V. Hessel, D. Kralisch, N. Kockmann, T. Noël and Q. Wang, *ChemSusChem*, 2013, **6**, 746; (*b*) S. C. Stouten, T. Noël, Q. Wang and V. Hessel, *Aust. J. Chem.*, 2013, **66**, 121; (*c*) D. T. McQuade and P. H. Seeberger, *J. Org. Chem.*, 2103, **78**, 6384; (*d*) T. Illg, P. Löb and V. Hessel, *Bioorg. Med. Chem.*, 2010, **18**, 3707; (*e*) K. Geyer, T. Gustafsson and P. H. Seeberger, *Synlett*, 2009, 2382; (*f*) B. P. Mason, K. E. Price, J. L. Steinbacher, A. R. Bogdan and D. T. McQuade, *Chem. Rev.*, 2007, **107**, 2300; (*g*) I. R. Baxendale, S. V. Ley, A. C. Mansfield and C. D. Smith, *Angew. Chem., Int. Ed.*, 2009, **48**, 4017; (*h*) I. R. Baxendale, J. J. Hayward, S. Lanners, S. V. Ley and C. D. Smith, in *Microreactors in Organic Synthesis and Catalysis*, ed. T. Wirth, Wiley-VCH, Weinheim, 2008, ch. 4.2, pp. 84; (*i*) A. R. Bogdan, S. L. Poe, D. C. Kubis, S. J. Broadwater and D. T. McQuade, *Angew. Chem., Int. Ed.*, 2009, **48**, 8547; (*j*) F. E. Valera, M. Quaranta, A. Moran, J. Blacker, A. Armstrong, J. T. Cabral and D. G. Blackmond, *Angew. Chem., Int. Ed.*, 2010, **49**, 2478; (*k*) L. Malet-Sanz and F. Susanne, *J. Med. Chem.*, 2012, **55**, 4062.

3 (*a*) C. G. Frost and L. Mutton, *Green Chem.*, 2010, **12**, 1687; (*b*) A. R. Bogdan, B. P. Mason, K. T. Sylvester and D. T. McQuade, *Angew. Chem., Int. Ed.*, 2007, **46**, 1698; (*c*) A. Kirschning, W. Solodenko and K. Mennecke, *Chem. – Eur. J.*, 2006, **12**, 5972; (*d*) M. Irfan, T. N. Glasnov and C. Oliver Kappe, *ChemSusChem*, 2011, **4**, 300.

4 (*a*) O. Bortolini, A. Cavazzini, P. Dambruoso, P. P. Giovannini, L. Caciolli, A. Massi, S. Pacifico and D. Ragno, *Green Chem.*, 2013, **15**, 2981; (*b*) O. Bortolini, A. Cavazzini, P. P. Giovannini, R. Greco, N. Marchetti, A. Massi and L. Pasti, *Chem. – Eur. J.*, 2013, **19**, 7802; (*c*) O. Bortolini, L. Caciolli, A. Cavazzini, V. Costa, R. Greco, A. Massi and L. Pasti, *Green Chem.*, 2012, **14**, 992; (*d*) A. Massi, A. Cavazzini, L. Del Zoppo, O. Pandoli, V. Costa, L. Pasti and P. P. Giovannini, *Tetrahedron Lett.*, 2011, **52**, 619; (*e*) A. Massi, O. Pandoli, A. Cavazzini, L. Del Zoppo, P. P. Giovannini and C. Bendazzoli, *Italian Patent*, 0001398243, 2013.

5 (*a*) G. Kardos and T. Soós, *Eur. J. Org. Chem.*, 2013, 4490; (*b*) P. Kasaplar, C. Rodríguez-Escrich and M. A. Pericàs, *Org. Lett.*, 2013, **15**, 3498; (*c*) Y. Arakawa and H. Wennemers, *ChemSusChem*, 2013, **6**, 242; (*d*) S. B. Otvos, I. M. Mandity and F. Fulop, *ChemSusChem*, 2012, **5**, 266; (*e*) L. Osorio-Planes, C. Rodríguez-Escrich and M. A. Pericàs, *Org. Lett.*, 2012, **14**, 1816; (*f*) C. Ayats, A. H. Henseler and M. A. Pericàs, *ChemSusChem*, 2012, **5**, 320; (*g*) X. C. Cambeiro, R. Martín-Rapún, P. O. Miranda, S. Sayalero, E. Alza, P. Llanes and M. A. Pericàs, *Beilstein J. Org. Chem.*, 2011, **7**, 1486; (*h*) A. L. W. Demuynck, L. Peng, F. de Clippel and J. Vanderleyden, *Adv. Synth. Catal.*, 2011, **353**, 725; (*i*) E. Alza, S. Sayalero, X. C. Cambeiro, R. Martín-Rapún, P. O. Miranda and M. A. Pericàs, *Synlett*, 2011, 464; (*j*) E. Alza, C. Rodríguez-Escrich, S. Sayalero, A. Bastero and M. A. Pericàs, *Chem. – Eur. J.*, 2009, **15**, 10167; (*k*) F. Bonfils, I. Cazaux, P. Hodge and C. Caze, *Org. Biomol. Chem.*, 2006, **4**, 493; (*l*) D. Bernstein, S. France, J. Wolfer and T. Lectka, *Tetrahedron: Asymmetry*, 2005, **16**, 3481; (*m*) S. France, D. Bernstein, A. Weatherwax and T. Lectka, *Org. Lett.*, 2005, **7**, 3009; (*n*) A. M. Hafez, A. E. Taggi, T. Dudding and T. Lectka, *J. Am. Chem. Soc.*, 2001, **123**, 18853; (*o*) R. Porta, M. Benaglia, V. Chiroli, F. Coccia and A. Puglisi, *Isr. J. Chem.*, 2014, DOI: 10.1002/ijch.201300106; (*p*) S. Martín, R. Porcar, E. Peris, M. I. Burguete, E. García-Verdugo and S. V. Luis, *Green Chem.*, 2014, **16**, 1639; (*q*) V. Chiroli, M. Benaglia, A. Puglisi, R. Porta, R. P. Jumde and A. Mandoli, *Green Chem.*, 2014, **16**, 2798; (*r*) R. Martín-Rapún, S. Sayalero and M. A. Pericàs, *Green Chem.*, 2013, **15**, 3295; (*s*) V. Chiroli, M. Benaglia, F. Cozzi, A. Puglisi, R. Annunziata and G. Celentano, *Org. Lett.*, 2013, **15**, 3590; (*t*) M. Rueping, C. Vila and T. Bootwicha, *ACS Catal.*, 2013, **3**, 1676; (*u*) E. Sugiono and M. Rueping, *Beilstein J. Org. Chem.*, 2013, **9**, 2457.

6 M. Movassaghi and E. N. Jacobsen, *Science*, 2002, **298**, 1904.

7 (*a*) A. Liese, K. Seebach and C. Wandrey, *Industrial Biotransformations*, Wiley-VCH, Weinheim, 2nd edn, 2006; (*b*) N. N. Rao, S. Lütz, K. Wurges and D. Minör, *Org. Process Res. Dev.*, 2009, **13**, 607; (*c*) G. Grogan, *Annu. Rep. Progr. Chem., Sect. B: Org. Chem.*, 2013, **109**, 15; (*d*) N. End and U. Schöning, *Top. Curr. Chem.*, 2004, **242**, 273.

8 (*a*) H. E. Schoemaker, D. Mink and M. G. Wubbolts, *Science*, 2003, **299**, 1694; (*b*) U. T. Bornscheuer, G. W. Huisman, R. J. Kazlauskas, S. Lutz, J. C. Moore and K. Robins, *Nature*, 2012, **485**, 185.

9 (*a*) P. Rasor, Immobilized enzymes in enantioselective organic synthesis, in *Chiral catalyst immobilization and recycling*, ed. D. E. De Vos, I. F. J. Vancelecom and P. A. Jacobs, Wiley-VCH, Weinheim, 2000, p. 97; (*b*) G. F. Bickerstaff, Immobilization of biocatalysts, in *Molecular biology and biotechnology*, ed. J. M. Walker and R. Rapley, RCS, London, 4th edn, 2000, p. 433; (*c*) L. Lalonde and A. Margolin, in *Enzyme catalysis in organic synthesis*, ed. K. Drauz and H. Waldmann, Wiley-VCH, Weinheim, 2nd revised edn, vol. 1, 2002, p. 163; (*d*) S. Pedersen and M. W. Christensen, in *Applied Biocatalysis*, ed. A. J. J. Straathof and P. Adlercreutz, CRC Press, Boca Raton, 2nd edn, 2000, p. 213.

10 (*a*) K. Faber and R. Patel, *Curr. Opin. Biotechnol.*, 2000, **11**, 517; (*b*) W. Keim and B. Driessen-Holscher, Supported catalysts. Deposition of active component. Heterogenization of complexes and enzymes, in *Preparation of solid catalysts*, ed. G. K. H. Ertl and J. Weitkamp, Wiley-VCH, Weinheim, 1999, p. 355.

11 (*a*) I. J. Dunn, E. Heinzle, J. Ingham and J. E. Prenosil, *Biological Reaction Engineering*, Wiley-VCH, Weinheim, 2003; (*b*) E. G. Vlakh and T. B. Tennikova, *J. Sep. Sci.*, 2013, **36**, 110; (*c*) E. G. Vlakh and T. B. Tennikova, *J. Sep. Sci.*, 2013, **36**, 1149.

12 (*a*) I. Itabaiana Jr., L. S. de Mariz e Miranda and R. O. M. Alves de Souza, *J. Mol. Catal. B: Enzym.*, 2013, **85–86**, 1; (*b*) R. Yuryev, S. Strompen and A. Liese, *Beilstein J. Org. Chem.*, 2011, **7**, 1449; (*c*) Z. Liu, J. Zhang, X. Chen and P. G. Wang, *ChemBioChem*, 2002, **3**, 348; (*d*) M. J. Fink, M. Scöhn, F. Rudroff, M. Schnürch and M. D. Mihovilovic, *ChemCatChem*, 2013, **5**, 724.

13 (*a*) P. Fernandes, *Int. J. Mol. Sci.*, 2010, **11**, 858; (*b*) M. S. Thomsen and B. Nidetzky, *Eng. Life Sci.*, 2008, **8**, 40; (*c*) J. M. Bolivar, J. Wiesbauer and B. Nidetzky, *Trends Biotechnol.*, 2011, **29**, 333; (*d*) M. Wu, H. Zhang, Z. Wang, S. Shen, X. C. Lea and X.-F. Li, *Chem. Commun.*, 2013, **49**, 1407; (*e*) R. de Oliveira Lopes, A. S. de Miranda, B. Reichart, T. Glasnov, C. O. Kappe, R. C. Simon, W. Kroutil, L. S. M. Miranda, I. C. R. Leal and R. O. M. A. de Souza, *J. Mol. Catal. B: Enzym.*, 2014, **104**, 107 For an interesting study on enzyme-catalyzed ring-opening polymerization in microreactors, see: (*f*) S. Kundu, A. S. Bhangale, W. E. Wallace, K. M. Flynn, C. M. Guttman, R. A. Gross and K. L. Beers, *J. Am. Chem. Soc.*, 2011, **133**, 6006.

14 (*a*) P. Chen, S. Han, G. Lin and Z. Li, *J. Org. Chem.*, 2002, **67**, 8251; (*b*) K. Koch, R. J. F. van den Berg, P. J. Nieuwland, R. Wijtmans, H. E. Schoemaker, J. C. M. van Hest and F. P. J. T. Rutjes, *Biotechnol. Bioeng.*, 2007, **99**, 1028.

15 L. Babich, A. F. Hartog, L. J. C. van Hemert, F. P. J. T. Rutjes and R. Wever, *ChemSusChem*, 2012, **5**, 2348.

16 (*a*) G. Dräger, C. Kiss, U. Kunz and A. Kirschning, *Org. Biomol. Chem.*, 2007, **5**, 3657; (*b*) N. Kurlemann and A. Liese, *Tetrahedron: Asymmetry*, 2004, **15**, 2955; (*c*) H. S. Shin and P. L. Rogers, *Biotechnol. Bioeng.*, 1996, **49**, 429; (*d*) F. Hildebrand, S. Khül, M. Pohl, D. Vasic-Racki, M. Müller, C. Wandrey and S. Lütz, *Biotechnol. Bioeng.*, 2006, **96**, 835; (*e*) R. Mikolajek, A. C. Spiess, M. Pohl, S. Lamare and J. Büchs, *ChemBioChem*, 2007, **8**, 1063; (*f*) T. Stillger, M. Pohl, C. Wandrey and A. Liese, *Org. Process Res. Dev.*, 2006, **10**, 1172; (*g*) A. A. Halima, N. Szitaa and F. Baganz, *J. Biotechnol.*, 2013, **168**, 567; (*h*) J. Lawrence, B. O'Sullivan, G. J. Lye, R. Wohlgemuth and N. Szitaa, *J. Mol. Catal. B: Enzym.*, 2013, **95**, 111; (*i*) B. O'Sullivan, H. Al-Bahrani, J. Lawrence, M. Campos, A. Cázares, F. Baganz, R. Wohlgemuth, H. C. Hailes and N. Szita, *J. Mol. Catal. B: Enzym.*, 2012, **77**, 1.

17 (*a*) G. Olack and H. Morrison, *J. Org. Chem.*, 1991, **56**, 4969; (*b*) F. A. Davis, C. Clark, A. Kumar and B.-C. Chen, *J. Org. Chem.*, 1994, **59**, 1184; (*c*) K. Tamaki, J. B. Shotwell, R. D. White, I. Drutu, D. T. Petsch, T. V. Nheu, H. He, Y. Hirokawa, H. Maruta and J. L. Wood, *Org. Lett.*, 2001, **3**, 1689; (*d*) F. Neuser, H. Zorn and R. G. Berger, *J. Agric. Food Chem.*, 2000, **48**, 6191; (*e*) P. E. Sum and P. Petersen, *Bioorg. Med. Chem. Lett.*, 1999, **9**, 1459; (*f*) W. E. Rose and M. J. Rybak, *Pharmacotherapy*, 2006, **26**, 1099.

18 P. P. Giovannini, G. Fantin, A. Massi, V. Venturi and P. Pedrini, *Org. Biomol. Chem.*, 2011, **9**, 8038 and references therein.

19 For approaches based on direct C–C bond formation, see: (*a*) C. A. Rose, S. Gundala, C.-L. Fagan, J. F. Franz, S. J. Connon and K. Zeitler, *Chem. Sci.*, 2012, **3**, 735; (*b*) O. Bortolini, G. Fantin, M. Fogagnolo, P. P. Giovannini, V. Venturi, S. Pacifico and A. Massi, *Tetrahedron*, 2011, **67**, 8110 For selected examples of more elaborated oxidative strategies, see: (*c*) J. Christoffers, *J. Org. Chem.*, 1999, **64**, 7668; (*d*) A. M. R. Smith, H. S. Rzepa, A. J. P. White, D. Billen and K. K. Hii, *J. Org. Chem.*, 2010, **75**, 3085 and references therein.

20 (*a*) P. P. Giovannini, P. Pedrini, V. Venturi, G. Fantin and A. Medici, *J. Mol. Catal. B: Enzym.*, 2010, **64**, 113; (*b*) O. Bortolini, P. P. Giovannini, S. Maietti, A. Massi, P. Pedrini, G. Sacchetti and V. Venturi, *J. Mol. Catal. B: Enzym.*, 2013, **85–86**, 93.

21 (*a*) P. Lehwald, M. Richter, C. Röhr, H.-w. Liu and M. Müller, *Angew. Chem., Int. Ed.*, 2010, **49**, 2389; (*b*) M. Müller, G. A. Sprenger and M. Pohl, *Curr. Opin. Chem. Biol.*, 2013, **17**, 261–270.

22 U. T. Bornscheuer, *Angew. Chem., Int. Ed.*, 2003, **42**, 3336.

23 H. H. Weetal, *Methods in Enzymology*, ed. K. Mosbach, Academic Press, New York, 1976, vol. 44, pp. 134.

24 (*a*) A. L. Ahmad, E. M. Low and S. R. A. Shukor, *J. Mol. Catal. B: Enzym.*, 2013, **88**, 26; (*b*) R. Lin, R. Wu, X. Huang and T. Xie, *Prep. Biochem. Biotechnol.*, 2011, **41**, 154; (*c*) L. Lloret, F. Hollmann, G. Eibes, G. Feijoo, M. T. Moreira and J. M. Lema, *Biodegradation*, 2012, **23**, 373.

25 M.-C. Yen, W.-H. Hsu and S.-C. Lin, *Process Biochem.*, 2010, **45**, 667.

26 (*a*) M. Guillén, M. D. Benaiges and F. Valero, *Biotechnol. Prog.*, 2011, **27**, 1232; (*b*) M. J. Hernaiz and D. H. G. Crout, *Enzyme Microb. Technol.*, 2000, **27**, 26.

27 W. J. Ting, K. Y. Tung, R. Giridhar and W. T. Wu, *J. Mol. Catal. B: Enzym.*, 2006, **42**, 32.

28 (*a*) A. M. Girelli, E. Mattei and A. Messina, *Sens. Actuators, B*, 2007, **121**, 515; (*b*) G. Felix and V. Descorps, *Chromatographia*, 1999, **49**, 595.

29 A slow but detectable decomposition of **1a** was observed in phosphate buffer (pH 6.5); the mechanism of this undesired side reaction is currently under investigation.

30 According to literature reports, we assumed that the absorbance at 280 and 215 nm of a 1% solution of the protein ($A_{280}^{1\%}$ and $A_{215}^{1\%}$) equals 13 and 200, respectively. The given values of protein concentration (Tables 1 and 2) result from the average of spectrophotometric measurements carried out at the above wavelengths.(*a*) W. J. Waddell, *J. Lab. Clin. Med.*, 1956, **48**, 311; (*b*) C. N. Pace, F. Vajdos, L. Fee, G. Grimsley and T. Gray, *Protein Sci.*, 1995, **4**, 2411.

31 J. Christoffers, T. Kauf, T. Werner and M. Rössle, *Eur. J. Org. Chem.*, 2006, 2601.

32 C. Clausen, I. Weidner and H. Butenschön, *Eur. J. Org. Chem.*, 2000, 3799.

33 R. M. McCormick and B. L. Karger, *Anal. Chem.*, 1980, **52**, 2249.

34 F. Gritti, Y. Kazakevich and G. Guiochon, *J. Chromatogr. A*, 2007, **1161**, 157.

Journal of Chromatography A, 1354 (2014) 43–55

Contents lists available at ScienceDirect

Journal of Chromatography A

journal homepage: www.elsevier.com/locate/chroma

Synthetic oligonucleotide separations by mixed-mode reversed-phase/weak anion-exchange liquid chromatography

Aleksandra Zimmermann[a], Roberto Greco[b], Isabel Walker[a], Jeannie Horak[a], Alberto Cavazzini[b], Michael Lämmerhofer[a,*]

[a] Institute of Pharmaceutical Sciences, University of Tübingen, Auf der Morgenstelle 8, 72076 Tübingen, Germany
[b] Department of Chemical and Pharmaceutical Sciences, University of Ferrara, via L. Borsari 46, 44121 Ferrara, Italy

ARTICLE INFO

Article history:
Received 26 March 2014
Received in revised form 2 May 2014
Accepted 18 May 2014
Available online 27 May 2014

Keywords:
Synthetic oligonucleotides
Mixed-mode chromatography
Reversed-phase/weak anion exchange stationary phase (RP-WAX)
Mixed-gradient elution technique
Single nucleotide exchange
Ion-pair reversed-phase chromatography

ABSTRACT

Synthetic oligonucleotides gain increasing importance in new therapeutic concepts and as probes in biological sciences. If pharmaceutical-grade purities are required, chromatographic purification using ion-pair reversed-phase chromatography is commonly carried out. However, separation selectivity for structurally closely related impurities is often insufficient, especially at high sample loads. In this study, a "mixed-mode" reversed-phase/weak anion exchanger stationary phase has been investigated as an alternative tool for chromatographic separation of synthetic oligonucleotides with minor sequence variations. The employed mixed-mode phase shows great flexibility in method development. It has been run in various gradient elution modes, viz. one, two or three parameter (mixed) gradients (altering buffer pH, buffer concentration, and organic modifier) to find optimal elution conditions and gain further insight into retention mechanisms. Compared to ion-pair reversed-phase and mere anion-exchange separation, enhanced selectivities were observed with the mixed-mode phase for 20–23 nucleotide (nt) long oligonucleotides with similar sequences. Oligonucleotides differing by 1, 2 or 3 nucleotides in length could be readily resolved and separation factors for single nucleotide replacements declined in the order Cytosine (C)/Guanine (G) > Adenine (A)/Guanine ~ Guanine/Thymine (T) > Adenine/Cytosine ~ Cytosine/Thymine > Adenine/Thymine. Selectivities were larger when the modification was at the 3′ terminal-end, declined when it was in the middle of the sequence and was smallest when it was located at the 5′ terminus. Due to the lower surface area of the 200 Å pore size mixed-mode stationary phase compared to the corresponding 100 Å material, lower retention times with equal selectivities under milder elution conditions were achievable. Considering high sample loading capacities of the mixed-mode anion-exchanger phase, it should have great potential for chromatographic oligonucleotide separation and purification.

1. Introduction

Over 30 years ago, short single-stranded DNA sequences have been used for the first time to suppress gene expression of the oncogenic Rous sarcoma virus by an antisense oligonucleotide approach [1]. This can be regarded as the beginning of targeted gene silencing which is gaining popularity as a new treatment strategy for various diseases such as cancer [1,2], viral diseases [3,4], skin diseases [5], and autosomal recessive diseases [6]. Nowadays, the development in the field of therapeutic oligonucleotides comprising antisense oligonucleotides, aptamers, small interfering RNAs (siRNA), micro-RNA-targeting oligonucleotides (anti-miRNA) and immune-stimulatory oligonucleotides is very dynamic [7]. For therapeutic purposes, structures of oligonucleotides are frequently chemically modified to prevent their degradation by cellular nucleases, increasing thereby their overall stability [7,8].

Commonly, oligonucleotides are efficiently synthesized using phosphoramidite chemistry. For small scale synthesis, an automated solid-phase synthesizer is used, because the coupling efficiency per addition of nucleotide is greater than 99% and achievable purities are usually greater than 70%. While for many mechanistic (biochemical) studies the quality of the desalted raw product may be satisfactory, for their pharmaceutical or medical application e.g. in clinical trials [9] oligonucleotide products must exhibit pharmaceutical grade purity. The most common impurities are oligonucleotides with deleted or extended sequences, i.e.

* Corresponding author at: Pharmaceutical (Bio)Analysis, Institute of Pharmaceutical Sciences, University of Tübingen, Auf der Morgenstelle 8, 72076 Tübingen, Germany. Tel.: +49 7071 29 78793; fax: +49 7071 29 4565.
E-mail address: michael.laemmerhofer@uni-tuebingen.de (M. Lämmerhofer).

http://dx.doi.org/10.1016/j.chroma.2014.05.048
0021-9673/

shorter or longer oligonucleotides due to one or more missing nucleotide couplings or double, triple, etc. couplings of nucleotides, respectively. Other impurities comprise incompletely deprotected products, oligonucleotides with a loss of a purine base and other degradation products [10–12].

For biological applications, where only diminutive quantities are needed, oligonucleotides can be purified by simple polyacrylamide gel electrophoresis (PAGE). However, for clinical trials, larger quantities of oligonucleotides with pharmaceutical purity are needed, for which the most widespread purification techniques are based on preparative liquid chromatography [13]. Reversed-phase liquid chromatography (RPLC) is the method of choice but due to insufficient hydrophobicity of oligonucleotides some particular strategies are needed. One option is to maintain the protecting group dimethoxytrityl (DMT) after the last synthesis step, in order to preserve it for the chromatographic purification by RPLC [14–17]. Such a lipophilic modification supports the separation of the product from other impurities. The 'DMT on' method is fast and efficient, providing an approximate purity of 95% for a 25 mer oligonucleotide [16], yet oligonucleotides with incorrect sequence cannot be separated from the main product using RPLC. Another drawback of this method is the requirement to cleave the protecting group after purification. Hence, an additional purification step is required to ensure that no further degradation products are generated during the post-purification processing step [14–17]. For this reason, ion-pair reversed phase high performance liquid chromatography (IP-RP-HPLC) has lately become the method of choice for oligonucleotide separation and purification [9,18–21]. Various cationic counterions have been suggested and tested as ion-pair agents [22], but most commonly triethylamine (TEA) is used, mainly as acetate (TEAA) [23–25] or bicarbonate (TEAB) salts [22,26]. Alternative ion-pair agents are tetraalkylammonium cations [27], which are stronger adsorbed on the stationary phase and lead to stronger retention behaviors. On the other hand, non-volatility of these quaternary ion-pair agents limit their elimination from the purified products [14,17,28] and precludes their use with mass spectrometric detection. In general, the retention of oligonucleotides is increasing with increasing concentration of the ion-pair agent in the mobile phase, which usually favorably affects resolution of structurally related oligonucleotide impurities. Hexafluoroisopropyl alcohol (HFIP) has been suggested as additive [15,29]. With HFIP in the mobile phase, TEA as ion-pairing agent becomes less soluble and thus binds more strongly to the stationary phase, forming thereby a more stable layer of ion-pairing agent on the stationary phase. Stronger retention is the result. However, in spite of all these advancements, the overall separation of structurally closely related oligonucleotide impurities by ion-pair RPLC is still challenging due to limited retentivity and selectivity.

Thus, a variety of alternative techniques have been elucidated for oligonucleotide separation. Due to the hydrophilic nature stemming from the polar ribosyl residues and ionizable phosphate groups, hydrophilic interaction chromatography (HILIC) has been determined as a successful separation technique for oligonucleotide samples [30–37]. However, for preparative chromatography, this technique is less attractive due to the low solubility of oligonucleotides in the mobile phase and excessive acetonitrile consumption. Nonetheless, anion exchange chromatography has been successfully used for both analytical [38–42] and preparative applications [43–45]. One of the main advantages of the latter is the possibility to perform elutions under non-denaturing conditions e.g. of siRNA duplexes [45]. However, negatively charged phosphate or phosphorothionate groups along the oligonucleotide backbone strongly interact with positively charged weak or strong anion-exchange sorbents. Due to the multivalent electrostatic interactions, efficient counterions are needed for elution and retention depends on the ionic strength of the mobile phase. Typical stationary phases that have been used for this separation mode include polyethyleneimine (PEI) functionalized silica [43,44], pellicular polystyrene–divinylbenzene anion exchange stationary phase [38–42] and monolithic anion-exchange stationary phases [46–50]. Anion-exchangers can be most efficiently applied for oligonucleotide purification, if they are employed in the displacement chromatography mode [51]. By combination of anion-exchange sites with some hydrophobic moieties or backbones, mixed-mode stationary phases are created. Such phases based on RP and anion-exchange principles have already been proposed some time ago by McLaughlin for oligonucleotide separations [52]. Recently, mixed-mode chromatographic materials have experienced some advancement for pharmaceutical ion, small molecule and peptide separations [53–61]. In mixed-mode chromatographic mode, nucleic acids may be separated by a combination of electrostatic interaction (size dependent) and hydrophobic interaction (sequence dependent). Note that Biba et al. has investigated factors influencing the separation of oligonucleotides using mixed-mode stationary phases containing C18, anion- and cation-exchanger groups [62].

In the present study, the chromatographic behavior of mixed-mode reversed-phase/weak anion exchange (RP/WAX) type stationary phases for the separation of structurally closely related oligonucleotides has been elucidated. The adsorbent is based on porous silica and is functionalized on the surface with a chromatographic ligand that contains a hydrophobic alkyl strand with embedded polar functional groups (a thioether and an amide group) and a terminal quinuclidinium weak anion-exchange site. This stationary phase was already successfully used for separation of peptides, metabolites and sugar phosphates [56–60]. A series of 20–23 nt long oligonucleotides with similar sequences has been used as probes to reveal structural effects on retention and selectivity in comparison to ion-pair-RPLC (HPLC and UHPLC) as well as mere weak anion-exchange chromatography. The samples were analyzed in different elution modes, employing one, two or three parameter gradients (changing buffer pH, buffer concentration, and organic modifier). Oligonucleotide structure variations have revealed sequence-retention and sequence-selectivity relationships. Furthermore, a 200 Å wide pore material has been prepared as well and tested in comparison to the 100 Å mixed-mode phase.

2. Experimental

2.1. Materials

Acetic acid (99.8%) and triethylamine (99.5%) were purchased from Sigma–Aldrich (Munich, Germany). Orthophosphoric acid was acquired from ABCR (Karlsruhe, Germany). Deionized water was purified using Elga PurLab Ultra purification system (Celle, Germany).

The oligonucleotide test samples (see Table 1) were synthesized by Sigma Genosys and purchased as desalted raw-products. Oligonucleotide samples were prepared in deionized water at concentrations of 8 mM.

The stationary phases and columns, respectively, used in this study are summarized in Table 2 along with their properties.

2.2. Synthesis and characterization of stationary phases

2.2.1. RP/WAX stationary phases based on N-(10-undecenoyl)-3-aminoquinuclidine

The reversed-phase/weak anion exchanger mixed-mode stationary phases were synthesized as described in Ref. [59].

Briefly, *N*-(10-undecenoyl)-3-aminoquinuclidine selector was obtained by reaction of *N*-10-undecenoic acid chloride with

Table 1
Synthetic oligonucleotides used as test samples in this study. They have been derived from oligonucleotide 1 by minor sequence variations which might occur during synthesis and represent potential impurities of synthetic oligonucleotide 1.

Oligonucleotide abbreviation	Sequence 5′–3′	Mix
1	GAATCTTACGAAATACCTGAGAA	I
2	GAATCTTA**G**GAA**T**TACCTGAGAA	
3	GAATCTTACGAAA_ACCTGAGAA	
4	**C**AATCTTACGAAATACCTGAGAA	II
5	**A**AATCTTACGAAATACCTGAGAA	
6	**T**AATCTTACGAAATACCTGAGAA	
7	GAATCTTACGAAATACCTGAGA**C**	III
8	GAATCTTACGAAATACCTGAGA**G**	
9	GAATCTTACGAAATACCTGAGA**T**	
10	GAATCTTACG**C**AATACCTGAGAA	IV
11	GAATCTTACG**G**AATACCTGAGAA	
12	GAATCTTACG**T**AATACCTGAGAA	
13	GAATCTTACGAAATACCTGAGA_	V
14	GAATCTTACGAAATACCTGAG__	
15	GAATCTTACGAAATACCTGA___	
16	_AATCTTACGAAATACCTGAGAA	VI
17	__ATCTTACGAAATACCTGAGAA	
18	___TCTTACGAAATACCTGAGAA	

3-aminoquinuclidine base and covalently bonded to thiol-silica gel, based on Kromasil 100 Å or 200 Å pore size and 5 μm particle size (Eka Chemicals, Bohus, Sweden). The selector coverage on the silica surface was determined by elemental analysis and the calculations based on nitrogen provided about 0.37 mmol/g (corresponding to 1.19 μmol/m^2) for the 100 Å pore size material and 0.20 mmol/g (corresponding to 1.33 μmol/m^2) for the 200 Å silica gel. The synthesized stationary phases were packed into stainless-steel HPLC columns (for dimensions see Table 2).

2.2.2. 3-(N,N-dimethylaminopropyl-silica based anion-exchanger

The anion-exchange stationary phase (Fig. 1b) was synthesized as previously described [58] by reaction of 3-(*N*,*N*-dimethylamino)propyl trimethoxysilane with Kromasil 100 silica gel – 5 μm (Eka Chemicals, Bohus, Sweden). Elemental analysis provided a selector coverage of 1.15 mmol/g of dimethylamino groups (based on nitrogen). The synthesized stationary phase was packed into a stainless-steel HPLC column (column dimension see Table 2).

2.3. Instrumentation and chromatographic conditions

All samples were analyzed on a 1290 series LC system from Agilent Technologies (Waldbronn, Germany) equipped with a

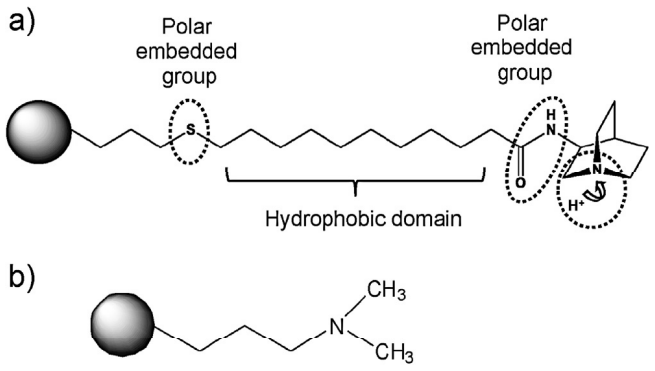

Fig. 1. Structure of (a) mixed-mode reversed-phase/weak anion-exchange stationary phase, and (b) 3-(*N*,*N*-dimethylamino)propyl-silica based weak anion-exchange stationary phase.

Table 2
Stationary phases and columns, respectively, used for the comparative column characterization.

Column name	Type	%C	%H	%N	Surface area (m^2/g)	Ligand coverage (WAX capacity) (mmol/g)	Ligand coverage (μmol/m^2)	Particle size (μm)	Pore size (Å)	Column dimension (mm × mm i.d.)
N-undecenoyl-3-aminoquinuclidine based (100 Å) (Fig. 1a)	MM	17.12	2.83	1.00	300	0.36	1.19	5	100	150 × 4
N-undecenoyl-3-aminoquinuclidine based (200 Å) (Fig. 1a)	MM	7.79	1.62	0.56	150	0.20	1.33	5	200	150 × 4
3-(*N*,*N*-dimethylamino)propyl-silica (WAX) (Fig. 1b)	WAX	6.93	1.68	1.46	320	1.15	3.59	5	100	150 × 4
Zorbax Rapid Resolution HD Eclipse Plus C18 (Agilent)	RP	9.00	–	–	160	–	–	1.8	95	50.1 × 2
Gemini C18 (Phenomenex)	RP	14.00	–	–	375	–	–	5	110	150.6 × 4

thermostated autosampler, degasser, binary pump, thermostated column compartment and diode array detector. The system was controlled by OpenLab CDS ChemStation – Edition for LC & LC/MS System (Rev. C.01.03 [37]). Data were analyzed using ChemStation software (Rev. B.04.03 [16]).

The samples were analyzed at a column temperature of 40 °C and a wavelength of 260 nm in different elution modes with one, two or three parameter gradients (altering buffer pH, buffer concentration, organic modifier) and in isocratic elution mode (see Table 3).

The mobile phase flow rate was 1.0 mL/min for the 150 × 4 mm i.d. columns and at equal linear flow velocity with other column dimensions. The injection volume was 20 μL. All detailed conditions can be found in the corresponding figures.

3. Results and discussion

3.1. Ion-pair reversed-phase vs mixed-mode RP/WAX chromatography

Oligonucleotides are highly hydrophilic and possess a multiple negatively charged backbone. Due to these properties, they interact very weakly with reversed phase stationary phases. To overcome this problem, oligonucleotide separations are nowadays commonly performed by ion-pair chromatography with cationic ion-pair agents such as triethylammonium acetate added to the mobile phase. The cationic ion-pair agent represents the counter-ion, which interacts with the negatively charged phosphate groups by electrostatic interactions and the hydrophobic moieties on the ion-pair agent eventually drive the interaction with the non-polar stationary phase of thus formed ion-paired oligonucleotides.

Herein, an oligonucleotide test mixture No. I consisting of oligonucleotide 1, 2, and 3 (the sequences of oligonucleotides are shown in Table 1) was first analyzed in ion-pair reversed-phase chromatography mode. Oligonucleotides 2 and 3 are potential impurities of oligonucleotide 1, whereby oligo 2 reveals a double nucleotide exchange of cytosine by guanine in position 9 from 5′ terminus and of adenine by thymine in nucleotide position 13 from the 5′ terminus. Compared to oligonucleotide 1, oligonucleotide 3 misses a single nucleotide thymine in position 13 from the 5′ end.

Fig. 2a illustrates the chromatogram obtained for the mixture of the 3 oligonucleotides on a Phenomenex Gemini C18, 5 μm HPLC column. It can be clearly seen that the C18 column does not exhibit sufficient selectivity for the three structurally closely related oligonucleotides, in spite of satisfactory retention which has been imposed by the ion-pair agent triethylamine. Switching to UHPLC employing an Agilent ZORBAX RRHD Eclipse Plus C18, 1.8 μm column and triethylamine containing eluents does not improve the situation (see Fig. 2b). Without reasonable selectivity, increased efficiencies will not provide a separation between structurally closely related oligonucleotides. Various parameters such as concentration of ion-pair agent triethylamine, its counter-ion (acetate and phosphate), buffer concentration, flow rate and temperature were investigated without success. The same test mixture No. I was then injected onto a previously proposed mixed-mode reversed-phase/weak anion exchanger (RP/WAX) column (based on 100 Å pore size silica particles) (Fig. 1a). All three oligonucleotides were nicely baseline separated from each other. The 22-mer oligonucleotide 3 eluted before the 23-mers (1 and 2). Substitution of a cytosine for guanine and an adenine for thymine somewhere in the middle of the sequence in oligonucleotide 1 induced stronger retention for oligonucleotide 2. Overall, this separation convincingly documented the potential of mixed-mode RP/WAX for oligonucleotide separations. A number of impurities were observed in each oligonucleotide mixture, which were also well resolved.

Since a plain RP i.e. hydrophobic interaction mechanism did not reveal reasonable selectivity, one might argue that the selectivity is merely due to an anion-exchange process. In order to elucidate this, an *N*,*N*-dimethylaminopropyl-modified silica-based weak anion-exchanger (WAX) analog, containing a comparable tertiary amine as WAX moiety like the above RP/WAX phase, was synthesized and examined for its selectivity for the same test mixture. As shown in Fig. 2d, low retention and lack of resolution was furnished when the oligonucleotides analyzed under identical conditions to the RP/WAX separation shown in Fig. 2c, in spite of a total anion-exchange capacity which was by about a factor of 3 larger on the dimethylaminopropyl-silica WAX phase. Adjusting similar elution time, the oligonucleotide test sample was still lacking resolution (Fig. 2e). Obviously, the selectivity on the RP/WAX phase was not solely based on differential interactions at the anion-exchanger site, but a more delicate interplay of a multitude of functionalities and interactions, i.e. a true mixed-mode mechanism.

Thus, the proposed RP/WAX stationary phase appeared to be highly suitable for synthetic oligonucleotide purification. In order to figure out the dominating contributions to retention and selectivity, various gradient elution modes were systematically investigated. A study on the effect of different modifications of the oligonucleotide structure and sequence were investigated in more detail.

3.2. Distinct gradient elution modes of mixed-mode RP/WAX stationary phase

The multi-functional character of the mixed-mode stationary phase endowed it with exceptional flexibility for method development. Solute interactions with the distinct functional moieties (anion-exchange site, lipophilic alkyl strand, polar-embedded groups) could be to some extent independently fine-tuned by particular elution conditions. Thus, depending on analyte character as well as mobile phase conditions, the currently investigated mixed-mode RP/WAX stationary phase was previously shown to be applicable for peptide separations in various elution modes, viz. reversed-phase (RP), (weak) anion-exchange (WAX), ion-exclusion, hydrophilic interaction (HILIC) and hydrophobic interaction chromatography (HIC) modes [57]. It can therefore be regarded as a truly multimodal stationary phase. Except for the ion-exclusion chromatographic mode, all other typical elution conditions for the distinct chromatographic modes of RP/WAX stationary phase ought to be applicable for oligonucleotide separation as well. Thus, the oligonucleotide separation of the test mixture composed of oligonucleotides 1, 2, and 3 was studied with different elution modes comprising one, two and three parameter gradients varying pH, buffer concentration, and organic modifier content in the course of the gradient run to find optimal elution conditions (Table 3). In all experiments, triethylammonium phosphate (TEAP) was chosen as buffer owing to its high elution strength and remarkable solubility even with high acetonitrile content as employed in HILIC mode.

Oligonucleotides are multiply negatively charged. Their retention on anion exchangers increases proportionally with the effective charge number z_{eff}. Typically, $\log k$ increases linearly with z_{eff} [56]. Resultant strong, potentially multivalent, Coulombic interactions can be effectively screened by free ions [63]. Hence, (phosphate) counterion concentrations >100 mM were necessary to achieve elution of the 20–23 nucleotide long oligonucleotides from the RP/WAX column at neutral pH (7–7.5). Besides the screening effect of elevated counterion concentrations, strong ionic interaction of the oligonucleotides on weak anion-exchange materials could also be modulated by pH variation. Full anion-exchange capacity was commonly reached at pH-values below 6, while with increasing pH from 7 to 7.5 the actual ion-exchange

Table 3
Distinct gradient elution modes of RP/WAX stationary phase and optimized isocratic elution conditions along with corresponding results for separation of oligonucleotide mixture No. I (oligos 1, 2, 3).

Method	Gradient mode	Constant parameter			Varied parameter						Retention time (min) of oligonucleotide			Resolution		Fig.
					A			B								
		pH	Buffer[a] (mM)	OM[b] (%)	pH	Buffer[a] (mM)	OM[b] (%)	pH	Buffer[a] (mM)	OM[b] (%)	No. 1	No. 2	No. 3	$Rs_{1,2}$	$Rs_{1,3}$	
One parameter gradient																
A	Buffer (low to high)	7.0	–	20	–	100	–	–	200	–	n.e.	n.e.	n.e.	–	–	
B	pH gradient (low to high)	–	100	20	7.0	–	–	8.0	–	–	n.e.	n.e.	n.e.	–	–	
C	Organic modifier (low to high)	8.0	200	–	–	–	–	–	–	40	4.63	5.24	4.37	0.94	0.49	Fig. 3a
D	Organic modifier (low to high)	7.5	200	–	–	–	–	–	–	40	25.99	29.79	23.00	2.30	2.01	Fig. 3b
E	Organic modifier (low to high)	7.0	100	–	–	–	20	–	–	50	n.e.	n.e.	n.e.	–	–	
F	Organic modifier (high to low)	8.0	200	–	–	-	75	–	–	–	7.74	9.46	6.80	1.60	1.01	Fig. 3c
G	Buffer (high to low)	8.0	–	–	–	200	–	–	100	–	n.e.	n.e.	n.e.	–	–	
Two parameter gradient																
H	pH/buffer (both low to high)	–	–	10	7.0	100	–	8.0	200	–	n.e.	n.e.	n.e.	–	–	
I	pH/buffer (both low to high)	–	–	20	7.0	100	–	8.0	200	–	31.00	34.30	28.53	2.53	2.34	Fig. 3d
J[c]	pH/buffer (both low to high)	–	–	20	7.0	100	–	8.0	200	–	39.49	44.04	35.92	2.59	2.51	Fig. 3e
K	pH/buffer (both low to high)	–	–	30	7.0	100	–	8.0	200	–	20.91	22.18	19.77	1.91	1.68	Fig. 3f
L	pH/buffer (both low to high)	–	–	40	7.0	100	–	8.0	200	–	13.03	14.34	12.18	2.26	1.49	Fig. 3g
M	pH/buffer (both low to high)	–	–	20[e]	7.0	100	–	8.0	200	–	22.17	24.25	21.00	2.36	1.38	Fig. 3h
N	pH/organic modifier (both low to high)	–	200	–	7.0	–	–	8.0	–	40	14.46	15.73	13.40	1.89	1.57	Fig. 3i
O	Buffer/organic modifier (both low to high)	8.0	–	–	–	100	–	–	200	40	16.55	17.65	15.62	1.87	1.54	Fig. 3j
P	Buffer (low to high)/organic modifier (high to low)	8.0	–	–	–	100	75	–	200	–	10.16	13.41	8.60	1.92	1.45	Fig. 3k
Q	pH (low to high)/organic modifier (high to low)	–	200	–	7.0	–	80	8.0	–	–	n.e.	n.e.	n.e.	–	–	
Three parameter gradient																
R	pH/buffer/organic modifier (all low to high)	–	–	–	7.0	40	–	8.0	200	40	19.97	20.99	19.15	1.58	1.22	Fig. 3l
S	pH/buffer (low to high)/organic modifier (high to low)	–	–	–	7.0	40	80	8.0	200	–	n.e.	n.e.	n.e.	–	–	
Isocratic conditions																
T[d]	–	7.5	200	40	–	–	–	–	–	–	n.a.	n.a.	n.a.	n.a.	n.a.	
U[d]	–	7.5	200	30	–	–	–	–	–	–	n.a.	n.a.	n.a.	n.a.	n.a.	

n.a., not available; n.e., not eluted; all gradient experiments used the following gradient profile: 50–100% B in 25 min, then 27 min hold at 100% B, followed by reequilibration.

[a] Buffer: triethylammonium phosphate TEAP (obtained by adjusting phosphoric acid of respective molarity with triethylamine to the specific pH); specified molarities refer to total phosphate contentration in the mixture (C_{tot}).

[b] As organic modifier (OM) acetonitrile was used.

[c] Gradient profile: 0–100% B in 25 min, then 27 min hold at 100% B, followed by reequilibration.

[d] [d]Isocratic elution.

[e] Isopropanol.

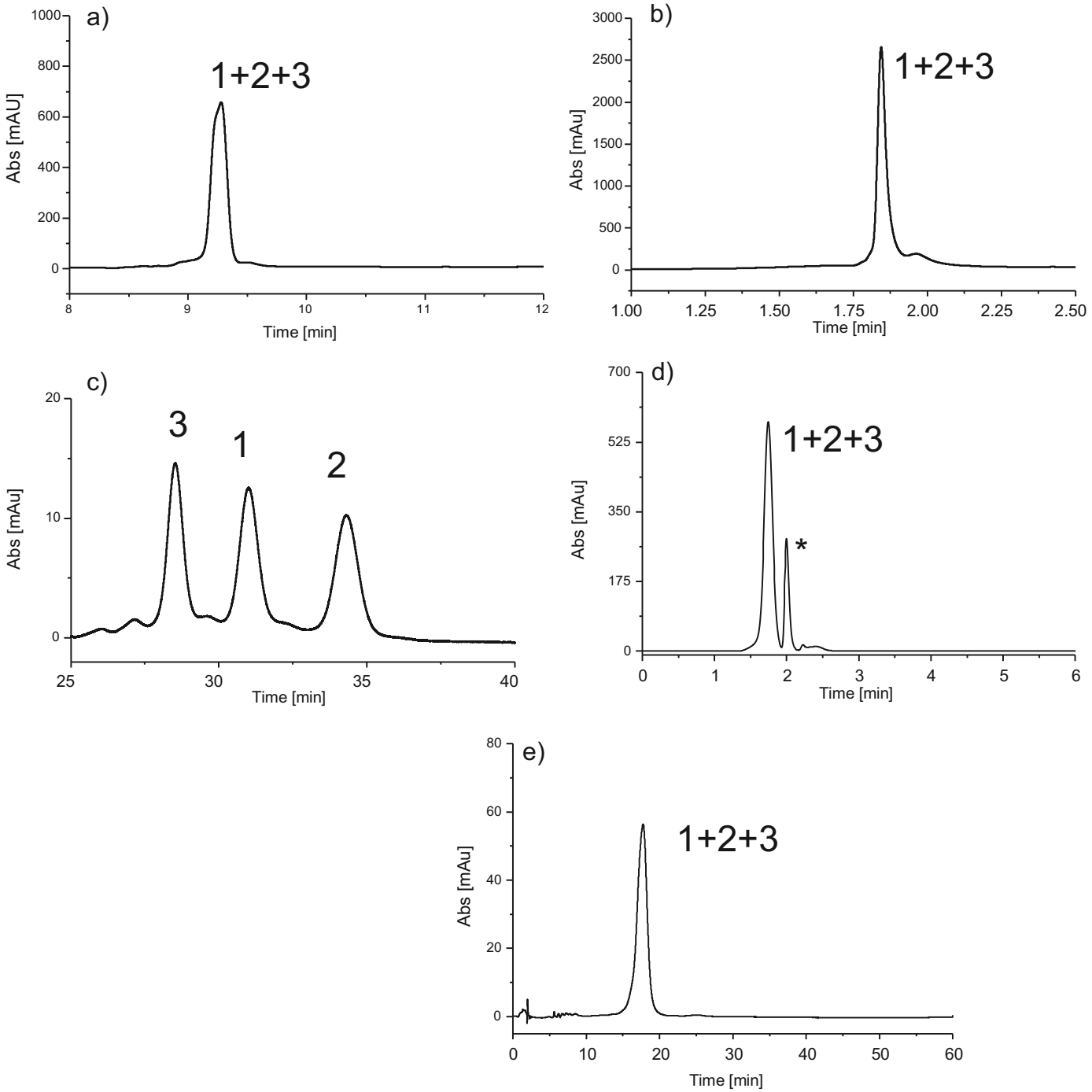

Fig. 2. Chromatograms of oligonucleotide test mix (1, 2, 3) by ion-pair reversed-phase HPLC (a), ion-pair reversed-phase UHPLC (b), mixed-mode RP/WAX chromatography (c), and weak anion-exchange chromatography (d, e). HPLC conditions: (a) column: Gemini C18; mobile phase: (A) 0.05 M triethylammonium acetate in water, pH 6.8; (B) acetonitrile/0.1 M triethylammonium acetate pH 6.8 (50:50, v/v); gradient: 0–100% B in 25 min, then 100% B until 52 min, followed by reequilibration at 100% A for 8 min. (b) Column: Zorbax Rapid Resolution HD Eclipse Plus C18 (1.8 μm); mobile phase: A and B like in (a); gradient: 0–100% mobile phase B in 3 min, then hold at 100% B until 4.40 min, followed by reequilibration at 100% A for 1.20 min. (c) RP/WAX (100 Å); mobile phase: (A) acetonitrile/0.1 M triethylammonium phosphate buffer pH 7.0 (20:80, v/v); (B) acetonitrile/0.2 M triethylammonium phosphate buffer pH 8.0 (20:80, v/v); gradient: 50–100% B in 25 min, then hold at 100% B until 52 min, followed by reequilibration for 8 min at 100% A. (d) Weak anion-exchange chromatography (*N*,*N*-dimethylaminopropyl-modified silica); mobile phase: (A) acetonitrile/0.1 M triethylammonium phosphate buffer pH 7.0 (20:80, v/v); (B) acetonitrile/0.2 M triethylammonium phosphate buffer pH 8.0 (20:80, v/v); gradient: 50–100% B in 25 min, then hold at 100% B until 52 min, followed by reequilibration for 8 min at 100% A; * indicates impurity contained in all 3 oligonucleotide standards. (e) Weak anion-exchange chromatography (*N*,*N*-dimethylaminopropyl-modified silica); mobile phase: (A) acetonitrile/0.01 M triethylammonium phosphate buffer pH 7.0 (20:80, v/v); (B) acetonitrile/0.05 M triethylammonium phosphate buffer pH 8.0 (20:80, v/v); gradient: 50–100% B in 25 min, then hold at 100% B until 52 min, followed by reequilibration for 8 min at 100% A. Flow rate: 1.0 mL/min (except for b) it was 0.25 mL/min); column temperature: 40 °C (25 °C in b); UV detection: 260 nm.

capacity was reduced and nearly absent at pH 8. The quinuclidine nitrogen was still positively charged at this pH. However, negatively charged residual silanol groups turn the net charge of the RP/WAX stationary phase surface into a negative surface potential at this pH [64], allowing thereby effective elution. Besides ionic interaction contributions, the RP/WAX phase possessed also hydrophobic retention increments. Without organic modifier addition the oligonucleotides were not eluted at all. An acetonitrile

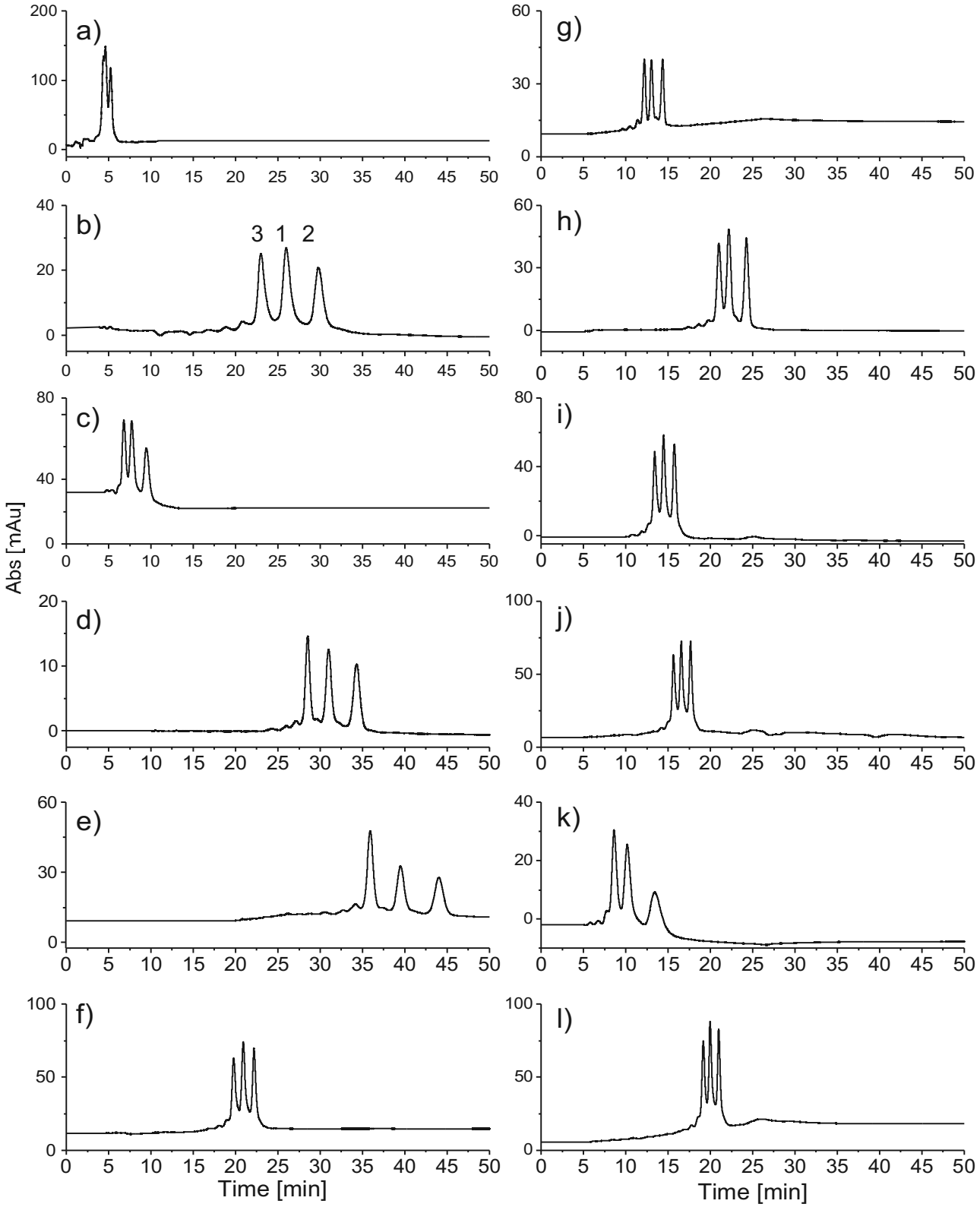

Fig. 3. Chromatograms of oligonucleotide test mixture 1, 2, 3 on RP/WAX (100 Å) column utilizing different gradient elution modes. In all cases the peaks are eluting in the same order. For conditions see Table 3.

content of at least 20% was required to elute the oligonucleotides, provided that pH and buffer concentrations were suitable as well (ca. pH 7.5 and at least 100 mM phosphate buffer).

Single parameter gradients were run initially (see methods A–G in Table 3). Increasing buffer (method A) and pH gradients (method B) did not allow the elution of oligonucleotides, because either the pH (method A) or the buffer concentration was too low (method B). An RP-like increase of the organic modifier gradient from 0 to 40% (v/v) acetonitrile (method C) provided low retention and resolution at pH 8 (Fig. 3a), while retention and resolution were significantly

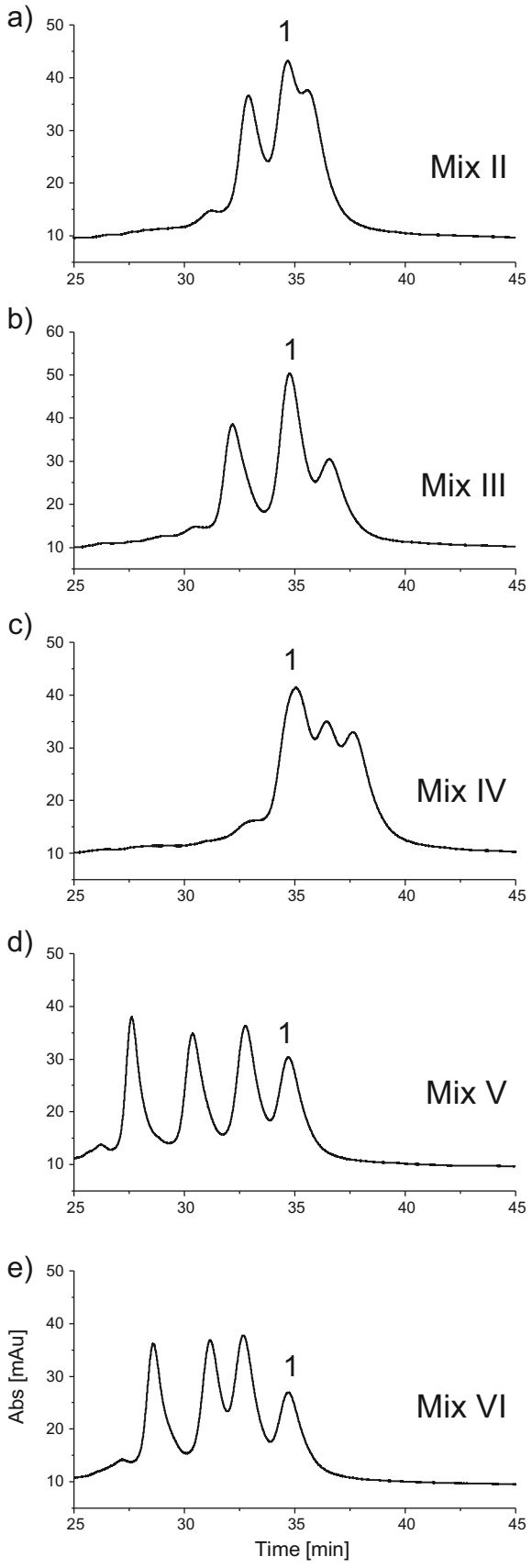

Fig. 4. Separation of oligonucleotide mixtures No. II (a), III (b), IV (c), V (d), VI (e) on mixed-mode RP/WAX stationary phase with a mixed-pH/buffer gradient. HPLC conditions: 100 Å RP/WAX column (see Table 2); mobile phase: (A) acetonitrile/0.1 M triethylammonium phosphate buffer pH 7.0 (20:80, v/v); (B) acetonitrile/0.2 M triethylammonium phosphate buffer pH 8.0 (20:80, v/v); gradient: 50–100% B in 25 min, then hold at 100% B until 52 min, followed by reequilibration for 8 min at 100% A. Flow rate: 1.0 mL/min; column temperature: 40 °C; UV detection: 260 nm.

enhanced at lower pH i.e. pH 7.5 under otherwise identical conditions (method D) (Fig. 3b). No elution was observed at pH 7 under otherwise identical gradient conditions (method E). It seemed that there was a relatively narrow elution window between pH 7 and 8. Aside of buffer and pH gradients typical for anion-exchange chromatography as well as increasing organic modifier gradients like in RPLC, a HILIC-like gradient from 75 to 0% (v/v) acetonitrile was tested as well (method F) (Fig. 3c). Fig. 3a and c shows a direct comparison of RPLC and HILIC gradients superimposed over the anion-exchange retention process. At constant 200 mM phosphate buffer at pH 8, the HILIC gradient (method F with decrease of acetonitrile from 75 to 0%) favorably affected resolution compared to the investigated RP gradient (method C with increase of acetonitrile from 0 to 40%) under otherwise identical conditions. Recently, the RP/WAX phase was successfully utilized in HIC mode for a basic lipophilic peptide [57]. Thus, it was finally examined whether such a HIC mode could be of use for oligonucleotide separation. A HIC gradient (i.e. a decreasing salt gradient) (method G) was run while pH was kept constant and no organic modifier (as common in HIC) was added. Unfortunately, under given salt concentrations (200–100 mM TEAP) no elution could be induced either due to too strong electrostatic or hydrophobic interactions.

Single parameter gradients had clearly revealed the narrow elution window for the oligonucleotide test samples (pH ≥ 7.5, phosphate buffer ≥100, acetonitrile ≥20%). More efficient elution should be achievable using two or three parameter gradients (see Table 3). A plethora of distinct mixed gradients are possible which may be helpful for optimization of separations. A series of mixed pH/buffer gradients (Table 3) were run at distinct constant modifier percentage and modifier type. Thereby, the pH was raised from 7 to 8 and simultaneously the phosphate buffer concentration was increased from 100 to 200 mM, both of which helped to overcome the otherwise strong ion-exchange interactions. By using various amounts of methanol (10, 20 and 40%, v/v) no elution was observed. Obviously, methanol is a weak organic modifier which could not disrupt the strong hydrophobic interactions in the range between 10 and 40%. The same problem was observed with 10% (v/v) acetonitrile (method H) or isopropanol. On the other hand, in such two parameter pH/buffer gradient mode, where the quantity of organic modifier was kept constant, it was observed that with increasing concentration of acetonitrile (methods H–L) or isopropanol (method M) the retention time and resolution were decreased (cf. chromatograms of Fig. 3d and g). This is a clear indication for retention contributions from hydrophobic interactions between RP/WAX phase and oligonucleotide bases. The best separation was achieved with 20% (v/v) acetonitrile (Fig. 3d). Isopropanol had higher elution strength than acetonitrile (cf. Fig. 3d and h; methods I vs M) but resolution, in particular between the first two peaks (oligonucleotides Nos. 1 and 3), was compromised. Other mixed two and three parameter gradients provided even worse results (Fig. 3e–g and i–l). In any case, regardless of the gradient type, the elution order did not change. This may be regarded as an indication that the primary driving force was always the anion-exchange process with some hydrophobic interaction contribution.

Mixed two and three parameter gradients may be very useful as generic gradients for screening experiments to quickly find the optimized elution conditions. For example, if the three parameter gradient (method R) of Fig. 3l is considered, the oligonucleotides elute at about 67% B, which means that the oligonucleotides elute at about 27% acetonitrile, 147 mM phosphate buffer and pH 7.7. Single and two parameter gradients could then be readily used for

Table 4
Retention time (bold) and retention time differences (Δt_R) in min compared to oligo in orthogonal cell ($\Delta t_R = t_{R,column} - t_{R,row}$; negative sign indicates shorter retention relative to oligo in respective row and positive sign longer retention).

		Single nucleotide substitution												Nucleotide deletions in the sequence					
	D / U	1	2	3	4	5	6	7	8	9	10	11	12	13	14	15	16	17	18
Single nucleotide substitution	1	**29.43** **36.22**	0.44	-6.42	-0.91	-0.91	-0.91	-1.00	4.81	0.56	1.34	5.17	1.34	-2.12	-4.97	-9.44	-3.97	-6.10	-8.29
	2	n.a	**28.87** **n.a.**	-6.86	-1.35	-1.35	-1.35	-1.44	4.37	0.12	0.90	4.73	0.90	-2.57	-5.41	-9.88	-4.41	-6.54	-8.74
	3	n.a	n.a	**23.01** **n.a.**	5.512	5.512	5.512	5.422	11.232	6.975	7.76	11.58	7.76	4.293	1.446	-3.03	2.445	0.32	-1.877
	4	-3.21	n.a	n.a	**28.52** **33.00**	0.00	0.00	-0.09	5.72	1.46	2.25	6.07	2.25	-1.22	-4.07	-8.54	-3.07	-5.19	-7.39
	5	-3.21	n.a	n.a	0.00	**28.52** **33.00**	0.00	-0.09	5.72	1.46	2.25	6.07	2.25	-1.22	11.54	-8.54	-3.07	-5.19	-7.39
	6	-3.21	n.a	n.a	0.00	0.00	**28.52** **33.00**	-0.09	5.72	1.46	2.25	6.07	2.25	-1.22	-4.07	-8.54	-3.07	-5.19	-7.39
	7	-3.85	n.a	n.a	-0.64	-0.64	-0.64	**28.43** **32.37**	5.81	1.55	2.34	6.16	2.34	-1.13	-3.98	-8.45	-2.98	-5.10	-7.30
	8	6.98	n.a	n.a	10.19	10.19	10.19	10.83	**34.24** **43.20**	-4.26	-3.47	0.35	-3.47	-6.94	-9.79	-14.258	-8.79	-10.91	-13.11
	9	-0.11	n.a	n.a	3.10	3.10	3.10	3.73	-7.09	**29.99** **36.10**	0.79	4.61	0.79	-2.68	-5.53	-10.00	-4.53	-6.66	-8.85
	10	1.52	n.a	n.a	4.73	4.73	4.73	5.37	-5.46	1.64	**30.77** **37.74**	3.82	0.00	-3.47	-6.31	-10.79	-5.32	-7.44	-9.64
	11	8.07	n.a	n.a	11.29	11.29	11.29	11.92	1.10	8.19	6.55	**34.60** **44.29**	-3.82	-7.29	-10.14	-14.61	-9.14	-11.26	-13.46
	12	1.52	n.a	n.a	4.73	4.73	4.73	5.37	-5.46	1.64	0.00	-6.55	**30.77** **37.74**	-3.47	-6.31	-10.79	-5.32	-7.44	-9.64
Nucleotide deletions in the sequence	13	-5.77	n.a	n.a	-2.56	-2.56	-2.56	-1.92	-12.75	-5.66	-7.29	-13.84	-7.29	**27.30** **30.45**	-2.85	-7.32	-1.85	-3.97	-6.17
	14	-11.13	n.a	n.a	-7.92	-7.92	-7.92	-7.28	-18.11	-11.01	-12.65	-19.20	-12.65	-5.36	**24.46** **25.09**	-4.47	1.00	-1.13	-3.32
	15	-18.24	n.a	n.a	-15.03	-15.03	-15.03	-14.39	-25.22	-18.12	-19.76	-26.31	-19.76	-12.47	-7.11	**19.99** **17.98**	5.47	3.35	1.15
	16	-8.66	n.a	n.a	-5.44	-5.44	-5.44	-4.81	-15.63	-8.54	-10.18	-16.73	-10.18	-2.89	2.47	9.58	**25.46** **27.56**	-2.13	-4.32
	17	12.66	n.a	n.a	-9.45	-9.45	-9.45	-8.82	19.64	12.55	14.18	20.74	14.18	-6.89	-1.54	5.58	-4.01	**23.33** **23.55**	-2.20
	18	16.47	n.a	n.a	13.26	13.26	13.26	12.62	23.45	16.35	17.99	24.54	17.99	10.70	-5.34	1.77	-7.81	-3.81	**21.13** **19.75**

n.a., data not available.

Method	Single nucleotide exchange at 5' end						Single nucleotide exchange in the middle						Single nucleotide exchange at 3' end						Average	SD
	1→5 G→A	1→6 G→T	1→4 G→C	5→6 A→T	4→5 C→A	6→4 T→C	1→12 A→T	1→10 A→C	1→11 A→G	10→12 C→T	11→12 G→T	10→11 C→G	1→9 A→T	1→7 A→C	1→8 A→G	7→9 C→T	8→9 G→T	7→8 C→G		
D	1.04	1.04	1.04	1.00	1.00	1.00	1.00	1.00	1.13	1.00	1.13	1.13	1.00	1.06	1.15	1.06	1.15	1.22	1.06	0.07
K	1.02	1.02	1.02	1.00	1.00	1.00	1.00	1.00	1.05	1.00	1.05	1.05	1.00	1.04	1.06	1.04	1.06	1.10	1.03	0.03
L	1.04	1.04	1.04	1.00	1.00	1.00	1.00	1.00	1.08	1.00	1.08	1.08	1.00	1.00	1.09	1.00	1.09	1.09	1.04	0.04
M	1.00	1.00	1.00	1.00	1.00	1.00	1.00	1.00	1.05	1.00	1.05	1.05	n.a.	n.a.	n.a.	n.a.	n.a.	n.a.	1.01	0.02
N	1.03	1.03	1.03	1.00	1.00	1.00	1.00	1.00	1.06	1.00	1.06	1.06	1.00	1.05	1.07	1.05	1.07	1.12	1.04	0.04
O	1.02	1.02	1.02	1.00	1.00	1.00	1.00	1.00	1.04	1.00	1.04	1.04	1.00	1.03	1.05	1.03	1.05	1.08	1.02	0.02
R	1.00	1.00	1.00	1.00	1.00	1.00	1.00	1.00	1.03	1.00	1.03	1.03	1.00	1.00	1.04	1.00	1.04	1.04	1.01	0.02
T	1.11	1.11	1.11	1.00	1.00	1.00	1.00	1.00	1.22	1.00	1.22	1.22	1.00	1.00	1.26	1.00	1.26	1.26	1.10	0.11
U	1.08	1.08	1.08	1.00	1.00	1.00	1.00	1.00	1.18	1.00	1.18	1.18	1.00	1.12	1.20	1.12	1.20	1.35	1.10	0.10
Average	1.04	1.04	1.04	1.00	1.00	1.00	1.00	1.00	1.09	1.00	1.09	1.09	1.00	1.04	1.12	1.04	1.12	1.16		
SD	0.04	0.04	0.04	0.00	0.00	0.00	0.00	0.00	0.07	0.00	0.07	0.07	0.00	0.04	0.08	0.04	0.08	0.11		

n.a. – not avaible

Separation factor:
1.0
1.01< <1.09
1.10< <1.19
1.20 <

Fig. 5. Separation factors between oligonucleotides with single nucleotide substitutions in the sequence.

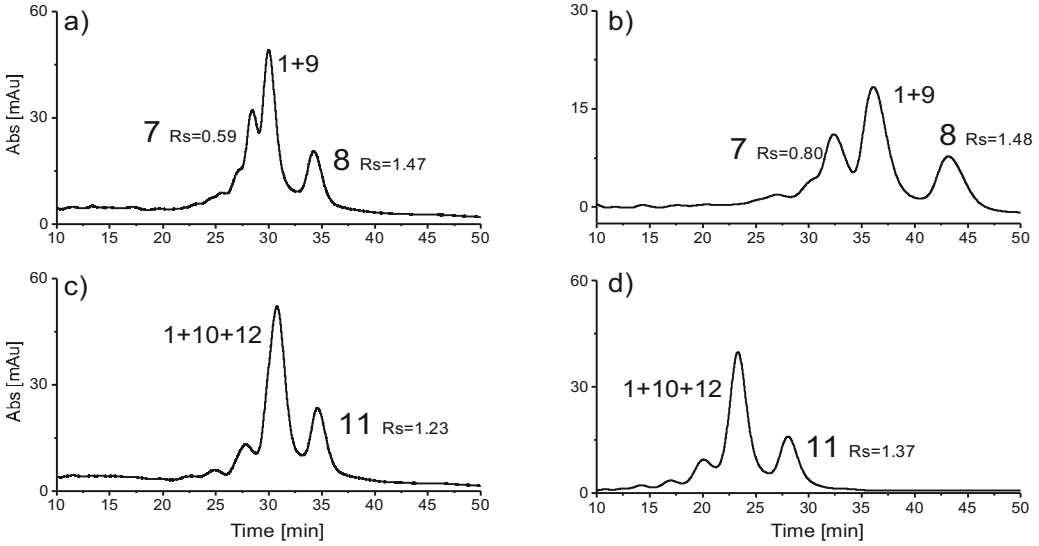

Fig. 6. Chromatographic separation of oligonucleotides differing by single nucleotide exchange at 3′-end (a, b) and in middle of sequence (c, d) on 100 Å RP/WAX stationary phase. Conditions (see Table 3): (a) D; (b) U; (c) D; (d) T. Other conditions see Fig. 2.

fine tuning of the separation. Overall, the experiments summarized in Table 3 clearly reveal that resolutions are better at lower pH (e.g. pH 7.5 is advantageous over pH 8) as well as lower acetonitrile percentage (e.g. 20% preferred over 40%). This clearly documents the beneficial effect of combined ionic and hydrophobic interaction on selectivity for structurally closely related oligonucleotides. A HILIC type gradient could be a successful alternative in terms of selectivity (cf. Fig. 3c), but it is more difficult to get the oligonucleotides eluted at low pH (7–7.5) and pH 8, on the other hand, is unfavorable in terms of selectivity. Finally, based on above screening experiments a new two-parameter mixed pH/buffer gradient at constant 20% (v/v) acetonitrile and variation of pH from 7 to 8 and phosphate

Method	Deletions at 5' end						Deletions at 3' end						Avarage	SD
	1→16 -1 Base	1→17 -2 Bases	1→18 -3 Bases	16→17 -1 Base	16→18 -2 Bases	17→18 -1 Base	1→13 -1 Base	1→14 -2 Bases	1→15 -3 Bases	13→14 -1 Base	13→15 -2 Bases	14→15 -1 Base		
D	1.19	1.31	1.46	1.10	1.22	1.11	1.11	1.24	1.54	1.12	1.39	1.24	1.25	0.15
K	1.09	1.14	1.22	1.05	1.12	1.06	1.03	1.11	1.27	1.08	1.23	1.14	1.13	0.08
L	1.13	1.21	1.28	1.07	1.14	1.07	1.05	1.13	1.34	1.07	1.27	1.19	1.16	0.10
M	1.05	1.09	1.18	1.04	1.12	1.08	1.04	1.10	1.24	1.06	1.19	1.12	1.11	0.06
N	1.09	1.15	1.23	1.05	1.13	1.08	1.05	1.12	1.29	1.07	1.23	1.15	1.14	0.08
O	1.07	1.10	1.16	1.04	1.09	1.05	1.03	1.08	1.20	1.05	1.16	1.10	1.09	0.05
R	1.05	1.07	1.10	1.02	1.05	1.03	1.02	1.05	1.12	1.03	1.10	1.07	1.06	0.03
T	1.37	1.61	1.86	1.17	1.35	1.16	1.17	1.40	2.01	1.19	1.72	1.44	1.45	0.29
U	1.32	1.55	1.88	1.18	1.43	1.21	1.19	1.46	2.08	1.23	1.75	1.43	1.48	0.29
Avarage	1.15	1.25	1.37	1.08	1.18	1.09	1.08	1.19	1.45	1.10	1.34	1.21		
SD	0.12	0.20	0.30	0.06	0.13	0.06	0.06	0.15	0.35	0.07	0.24	0.14		

Separation factor:
1.0
1.01 < <1.09
1.10 < <1.19
1.20 < <1.49
1.50 < <1.99
2.00 <

Fig. 7. Separation factors between oligonucleotides with nucleotide deletions in the sequence.

buffer from 100 to 200 mM was investigated (method J). In fact, the best separation of the test mixture composed of oligonucleotide 1, 2 and 3 was obtained with this gradient and was already shown in Fig. 2c.

3.3. Oligonucleotide structure–retention (separation) relationships

Minor structural variations such as single nucleotide exchanges were difficult to resolve. It would be desirable to be able to predict the effect of such modifications on retention and this was accomplished for ion-pair RPLC [15,65]. For the current mixed-mode phase this aim turned out to be more challenging, but it was nonetheless desirable to derive some more in-depth information about structural effects on retention/selectivity relationships. For this study the analyte set was extended with oligonucleotides 4–18. They contained essentially the same sequence as oligonucleotide 1, but displayed minor structural modifications, such as (i) single nucleotide substitutions (single nucleotide polymorphisms, SNPs) (4–12) either at the 5′ terminus, the 3′ terminus or somewhere in the middle of the sequence, or (ii) deletions of one, two or three nucleotides (N–*x*; with *x* is 1, 2, or 3) at the 3′ terminus (13–15) or 5′ terminus (16–18) (see Table 1).

All the gradient elution modes, which gave good results in previous experiments with test mix No. I (oligonucleotides 1, 2 and 3) were utilized in this study, together with some additional isocratic elution conditions. Representative chromatograms of oligonucleotide mixtures II–VI eluted with the same conditions are shown in Fig. 4.

Table 4 presents a retention time map for the different oligonucleotides under two distinct conditions, for a single parameter (organic modifier) gradient D and isocratic condition U (see Table 3). The data for conditions D were displayed above and those for conditions U below the diagonal line. Retention times of each oligonucleotide were depicted in bold just above or below the diagonal line and all the other values represented retention time differences between orthogonal cells. A negative value means that the oligonucleotide of the respective column shows lower retention than the oligonucleotide in the respective row, a positive value that it is stronger retained. For example, with condition D oligonucleotide 18 (GAA deletion at the 5′ terminus) elutes 8.29 min earlier than oligonucleotide 1. In contrast, oligonucleotide 8 (3′ terminal A of 1 exchanged against G in 8) elutes 4.81 min later than oligonucleotide 1. Substitutions of A, C or T for G leads to a significant retention shift towards longer retention times. For other substitutions, there seems to be some dependency on the position of the nucleotide exchange. For comparison of retention time differences using two distinct conditions, a diagonal line can be drawn from bottom left to top right through the cells and then the values in the corresponding cells on this line can be compared. For example, the retention time shift towards earlier elution of oligonucleotide 18 compared to 1 is larger (−16.47 min) under condition U (isocratic conditions) than conditions D (−8.29 min). This trend is obeyed by the majority of cases, in other words isocratic conditions U provide better selectivity between closely related oligonucleotide structures than the organic modifier gradient D used in this study. These could be favorable conditions for preparative scale oligonucleotide purification. In fact, all oligonucleotides with single, double and triple nucleotide deletions (oligos 13–18) which are most realistic impurities in synthetic oligonucleotides show significant retention time shifts (>1.5 min). Thus, the current RP/WAX phase could be quite useful for oligonucleotide purifications.

Separation factors resulting between nucleotide pairs possessing SNPs are depicted in Fig. 5. Oligonucleotides with SNPs at 5′ terminus can be resolved, when G is involved in the nucleotide exchange and typical separation factors up to 1.1 were furnished

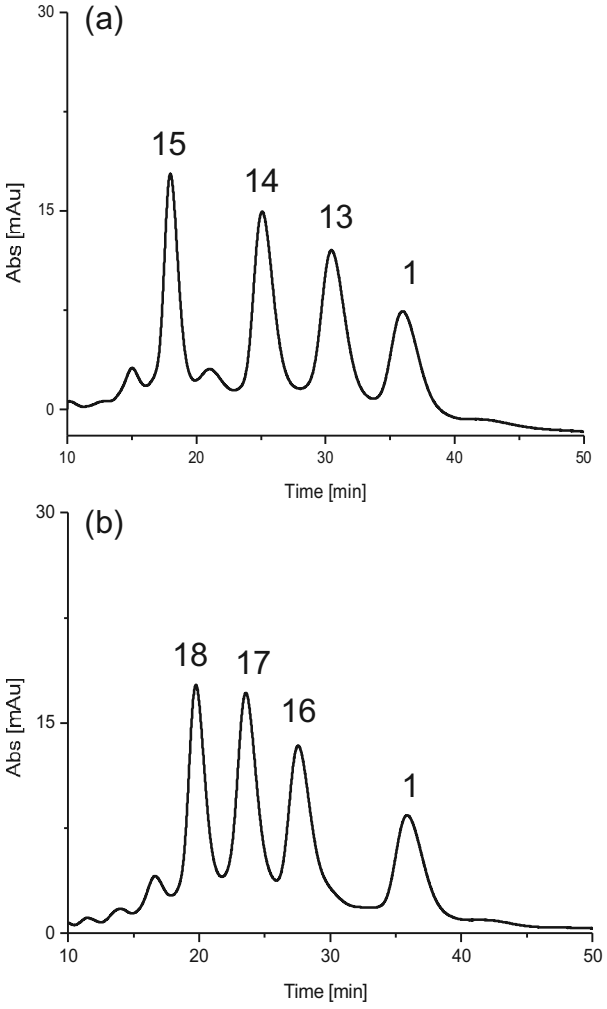

Fig. 8. Isocratic separation of oligonucleotide mixture (a) No. V (1, 13, 14, 15) and (b) No. VI (1, 16, 17, 18) with similar sequences but different chain lengths on the 100 Å mixed-mode RP/WAX stationary phase. HPLC conditions: mobile phase: acetonitrile/0.2 M triethylammonium phosphate buffer pH 7.5 (30:70, v/v); flow rate: 1.0 mL/min; column temperature: 40 °C; UV detection: 260 nm.

with the tested conditions (Fig. 5). Similarly, SNPs somewhere in the middle of the oligonucleotide sequence are more challenging. No resolution was observed when A/C, A/T, or C/T nt exchanges were concerned. Again, involvement of G led to resolution, with typically larger separation factors compared to the corresponding SNPs at the 5′ terminus (Figs. 5 and 6). When SNPs occurred at the 3′-terminus, some selectivity was observed for all mutations except for A/T (Figs. 5 and 6). Separation factors achieved, e.g. with condition D (organic modifier gradient) and U (isocratic), typically decline in the order C/G > A/G ∼ G/T > A/C ∼ C/T > A/T (Fig. 4). Overall it appeared that single nucleotide exchanges were easier to resolve, the further they are away from the 5′-terminus and when G is involved. Isocratic elution method U and gradient elution method D turned out to be the best elution conditions with which 11 out of 18 SNP oligonucleotide pairs revealed at least some selectivity.

Impurities due to single nucleotide exchanges are less likely occurring during oligonucleotide synthesis. More realistic modifications are nucleotide deletions (N–*x*; wherein *x* = 1, 2 or 3). To probe the selectivity of the RP/WAX stationary phase for such oligonucleotide modifications, test mixture V consisting of oligonucleotides 1, 13, 14 and 15 as well as test mix VI containing

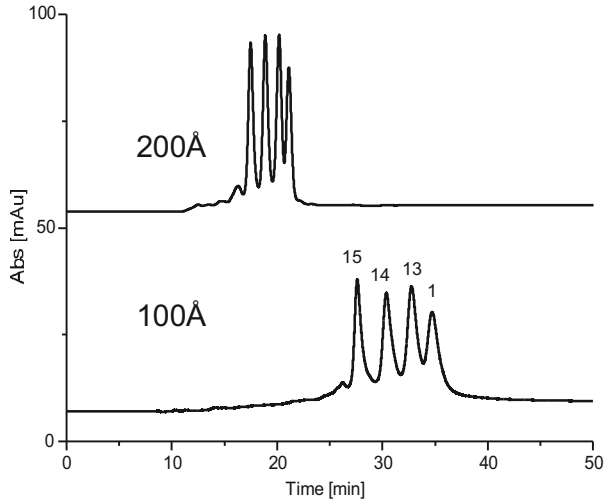

Fig. 9. Effect of pore size on chromatographic separations of oligonucleotide mixture No. V (1, 13, 14, 15) on mixed-mode RP/WAX stationary phase with 100 Å and 200 Å pore diameter. In both cases the peaks are eluting in the same order. HPLC conditions: mobile phase: (A) acetonitrile/0.05 M triethylammonium phosphate buffer pH 7.0 (20:80, v/v); (B) acetonitrile/0.1 M triethylammonium phosphate buffer pH 8.0 (20:80, v/v); gradient: 50–100% B in 25 min, then hold at 100% B until 52 min, followed by reequilibration for 8 min at 100% A; flow rate: 1.0 mL/min; column temperature: 40 °C; UV detection: 260 nm. For the 100 Å material the TEAP buffer concentration was 0.1 M in A and 0.2 M in B; other conditions identical.

oligonucleotides 1, 16, 17 and 18 were analyzed on the 100 Å RP/WAX column.

It was derived from Fig. 7 that selectivity increased with the number of nucleotide deletions in the investigated oligonucleotides. Separation factors were typically in the range of 1.1–1.4 in the group of N−1 nt, between 1.2 and 1.7 in the group of N−2 nts, and between 1.5 and 2.0 in the group of N−3 nts under optimized conditions (D, U).

Representative chromatograms of oligonucleotide mixtures with deleted sequences obtained under isocratic elution conditions are shown in Fig. 8. It can be seen that with each deleted nt the oligonucleotides elute earlier regardless whether the deletion is at the 3′ terminus (Fig. 8a) or 5′ terminus (Fig. 8b). In general, selectivity appeared to be larger when the deletion was at the 3′ terminus than when it was at the 5′ terminus. Also deletions somewhere in the middle of the sequence were resolved as demonstrated above cf. resolutions between nucleotide 1 and 3. Other impurities such as missing cleavages of protection groups were not investigated herein, but could be expected to be readily separated on the present RP/WAX stationary phase as well.

3.4. Pore size effect

The earlier described 100 Å pore size RP/WAX stationary phase possessed a large adsorption surface. However, for oligonucleotides with a length of about 20–23 nts, the intra-particulate diffusional pores could be too narrow to allow unhindered diffusion of the oligonucleotides to the adsorption sites within the pores. Furthermore, due to the polyelectrolyte nature, adsorption isotherms are typically very steep owing to the multivalent ionic binding mechanism [66]. High buffer concentrations and/or high pH were required for elution within reasonable run times. Favorable milder elution conditions can be achieved by using wide pore materials which possessed lower surface areas and thus provide lower net retention under equal chromatographic conditions. To realize this, the RP/WAX selector was immobilized onto 5 μm silica particles with 200 Å pore size.

A sample containing the four synthetic oligonucleotides 1, 13, 14 and 15 with different chain lengths was comparatively evaluated on the 100 Å and 200 Å RP/WAX columns. Due to the lower surface area of a factor of about 2 per unit mass for the 200 Å material compared to the 100 Å stationary phase, the phosphate buffer concentration could be reduced by a factor of 2 (from 100 mM to 50 mM in channel A and 200 mM to 100 mM in channel B) and the oligonucleotides still eluted much faster than on the 100 Å RP/WAX column under otherwise identical conditions (Fig. 9). When the same elution conditions as for the 100 Å material were used, all sample constituents eluted with t_0 on the 200 Å material. A further reduction to 25 mM in A and 50 mM in B channels did not promote elution of the oligonucleotides in spite of setting a pH of 8 in channel B. Whatsoever, selectivity and resolution were not compromised significantly by the reduction of the surface area, because the selector coverage per square meter was essentially identical. The 200 Å pore size material thus has some advantages and a further increase of the pore size to 300 Å seems promising.

4. Conclusions

Oligonucleotides of the typical size range of small interfering RNA with 20–23 nucleotides have been separated by mixed-mode chromatography on a reversed-phase/weak anion-exchange stationary phase with surface-bonded *N*-11-undecenyl-3-aminoquinuclidine based on 5 μm thiol-silica. This stationary phase features multiple functionalities for mixed-mode retention mechanisms comprising a lipophilic alkyl strand for hydrophobic interaction like in RP separation, a quinuclidinium moiety for ionic interactions which stands in accordance with an anion-exchange process and polar embedded groups for polar retention increments, most notably an amide group for hydrogen bonding. This RP/WAX stationary phase has revealed improved resolution over ion-pair RPLC for structurally closely related oligonucleotides, which may be found as impurities in synthetic oligonucleotide production. Various single, double, triple parameter gradients have been examined. Results revealed that anion-exchange is the dominating retention principle, yet other binding increments in particular hydrophobic interactions contribute to selectivity.

The most realistic impurities in synthetic oligonucleotides, besides incompletely deprotected oligonucleotides, result from nucleotide deletions (N−1, N−2 and N−3) and double couplings of nt (N+*x*). In both situations, the number of nucleotides is different and such impurities can be well resolved on the RP/WAX phase, regardless whether the oligonucleotides differ by one, two or three nts. Single nucleotide polymorphisms are more challenging to resolve. Two general trends have been observed: resolution depended on the location of SNP and decreased in the order: SNP at 3′ terminus > somewhere in the middle > at 5′ terminus. Regarding the type of bases that were exchanged, selectivities (and thus resolutions) decline in the order C/G > A/G ~ G/T > A/C ~ C/T > A/T. A 200 Å pore size RP/WAX phase turned out to be advantageous in terms of reduced retention at comparable resolutions allowing the use of milder elution conditions. The proposed RP/WAX phase shows remarkable promise for purification of synthetic oligonucleotides. A high loading capacity can be expected as proven for peptide separations in earlier studies [59]. Tailoring of the surface chemistry with the goal of some further optimization of selectivities and efficiencies combined with milder elution conditions will be addressed in future studies to enable resolution of oligonucleotides with all kinds of sequence modifications employing MS compatible conditions at fast speed and high efficiency.

Acknowledgements

R.G. thanks the University of Ferrara (grant: Fondo Giovani-2012).

References

[1] I. Tamm, B. Dörken, G. Hartmann, Lancet 358 (2001) 489.
[2] B. Jansen, U. Zangemeister-Wittke, Lancet Oncol. 3 (2002) 672.
[3] B.E. Korba, J.L. Gerin, Antiviral Res. 28 (1995) 225.
[4] A. Kirk Field, Antiviral Res. 37 (1998) 67.
[5] C.J. Wraight, P.J. White, Pharmacol. Ther. 90 (2001) 89.
[6] F. Rigo, Y. Hua, A.R. Krainer, C.F. Bennett, J. Cell Biol. 199 (2012) 21.
[7] G.F. Deleavey, M.J. Damha, Chem. Biol. 19 (2012) 937.
[8] R. Kole, A.R. Krainer, S. Altman, Nat. Rev. Drug Discov. 11 (2012) 125.
[9] A.C. McGinnis, B. Chen, M.G. Bartlett, J. Chromatogr. B: Analyt. Technol. Biomed. Life Sci. 883–884 (2012) 76.
[10] R.R. Deshmukh, K.O. Eriksson, P. Moore, D.L. Cole, Y.S. Sanghvi, Nucleosides Nucleotides Nucleic Acids 20 (2001) 567.
[11] K.T. York, R.C. Smith, R. Yang, P.C. Melnyk, M.M. Wiley, C.M. Turk, M. Ronaghi, K.L. Gunderson, F.J. Steemers, Nucleic Acids Res. 40 (2012) e4.
[12] G.M. Blackburn, M.J. Gait, D. Loakes, D.M. Williams (Eds.), Nucleic Acids in Chemistry and Biology, The Royal Society of Chemistry, Great Britain, 2006.
[13] R.R. Deshmukh, W.E. Leitch II, Y.S. Sanghvi, D.L. Cole, Sep. Sci. Technol. (San Diego, CA, U.S.) 2 (2000) 511.
[14] M. Gilar, Anal. Biochem. 298 (2001) 196.
[15] M. Gilar, K.J. Fountain, Y. Budman, U.D. Neue, K.R. Yardley, P.D. Rainville, R.J. Russell II, J.C. Gebler, J. Chromatogr. A 958 (2002) 167.
[16] M. Gilar, E.S.P. Bouvier, J. Chromatogr. A 890 (2000) 167.
[17] Y.S. Sanghvi, M. Schulte, Curr. Opin. Drug Discov. Devel. 7 (2004) 765.
[18] C.G. Huber, J. Chromatogr. A 806 (1998) 3.
[19] H. Oberacher, C.G. Huber, TrAC, Trends Anal. Chem. 21 (2002) 166.
[20] P.J. Oefner, C.G. Huber, J. Chromatogr. B: Analyt. Technol. Biomed. Life Sci. 782 (2002) 27.
[21] B. Noll, S. Seiffert, H.-P. Vornlocher, I. Roehl, J. Chromatogr. A 1218 (2011) 5609.
[22] V.K. Sharma, J. Glick, P. Vouros, J. Chromatogr. A 1245 (2012) 65.
[23] K. Ashman, A. Bosserhoff, R. Frank, J. Chromatogr. 397 (1987) 137.
[24] S.M. McCarthy, M. Gilar, J. Gebler, Anal. Biochem. 390 (2009) 181.
[25] C.G. Huber, P.J. Oefner, G.K. Bonn, J. Chromatogr. 599 (1992) 113.
[26] C.G. Huber, H. Oberacher, Mass Spectrom. Rev. 20 (2002) 310.
[27] T. Victor, A.M. Jordaan, A.J. Bester, A. Lochner, J. Chromatogr. 389 (1987) 339.
[28] D.S. Levin, B.T. Shepperd, C.J. Gruenloh, J. Chromatogr. B: Analyt. Technol. Biomed. Life Sci. 879 (2011) 1587.
[29] A. Apffel, J.A. Chakel, S. Fischer, K. Lichtenwalter, W.S. Hancock, J. Chromatogr. A 777 (1997) 3.
[30] Q. Li, F. Lynen, J. Wang, H. Li, G. Xu, P. Sandra, J. Chromatogr. A 1255 (2012) 237.
[31] L. Gong, J.S.O. McCullagh, J. Chromatogr. A 1218 (2011) 5480.
[32] A.J. Alpert, J. Chromatogr. 499 (1990) 177.
[33] B. Buszewski, S. Noga, Anal. Bioanal. Chem. 402 (2012) 231.
[34] R. Easter, C. Barry, J. Caruso, P. Limbach, Anal. Methods 5 (2013) 2657.
[35] R.N. Easter, K.K. Kroening, J.A. Caruso, P.A. Limbach, Analyst (Cambridge, U.K.) 135 (2010) 2560.
[36] P. Holdsvendova, J. Suchankova, M. Buncek, V. Backovska, P. Coufal, J. Biochem. Biophys. Methods 70 (2007) 23.
[37] M. Bittová, J. Havliš, H. Fuksová, B. Vrbková, L. Trnková, J. Sep. Sci. 35 (2012) 3227.
[38] K. Rahman, U. Voss, P.J. Nicholls, A.D.B. Malcolm, Biochem. Soc. Trans. 16 (1988) 368.
[39] F. Wincott, A. DiRenzo, C. Shaffer, S. Grimm, D. Tracz, C. Workman, D. Sweedler, C. Gonzalez, S. Scaringe, N. Usman, Nucleic Acids Res. 23 (1995) 2677.
[40] A.J. Bourque, A.S. Cohen, J. Chromatogr. B: Biomed. Sci. Appl. 662 (1994) 343.
[41] Y.Z. Xu, P.F. Swann, Anal. Biochem. 204 (1992) 185.
[42] J.R. Thayer, Y. Wu, E. Hansen, M.D. Angelino, S. Rao, J. Chromatogr. A 1218 (2011) 802.
[43] J.D. Pearson, F.E. Regnier, J. Chromatogr. 255 (1983) 137.
[44] R.R. Drager, F.E. Regnier, Anal. Biochem. 145 (1985) 47.
[45] B. Noll, S. Seiffert, F. Hertel, H. Debelak, P. Hadwiger, H.-P. Vornlocher, I. Roehl, Nucleic Acid Ther. 21 (2011) 383.
[46] J.R. Thayer, K.J. Flook, A. Woodruff, S. Rao, C.A. Pohl, J. Chromatogr. B 878 (2010) 933.
[47] W. Wieder, C.P. Bisjak, C.W. Huck, R. Bakry, G.K. Bonn, J. Sep. Sci. 29 (2006) 2478.
[48] S. Yamamoto, M. Nakamura, C. Tarmann, A. Jungbauer, J. Chromatogr. A 1144 (2007) 155.
[49] D. Sykora, F. Svec, J.M.J. Frechet, J. Chromatogr. A 852 (1999) 297.
[50] S.D. Woodward, I. Urbanova, D. Nurok, F. Svec, Anal. Chem. (Washington, DC, U.S.) 82 (2010) 3445.
[51] R.R. Deshmukh, W.E. Leitch II, D.L. Cole, J. Chromatogr. A 806 (1998) 77.
[52] L.W. McLaughlin, Chem. Rev. 89 (1989) 309.
[53] X. Liu, C. Pohl, A. Woodruff, J. Chen, J. Chromatogr. A 1218 (2011) 3407.
[54] X. Liu, C.A. Pohl, J. Sep. Sci. 33 (2010) 779.
[55] X. Liu, C.A. Pohl, J. Chromatogr. A 1232 (2012) 190.
[56] H. Hinterwirth, M. Lämmerhofer, B. Preinerstorfer, A. Gargano, R. Reischl, W. Bicker, O. Trapp, L. Brecker, W. Lindner, J. Sep. Sci. 33 (2010) 3273.
[57] M. Laemmerhofer, R. Nogueira, W. Lindner, Anal. Bioanal. Chem. 400 (2011) 2517.
[58] M. Lämmerhofer, M. Richter, J. Wu, R. Nogueira, W. Bicker, W. Lindner, J. Sep. Sci. 31 (2008) 2572.
[59] R. Nogueira, M. Lämmerhofer, W. Lindner, J. Chromatogr. A 1089 (2005) 158.
[60] R. Dabre, N. Azad, A. Schwaemmle, M. Laemmerhofer, W. Lindner, J. Sep. Sci. 34 (2011) 761.
[61] A.F.G. Gargano, T. Leek, W. Lindner, M. Laemmerhofer, J. Chromatogr. A 1317 (2013) 12.
[62] M. Biba, E. Jiang, B. Mao, D. Zewge, J.P. Foley, C.J. Welch, J. Chromatogr. A 1304 (2013) 69–77.
[63] J. Stahlberg, J. Chromatogr. A 855 (1999) 3.
[64] O.L. Sánchez Muñoz, E.P. Hernández, M. Lämmerhofer, W. Lindner, E. Kenndler, Electrophoresis 24 (2003) 390.
[65] O. Kohlbacher, S. Quinten, M. Sturm, B.M. Mayr, C.G. Huber, Angew. Chem. Int. Ed. 45 (2006) 7009.
[66] G. Carta, A. Jungbauer, Protein Chromatography: Process Development and Scale-Up, Wiley-VCH, Weinheim, 2010.

analytical chemistry

Letter

pubs.acs.org/ac

A New Method to Investigate the Intrusion of Water into Porous Hydrophobic Structures under Dynamic Conditions

Alberto Cavazzini,*[,†] Nicola Marchetti,[†] Luisa Pasti,[†] Roberto Greco,[†] Francesco Dondi,[†] Aldo Laganà,[‡] Alessia Ciogli,[¶] and Francesco Gasparrini[¶]

[†]Department of Chemistry and Pharmaceutical Sciences, University of Ferrara, via L. Borsari 46, 44121 Ferrara, Italy

[‡]Department of Chemistry, University of Rome "La Sapienza", Piazzale A. Moro 5, 00185 Rome, Italy

[¶]Dipartimento di Chimica e Tecnologia del Farmaco, University of Rome "La Sapienza", Piazzale A. Moro 5, 00185 Rome, Italy

Supporting Information

ABSTRACT: The intrusion of water into the pores of hydrophobic materials is investigated by means of a dynamic flow system. The porous hydrophobic material is packed into a stainless steel chromatographic column, and water is flushed through by means of a high-pressure pump. Back-pressure control is provided by flow restrictors after the column. The applied pressure forces the water to penetrate the pores of the hydrophobic material. The water volume contained in the column, as a function of the applied pressure, reflects the degree of wetting of the solid by water. This volume is determined by measuring, through a mass spectrometer, the retention time of deuterium oxide injected in the column. The method is applied with alkyl-modified (*n*-octyl and *n*-octadecyl) and perfluorinated (alkyl and phenyl) silica surfaces. The information gathered by this study may contribute to explain the retention behavior of reversed-phase chromatographic columns when used under highly aqueous mobile-phase conditions.

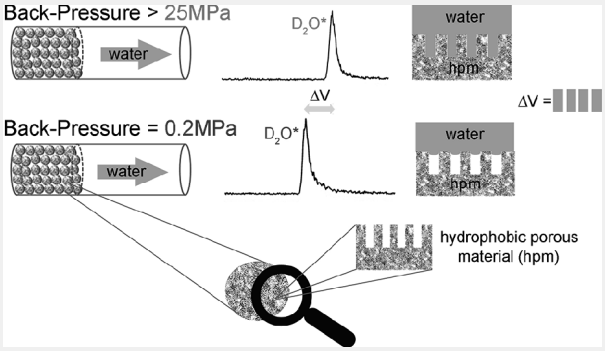

A renewed interest toward the characterization of hydrophobic porous materials has arisen in recent years among scientists and industrialists in different fields such as catalysis, material and biomedical sciences (including building materials, biomedical fibers, and synthetic bones), energy and sensor technology, energy storage,[1] adsorption, separation and purification (e.g., chromatography, liquid purification, gas separation or storage), pharmaceutical sciences, petroleum science and technology, etc.[2] Useful information about the microstructure of porous materials can be achieved if the solid is placed in contact with a nonwetting liquid and external pressure is applied. This is indeed the principle of mercury intrusion porosimetry (MIP), which is undoubtedly the most popular method of investigation of porous solids by forcing a liquid into their pores. Due to the extremely high surface tension and energy surface of mercury, in fact, it poorly wets most surfaces. However, the use of mercury presents both technical and environmental issues. First of all, the working pressures required in MIP experiments are on the order of a hundred MPa (i.e., thousand bar). This provokes the deformation of the porous structure during measurements, which may be irreversible in some cases.[3] In addition, mercury is highly toxic so that its replacement with "greener" solvents is greatly desirable. For these reasons, other less hazardous liquid metals or metallic alloys have been proposed as nonwetting liquids for intrusion experiments but, admittedly, they were not as successful.[2]

Water has also been suggested as intruding liquid. By analogy to MIP, water intrusion porosimetry (WIP) lies in forcing water into the pores of a hydrophobic surface under the effect of external pressure. The technique was described in the late nineties by Eroshenko and Fadeev,[4−6] who employed a homemade water porosimeter to study the penetration of water into hydrophobized porous silica. Essentially, the water−silica system under study was placed into a flexible envelope, which was subjected to an isostatic pressure applied by an oil system. As a result of increasing compression, the envelope shrinked and the change in volume due to the intrusion of water in the pores was measured. The commercial water porosimeter is essentially based on the same principle.[7]

The fundamental equation of both mercury and water intrusion porosimetry is the modified Young−Laplace equation for cylindrical pores,[3] most of the time referred to as the Washburn's equation,[8] which establishes the relationship between the applied pressure P (Laplace's capillary pressure) and the pore diameter d_p:

Received: November 8, 2012
Accepted: December 10, 2012
Published: December 10, 2012

dx.doi.org/10.1021/ac303253b | *Anal. Chem.* 2013, 85, 19−22

$$P = -\frac{4\gamma}{d_p}\cos\theta \quad (1)$$

where γ is the surface tension of the nonwetting liquid and θ is the contact wetting angle in the liquid−surface−air system (for a nonwetting situation, $\theta > 90°$ and this explains the minus sign in the Washburn's equation). In MIP applications, γ is usually assumed to be 484 mN·m ^{1} (or dyne·cm^{-1}), i.e., the surface tension of pure mercury in air at 25 °C. The surface tension of water for the water−air interface at 25 °C is instead only 72 mN·m^{-1}. Regarding the contact angle θ, a customary value of 130° or 140° is generally accepted in MIP.[9,2,10] On the other hand, different values have been reported for the contact angle of water at hydrophobic surfaces, such as 93° (for silica plate bonded with octadecyldimethylchlorosilane and end-capped with trimethylchlorosilane),[11] 110−112° (for pure water on a self-assembled monolayer of octadecyltrichlorosilane on glass slides,[12] for pure water on films formed from alkyltrichlorosilanes on the silica surface of silicon wafers,[13] and for pure water on film of paraffins[14]), or 126° (for commercial hydrophobic porous silica grafted with C18 chains and end-capped with trimethylchlorosilane[15]). This variability reflects the observation that, particularly for thin hydrophobic layers applied onto surfaces of hydrophilic supports, water porosimetry is expected to give much more detailed information about the structure and the properties of the surface than MIP.[5] A simple calculation based on the Washburn's equation (by assuming a contact angle of 140°) shows that pressures as large as 150 MPa (1 MPa ≡ 10 N·m^{-2} = 10 bar = 147 psi) are required to intrude mercury into a cylindrical pore of 10 nm (100 Å). The same calculation, but with water as the nonwetting liquid (and by assuming θ = 120°[16]), would lead to only about 15 MPa.

In this work, we present a new method, based on the sound principle of tracer-pulse chromatography,[17−30] for studying the intrusion of water into hydrophobic porous solids under dynamic conditions. This last aspect is particularly relevant as intrusion phenomena are usually studied under quasi-static conditions, while only a few experiments have been devoted to evaluating the dynamic aspects of wetting.[31,32] As a first example of applications, we focused on some hydrophobized porous silica (including alkyl and perfluoro-alkyl grafting), which are commonly used as stationary phases in liquid chromatography. For the reasons explained above, in fact, chemically modified porous silica are particularly good candidates for this kind of investigation.

The purpose of this work is, on the one side, to show that this method is promising to provide information about the dynamic behavior of water at hydrophobic interfaces and, on the other, to contribute to the investigation of the chromatographic behavior of reversed-phase adsorbents used with highly aqueous mobile phases.[33−36] We refer, in particular, to the dramatic decrease of chromatographic performances, associated to a sudden loss of retention after a drop in the column pressure (either by accident or by a reduction in flow rate), that has been observed on both typical C8- or C18-silica based sorbents[33,37] and perfluorinated stationary phases[38] at very high water content (usually 95% or larger). This phenomenon, sometimes attributed to the collapse of hydrophobic chains grafted to the stationary phase, is more likely due to the extrusion of water from the pores of the adsorbents when pressure is released.[33,37]

■ EXPERIMENTAL SECTION

Materials and Methods. Four chromatographic columns were employed in this work. Two of them were traditional reversed-phase columns, packed with octyl (C8)- and octadecyl (C18)-bonded silica (respectively, Biobasic8 from Thermo Scientific and Ultra-C18 from Restek). The other two were homemade columns packed with perfluorohexylethylsiloxane- and pentafluorophenylpropylsiloxane-bonded silica (abbreviated as PFH- and PFP-silica, respectively). The synthesis and the chemical structures of the perfluorinated materials, as well as the packing conditions, are given in the Supporting Information. The dimensions of the columns and the geometric characteristics of the packing materials are reported in Table 1.

Table 1. Packing Type, Particle Size, Pore Size, Column Dimension (Length × Internal Diameter), Void (Pycnometric) Volume, Interstitial Volume, Total (ε_t) and Interstitial (ε_e) Porosity of the Four Columns Considered in This Work

packing type	p_s (μm)	d_p (nm)	L × I.D. (mm)	V_0 (μL)	V_e (μL)	ε_t	ε_e
C8-silica	5	300	150 × 1	89	48	0.75	0.41
C18-silica	5	100	50 × 2.1	115	64	0.66	0.37
PFH-silica	2.6	100	100 × 3	471	260	0.67	0.37
PFP-silica	2.6	100	100 × 3	480	262	0.68	0.37

Ultrahigh grade milli-Q water was obtained by water purification system (Millipore). Solvents for pycnometry were HPLC-grade methanol, tetrahydrofuran, and dichloromethane (from Sigma Aldrich). Deuterium oxide, D_2O, was from Cambridge Isotope Laboratories Inc. Polystyrene standards for inverse size exclusion measurements were from Supelco. Fused silica tubings (20 μm I.D. × 360 μm O.D., from Upchurch Scientific) were used as back pressure regulators.

Equipment. A LC/MS instrumentation composed by a micro-HPLC (Finnigan Surveyor Plus) interfaced to a LTQ-XL linear ion trap MS detector (Thermo Scientific) with an APCI interface was used for all measurements.[39] Details about ion source operational conditions are reported under the Supporting Information.

■ RESULTS AND DISCUSSION

The herein proposed method for studying the intrusion of water into the pores of hydrophobic materials is based on the theory of tracer pulse chromatography.[17−29] When the mobile phase is made of only one component (let us say A), this theory shows that the void volume of the column, V_0, is given by the retention volume, V_A^*, of a detectable tracer of that component (provided that there is no isotopic effect, i.e., that the labeled and the unlabeled components have the same isotherm):[22]

$$V_0 = V_A^* \quad (2)$$

In eq 2, it is implicitly assumed that the liquid A completely wets the solid. In case this does not happen, the "actual" volume of the liquid in the column is expected to differ from the void volume. In particular, if the liquid will not be able to penetrate the pores of the adsorbent, the actual volume will correspond to the volume of interstitial or through-pores. In the case water is the intruding liquid, eq 2 can be conveniently rewritten as:

$$V_{H_2O} = V_{D_2O}^* \quad (3)$$

dx.doi.org/10.1021/ac303253b | Anal. Chem. 2013, 85, 19−22

where $V^*_{D_2O}$ is the retention volume of deuterium oxide and V_{H_2O} is the "actual" volume of the water in the column. For a hydrophobic material, V_{H_2O} will not necessarily match V_0. However, since the penetration of a nonwetting liquid in the pores can be forced by the action of an external pressure, the dependence of the actual volume V_{H_2O} on the applied pressure can be taken as an estimate of the degree of wetting of the porous material by water.

The pressure drop of a fluid flowing through a packed chromatographic column depends in a complex way on several factors, including the flow rate, the viscosity of the mobile phase, the length and the radius of the column, the interstitial (also referred to as external or interparticle) porosity, and the particle size.[37] Under the hypothesis of an homogeneous packing, it is a good approximation to assume that the pressure decreases linearly from the column inlet to the column outlet (that it is usually close to atmospheric pressure). Thus, as a function of the position along the column, the water inside is subjected to different pressures and may penetrate the pores of the solid at different levels. In order to minimize this effect, in this work, the flow rate was set up (20 μL·min^{-1}) to make the back-pressure coming from the water stream through the packed bed negligible (maximum 0.4 MPa for the columns packed with PFH- and PFP-silica). The (constant) back-pressure was instead generated using a series of restrictors placed after the column. The pressure drop over the restrictor was adjusted by changing its length.[40] Under the Supporting Information, the length vs back-pressure plot at constant flow rate is reported.

As it was stated, the limits within which the actual volume is expected to vary are given by the interstitial volume of the column V_e, if water is totally excluded from the pores of the solid, and by V_0, if penetration of water into the pores is complete. Since it is generally agreed upon that the pycnometric or weight difference method provides the best estimate of the maximum possible hold-up volume,[22,41,42] this value was taken as V_0 (see Table 1, column 5).

Figure 1 shows the dependence of the actual volume on the applied pressure. Before starting the experiments, all columns were thoroughly flushed with water. In order to summarize in the same chart the results for the four employed columns, the actual volumes (calculated according to eq 3) have been normalized by the corresponding V_0s.

The horizontal line in the upper part of the figure represents the condition $V_{H_2O} = V_0$ (that is, the situation of total wetting). On the other hand, the lines in the lower part of the graph correspond to the normalized interstitial volumes (i.e., the volume fraction of the void volume occupied by interstitial pores) of the four columns. The interstitial volumes were determined by inverse size exclusion chromatography (ISEC).[43,44] For the sake of conciseness, ISEC plots and experimental details are reported in the Supporting Information. The estimated interstitial volumes have been reported in Table 1, column 6.

It is remarkable to observe the different behavior exhibited by water on the four adsorbents. In particular, two different trends may be recognized by considering the plots in Figure 1. The C18- and the PFH-silica adsorbents (red squares and green triangles, respectively), in fact, exhibit a qualitatively analogous S-shaped course starting approximatively from the normalized interstitial volume for the C18-silica or from about 15% more

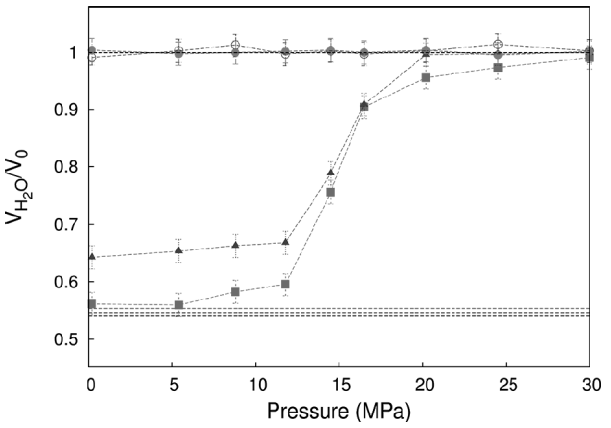

Figure 1. The dependence of the normalized volume of the water contained in the column on the applied pressure. The line $V_{H_2O}/V_0 = 1$ represents the condition of total wetting. The dashed colored lines in the lower part of the figure are the normalized interstitial volumes of the four columns. Red squares and line: C18-silica; green triangles and line: PFH-silica; blue empty circles and line: C8-silica; fuchsia circles and line: PFP-silica. Errors given as ± one standard deviation.

for the PFH-silica and ending at one, when the applied pressures are about 20 and 25 MPa, respectively, for the PFH- and the C18-adsorbent.

On the other hand, the actual volumes measured for the other two adsorbents (C8- and PFP-silica, respectively, blue empty circles and fuchsia circles) practically do not depend on the pressure and, with an acceptable approximation, correspond to the hold-up volume (admittedly, in these cases, the plotted data are redundant, inasmuch as there is no reason to further increase the pressure after achieving a situation of complete wetting). The interpretation of these results is consistent with the characteristics of the adsobents. C18- and PFH-silicas are, in fact, the most hydrophobic ones[38,45] and their pore size is comparable. On the other hand, the C8-silica adsorbent, which is definitely less hydrophobic than the C18-silica but still considered highly hydrophobic, has pores of 30 nm in diameter, i.e., about three times larger than those of C18-silica. Equation 1 shows that wetting is greatly affected by the dimension of the pores.[4,5,33] Thus, it is the increased dimension of pores that explains why in this case the actual volume of water is substantially constant and close to the pycnometric hold-up volume of the column. Finally, the PFP-silica is the least hydrophobic among the considered adsorbents, and wetting by water is not an issue even at very low pressures.

A further generalization of these results is, however, hindered by the heterogeneous nature of the adsorbents, in terms of both pore size distribution and chemical characteristics of the surface. The different behavior observed at low pressure between C18- and PFH-silica (the latter being partially wetted by water), for instance, may be caused either by the different hydrophobicity of the two materials or by the presence of accessible hydrophilic groups on the matrix. It is well-known, in fact, that the presence of free (uncapped) silanols on the surface of a functionalized silica may dramatically improve the wetting properties of that material.[33]

In conclusion, the proposed method seems to be a very promising, environmentally friendly tool for the characterization of porous materials under dynamic conditions. In a large number of applications (heterogeneous catalysis in flow,[46]

dx.doi.org/10.1021/ac303253b | *Anal. Chem.* 2013, 85, 19−22

chromatography, solid-phase extraction, etc.), these are the conditions in which the materials will be effectively employed. In comparison to other approaches aimed at characterizing, under dynamical conditions, the degree of wetting of hydrophobic porous materials by water, which have the drawbacks of needing so-called "unretained" probes[34] or buffered systems,[33] this one gives a direct, physically sound estimation of the phenomenon in pure water.

■ ASSOCIATED CONTENT

Supporting Information

Additional information as noted in text. This material is available free of charge via the Internet at http://pubs.acs.org/.

■ AUTHOR INFORMATION

Corresponding Author

*E-mail: cvz@unife.it. Phone: +39 0532 455331. Fax: +39 0532 240709.

Notes

The authors declare no competing financial interest.

■ ACKNOWLEDGMENTS

The authors thank the Italian University and Scientific Research Ministry (PRIN 20098SJX4F_004 and PRIN 2009ZSC5K2_004), the University of Ferrara (FAR 2010), and the Regional Operational Programme of the European Regional Development Fund, Industrial Research and Technological Transfer (POR FESR 2007-2013 Priority 1). Thanks also to Dr. E. Bianchini from the Department of Chemistry and Pharmaceutical Sciences, University of Ferrara (Ferrara, Italy), for elemental analysis measurements

■ REFERENCES

(1) Eroshenko, V.; Regis, R. C.; Soulard, M.; Patarin, J. *J. Am. Chem. Soc.* **2001**, *123*, 8129−8130.
(2) Rouquerol, J.; Baron, G.; Denoyel, R.; Giesche, H.; Groen, J.; Klobes, P.; Levitz, P.; Neimark, A. V.; Rigby, S.; Skudas, R.; Sing, K.; Thommes, M.; Unger, K. *Pure Appl. Chem.* **2012**, *84*, 107−136.
(3) Gregg, S. J.; Sing, K. S. W. *Adsorption, Surface Area and Porosity*; Academic Press: New York, 1967.
(4) Eroshenko, V. A.; Fadeev, A. Y. *Colloid J.* **1995**, 480−483.
(5) Eroshenko, V. A.; Fadeev, A. Y. *Russ. J. Phys. Chem.* **1996**, 1380−1383.
(6) Fadeev, A. Y.; Eroshenko, V. A. *J. Colloid Interface Sci.* **1997**, *187*, 275−282.
(7) http://www.pmiapp.com/products/water_intrusion_porosimeter.html.
(8) Washburn, E. W. *Phys. Rev.* **1921**, *17*, 273−283.
(9) Giesche, H. *Part. Part. Syst. Charact.* **2006**, *23*, 1−11.
(10) Guan-Sajonz, H.; Guiochon, G.; Davis, E.; Gulakowski, K.; Smith, D. W. *J. Chromatogr., A* **1997**, *773*, 33−51.
(11) Montgomery, M. E.; Green, M. A.; Green, M. J. *Anal. Chem.* **1992**, *64*, 1170.
(12) Maoz, R.; Sagiv, J. *J. Colloid Interface Sci.* **1984**, *100*, 465−496.
(13) Wasserman, S. R.; Tao, Y. T.; Whitesides, G. M. *Langmuir* **1989**, *5*, 1074−1087.
(14) Janczuk, B.; Bialopiotrowicz, T.; Wojcik, W. *Colloids Surf., A* **1989**, *36*, 391−403.
(15) Gomez, F.; Denoyel, R.; Rouquerol, J. *Langmuir* **2000**, *16*, 4374−4379.
(16) Lefevre, B.; Saugey, A.; Barrat, J. L.; Bocquet, L.; Charlaix, E.; Gobin, P. F.; Vigier, G. *J. Chem. Phys.* **2004**, *120*, 4927−4938.
(17) Helfferich, F.; Peterson, D. L. *Science* **1963**, *142*, 661−663.
(18) Helfferich, F. *J. Chem. Educ.* **1964**, *41*, 410−413.
(19) Peterson, D. L.; Helfferich, F. *J. Phys. Chem.* **1965**, *69*, 1283−1293.
(20) Helfferich, F.; Klein, G. *Multicomponent Chromatography*; Marcel Dekker Inc.: New York, 1970.
(21) McCormick, R. M.; Karger, B. L. *Anal. Chem.* **1980**, *52*, 2249−2257.
(22) Knox, J. H.; Kaliszan, R. *J. Chromatogr.* **1985**, *349*, 211−234.
(23) Weng, M.; Mallette, J.; Parcher, J. F. *J. Chromatogr., A* **2008**, *1190*, 1−7.
(24) Yun, K. S.; Zhu, C.; Parcher, J. F. *Anal. Chem.* **1995**, *67*, 613−619.
(25) Mallette, J.; Wang, M.; Parcher, J. F. *Anal. Chem.* **2010**, *82*, 3329−3336.
(26) Lindholm, J.; Forssen, P.; Fornstedt, T. *Anal. Chem.* **2004**, 4856−4865.
(27) Lindholm, J.; Forssen, P.; Fornstedt, T. *Anal. Chem.* **2004**, 5472−5478.
(28) Arnell, R.; Ferraz, N.; Fornstedt, T. *Anal. Chem.* **2006**, *78*, 1682−1689.
(29) Fornstedt, T. *J. Chromatogr., A* **2010**, *1217*, 792−812.
(30) Gritti, F.; Kazakevich, Y.; Guiochon, G. *J. Chromatogr., A* **2007**, *1161*, 157−169.
(31) Tretinnikov, O. N.; Ikada, Y. *Langmuir* **1994**, *10*, 1606−1614.
(32) Guillemot, L.; Galarneau, A.; Vigier, G.; Abensur, T.; Charlaix, E. *Rev. Sci. Instrum.* **2012**, *83*, 105105-1−105105-6.
(33) Walter, T. H.; Iraneta, P.; Capparella, M. *J. Chromatogr., A* **2006**, *1075*, 177−183.
(34) Nagae, N.; Enami, T.; Doshi, S. *LC-GC North Am.* **2002**, *20*, 964−972.
(35) Bidlingmeyer, B. A.; Broske, A. D. *J. Chromatogr. Sci.* **2004**, *42*, 100−106.
(36) Gritti, F.; Guiochon, G. *J. Chromatogr., A* **2003**, *1010*, 153−176.
(37) Neue, U. D. *HPLC Columns: Theory, Technology and Practice*; Wiley-VCH: New York, 1997.
(38) Billiet, H. A. H.; Schoenmakers, P. J.; de Galan, L. *J. Chromatogr.* **1981**, *218*, 443−454.
(39) Marchetti, N.; Caciolli, L.; Laganà, A.; Gasparrini, F.; Pasti, L.; Dondi, F.; Cavazzini, A. *Anal. Chem.* **2012**, *84*, 7138−7145.
(40) Szabelski, P.; Cavazzini, A.; Kaczmarski, K.; Liu, X.; van Horn, J.; Guiochon, G. *J. Chromatogr., A* **2002**, 41−53.
(41) Rimmer, C. A.; Simmons, C. R.; Dorsey, J. D. *J. Chromatogr., A* **2002**, *965*, 219−232.
(42) Gritti, F.; Kazakevich, Y. V.; Guiochon, G. *J. Chromatogr., A* **2007**, *1169*, 111−124.
(43) Guan, H.; Guiochon, G. *J. Chromatogr., A* **1996**, *731*, 27−40.
(44) Cavazzini, A.; Gritti, F.; Kaczmarski, K.; Marchetti, N.; Guiochon, G. *Anal. Chem.* **2007**, *79*, 5972−5979.
(45) Schoenmakers, P. J.; Billiet, H. A. H.; de Galan, L. *Chromatographia* **1982**, *15*, 205−214.
(46) Bortolini, O.; Caciolli, L.; Cavazzini, A.; Costa, V.; Greco, R.; Massi, A.; Pasti, L. *Green Chem.* **2012**, *14*, 992−1000.

Journal of Chromatography A, 1286 (2013) 47–54

Contents lists available at SciVerse ScienceDirect

Journal of Chromatography A

journal homepage: www.elsevier.com/locate/chroma

Geometric characterization of straight-chain perfluorohexylpropyl adsorbents for high performance liquid chromatography

Alberto Cavazzini[a,*], Luisa Pasti[a], Roberto Greco[a], Valentina Costa[a], Damiano Solera[a], Francesco Dondi[a], Nicola Marchetti[a,b], Aldo Laganà[c], Francesco Gasparrini[d]

[a] Department of Chemistry and Pharmaceutical Sciences, University of Ferrara, via L. Borsari, 46, 44121 Ferrara, Italy
[b] Lab. "Terra&Acqua Tech" – Water Quality, Technopole of Ferrara, Ferrara, Italy
[c] Department of Chemistry, University of Rome, "La Sapienza", Piazzale Aldo Moro 5, 00185 Rome, Italy
[d] Dipartimento di Chimica e Tecnologia del Farmaco, University "La Sapienza", Rome, Italy

ARTICLE INFO

Article history:
Received 21 November 2012
Received in revised form 12 February 2013
Accepted 15 February 2013
Available online 26 February 2013

Keywords:
Perfluoroalkyl-based adsorbents
Stationary phase geometry
Hydrophobic surface wettability
Tracer pulse chromatography

ABSTRACT

The geometric characterization of porous adsorbents used as stationary phases in high performance liquid chromatography is a key aspect for the understanding and the description of retention mechanisms. Herein, we present a study aimed at describing the geometric characteristics of alkyl-perfluorinated silica stationary phases by employing chromatographic and non-chromatographic techniques. This study shows that, under typical chromatographic conditions, the perfluorohexylpropyl straight chains grafted to the silica surface assume a compact arrangement. As perfluorinated stationary phases are highly hydrophobic, their wetting behavior in water was investigated. To this end, a novel approach based on tracer pulse chromatography with pure water as the mobile phase and deuterium oxide as the labeled marker was employed. Experimentally it was found that, unless a high back-pressure is applied, water is expelled by the pores of the adsorbent. On the other hand, wetting can be significantly improved if 5–10% (v/v) of organic modifier is added to the mobile phase. The practical consequences of limited wettability are discussed, in particular with reference to fluorous-SPE (F-SPE) applications.

1. Introduction

Alkyl perfluorinated silica-based materials were employed as stationary phases for gas chromatography in the late 1970s [1]. A few years later, they were introduced as stationary phases in reversed-phase liquid chromatography, firstly by Berendsen et al. [2], Billiet et al. [3], Haas et al. [4] and Schoenmakers et al. [5]. Some characteristics made alkyl-perfluorinated silica-based stationary phases particularly interesting for HPLC applications. In particular, they exhibited a specific affinity towards fluorine-containing compounds (this property, referred to as fluorophilicity or fluorous-affinity, arises from strong noncovalent interactions between highly fluorinated chemical moieties) and an extremely low polarity. In the solubility scale of Hildebrand and Scott [6], the solubility parameter estimated for fluoroalkanes is roughly 5 $cal^{1/2}/cm^{3/2}$, against values for instance of 7, 15, 16 and 13 $cal^{1/2}/cm^{3/2}$ for n-alkanes, water, methanol and acetonitrile, respectively. As the solubility parameter strongly correlates with polarity (essentially, it represents the square root of the cohesive energy density of a substance that is, the energy necessary to vaporize one mole of a substance divided by the molar volume of the liquid [7]), the polarity of alkyl perfluorinated stationary phases is lower than that of their alkyl counterparts. On the other hand, alkyl perfluorinated materials are immiscible also with most common organic solvents at room temperature (in the older patent literature [8,9], the term "oleophobic" has been used to characterize this feature) and they are less polarizable than the corresponding hydrocarbons, as indicated by Kamlet–Taft dipolarity/polarizability parameters and refractive indexes remarkably lower than for hydrocarbons [10,11].

Based on the "solubility parameter model" [12,13], the extreme low polarity of perfluoroalkyl stationary phases was invoked to explain the expected enhanced selectivity of these materials, with respect to the alkyl phases, towards low and moderately polar solutes [5] and was even claimed to be the key for the development of reversed-phase separations of proteins with considerably less organic modifier in the mobile phase [14]. Detailed data supporting these suggestions, however, were not provided and, as a matter of fact, alkyl perfluorinated phases did not have the same success as the alkyl phases (e.g., C8, C18) [3,15–19].

At the same time, the main manufacturers of HPLC columns focused the development and the production of fluorinated phases almost exclusively on the perfluorophenyl (PFP) type,

* Corresponding author. Tel.: +39 0532 455331; fax: +39 0539 240709.
E-mail address: cvz@unife.it (A. Cavazzini).

0021-9673/$ – see front matter © 2013 Elsevier B.V. All rights reserved.
http://dx.doi.org/10.1016/j.chroma.2013.02.050

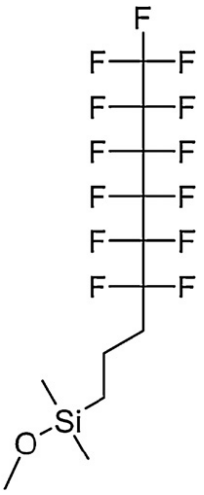

Fig. 1. Perfluorohexylpropyl silica gel structure.

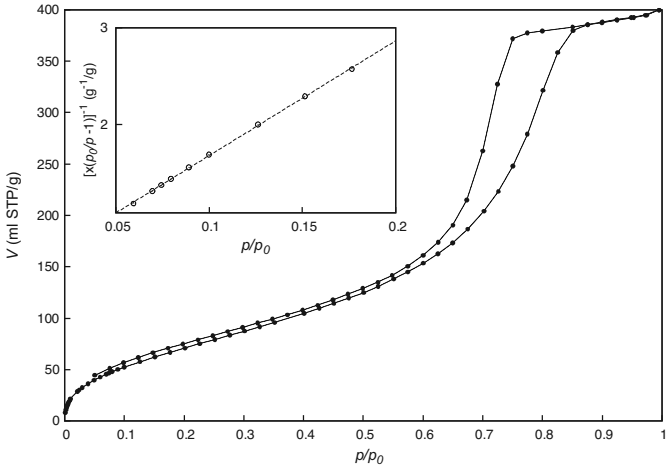

Fig. 2. LTNA isotherm measured for the perfluorohexylpropyl silica. *y*-axis: N_2 adsorbed volume at standard temperature and pressure, STP (P = 1 atm, T = 273 K) per gram of functionalized material. Inset: linear transformed BET equation in the range $0.05 \leq p/p_0 \leq 0.2$. Empty circles: experimental data; dashed line: linear regression (R^2 = 0.9989).

perfluoroalkyl adsorbents being mainly prepared as bulk materials for fluorous flash-chromatography by dedicated companies (e.g., [20]). While the concept of fluorophilicity had been widely exploited in fields such as synthesis [21], catalyst technology [22], purification of synthetic peptides [23] and oligosaccharides [24], HPLC separations on perfluoroalkyl silica-based stationary phases were limited to niche applications for a long time. In the last years, however, a renewed interest in these materials as stationary phases for HPLC applications in proteomics [25], metabolomics [26], determination of biogenic amines [27] and for the enrichment and analysis of perfluorinated emergent contaminants [19] has arisen.

In this work, we propose a study aimed at characterizing the geometric features of a straight-chain perfluorohexylpropyl silica gel (see Fig. 1), by combining the information from low temperature nitrogen adsorption (LTNA) isotherm and elemental analysis with that coming from different types of chromatographic measurements, including tracer-pulse (TP) and inverse size exclusion chromatography (ISEC). We believe this information may help the understanding of retention mechanisms on alkyl perfluorinated stationary phases, inasmuch as the chromatographic retention behavior of solutes should be referred to the geometric properties of the adsorbent after functionalization and not to those of the base silica. It is well known, in fact, that quantities such as specific surface area, pore size and pore volume change after functionalization. Analogous studies performed on alkyl [28–30] and phenyl (including PFP) modified silica gels [31,32] demonstrated the importance of this information for the interpretation of the chromatographic process.

Since alkyl perfluorinated stationary phases are extremely apolar, wetting by water is expected to be an issue under some circumstances such as, for instance, if they are in contact with highly aqueous mobile phases. This behavior is well-known in reversed-phase liquid chromatography with hydrophobic C8 or C18 stationary phases, where a sudden drop in the column pressure, either by accident or by reduction of the flow rate, may provoke loss of efficiency and retention when highly aqueous mobile phases are employed [33–36]. The expression "phase collapse" has been used to describe this effect, even though it is due to the expulsion of water from the pores of the hydrophobic surface [33,34]. The wetting behavior of perfluorocarbon bonded phases in water has been thus studied by means of a recent application of TP chromatography, in which pure water is the mobile phase and deuterium oxide the labeled marker [37].

2. Theory

2.1. Surface area, pore size distribution and bonding density determination

Over the last 60 years, the Brunauer–Emmett–Teller (BET) method has become extremely popular for determining the surface area of adsorbents, catalysts and other porous materials [38]. The principle is based on the construction of the LTNA isotherm (commonly said BET plot) that reports the amount adsorbed by unit mass of solid (specific amount adsorbed) as a function of the equilibrium (or relative) pressure, at a constant temperature. Therefrom, both the monolayer capacity and the mesopore (i.e., pores of 20–500 Å diameter) size distribution can be estimated. Nitrogen is generally accepted as the most suitable adsorptive for mesopore size analysis as the thickness of the N_2 multilayer is largely insensitive to differences in adsorbent particle size or surface structure. On the other hand, from monolayer capacity the estimation of the specific surface area is straightforward. The average area occupied by a N_2 molecule in the completed monolayer, $a_s(N_2)$, is usually taken equal to 16.2 Å^2. However, this is a reasonable estimate for $a_s(N_2)$ on hydrophilic surfaces (such as bare silica), while on the hydrophobic ones, being nitrogen adsorption less localized, larger values have been suggested [39,40]. For instance, Buyanova et al. [41] and Giaquinto et al. [30] proposed for $a_s(N_2)$ values of 20.5 and 20.6 Å^2, respectively.

In case of so-called type-IV isotherm (see Fig. 2) [38], the specific mesopore volume can be evaluated by the amount adsorbed at the plateau by assuming that the adsorbate has the normal molar volume of the liquid at the operational temperature (Gurvich rule [42]). The determination of the pore size distribution from LTNA can instead be achieved by different methods. The "classical" ones rely on the Kelvin equation that essentially relates the nitrogen pressure to the size of pores in which capillary/condensation of the adsorbate takes place [40,38]. These classical pore-filling models are accurate enough to describe adsorption in mesopores while they are not suitable for characterizing microporous materials [43]. On the other hand, more advanced approaches, such as those based upon the density functional theory (DFT), have the advantage of describing adsorption over the entire range of pore size (including micropores) [44].

Bonding density is traditionally obtained from organic elemental micro-analysis of the chemically bonded phase. Organic

elemental micro-analysis generally allows for the determination of carbon, hydrogen, nitrogen and heteroatoms, such as halogens or sulfur. The measured percentage (w/w) of an element i, P_i%, is readily expressed in the number of ligand attached to the bare silica surface (bonding density), N, as [45]:

$$P_i\% = \frac{N \times w_i \times n_i}{1 + N \times (M_w - 1)} \times 100 \quad (1)$$

where n_i and w_i are the number of atoms of element i in the bonded ligand and the molecular weight of the element i, respectively, and M_w is the molecular weight of the ligand. The term $N \times (M_w - 1)$, in the denominator of Eq. (1), corrects for the weight increase of silica after functionalization and accounts for one hydrogen atom lost in the surface reaction. According to Eq. (1), N is expressed as number of moles of ligand per gram of unmodified (bare) silica and it is assumed that monofunctional ligands (i.e., ligands with only one group able to react with the surface) have been employed in the derivatization process.

2.2. Void volume measurement

There are several techniques available for the determination of the void volume of a chromatographic column [47–49]. In this work, we will only focus on the TP and the pycnometric method.

In the framework of TP chromatography [46,47,50–57], when the eluent contains one or more component that can interact with the stationary phase, the integral mass balance equation for the component i is given by:

$$V^*_{R,i} = \frac{n_i^{tot}}{C_i^M} \quad (2)$$

where $V^*_{R,i}$ is the retention volume of the isotopically labeled i compound, and n_i^{tot} and C_i^M are the total amount of unlabeled species i in the column (taken as a whole) and its molar concentration in the mobile phase, respectively. The theory of TP chromatography assumes that the distribution coefficients for molecules of the labelled components are identical to those of the unlabelled materials, that is, that there is no isotope effect [46,47]. By assuming, then, the same partial molar volumes of the organic modifier upon adsorption or mixing to form the binary eluent, from Eq. (2) one obtains [47]:

$$V^*_{R,i} = \frac{V_i^{tot}}{\mathcal{O}_i^M} \quad (3)$$

being V_i^{tot} and $\mathcal{O}_i^M$ the total volume of i in the column and its volume fraction in the bulk eluent, respectively. Owing to the complexity of the interfacial region in liquid chromatography with stationary phases consisting of organic moieties, the exact volume of adsorbed and bulk-liquid phases cannot be unambiguously delineated [58]. The way out to this cumbersome problem involves the specification of the hypothetical gibbs dividing surface (GDS) which delineates the boundary between the stationary phase and the mobile phase. Two conventions are commonly used in LC for establishing the position of GDS: either the GDS is assumed to coincide with the physical surface of the solid adsorbent (so-called "nothing is adsorbed in terms of volume", or *vNA*, convention [59]) or the GDS is established at the interface between an adsorbed film (that constitutes the stationary phase volume, V_S) and the bulk fluid (this convention is said "component J not adsorbed", or *JNA*, convention [59]). With *vNA* convention, the void volume of the column (also referred to as "thermodynamic dead volume") is given by the total volume of the eluent in the column, V_0. If the *JNA* convention is adopted, instead, the pertinent void volume is the so-defined "kinetic void volume", V_M. The relationship between V_M and V_0 is given by:

$$V_M = V_0 - V_S \quad (4)$$

Literature is replete with discussions concerning the difficulties involved in the accurate estimation of V_M (primarily due to the problem of finding a truly unretained and unexcluded compound) [47–49]. On the other hand, V_0 can be easily estimated for instance, through pycnometry, perturbation on the plateau technique or TP experiments [48]. In the context of TP method, summation over all eluent components (i and j, for a binary system) leads to V_0 [47,52]:

$$V_{0,\mathrm{TP}} = V^*_{R,i}\mathcal{O}_i^M + V^*_{R,j}\mathcal{O}_j^M \quad (5)$$

V_0 is accordingly obtained by injecting small samples of eluent with isotopically labeled solute components and determining the elution volume ($V^*_{R,i}$ and $V^*_{R,j}$) for each labeled component. Obviously, the method can be used with a pure eluent ($\mathcal{O}_i^M$ or $\mathcal{O}_j^M = 1$) and this is by far the simplest way of determining V_0.

The most popular of the static methods for the determination of void volume is pycnometry (or the weight difference method). The method consists in weighing the chromatographic column sequentially filled with solvents of different densities. The pycnometric void volume, $V_{0,\mathrm{pycn}}$ is thus calculated as [47,60,48,49]:

$$V_{0,\mathrm{pycn}} = \frac{w_1 - w_2}{\delta_1 - \delta_2} \quad (6)$$

where w_1 and w_2 are the weights of the column filled with solvent 1 and 2, respectively, and δ_1 and δ_2 their densities. It is generally agreed upon that $V_{0,\mathrm{pycn}}$ gives the maximum possible void volume.

3. Materials and methods

3.1. Chromatographic measurements

3.1.1. Columns and materials

Two commercial stainless steel columns (50 and 150 mm × 2.1 mm, respectively) packed with perfluorohexylpropyl straight-chain functionalized silica gel, particle size 5 μm, pore size 100 Å (Fluophase-RP from Thermo Scientific) were used. Ultra high quality Milli-Q water was obtained by a Milli-Q water purification system (Millipore). Acetonitrile (ACN) was LC–MS grade (from Sigma–Aldrich). HPLC-grade methanol (MeOH), tetrahydrofuran (THF) and dichloromethane (DCM) were also purchased from Sigma–Aldrich. Deuterated water, D_2O, and deuterated ACN, D_3-ACN, were from Cambridge Isotope Laboratories Inc. Polystyrene standards were from Supelco. Fused silica tubings (20 μm I.D. × 360 μm O.D. from Upchurch Scientific) of different length were used as back pressure regulators.

3.1.2. Equipment

A LC/MS instrumentation composed by a micro-HPLC (Finnigan Surveyor Plus) equipped with a low-pressure four-channel pump, a column thermostat and an autosampler and interfaced to a LTQ-XL linear ion trap MS detector (Thermo Scientific) with an APCI ion source was used for tracer pulse measurements (Section 3.1.3). A micro-HPLC Agilent 1100 composed by a binary high-pressure pump system, a column thermostat, a DAD-UV detector and a micro-autosampler was employed for ISEC measurements (Section 3.1.4).

3.1.3. TP chromatography

5 μl of D_3-ACN and D_2O were injected separately in columns equilibrated with different ACN aqueous solutions. ACN concentration was varied with increments of 10% in the range 0–80%.

Between 80 and 100%, the following concentrations were prepared: 85, 90, 93, 95, 97 and 100. The flow rate was 0.1 ml/min on the shorter column and 0.25 ml/min on the longer one. The temperature was 25 ± 0.2 °C. APCI (positive polarity) operational conditions were: source current 5 μA; source voltage 6 kV; capillary temperature 275 °C; vaporizer temperature 375 °C; capillary voltage 46 V; tube lens 75 V. D_2O and D_3-ACN were monitored in SIM mode at m/z = 21 and 45, respectively ($[M+H]^+$). All measurements were done triplicate. Retention times of perturbations determined through peak moments were corrected by extra-column contributions.

3.1.4. ISEC

Samples of polystyrene of known average molecular weight (0.5, 2 2.5, 5, 9, 17.5, 30, 34.5, 50, 110, 200, 402, 565, 655, 1030, 1570, 1800, 2700 and 3800 kDa) and narrow molecular weight distributions were injected into the columns equilibrated with THF and their retention volumes, determined through peak moments and corrected by extra-column volume, plotted versus the cubic root of their molecular weight (see Section 4.3). Work wavelength, temperature and flow rate were 226 nm, 25.0 ± 0.2 °C and 0.2 ml/min, respectively. Measurements were repeated twice.

3.2. Non-chromatographic measurements

After completion of measurements, the columns were washed with ACN, unpacked, and the packing was dried at 100 °C under slow nitrogen flow followed by vacuum until constant weight. This material was used for LTNA determination and elemental analysis.

3.2.1. LTNA measurements

Nitrogen physisorption measurements were carried out at 77 K in the relative pressure range p/p_0 (p and p_0: pressure and saturated vapour pressure, respectively) from 1×10^{-6} to 1. A Quantachrome Autosorb 1-MP/TCD instrument (from Quantachrome Instruments) was used. Prior to the analysis the samples were outgassed (residual pressure lower than 10^{-6} mbar) at 200 °C for 16 h. Specific surface areas were determined by using the BET in the relative pressure range from 0.05 to 0.20 p/p_0. Pore size distributions were obtained by applying the nonlocal density functional theory (NLDFT) method (N_2 silica kernel based on a cylindrical pore model applied to the desorption branch) [61].

3.2.2. Elemental analysis

C, H, N, S elemental micro-analysis were performed on a Flash2000 elemental analyzer from Thermo Scientific. Samples were dried under vacuum for 6 h at 100 °C before analysis. Fluorine (F) analysis were executed by the Laboratory for Elemental Analysis of the University of Wien [62].

3.2.3. Pycnometry

DCM (density: 1.33 g/ml) and MeOH (0.79 g/ml) were used as solvents for pycnometric measurements. Column weighing was repeated three times per each solvent.

4. Results and discussion

4.1. Surface area, pore volume and pore size determination from LTNA measurements

The full nitrogen (adsorption and desorption) isotherm measured for the perfluorinated silica gel is represented in the main part of Fig. 2. According to the IUPAC classification, the isotherm belongs to type-IV [63]. The upper plateau of the adsorption isotherm corresponds to complete pore filling, while the lower and the upper branches of the hysteresis loop represent measurements obtained by progressive addition and withdrawal of gas of the adsorbent, respectively. V is the volume (ml) of adsorbed N_2 gas at standard temperature and pressure (STP) per gram of functionalized silica gel and p/p_0 is the relative pressure. The form of the BET equation most often employed for analysis of experimental data (so-called linear transformed BET equation) is given by:

$$\frac{1}{x(p_0/p-1)} = \frac{1}{x_m c} + \frac{c-1}{x_m c}\frac{p}{p_0} \tag{7}$$

where x and x_m are, respectively, the weight of gaseous nitrogen adsorbed at a given p/p_0 and that to give monolayer coverage. x is readily achievable from data of Fig. 2 by considering that gaseous N_2 density at STP is 0.00125 g/ml. The c-constant is a dimensionless quantity related to the energy of adsorption:

$$c = \exp\left(\frac{E_a - E_L}{RT}\right) \tag{8}$$

where E_a is the energy of adsorption in the first adsorption layer, E_L the liquefaction energy, R and T, respectively, the universal gas constant and the absolute temperature [38].

When the plot $1/x(p_0/p-1)$ against p/p_0 yields a straight line, by its slope, $s = (c-1)/(x_m c)$, and intercept, $i = 1/x_m c$, the calculation of x_m and c-constant is straightforward being:

$$c = \frac{s}{i} + 1 \tag{9}$$

and

$$x_m = \frac{1}{s+i} \tag{10}$$

From x_m the specific surface area S (m^2/g) can be calculated through:

$$S = \frac{x_m}{w_{N_2}} \times N_a \times a(N_2) \tag{11}$$

where w_{N_2} and N_a are the molar mass of N_2 and the Avogadro's constant, respectively.

The inset of Fig. 2 shows the application of Eq. (7) to the relative pressure range of the adsorption isotherm $0.05 \leq p/p_0 \leq 0.2$. From Eq. (9), one gets a value for the c-constant equal to 24.8 while, from Eqs. (10) and (11) and by assuming the customary value $a(N_2) = 16.2 Å^2$, S was estimated for the functionalized silica to be 286 m^2/g. Kazakevich and coworkers measured the c constants for different stationary phases [64,65]. They reported values of c ranging from 80 to 200 for bare silica, 16 to 20 for alkyl-modified adsorbents of C-18 type, 10 to 12 for hydrophobic methyl-terminated surfaces and of the order of about 40 for PFP and 30 for phenyl-modified stationary phases. The slightly larger c value estimated for perfluorohexylpropyl adsorbents with respect to the C18 ones can be possibly explained in light of the higher electron density of perfluorinated chains.

Since $a(N_2)$ is correlated to c [30], this finding would seem to suggest that the value of the cross sectional area of nitrogen to be employed for the evaluation of the surface area of alkyl perfluorinated adsorbents through the BET method should be similar to that suggested for C18 phases [30,41]. However, as the information gathered in this work was based on the evaluation of only one material that, in addition, was not fully characterized by the manufacturer (see later on) we decided to use the traditional 16.2 $Å^2$ value. According to Jelinek and Kováts [66], in fact, this should be a reasonable estimate for perfluoro-polymer surfaces. On the other hand, these aspects will be detailedly investigated in to a future work. To this end, home-made perfluorinated silica adsorbents (both straight-chain and PFP) have been already prepared in the lab [37] and additional measurements are been carried out.

Fig. 3 shows the calculated pore size distribution for the perfluorohexylpropyl silica gel obtained by NLDFT [61]. The relation

Table 1
Geometric parameters of bare- and perfluorohexylpropyl-silica gel by LTNA and elemental analysis.

Adsorbent	Surface area, S (m^2/g)	Pore volume and corrected pore volume		Pore size, d_p (Å)	Percentage, P_i% (w/w)		Bonding density, d_b (μmol/m^2)	
		$V_{p,LTNA}$ (ml/g)	$V^*_{p,LTNA}$ (ml/g)		C	F	C	F
Bare silica	310[a]	1.03[a]	N/A[b]	100[a]	0	0	0	0
Fluophase-RP	286[c]	0.58	0.799[d]	92	9.7	16.2	N/A[b],[e]	2.91[f]

[a] From manufacturer.
[b] N/A: not applicable.
[c] Calculated by assuming $a_s(N_2) = 16.2$ Å^2. See Section 4 for details.
[d] Corrected pore volume, $V^*_{p,LTNA}$, refers to 1 g of bare silica (see Section 4.7).
[e] See Section 4.2.
[f] μmol/m^2 bare silica (see Eq. (13))

between pore volume, V_p, and pore dimension, d_p, is presented graphically both in the form of a frequency curve, dV_p/dd_p vs d_p, and as a cumulative plot, V_p vs d_p. From these calculations, one gets 92 Åas the averaged pore size of the functionalized silica and 0.58 ml/g as its specific pore volume. Exactly the same V_p result can be achieved by dividing the plateau value of the adsorption isotherm, roughly 375 ml STP/g (see Fig. 2), by 646 (i.e., the ratio between the density of liquid nitrogen at 77 K, 0.807 g/ml, and its gas density at STP) [67]. For the sake of clarity and for future reference, S and V_p values for the Fluophase-RP material have been listed in row 2 of Table 1, columns 2 and 3 (the subscript "LTNA" was used to indicate the type of measurement used for the estimation of the parameter).

4.2. Bonding density from elemental analysis

Eq. (1) can be recast to express the bonding density (mol/g) as:

$$N\,(\mathrm{mol/g}) = \frac{P_i\%}{(100 \times n_i \times w_i) - P_i\% \times (M_w - 1)} \tag{12}$$

In chromatographic works, the bonding density is usually given in μmol/m^2 and indicated by d_b:

$$d_b\,(\mu\mathrm{mol/m^2}) = N \times \frac{10^6}{S_{SiO_2}} \tag{13}$$

S_{SiO_2} being the specific surface area of bare silica.

P_C% and P_F% obtained by elemental analysis are reported in Table 1, row 2, columns 6 and 7. From P_F%, through Eqs. (12) and (13), d_b can be calculated (last column of Table 1). On the other hand, carbon load cannot be directly used to estimate the bonding density of ligands inasmuch as, according to manufacturer, commercial Fluophase-RP was end-capped after functionalization [68] (unfortunately, no details were given about the end-capping procedure). P_C%, accordingly, includes the contribution to carbon coming from both the end-capping agent and the ligand (this explains the symbol N/A appearing in Table 1, row 2, column 8).

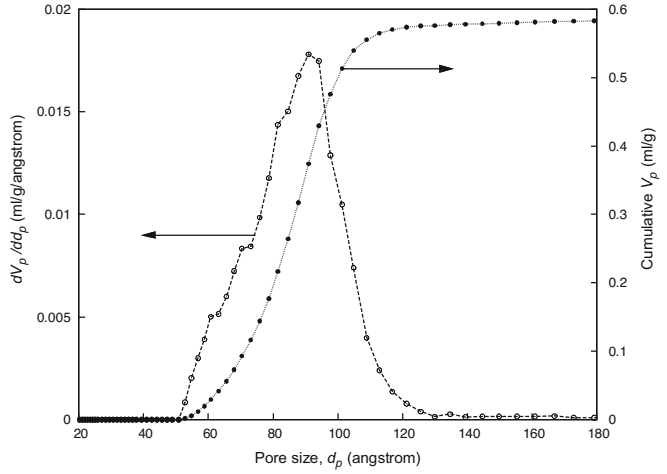

Fig. 3. Pore size distribution curve (empty circles connected by a dashed line, left y-axis) and cumulative pore volume distribution (filled circles connected by a dotted line, right y-axis). Arrows simply indicate the pertinent y-axis for the two plots.

By considering the P_F% value (16.2% (w/w), Table 1, column 7) and the chemical structure of the ligand (containing 13 fluorine and 11 carbon atoms, Fig. 1), the two contributions can however be estimated. In fact, by simply dividing the weight of fluorine in one gram of functionalized silica (0.162 g) by the product between the number of fluorine in the ligand (13) and the molar mass of fluorine (19 g/mol), one obtains 6.56×10^{-4} moles of ligand per gram of functionalized silica. This corresponds to 0.087 g of carbon ($6.56 \times 10^{-4} \times 11 \times 12$). Accordingly, from the difference between the total mass of carbon in one gram of functionalized silica (0.097 g, Table 1, row 2, column 6) and the carbon mass from the ligand (0.087 g), the amount of carbon coming from end-capping is 0.010 g per gram of functionalized silica. Let us assume that trimethylsilylchloride was used for end-capping: one gets to the conclusion that 2.78×10^{-4} (= 0.010/3/12) moles of silanols/g functionalized silica were capped, that is 0.97 μmol of capped silanols per square meter of functionalized silica (= 2.78×10^{-4}/286). The surface concentration of free silanols after end-capping can be finally estimated by assuming an initial surface concentration of silanols equal to 8 μmol/m^2 [36] and by subtracting to this both the number of silanols covered by the introduction of the ligand onto the surface, 2.29 μmol/m^2 (= 6.56×10^{-4}/286), and the number of capped silanols (0.97 μmol/m^2). This simple calculation leads to 4.74 μmol of free silanols per square meter of functionalized silica, which shows that about 40% of the total silanols were functionalized. Within the limits of experimental errors, this value is consistent with typical silanol coverage reported for alkyl reversed-phase adsorbents (usually in the range of 50% [36,69]).

4.3. Interstitial pore volume through ISEC

In Fig. 4, the retention volumes, V_r, of standard polystyrenes are plotted against the cubic root of their molecular weights, $M_{w,polys}$, for both columns (ISEC plots). The dotted and dashed lines represent the linear regressions calculated for the volumes of totally excluded polystyrenes [70]. The ISEC estimation of interstitial volume, V_e, is derived from the extrapolation to $M_{w,polys} = 0$ of these linear regressions. V_e equal to 0.073 and 0.218 ml were obtained for the 5- and the 15-cm column, respectively.

4.4. Void volume determination

Fig. 5 shows how $V_{0,TP}$ changes by changing the mobile phase composition for the shorter (black circles) and the longer (empty circles) column employed in this work. From these data, averaged

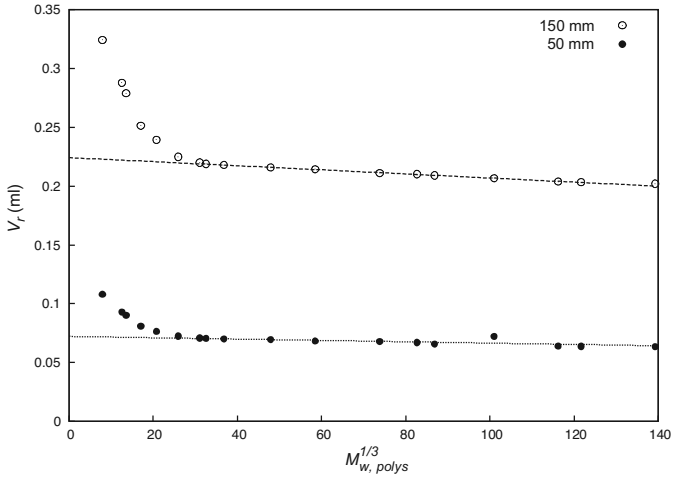

Fig. 4. ISEC plot for the 150 mm (empty circles) and 50 mm (black circles) column. Straight lines: linear fittings of excluded polystyrene retention volumes.

void volume values (calculated over the entire $V_{0,TP}$ experimental datasets) were found to be equal to 0.124 and 0.365 ml (they are represented in figure with dashed lines). Pycnometric void volumes, calculated according to Eq. (6), have been also represented in Fig. 5 (dotted lines). Their values are listed, together with the $V_{0,TP}$ averages in Table 2, row 2, columns 3 and 4. As it can be observed, a significant agreement was found between pycnometric and chromatographic measurements.

A closer look to Fig. 5 reveals some interesting aspects. When water is used as the mobile phase, the calculated void volume drops to values noticeably smaller than the averages. This is so for both columns. In the case of the 5-cm column, the calculated hold-up volume in water is only about 60% of the average value (0.074 vs. 0.124 ml) and it practically corresponds to the interstitial volume estimated by ISEC. For the 15-cm column the difference among the two volumes is slightly smaller (0.255 vs. 0.365, see Table 2). Due to the extremely low polarity of perfluorocarbon bonded phases and the operative conditions employed (see further on), the water cannot completely fill the intraparticle volume of the packed bed. A similar suggestion was proposed by Billiet and coworkers to explain the sudden loss of chromatographic performances of

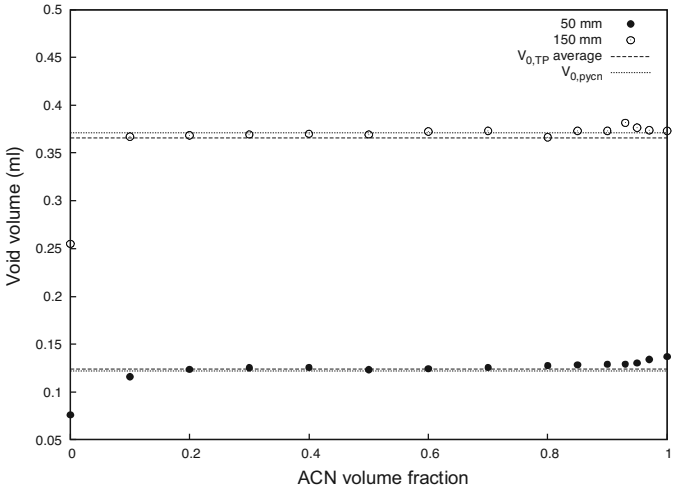

Fig. 5. Void volume, $V_{0,TP}$, vs ACN volume fraction (black circles: 50 mm × 2.1 mm column; empty circles: 150 mm × 2.1 mm column). $V_{0,TP}$s were calculated according to Eq. (5). Dashed lines: $V_{0,TP}$ average values (calculated over the entire datasets). Dotted lines: void volumes calculated by pycnometry, $V_{0,TP}$. $V_{0,TP}$s were calculated through Eq. (6).

Table 2
Geometric parameters of perfluorohexylpropyl-silica by chromatographic measurements. Errors on $V_{0,pycn}$ calculated by error propagation (weighing standard deviation upon triplicate measurements: ±0.001 g). Errors on $V_{0,TP}$ given as ± one standard deviation (calculated upon the entire data set of Fig. 5 with the exclusion of the point at 100% water. See text for details).

Parameter		Column	
		50 mm	150 mm
Void volume (ml)	$V_{0,pycn}$	0.122 ± 0.003	0.370 ± 0.003
	$V_{0,TP}$	0.124 ± 0.005	0.365 ± 0.005
Interstitial volume (ml)	V_e	0.073	0.218
Internal volume (ml)	$V_{i,pycn}$	0.049	0.154
	$V_{i,TP}$	0.051	0.153
Adsorbent mass (g)[a]	w_{pack}	0.092	0.270
Specific pore volume (ml/g)	$V_{p,pycn}$	0.533	0.570
	$V_{p,TP}$	0.554	0.566
Corrected pore volume (ml/g)[b]	$V^*_{p,pycn}$	0.734	0.785
	$V^*_{p,TP}$	0.763	0.781

[a] Determined by weighing after unpacking the columns.
[b] Corrected pore volumes, $V^*_{p,pycn}$ and $V^*_{p,TP}$, refer to 1 g of bare silica (see Section 4.7).

perfluorinated stationary phases at low organic content [3]. The wetting behavior of alkyl perfluorinated stationary phases in pure water has been further investigated through a novel method [37], based on the physically sound theory of TP chromatography, that will be described in the next section.

4.5. The effect of the applied back pressure on the water volume contained in the column

Eq. (5) shows that, if pure water is employed as the eluent, the void volume is given by:

$$V_{0,TP} = V^*_{R,D_2O} \tag{14}$$

where V^*_{R,D_2O} is the retention volume of the deuterated water peak. This equation holds in case of complete wetting of the adsorbent. On the other hand, if water cannot entirely penetrate the pores of the adsorbent, Eq. (14) provides what is more correctly termed the "actual" volume of water in the column, V_{H_2O}. By analogy to Eq. (14), it is convenient to write:

$$V_{H_2O} = V^*_{R,D_2O} \tag{15}$$

Fig. 6 shows how the actual volume of water changes by changing the applied back pressure.[1] The pressure was generated by restrictors placed after the column. The pressure drop over the restrictor was adjusted by changing its length [72]. The measurements were performed at constant flow rate. The flow rate was kept at 20 μl/min (checked by weighing) as, under these conditions, the back-pressure given by the HPLC system (including the column) was negligible, about 2 bar, if compared to that generated by the restrictor. As to minimize extra-column effects, the longer column was used in these measurements.

The course of the V_{H_2O} as a function of the applied pressure presents a characteristic S-shape from a value that is about 15% larger than V_e up to the pycnometric void volume. For the sake of clarity, V_0 and V_e have been represented in the plot (upper and lower dashed lined).

This study shows that a pressure larger than 200 bar is needed to completely fill with water the intraparticle volume of the alkyl-perfluorinated stationary phase. On the other hand, the back-pressure generated by the 15-cm column operated at 0.25 ml/min

[1] At these pressures, water compressibility can be neglected [71].

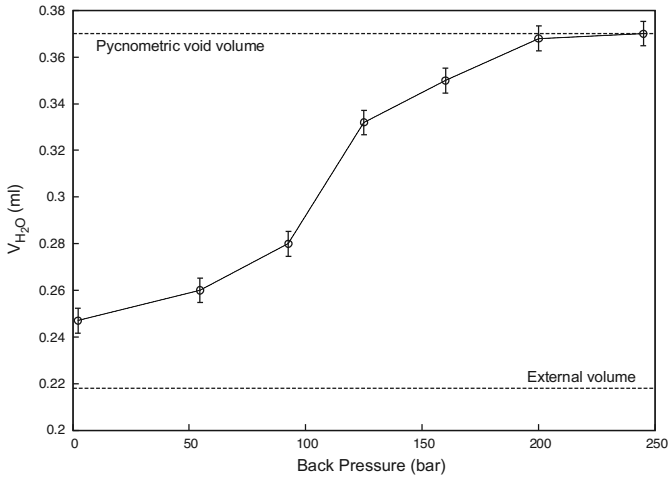

Fig. 6. Actual volume of water contained in the column as a function of the applied back pressure. V_{H_2O} was calculated through Eq. (15). Errors given as ± one standard deviation (triplicate measurements).

with pure water as the mobile phase (that are the conditions of Fig. 5) was 60 bars. This explains why the water volume in the column is only 0.255 ml. The slight difference between this volume and the one achievable by Fig. 6 at the same pressure (at 60 bar one reads a volume slightly larger 0.265 ml) is due to the fact that, in the first case (Fig. 5), the pressure was generated by the fluid stream through the packed bed while, in the second one, it was given by the restrictor. If the packing is homogeneous, it is a good approximation to assume that the back pressure decreases linearly from the inlet of the column to its outlet, where the pressure is close to the atmospheric one. Therefore, under the conditions of Fig. 5, only a short part of the column, near to the inlet, is effectively subjected to a pressure close to 60 bar.

There are some important, practical consequences which follow from this finding. First of all, it explains the poor column performances observed with these materials and highly aqueous mobile phases [3] as a consequence of the fact that, being the water expelled from the pores of the porous hydrophobic material, the effective adsorption surface available to analytes is remarkably reduced. Secondly, it warns about the use of alkyl perfluorinated materials as pre-concentration media in fluorous solid phase extraction (F-SPE) of aqueous solutions. On the other hand, this has been recently demonstrated to be a potentially very promising field of application of these materials, especially for environmental purposes [19]. The typical pressures in SPE applications do not allow water to penetrate the pores of the adsorbent. As a consequence, if pure water is used as the solvent during phase-conditioning and sample-loading in F-SPE, the perfluorinated material will not be completely wet and the surface area effectively available for adsorption will result much smaller than expected. This will affect the performances of F-SPE in terms of both loss of mass (and thus mass recovery) and reproducibility. As shown in Fig. 5, however, the addition of 5–10% (v/v) organic to the eluent permits the recovery of efficient operational conditions.

4.6. Internal and specific pore volume

The difference between void and interstitial volume defines the internal volume, V_i. As void volumes were measured by both pycnometry and TP chromatography, two V_i estimates for each column, $V_{i,\mathrm{pycn}}$ and $V_{i,\mathrm{TP}}$, are reported in Table 2 (third row). Their values, however, are practically coincident.

From the internal volume and the mass of adsorbent inside the column, w_{pack}, finally, a chromatographic estimation of the specific pore volume can be achieved, being:

$$V_p = \frac{V_i}{w_{\mathrm{pack}}} \tag{16}$$

Pore volumes obtained by Eq. (16) are listed in the sixth row of Table 2. The average value of the four measurements is 0.56 ml per gram of functionalized silica. When compared with the pore volume estimated by LTNA, $V_{p,\mathrm{LTNA}} = 0.58$ (see Table 1), one concludes that the molecular arrangement of the organic bonded layer exposed to the HPLC eluent at ambient temperature does not significantly differ from that in vacuum at liquid nitrogen temperature. This finding agrees with the results of previous investigations conducted on alkyl- and phenyl-modified adsorbents by Kazakevich's group [29,31,73,74,28,30] and would seem to suggest that perfluorinated chains are in a "collapsed-like state" [29], due to the fact that intermolecular interactions are stronger than the interaction between eluent and perfluoroalkyl chains.

4.7. Bonded layer volume and effective molecular volume of bonded ligands

Another consideration that can be done with the data in our possess is about the change of specific pore volume before and after functionalization of bare silica. As reported in the second row of Table 1, third column, the pore volume estimated by LTNA isotherm for bare silica is $V_{p,\mathrm{LTNA}} = 1.03$ ml/g. As it has been just demonstrated there is not any significant difference between pore volume measured by LTNA and chromatography. Therefore, the difference between specific pore volumes of bare and functionalized silica gel can be used to estimate the volume of the bonded layer [74]. In order to make a valid comparison between these series of data, however, it is necessary to relate the specific pore volume, measured for the functionalized material, to 1 g of bare silica. This can be easily accomplished by considering the specific mass increment of silica after functionalization, given by (see Eqs. (1) and (13)):

$$N \times (M_w - 1) = d_b \times S_{\mathrm{SiO_2}} \times (M_w - 1) \times 10^{-6} \tag{17}$$

Accordingly the weight fraction, f, of bare silica over the functionalized material is [75,28]:

$$f = \frac{1}{1 + (d_b \times S_{\mathrm{SiO_2}} \times (M_w - 1) \times 10^{-6})} \tag{18}$$

The specific pore volume measured on the functionalized material can be thus related to one gram of bare silica by division by f. We define this as the corrected volume (represented with a superscript *). With the data reported in Tables 1 and 2, one obtains $f = 0.726$. Corrected specific pore volumes, $V^*_{p,\mathrm{LTNA}}$, $V^*_{p,\mathrm{pycn}}$ and $V^*_{p,\mathrm{TP}}$ are reported in Tables 1 and 2. The bonded layer volume, V_{layer}, can be, finally, calculated by the difference between the specific pore volume of bare silica, 1.03 ml/g (see Table 1) and 0.77 ml/g, which is the average of the five estimations of corrected pore volumes obtained on the functionalized material through chromatographic methods (Table 2) and LTNA measurements (Table 1). Accordingly, $V_{\mathrm{layer}} = 0.26$ ml/g. Through V_{layer}, d_b, N_a and the surface area of bare silica, it is also possible to estimate the effective molecular volume of bonded ligands, V_{ligand}, as [32]:

$$V_{\mathrm{ligand}} = \frac{V_{\mathrm{layer}}}{S_{\mathrm{SiO_2}} \times d_b \times N_a} \tag{19}$$

A value of about 480 Å^3/molecule is obtained as the estimate of the volume of one perfluorohexylpropyl chain. For the sake of comparison, the effective molecular volume of a C18 bonded chain was estimated to be about 600 Å^3/molecule [29].

5. Conclusions

This study has evidenced some important characteristics of perfluorohexylpropyl silica-based stationary phases. In particular, it has been shown that under typical chromatographic conditions perfluorinated chains assume a compact arrangement, in analogy with what reported for alkyl [29] and phenyl [64] bonded phases in reversed phase chromatography. The other important aspect is related to the poor wettability of these media by water. The approach proposed to investigate the wetting behavior of perfluorinated adsorbents in water, based on tracer pulse chromatography with water as the mobile phase and deuterium oxide as the labeled tracer, seems to be very promising to investigate other situations in which wettability issues are suspected (including traditional C8 and C18 stationary phases). This method in fact does not require the choice of an unretained compound [34] nor the use of buffered solutions [33]. In the case of perfluorohexylpropyl adsorbents, it was shown that, unless a back-pressure of the order of 200 bars or larger is applied, the accessible pore volume of the packing particles is not completely accessible to water molecules. Therefore, the surface available for adsorption under these conditions is significantly smaller than the theoretical value, with important repercussions both for chromatographic (e.g., loss of retention and efficiency) and F-SPE (e.g., low recovery and scarce reproducibility) applications. The situation improves significantly when 5–10% (v/v) organic is added to the mobile phase.

Acknowledgments

The authors thank the Italian University and Scientific Research Ministry (PRIN 20098SJX4F_004 and PRIN 2009ZSC5K2_004), the University of Ferrara (FAR 2010) and the Regional Operational Programme of the European Regional Development Fund, Industrial Research and Technological Transfer (POR FESR 2007-2013 Priority 1). The authors also thank Dr. E. Bianchini from the Department of Chemistry and Pharmaceutical Sciences, University of Ferrara (Ferrara, Italy) for elemental analysis measurements and Dr. G. Gatti from the Dipartimento di Scienze e Tecnologie Avanzate, Università del Piemonte Orientale "Amedeo Avogadro" (Alessandria, Italy) for LTNA isotherm determination and NLDFT calculations.

References

[1] S.H. Langer, D.T. Hein, M.W. Bolme, Anal. Chem. 50 (1978) 1578.
[2] G.E. Berendsen, K.A. Pikaart, L. de Galan, C. Olleman, Anal. Chem. 52 (1980) 1990.
[3] H.A.H. Billiet, P.J. Schoenmakers, L. de Galan, J. Chromatogr. 218 (1981) 443.
[4] A. Haas, J. Kohler, H. Hemetsberger, Chromatographia 14 (1981) 341.
[5] P.J. Schoenmakers, H.A.H. Billiet, L. de Galan, Chromatographia 15 (1982) 205.
[6] J.H. Hildebrand, R.L. Scott, The Solubility OD Nonelectrolytes, 3rd ed., Dover, New York, 1964.
[7] J.C. Giddings, Unified Separation Science, Wiley-Interscience, New York, 1991.
[8] D.R. Husted, A.H. Ahlbrecht, US Patent 2,782,184 (Minnesota Mining and Manufacturing Company), February 19, 1957 (application: July 17, 1953).
[9] J.A. Gladysz, D.P. Curran, I.T. Horváth (Eds.), Handbook of Fluorous Chemistry, Wiley-VCH, Darmstadt, 2004.
[10] L.E. Brady, P.W. Carr, Anal. Chem. 54 (1982) 1751.
[11] J.A. Riddick, W. Bunger, T.K. Sakano, Organic Solvents: Physical Properties and Methods of Purification, 4th ed., Wiley-Interscience, New York, 1986.
[12] B.L. Karger, C.E.L.R. Snyder, J. Chromatogr. 125 (1976) 71.
[13] B.L. Karger, L.R. Snyder, C. Eon, Anal. Chem. 50 (1978) 2126.
[14] G. Xindu, P.W. Carr, J. Chromatogr. 269 (1983) 96.
[15] F.M. Yamamoto, S. Rokushika, J. Chromatogr. A 898 (2000) 141.
[16] M. Turowski, T. Morimoto, K. Kimata, H. Monde, T. Ikegami, K. Hosoya, N. Tanaka, J. Chromatogr. A 911 (2001) 177.
[17] C.F. Poole, H. Ahmed, W. Kiridena, C. DeKay, W.W. Koziol, Chromatographia 65 (2007) 127.
[18] Y. Sakaguchi, H. Yoshida, K. Todoroki, H. Nohta, M. Yamaguchi, Anal. Chem. 81 (2009) 5039.
[19] N. Marchetti, L. Caciolli, A. Laganà, F. Gasparrini, L. Pasti, F. Dondi, A. Cavazzini, Anal. Chem. 84 (2012) 7138.
[20] www.fluorous.com
[21] H. Zhou, W. Zhang, B. Yan, J. Comb. Chem. 12 (2010) 206.
[22] Y. Nakamura, S. Takeuchi, Y. Ohgo, D.P. Curran, Tetrahedron Lett. 41 (2000) 57.
[23] J.K. Kim, J.R. Lee, J.W. Kang, S.J. Lee, G.C. Shin, W.S. Yeo, K.H. Kim, H.S. Park, K.P. Kim, Anal. Chem. 83 (2011) 157.
[24] T. Miura, K.G. snd, D. Hosaka, T. Inazu, Angew. Chem. Int. Ed. 42 (2003) 2047.
[25] S.M. Brittain, S.B. Ficarro, A. Brock, E.C. Peters, Nat. Biotechnol. 23 (2005) 463.
[26] E.P. Go, W. Uritboonthai, J.V. Apo, S.A. Trauger, A. Nordstrom, G. O'Maille, S.M. Brittain, E.C. Peters, G. Siuzdak, J. Proteome Res. 6 (2007) 1492.
[27] T. Hayama, Y. Sakaguchi, H. Yoshida, M. Itoyama, K. Todoroki, M. Yamaguchi, H. Nohta, Anal. Chem. 84 (2012) 8407.
[28] Y.V. Kazakevich, R. LoBrutto, F. Chan, T. Patel, J. Chromatogr. A 913 (2001) 75.
[29] I. Rustamov, T. Farcas, F. Ahmed, F. Chan, R. LoBrutto, H.M. McNair, Y.V. Kazakevich, J. Chromatogr. A 913 (2001) 49.
[30] A. Giaquinto, Z. Liu, A. Bach, Y. Kazakevich, Anal. Chem. 80 (2008) 6358.
[31] F. Chan, L.S. Yeung, R. LoBrutto, Y.V. Kazakevich, J. Chromatogr. A 1082 (2005) 158.
[32] F. Chan, L.S. Yeung, R. LoBrutto, Y.V. Kazakevich, J. Chromatogr. A 1069 (2005) 217.
[33] T.H. Walter, P. Iraneta, M. Capparella, J. Chromatogr. A 1075 (2005) 177.
[34] N. Nagae, T. Enami, S. Doshi, LC–GC N. Am. 20 (2002) 964.
[35] B.A. Bidlingmeyer, A.D. Broske, J. Chromatogr. Sci. 42 (2004) 100.
[36] U.D. Neue, HPLC Columns: Theory, Technology and Practice, Wiley-VCH, New York, 1997.
[37] A. Cavazzini, N. Marchetti, L. Pasti, R. Greco, F. Dondi, A. Laganà, A. Ciogli, F. Gasparrini, Anal. Chem. 85 (2013).
[38] F. Rouquerol, J. Rouquerol, K. Sing, Adsorption by Powders and Porous Solids, Academic Press, San Diego, 1999.
[39] D. Amati, E.S. Kováts, Langmuir 3 (1987) 687.
[40] S.J. Gregg, K.S.W. Sing, Adsorption, Surface Area and Porosity, Academic Press, London, 1967.
[41] N.E. Buyanova, R.V. Zagrafskaya, A.P. Karnaukhov, A.S. Shepelina, Kinet. Catal. 24 (1983) 1011.
[42] L. Gurvich, J. Phys. Chem. Russ. 47 (1915) 805.
[43] R.J. Dombrowski, D.H. Hyduke, C.M. Lastoskie, Langmuir 16 (2000) 5041.
[44] C. Lastoskie, K.E. Gubbins, N.J. Quirke, J. Phys. Chem. 97 (1993) 4786.
[45] G.E. Berendsen, L. de Galan, J. Liq. Chromatogr. (1978) 561.
[46] F. Helfferich, D.L. Peterson, Science 142 (1963) 661.
[47] J.H. Knox, R. Kaliszan, J. Chromatogr. 349 (1985) 211.
[48] C.A. Rimmer, C.R. Simmons, J.D. Dorsey, J. Chromatogr. A 965 (2002) 219.
[49] F. Gritti, Y.V. Kazakevich, G. Guiochon, J. Chromatogr. A 1169 (2007) 111.
[50] K.S. Yun, C. Zhu, J.F. Parcher, Anal. Chem. 67 (1995) 613.
[51] M. Weng, J. Mallette, J.F. Parcher, J. Chromatogr. A 1190 (2008) 1.
[52] J. Mallette, M. Wang, J.F. Parcher, Anal. Chem. 82 (2010) 3329.
[53] J. Lindholm, P. Forssen, T. Fornstedt, Anal. Chem. 76 (2004) 4856.
[54] J. Lindholm, P. Forssen, T. Fornstedt, Anal. Chem. 76 (2004) 5472.
[55] R. Arnell, P. Fórsen, T. Fornstedt, J. Chromatogr. A 1099 (2005) 167.
[56] R. Arnell, N. Ferraz, T. Fornstedt, Anal. Chem. 78 (2006) 1682.
[57] T. Fornstedt, J. Chromatogr. A 1217 (2010) 792.
[58] M. Wang, B. Avula, Y.H. Wang, J.F. Parcher, I.A. Khan, J. Chromatogr. A 1220 (2012) 75.
[59] F. Riedo, E.S. Kováts, J. Chromatogr. 239 (1982) 1.
[60] R.M. McCormick, B. Karger, Anal. Chem. 52 (1980) 2249.
[61] C. Bisio, G. Gatti, E. Boccaleri, L. Marchese, G.B. Superti, H.O. Pastore, M. Thommes, Micropor. Mesopor. Mater. 107 (2008) 90.
[62] http://chemie.univie.ac.at/en/service-facilities/laboratory-for-elemental-analysis/
[63] K.S. Sing, D.H. everett, R.A.W. Haul, L. Moscou, R.A. Pierotti, J. Rouquerol, T. Siemieniewska, Pure Appl. Chem. 57 (1985) 603.
[64] F. Chan, L.S. Yeung, R. LoBrutto, Y.V. Kazakevich, J. Chromatogr. A 1069 (2005) 217.
[65] Y.V. Kazakevich, A.Y. Fadeev, Langmuir 18 (2002) 3117.
[66] L. Jelinek, E.sz. Kováts, Langmuir 10 (1994) 4225.
[67] A. Galarneau, H. Cambon, F. Di Renzo, F. Fajula, Langmuir 17 (2001) 8328.
[68] Thermo Scientific, Technical Guide TG 01-08 "Fluophase and Fluofix Column".
[69] L.R. Snyder, J.J. Kirkland, J.W. Dolan, Introduction to Modern Liquid Chromatography, 3rd ed., Wiley & Sons, United States of America, 2010.
[70] A. Cavazzini, F. Gritti, K. Kaczmarski, N. Marchetti, G. Guiochon, Anal. Chem. 79 (2007) 5972.
[71] M. Martin, G. Guiochon, J. Chromatogr. A 1090 (2005) 16.
[72] P. Szabelski, A. Cavazzini, K. Kaczmarski, X. Liu, J. van Horn, G. Guiochon, J. Chromatogr. A 950 (2002) 41.
[73] F. Chan, L.S. Yeung, R. LoBrutto, Y.V. Kazakevich, J. Chromatogr. A 1082 (2005) 158.
[74] Y.V. Kazakevich, R. LoBrutto, R. Vivilecchia, J. Chromatogr. A 1064 (2005) 9.
[75] G.E. Berendsen, L. de Galan, J. Liq. Chromatogr. 1 (1978) 403.

Desidero ringraziare il Professor Alberto Cavazzini e il Professor Alessandro Massi, miei tutor durante questo dottorato, per la grande disponibilità e cortesia dimostratemi e per gli insegnamenti che mi hanno trasferito.

Desidero ringraziare il Dott. Pierpaolo Giovannini per la guida e l'aiuto durante questi anni di dottorato.

Ringrazio il Prof. Michael Lämmerhofer e il Prof. C. Oliver Kappe per l'opportunità datami di lavorare nel proprio gruppo di ricerca durante i miei due periodi di studio all'estero, ed avermi dato l'occasione di fare una meravigliosa esperienza.

Ringrazio la Dott.ssa Valentina Costa per avermi trasmesso un bagaglio scientifico prezioso.
Ringrazio i miei colleghi dottoranti ed in particolare la Dott.ssa Chiara Massarenti che ha condiviso con me questo periodo di scrittura della Tesi.
Ringrazio il Dottor Salvatore Pacifico, mio riferimento scientifico. Ringrazio i colleghi e gli amici Daniele Ragno, Anna Zaghi, Adelaide Donvito per tutto quel che concerne il percorso fatto insieme in questi anni di dottorato
Desidero ringraziare la Dott.ssa Tatiana Bernardi, la Dott.ssa Nikla Baricordi, il Dott. Paolo Formaglio, il Dott. Marco Carmosino, la Dott.ssa Ercolina Bianchini per la disponibilità e la gentilezza dimostratemi.
Un ringraziamento speciale alla mia amatissima famiglia per avermi sempre sostenuto in tutte le mie decisioni permettendomi di raggiungere questo traguardo.

Ringrazio gli amici di sempre - quelli di Bologna in particolare… per essermi stati vicini sia nei momenti difficili, sia nei momenti felici, troppi da menzionare uno ad uno ma insostituibili - ringrazio i Minimal Joy e i Massimo Volume, ringrazio i Cure e i Joy Division per non avermi fatto mollare la presa, mai!

"Remembering
You standing quiet in the rain
As I ran to your heart to be near
And we kissed as the sky fell in
Holding you close
How I always held close in your fear
Remembering
You running soft through the night
You were bigger and brighter and wider than snow
And screamed at the make-believe
Screamed at the sky
And you finally found all your courage
To let it all go"

UNIVERSITÀ DEGLI STUDI DI FERRARA
- EX LABORE FRUCTUS -

Sezioni

Dottorati di ricerca

Il tuo indirizzo e-mail

grcrrt@unife.it

Oggetto:

Dichiarazione di conformità della tesi di Dottorato

Io sottoscritto Dott. (Cognome e Nome)

Greco Roberto

Nato a:

Maglie

Provincia:

Lecce

Il giorno:

09/05/1985

Avendo frequentato il Dottorato di Ricerca in:

Scienze Chimiche

Ciclo di Dottorato

27

Titolo della tesi:

Studio, sintesi e caratterizzazione di nuovi materiali microporosi funzionalizzati per la realizzazione di processi reattivi e separativi in sistemi dinamici

Titolo della tesi (traduzione):

Tutore: Prof. (Cognome e Nome)

Cavazzini Alberto

Settore Scientifico Disciplinare (S.S.D.)

CHIM/06

Parole chiave della tesi (max 10):

materiali porosi, porous materials, chimica in flusso, flow chemistry, organocatalisi, organocatalysis, microreattori,microreactors, catalisi eterogenea, heterogeneous catalysis, isoterma di eccesso, excess isotherm, adsorbimento, adsorption.

Consapevole, dichiara

CONSAPEVOLE: (1) del fatto che in caso di dichiarazioni mendaci, oltre alle sanzioni previste dal codice penale e dalle Leggi speciali per l'ipotesi di falsità in atti ed uso di atti falsi, decade fin dall'inizio e senza necessità di alcuna formalità dai benefici conseguenti al provvedimento emanato sulla base di tali dichiarazioni; (2) dell'obbligo per l'Università di provvedere al deposito di legge delle tesi di dottorato al fine di assicurarne la conservazione e la consultabilità da parte di terzi; (3) della procedura adottata dall'Università di Ferrara ove si richiede che la tesi sia consegnata dal dottorando in 2 copie di cui una in formato cartaceo e una in formato pdf non modificabile su idonei supporti (CD-ROM, DVD) secondo le istruzioni pubblicate sul sito: http://www.unife.it/studenti/dottorato alla voce ESAME FINALE –

disposizioni e modulistica; (4) del fatto che l'Università, sulla base dei dati forniti, archivierà e renderà consultabile in rete il testo completo della tesi di dottorato di cui alla presente dichiarazione attraverso l'Archivio istituzionale ad accesso aperto "EPRINTS.unife.it" oltre che attraverso i Cataloghi delle Biblioteche Nazionali Centrali di Roma e Firenze; DICHIARO SOTTO LA MIA RESPONSABILITA': (1) che la copia della tesi depositata presso l'Università di Ferrara in formato cartaceo è del tutto identica a quella presentata in formato elettronico (CD-ROM, DVD), a quelle da inviare ai Commissari di esame finale e alla copia che produrrò in seduta d'esame finale. Di conseguenza va esclusa qualsiasi responsabilità dell'Ateneo stesso per quanto riguarda eventuali errori, imprecisioni o omissioni nei contenuti della tesi; (2) di prendere atto che la tesi in formato cartaceo è l'unica alla quale farà riferimento l'Università per rilasciare, a mia richiesta, la dichiarazione di conformità di eventuali copie; (3) che il contenuto e l'organizzazione della tesi è opera originale da me realizzata e non compromette in alcun modo i diritti di terzi, ivi compresi quelli relativi alla sicurezza dei dati personali; che pertanto l'Università è in ogni caso esente da responsabilità di qualsivoglia natura civile, amministrativa o penale e sarà da me tenuta indenne da qualsiasi richiesta o rivendicazione da parte di terzi; (4) che la tesi di dottorato non è il risultato di attività rientranti nella normativa sulla proprietà industriale, non è stata prodotta nell'ambito di progetti finanziati da soggetti pubblici o privati con vincoli alla divulgazione dei risultati, non è oggetto di eventuali registrazioni di tipo brevettale o di tutela. PER ACCETTAZIONE DI QUANTO SOPRA RIPORTATO

Firma del dottorando

Ferrara, li _____26/03/2015_____ (data) Firma del Dottorando

_____

Firma del Tutore

Visto: Il Tutore Si approva Firma del Tutore _____